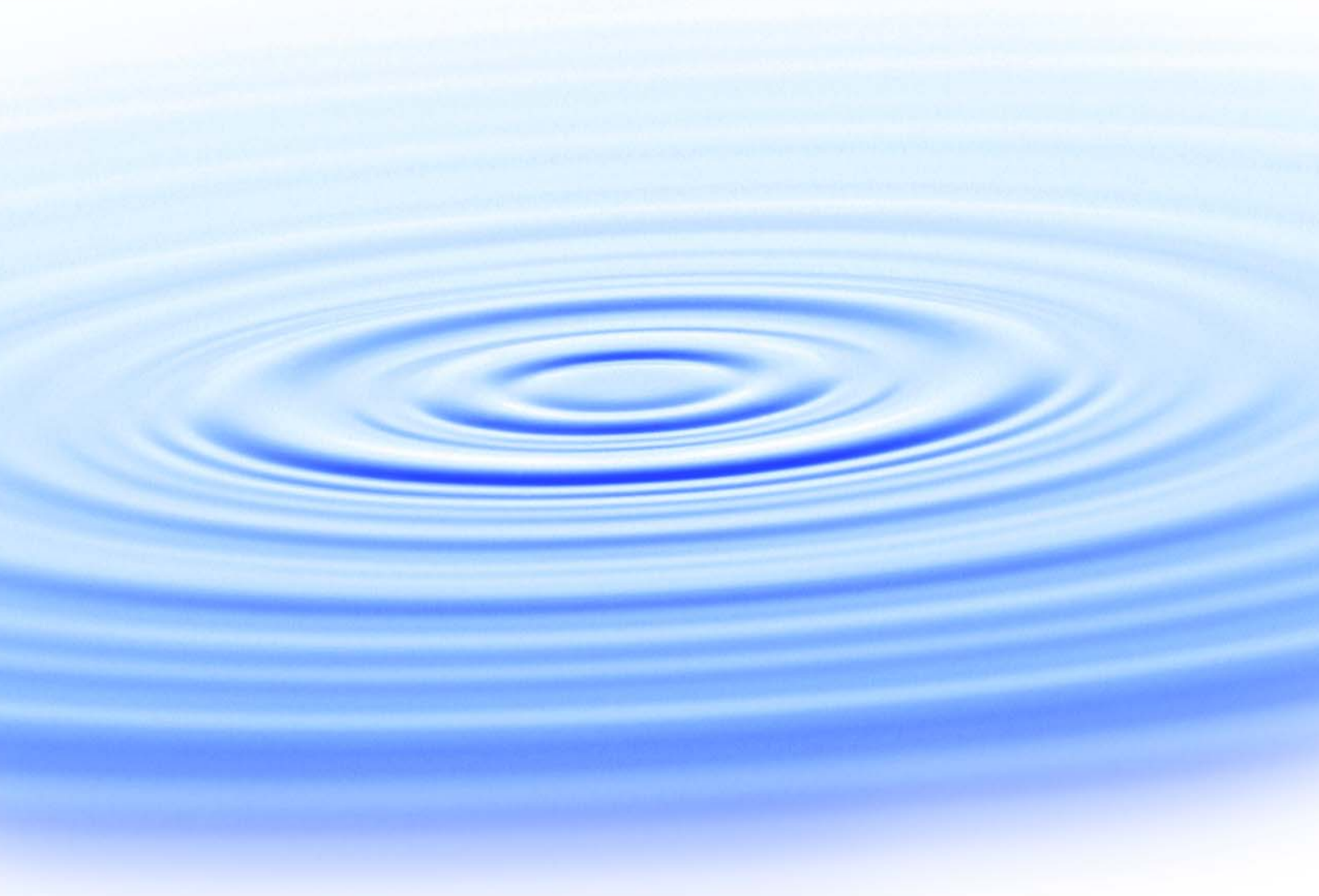




Pilot-Scale Oxidative Technologies for Reducing Fouling Potential in Water Reuse and Drinking Water Membranes



WaterReuse Research Foundation

Pilot-Scale Oxidative Technologies for Reducing Fouling Potential in Water Reuse and Drinking Water Membranes

About the WateReuse Research Foundation

The mission of the WateReuse Research Foundation is to conduct and promote applied research on the reclamation, recycling, reuse, and desalination of water. The Foundation's research advances the science of water reuse and supports communities across the United States and abroad in their efforts to create new sources of high-quality water through reclamation, recycling, reuse, and desalination while protecting public health and the environment.

The Foundation sponsors research on all aspects of water reuse, including emerging chemical contaminants, microbiological agents, treatment technologies, salinity management and desalination, public perception and acceptance, economics, and marketing. The Foundation's research informs the public of the safety of reclaimed water and provides water professionals with the tools and knowledge to meet their commitment of increasing reliability and quality.

The Foundation's funding partners include the Bureau of Reclamation, the California State Water Resources Control Board, the California Energy Commission, and the California Department of Water Resources. Funding is also provided by the Foundation's subscribers, water and wastewater agencies, and other interested organizations.

Pilot-Scale Oxidative Technologies for Reducing Fouling Potential in Water Reuse and Drinking Water Membranes

Benjamin D. Stanford, Ph.D.¹
Aleksey N. Pisarenko, Ph.D.²
Shane A. Snyder, Ph.D.³
Southern Nevada Water Authority

R. David Holbrook, Ph.D, P.E.
National Institute of Standards and Technology

¹*Currently at Hazen and Sawyer, P.C.*

²*Currently at Trussell Technologies, Inc.*

³*Currently at University of Arizona*

Cosponsors

Bureau of Reclamation
Southern Nevada Water Authority
Clean Water Coalition
Air Products
Clark County Water Reclamation District
West Basin Municipal Water District



WateReuse Research Foundation
Alexandria, VA



Disclaimer

This report was sponsored by the WateReuse Research Foundation and cosponsored by the Bureau of Reclamation, Southern Nevada Water Authority, Clean Water Coalition, Air Products, Clark County Water Reclamation District, and West Basin Municipal Water District. The Foundation, its Board Members, and the project cosponsors assume no responsibility for the content of this publication or for the opinions or statements of facts expressed in the report. The mention of trade names of commercial products does not represent or imply the approval or endorsement of the WateReuse Research Foundation, its Board Members, or the cosponsors. This report is published solely for informational purposes.

For more information, contact:

WateReuse Research Foundation
1199 North Fairfax Street, Suite 410
Alexandria, VA 22314
703-548-0880
703-548-5085 (fax)
www.WateReuse.org/Foundation

© Copyright 2013 by the WateReuse Research Foundation. All rights reserved. Permission to reproduce must be obtained from the WateReuse Research Foundation.

WateReuse Research Foundation Project Number: WRRF-08-08
WateReuse Research Foundation Product Number: 08-08-1

ISBN: 978-1-934183-98-4
Library of Congress Control Number: 2013956570

Printed in the United States of America

Printed on Recycled Paper

Contents

List of Figures	ix
List of Tables	xiii
Acronyms.....	xvi
Foreword.....	xix
Acknowledgements.....	xx
Executive Summary	xxiii
Chapter 1. Introduction, Background, and Study Design.....	1
1.1 Introduction to Membranes and Water Reuse	1
1.2 Fouling and Options for Fouling Control and NF and RO Membranes	3
1.2.1 Types of Fouling in NF and RO Membrane Applications	3
1.2.2 Implications of Fouling in NF and RO Membranes.....	5
1.2.3 Control of Reversible Fouling in NF and RO Membranes	5
1.2.4 Control of Irreversible Fouling from NOM	6
1.2.5 Hybridized Biological Treatment, Oxidation, and Membrane Separation Systems	7
1.2.6 Potential Drawbacks to Preoxidation Strategies in Hybrid Treatment Systems	8
1.3 Summary and Study Overview	9
Chapter 2. Experimental Design and Analytical Methods.....	11
2.1 Project Approach and Experimental Design.....	11
2.1.1 Research Objectives.....	11
2.1.2 Project Overview	12
2.1.3 Project Approach	13
2.2 Overview of Analytical Methods.....	15
2.2.1 Dissolved Organic Matter Characterization Techniques	16
2.2.2 Trace Organic Contaminant and Inorganic Constituent Analyses	19
2.2.3 Membrane Autopsy and Surface Analyses	20
2.2.4 Determination of the UV Dose at the Pilot-Scale UV/H ₂ O ₂ Reactor	22
Chapter 3. Oxidation Impacts on Dissolved Organic Matter	25
3.1 Chapter Overview	25
3.2 Experimental Setup.....	26
3.3 Results and Discussion	27
3.3.1 Oxidation Impacts on NOM in Colorado River Water	27
3.3.2 Oxidation Impacts on EfOM in Tertiary Effluent from Water Reclamation Facility 2	30
3.3.3 Oxidation Impacts on EfOM in UF Filtrate	31
3.3.4 Oxidation Impacts on EfOM in MBR Filtrate	40
3.4 Conclusions.....	47

Chapter 4. Bench-Scale Evaluation of Preoxidation Impacts on RO Membrane Fouling.....	49
4.1 Chapter Overview	49
4.2 Experimental Setup.....	49
4.2.1 Flat Sheet Membrane Test System.....	49
4.2.2 Application of Preoxidation Technologies for Flat Sheet Tests.....	50
4.3 Data from Flat Sheet Tests.....	51
4.3.1 Colorado River Water Tests	51
4.3.2 MBR Filtrate Pretreatment with Ozone and Ozone/Peroxide Tests	52
4.3.3 Tertiary Effluent and UF Filtrate Pretreatment with UV and UV/Peroxide Tests (WWF 2).....	55
4.4 Result Summary and Conclusions	57
Chapter 5. Pilot-Scale Evaluation of the MBR-O₃-RO System at Water Reclamation Facility 1.....	59
5.1 Chapter Overview	59
5.2 Description of MBR-O ₃ -RO Pilot-Scale Equipment	59
5.2.1 Description of MBR Equipment.....	60
5.2.2 Description of HiPOx [®] Equipment	62
5.2.3 Description of RO Equipment.....	62
5.3 Results and Discussion	64
5.3.1 Phase I: 14-gfd Conditions	64
5.3.2 Phase II: 15.5-gfd Conditions.....	67
5.3.3 Phase III: 17-gfd Conditions	70
5.3.4 Phase IV: 19-gfd Conditions	77
5.3.5 End-of-Study Microscopy Analysis and Discussion.....	80
5.4 Conclusions.....	84
Chapter 6. Pilot-Scale Evaluation of the UF-O₃-RO and UF-UV/H₂O₂-RO System at Water Reclamation Facility 2	85
6.1 Chapter Overview	85
6.2 Description of the UF-UV/H ₂ O ₂ -RO and UF-O ₃ -RO Pilot-Scale Equipment.....	85
6.2.1 Description of the UF Equipment	86
6.2.2 Description of the Ozonia [®] Equipment	87
6.2.3 Description of the TrojanUVPhox [®] UV Equipment	87
6.2.4 Description of the RO Equipment.....	87
6.3 Results and Discussion	88
6.3.1 Phase I: 14-gfd Conditions for UF-RO and UF-O ₃ -RO Trains	88
6.3.2 Phase II: 14-gfd Conditions for UF-RO and UF-UV/H ₂ O ₂ -RO Trains.....	91
6.3.3 Phase III: 15-gfd Conditions for UV/H ₂ O ₂ Pretreatment	94
6.3.4 End-of-Study Autopsy and Microscopy Analysis	96
6.4 Conclusions.....	100

Chapter 7. Preoxidation Impacts on Trace Organic Contaminant Concentrations.....	101
7.1 Introduction and Background	101
7.2 Experimental Methods and Equipment.....	102
7.2.1 Drinking Water Treatment Plant 1 (DWTP 1), Colorado River Water Tests	102
7.2.2 Water Reclamation Facility 1, MBR-O ₃ -RO Tests.....	102
7.2.3 Water Reclamation Facility 2, UF-UV/Peroxide/RO Tests.....	102
7.2.4 Analytical Methods.....	102
7.2.5 Energy Calculations for Contaminant Destruction	103
7.3 Experimental Results	103
7.3.1 Background Water Quality Data	103
7.3.2 TO _{RC} Removal/Oxidation from Colorado River with Ozone and RO Treatment.....	104
7.3.3 TO _{RC} Removal/Oxidation through MBR, Ozone, and RO Treatments at WRF 1	107
7.3.4 TO _{RC} Removal/Oxidation through UF, UV/Peroxide, and RO Treatments at Water Reclamation Facility 2	114
7.4 Implications of Findings	119
7.5 Concluding Remarks	121
Chapter 8. Cost Comparison of Oxidative Pretreatment Strategies.....	123
8.1 Introduction.....	123
8.2 Basis for Energy Calculations.....	123
8.2.1 RO Membrane Pressure and Pumping Power	123
8.2.2 UV and UV/Peroxide	126
8.2.3 Ozone	129
8.3 Combined Energy Projections	129
8.4 Comparison of Costs and Summary	133
Chapter 9. Summary and Conclusions	135
9.1 Overview and Restatement of Project Objectives	135
9.2 Summary of Results from This Study.....	136
9.2.1 Impact of Oxidation on Organic Matter	136
9.2.2 Bench-Scale Membrane Fouling Results	136
9.2.3 Pilot-Scale Fouling Results: MBR-O ₃ -RO	137
9.2.4 Pilot-Scale Fouling Results: UF-UV/H ₂ O ₂ -RO.....	137
9.2.5 Impact of Preoxidation on Trace Organic Contaminants	137
9.2.6 Cost Considerations for Preoxidation Strategies	138
9.3 Conclusions and Recommendations	138
References.....	141

Appendix A.....	151
Appendix B.....	191
Appendix C.....	197
Appendix D.....	205

Figures

2.1	A fluorescence EEM image, with outlined boundaries for integration regions and data collection.	18
2.2	Image from sessile drop method using water on a fouled membrane surface.	21
2.3	A plot of atrazine concentration, as $\ln(C_i/C_o)$, vs. fluence (UV dose), as determined by radiometer measurements.	23
2.4	A plot of UV dose determined by actinometry vs. radiometer measurements.	23
2.5	A plot of UV dose values determined by actinometry vs. the feed flow to the UV skid running with 17 active lamps at 60% power.	24
3.1	Ozone demand/decay curve for Colorado River water.	27
3.2	Fluorescence EEM spectra for (A) raw Colorado River water, (B) after 1.5-mg/L O_3 and 0.5-mg/L H_2O_2 , (C) after 3-mg/L O_3 and 1.1-mg/L H_2O_2 , (D) after 3 mg/L.	28
3.3	Size exclusion chromatography/UV/fluorescence data for Colorado River water samples.	30
3.4	Fluorescence EEM spectra of (A) tertiary effluent, (B) tertiary effluent treated with UV dose of 2300 mJ/cm^2 (UV dose is approximate), (C) tertiary effluent treated with a UV dose of 1900 mJ/cm^2 and 7-mg/L H_2O_2 , (D) tertiary effluent treated with a UV dose of 2500 mJ/cm^2 and 10-mg/L H_2O_2	31
3.5	Ozone decay curves in the UF feed (“Pre-UF”) and filtrate (“Post-UF”) from test no. 1.	33
3.6	Ozone decay curves in UF feed and UF filtrate at various ozone doses (test no. 2).	33
3.7	UV_{254} plotted versus applied ozone dose in UF feed (pre-UF) and UF filtrate (post-UF).	35
3.8	Fluorescence EEM spectra of (A) UF feed (without ozone), (B) UF filtrate (without ozone), (C) UF feed with 1.5-mg/L ozone, and (D) UF filtrate with 1.5-mg/L ozone.	35
3.9	Overlaid size exclusion chromatography–UV chromatograms for UF filtrate at various ozone doses.	37
3.10	Overlaid size exclusion chromatography–fluorescence chromatograms for UF filtrate treated with various ozone doses.	37
3.11	Polarity rapid assessment method analysis results for UF filtrate treated with various ozone doses.	38
3.12	Fluorescence EEM spectra of (A) UF filtrate after 400 mJ/cm^2 and 10-mg/L H_2O_2 , (B) UF filtrate after 1000 mJ/cm^2 (no H_2O_2), (C) UF filtrate after 1000 mJ/cm^2 and 5-mg/L H_2O_2 , (D) UF filtrate after 1000 mJ/cm^2 and 10-mg/L H_2O_2	39
3.13	Ozone decay curves in MBR filtrate at various ozone doses.	40
3.14	UV_{254} plotted versus measured ozone residual and applied ozone dose.	40
3.15	Size exclusion chromatography–UV overlaid chromatograms for MBR filtrate samples treated with various ozone and ozone/hydrogen peroxide doses.	42

3.16	(Ozone alone) Overlaid size exclusion chromatography–UV chromatograms normalized by higher-molecular-weight peak at 42 min for MBR filtrate samples treated with various ozone doses.	43
3.17	(Ozone + peroxide) Overlaid size exclusion chromatography–UV chromatograms normalized by higher-molecular-weight peak at 42 min for MBR filtrate samples treated with various ozone/hydrogen peroxide doses.	43
3.18	Overlaid size exclusion chromatography–UV chromatograms normalized by lower-molecular-weight peak at 72.5 min for MBR filtrate samples treated with various ozone doses.	44
3.19	Overlaid size exclusion chromatography–UV chromatograms normalized by lower-molecular-weight peak at 72.5 min for MBR filtrate samples treated with various ozone/hydrogen peroxide doses.	44
3.20	Size exclusion chromatogram with TOC detector of MBR influent and effluent samples.	45
3.21	Size exclusion chromatogram with TOC detector of MBR effluent without and with ozone spiked at 6 mg/L (O_3 :TOC ~ 1.0).	45
3.22	Biodegradable dissolved organic carbon over time in control samples spiked with sodium acetate and MBR filtrate. Error bars are based on duplicate sample.	46
4.1	ESEM images from left to right: virgin ESPA-2 membrane, ESPA-2 after 72-h fouling test with Colorado River water, and ESPA-2 membrane after 72-h fouling test with Colorado River water + 3-mg/L ozone.	52
4.2	Contact angle measurements for clean and fouled ESPA-2 membranes (3-mg/L ozone dose and raw Colorado River water).	52
4.3	Change in normalized TCSF (J/J_o) in RO flat sheet tests using MBR filtrate and MBR filtrate + 3-mg/L ozone.	54
4.4	Change in normalized TCSF (J/J_o) in RO flat sheet tests using MBR filtrate treated with 1.5-mg/L ozone and 6-mg/L ozone.	54
4.5	Change in normalized TCSF (J/J_o) in RO flat sheet tests using MBR filtrate treated with 3-mg/L ozone and 3-mg/L ozone + peroxide (0.5-mol ratio).	55
4.6	Overlaid changes in normalized RO permeate flux (J/J_o) over time for tertiary effluent with various UV and UV/peroxide treatments and UF filtrate with and without UV/peroxide preoxidation.	57
5.1	Photographs of MBR setup, HiPOx [®] , and RO at WRF 1 (series of aeration and anoxic tanks in top panel; HiPOx [®] unit, bottom right panel; RO unit, bottom left panel).	60
5.2	Process layout of MBR-RO and MBR- O_3 -RO treatment trains.	60
5.3	Process flow diagram of Hydranautics MBR and wastewater treatment skid.	61
5.4	Schematic of Hydranautics twin RO system.	63
5.5	Changes in temperature-corrected specific flux (TCSF) (gfd/psi) for the two treatments under 14-gfd conditions.	65
5.6	Changes in temperature-corrected specific flux (TCSF) decline (%) for the two treatments under 14-gfd conditions.	65
5.7	Changes in normalized salt transport coefficient (STCn) for the two treatments under 14-gfd conditions.	66

5.8	Changes in differential pressure (dP) for the two treatments under 14-gfd conditions.....	66
5.9	Changes in temperature-corrected specific flux (TCSF) (gfd/psi) for the two treatments under 15.5-gfd conditions.....	67
5.10	SEM image (the scale bar in red is for 5 μ m) of a clean ESPA-2 membrane (left image) and a table generated from EDAX analysis.....	68
5.11	SEM image (the scale bar in red is for 20 μ m) of Train 1 (MBR-O ₃ -RO) membrane (left image) and a table generated from EDAX analysis.....	68
5.12	SEM image (the scale bar in red is for 5 μ m) of Train 1 (MBR-O ₃ -RO) membrane showing paired cells (left image) and a diatom (right image) at higher magnification.....	69
5.13	SEM image (the scale bar in red is for 5 μ m) of Train 2 (MBR-RO) membrane showing paired cells (left image) and a diatom (right image) at higher magnification.....	69
5.14	Changes in temperature-corrected specific flux (TCSF) (gfd/psi) for the two treatments under 17-gfd conditions.....	70
5.15	Change in temperature-corrected specific flux (TCSF) for CLV pilot system for the 17-gfd testing upon restart on February 28, 2011.....	71
5.16	Change in differential pressure for CLV pilot system for the 17-gfd testing at restart on Feb. 28, 2011 (1 = MBR-O ₃ -RO train; 2 = MBR-RO train).	71
5.17	Photographs illustrating the process of opening the RO elements.....	72
5.18	Photographs illustrating the process of sampling RO elements for microscopy analysis.....	72
5.19	SEM image at $\times 3000$ (the scale bar in red is for 5 μ m) of a clean ESPA-2 membrane (left image) and a table generated from EDAX analysis.....	73
5.20	SEM image at $\times 3000$ (the scale bar in red is for 5 μ m) of a sample of MBR-O ₃ -RO lead element (left image) and a table generated from EDAX analysis.....	73
5.21	SEM image at $\times 3000$ (the scale bar in red is for 5 μ m) of a sample of MBR-RO lead element (left image) and a table generated from EDAX analysis.....	74
5.22	SEM image at $\times 40$ (the scale bar in red is for 200 μ m) of a sample of MBR-O ₃ -RO tail element (left image) and a table generated from EDAX analysis... ..	74
5.23	SEM image at $\times 80$ (the scale bar in red is for 200 μ m) of a sample of MBR-RO tail element (left image) and a table generated from EDAX analysis.....	75
5.24	Change in temperature-corrected specific flux (TCSF) for CLV pilot system for the 17-gfd testing with new elements.....	76
5.25	Changes in temperature-corrected specific flux (TCSF) for the MBR-RO trains over time for 17-gfd conditions.....	76
5.26	Changes in % temperature-corrected specific flux decline for the MBR-RO trains over time for 17-gfd conditions.....	77
5.27	Changes in temperature-corrected specific flux (TCSF) for the MBR-RO trains over time for 19-gfd conditions.....	78
5.28	Changes in temperature-corrected specific flux for the MBR-RO trains over time for 19-gfd conditions.....	78
5.29	Changes in normalized temperature-corrected specific flux (TCSF) and percentge difference for the MBR-RO trains over time for 19-gfd conditions.....	79

6.1	Photographs of UF, Ozonia, TrojanUVPhox [®] , chemical feed, and RO systems at Water Reclamation Facility 2.	86
6.2	Process layout of UF-RO, UF-O ₃ -RO, and UF-UV/H ₂ O ₂ -RO treatment trains.	86
6.3	Changes in temperature-corrected specific flux (TCSF) (gfd/psi) for the UF-RO and UF-O ₃ -RO treatments at 14 gfd during Phase I.	89
6.4	SEM image at ×3000 (the scale bar in red is for 5 μm) of a sample of UF-O ₃ -RO tail element (left image) and a table generated from EDAX analysis.	90
6.5	SEM image at ×6000 (the scale bar in red is for 2 μm) of a sample of UF-RO tail element (left image) and a table generated from EDAX analysis.	91
6.6	Changes in temperature-corrected specific flux (TCSF) (gfd/psi) for the UF-RO and UF-UV/H ₂ O ₂ -RO trains under 14-gfd conditions.	92
6.7	Changes in percentage of temperature-corrected specific flux decline for the UF-RO and UF-UV/H ₂ O ₂ -RO trains under 14-gfd conditions.	92
6.8	Changes in normalized salt transport coefficient for the UF-RO and UF-UV/H ₂ O ₂ -RO trains under 14-gfd conditions.	93
6.9	Changes in differential pressure for the UF-RO and UF-UV/H ₂ O ₂ -RO trains under 14-gfd conditions.	93
6.10	Photograph of cartridge filters from UF-UV/H ₂ O ₂ -RO (Train 1) and UF-RO (Train 2) trains under 14-gfd conditions.	94
6.11	Changes in temperature-corrected specific flux (TCSF) (gfd/psi) for the UF-RO and UF-UV/H ₂ O ₂ -RO trains under 15.5-gfd conditions.	95
6.12	Changes in percentage of temperature-corrected specific flux decline for the UF-RO and UF-UV/H ₂ O ₂ -RO trains under 15.5-gfd conditions.	95
6.13	Changes in normalized salt transport coefficient and normalized differential pressure (dPn) for the UF-RO and UF-UV/H ₂ O ₂ -RO trains under 15.5-gfd conditions.	96
7.1	Removal of NDMA by ozone and ozone/peroxide in spiked Colorado River water	105
7.2	Concentration of TOxCs through MBR treatment at WRF 1.	108
8.1	Changes in RO system operating pressure over time with different flux decline scenarios using WRF 2 post-UF water.	124
8.2	Changes in RO system operating pressure over time with different flux decline scenarios and CIP events, assuming 85% restoration of original flux using WRF 2 post-UF water.	125
8.3	Relationship between feed pressure and power to drive water across the RO membranes, scaled to low-salt water, reuse application ranges.	125
8.4	Power usage for 3-mg/L ozone pretreatment vs. control with no ozone for Scenarios A, B, C, and D as described in Table 8.4.	131
8.5	Ozone generation, pumping, and CIP chemical costs for a 3-mg/L O ₃ -RO system versus a control RO system.	132
8.6	Ozone generation, pumping, and CIP chemical costs for a 1.5-mg/L O ₃ -RO system vs. a control RO system.	133

Tables

1.1	Delineation of Fluorescence Regional Integration Volumes	17
3.1	Water Quality Parameters for MBR Filtrate and Colorado River Water.....	26
3.2	Change in Specific UV Absorbance for Ozone- and Ozone/Peroxide-Treated Samples	28
3.3	Bulk Water Quality Parameters for UF Feed and Permeate	32
3.4	Changes in UV ₂₅₄ and UV ₂₈₀ of UF Feed and UF Filtrate When Treated with Various Doses of Ozone	34
3.5	Fluorescence Regional Integration of UF Feed and UF Filtrate Treated with Various Doses of Ozone	36
3.6	Changes in UV ₂₅₄ of UF Filtrate When Treated with Various Doses of UV and UV/H ₂ O ₂	38
3.7	Fluorescence Regional Integration of Samples from UF Filtrate Treated with Various UV and UV/H ₂ O ₂ Doses	39
3.8	Changes in UV ₂₅₄ and UV ₂₈₀ of MBR Filtrate Treated with Various Doses of Ozone and Hydrogen Peroxide.....	41
3.9	Fluorescence Regional Integration on MBR Filtrate Treated with Various Doses of Ozone and Hydrogen Peroxide.....	41
3.10	Summary of Biodegradable Dissolved Organic Carbon Results for MBR Filtrate Samples Treated with Various Ozone and Ozone/Hydrogen Peroxide Doses	47
4.1	Comparison of Changes in Specific Flux (SF) after i Hours of Operation (SF _i), Targeted Flux, Initial Pressure (P ₀), and Initial Specific Flux (SF ₀) for Colorado River Water	51
4.2	Comparison of Changes in Specific Flux (SF) after i Hours of Operation (SF _i), Targeted Flux, Initial Pressure (P ₀), And Initial Specific Flux (SF ₀) for MBR Filtrate (MBR-F).....	53
4.3	Comparison of Changes in Specific Flux (SF) after i Hours of Operation, Targeted Flux, Initial Pressure (P ₀), and Initial Specific Flux (SF ₀) for Tertiary Effluent and UF Filtrate from Water Reclamation Facility 2 Treated under Various UV and UV/Peroxide Conditions.....	56
5.1	Typical Operating Parameters for Hydranautics MBR Pilot System	61
5.2	Typical MBR Feed and Filtrate Water Quality for BOD/COD, Ammonia, and Phosphorus Removal	62
5.3	Selected Analysis for RO Grab Samples and Frequency.....	63
5.4	14-gfd RO Operating Parameters for 1 × 6 Array	64
5.5	15.5-gfd RO Operating Parameters for 1 × 6 Array	67
5.6	17-gfd RO Operating Parameters for 1 × 5 Array	70
5.7	Wet Tests of the Lead and Tail Elements from MBR-RO Treatment Trains at 17 gfd...	72
5.8	19-gfd RO Operating Parameters for 1 × 4 Array	77

5.9	Wet Tests of the Lead and Tail Elements from MBR-RO Treatment Trains at 19 gfd	79
5.10	Contact Angle Measurements for MBR-RO Treatment Trains at 19 gfd	81
5.11	TOC Analysis (in mg/cm ² of Membrane Surface) for MBR-RO Trains	81
5.12	Fluorescence Analysis of Foulant Extraction of MBR-RO Trains	82
5.13	Summary of the ESEM and EDS Characterization Results of MBR-RO Trains	83
6.1	Typical UF Feed and Filtrate Water Quality for Phosphorus Removal	87
6.2	Selected Analysis for RO Pilot Grab Samples and Frequency	88
6.3	14-gfd RO Operating Parameters for 1 × 6 Array	89
6.4	Wet Tests of the Lead and Tail Elements from UF-RO Pilots	90
6.5	15.5-gfd RO Operating Parameters for 1 × 6 Array	94
6.6	Wet Tests of the Lead and Tail Elements from UF-RO and UF-UV/H ₂ O ₂ -RO Trains	96
6.7	Contact Angle Measurements for UF/RO Treatment Trains at 15.5 gfd	98
6.8	TOC Analysis (as mg/cm ² of Membrane Surface) for UF-RO Trains	98
6.9	Fluorescence Analysis of Foulant Extraction of UF-RO Trains	99
6.10	Summary of the ESEM and EDS Characterization Results of UF-RO Trains	100
7.1	Water Quality Parameters for MBR Filtrate and Colorado River Water	104
7.2	Percentage Removal of TOxCs by Ozone in Colorado River Water at Various O ₃ :DOC Ratios	106
7.3	Percent age Removal of TOxCs by Ozone + Peroxide in Colorado River Water at Various O ₃ :DOC Ratios	106
7.4	Summary of the Effects of RO (ESPA-2) and Preozonation on TOxC Concentration (ng/L)	107
7.5	Percentage Removal of TOxCs by Ozone in MBR Filtrate at Various O ₃ :DOC Ratios	108
7.6	Percentage Removal of TOxCs by Ozone + Peroxide in MBR Filtrate at Various O ₃ :DOC Ratios	109
7.7	Removal of TOxCs (ng/L) by MBR, Ozone, and RO	110
7.8	Transport of TOxCs and Bromate through MBR-RO Trains	111
7.9	Direct NDMA and Bromate Formation from Ozone and Ozone/Peroxide of MBR Filtrate	112
7.10	Direct NDMA Formation by Ozone (Day 0) and NDMA Formation Potential (Day 10–Day 0)	113
7.11	Direct Bromate Formation from Ozone and Ozone/Peroxide of MBR Filtrate	114
7.12	Percentage Removal of TOxCs by UV/Peroxide in UF Filtrate in Bench-Scale UV Experiments	115
7.13	Removal of TOxCs by UV/Peroxide and RO in UF Filtrate in Pilot-Scale Tests	116
7.14	Transport of TOxCs and Bromate through UF-RO Trains	117
7.15	NDMA Destruction and Bromate Formation from UV/Peroxide Treatment of UF Filtrate (UF-F)	118

7.16	Impact of UV/Peroxide on NDMA Formation Potential in UF Filtrate (UF-F)	118
7.17	Electrical Energy per Order (EEO) of TOrC Removal by Ozone (O ₃) and Ozone/Peroxide (O ₃ /H ₂ O ₂) in CRW and MBR Filtrate, Sorted by Ozone-Based EEO in MBR Filtrate	119
7.18	Electrical Energy per Order (EEO) of TOrC Removal by UV and UV/Peroxide in UF Filtrate	120
8.1	Water Quality Parameters for UV Power Calculations.....	126
8.2	Description of Baseline and Adjusted Comparison Scenarios for UV Power Calculations.....	128
8.3	Calculated Ratio of UV-Only Power Requirements for Test Case Scenarios.....	128
8.4	Parameters Used for Cost Curve Development.....	130
8.5	Summary of Capital and O&M Costs from WateReuse-08-05.....	134
8.6	Flow-Normalized Capital Costs for Combined Process Trains	134
8.7	Flow-Normalized Annual O&M Costs for Combined Process Trains.....	134

Acronyms

AOC	assimilable organic carbon
AOP	advanced oxidation process
ATD	antitelescoping device
BDOC	biodegradable dissolved organic carbon
BOD	biological oxygen demand
CIP	clean-in-place
CRW	Colorado River water
DBNPA	2,2-dibromo-3-nitrilopropionamide
DI	deionized (water)
DOC	dissolved organic carbon
DOM	dissolved organic matter
DWTP	drinking water treatment plant
EDCs	endocrine disrupting compounds
EDS	energy dispersive spectroscopy
EEM	excitation–emission matrix (spectroscopy)
EffOM	effluent organic matter
EPA	Environmental Protection Agency (U.S.)
EPS	extracellular polymeric substances
ESEM	environmental SEM
FI	fluorescence index
FL	fluorescence (detectors)
FP	formation potential
FRI	fluorescence regional integration
GC	gas chromatography
HLB	hydrophilic-lipophilic balance
ICP	inductively coupled plasma
IPR	indirect potable reuse
LC	liquid chromatography
MBR	membrane bioreactor
MF	microfiltration
MFI	modified fouling index
MS	mass spectrometry
NDMA	<i>N</i> -nitrosodimethylamine
NF	nanofiltration (membranes)
NIST	National Institute of Standards and Technology
NOM	natural organic matter
NTU	nephelometric turbidity unit
O&M	operations and maintenance

OBM	oxidation biofiltration membrane
PAC	Project Advisory Committee
PhACs	pharmaceutically active compounds
PRAM	polarity rapid assessment method
PVDF	polyvinylidene fluoride
RC	retention coefficients
RO	reverse osmosis (membranes)
SDI	silt density index
SEC	size exclusion chromatography
SEM	scanning electron microscopy
SPE	solid phase extraction
TAC	Technical Advisory Committee
TDS	total dissolved solids
TMP	transmembrane pressure
TOC	total organic carbon
TOrC	trace organic contaminant
UF	ultrafiltration
UV	ultraviolet light
UVT	UV transmittance at 254 nm
WHO	World Health Organization
WRF 1	Water Reclamation Facility 1
WRF 2	Water Reclamation Facility 2

Foreword

The WaterReuse Research Foundation, a nonprofit corporation, sponsors research that advances the science of water reclamation, recycling, reuse, and desalination. The Foundation funds projects that meet the water reuse and desalination research needs of water and wastewater agencies and the public. The goal of the Foundation's research is to ensure that water reuse and desalination projects provide high-quality water, protect public health, and improve the environment.

An Operating Plan guides the Foundation's research program. Under the plan, a research agenda of high-priority topics is maintained. The agenda is developed in cooperation with the water reuse and desalination communities including water professionals, academics, and Foundation subscribers. The Foundation's research focuses on a broad range of water reuse research topics including the following:

- Definition of and addressing emerging contaminants
- Public perceptions of the benefits and risks of water reuse
- Management practices related to indirect potable reuse
- Groundwater recharge and aquifer storage and recovery
- Evaluation and methods for managing salinity and desalination
- Economics and marketing of water reuse

The Operating Plan outlines the role of the Foundation's Research Advisory Committee (RAC), Project Advisory Committees (PACs), and Foundation staff. The RAC sets priorities, recommends projects for funding, and provides advice and recommendations on the Foundation's research agenda and other related efforts. PACs are convened for each project and provide technical review and oversight. The Foundation's RAC and PACs consist of experts in their fields and provide the Foundation with an independent review, which ensures the credibility of the Foundation's research results. The Foundation's Project Managers facilitate the efforts of the RAC and PACs and provide overall management of projects.

This multiyear study was designed to evaluate a novel approach of using oxidative technologies as a pretreatment for RO membrane feed water to address issues associated with organic fouling: instead of using oxidation as a final treatment step for system redundancy and removal of trace organic contaminants (TOrcs), the study was designed to investigate the use of ozone, ozone/peroxide, UV, and UV/peroxide, at bench and pilot scale, prior to membrane treatment in order to reduce the fouling associated with natural organic matter while also achieving TOrc removal. Ozone preoxidation had the most potential to provide additional fouling control in a cost-effective manner, as demonstrated during multiple pilot tests at two wastewater treatment facilities. The data, cost analysis, and interpretation of findings are provided in this Final Report Document.

Richard Nagel

Chair

WaterReuse Research Foundation

G. Wade Miller

Executive Director

WaterReuse Research Foundation

Acknowledgments

This study began as a research initiative of the Southern Nevada Water Authority, and the authors are grateful for its support (financial, in-kind, and staff time) throughout this project. We especially thank Ron Zegers, Dave Rexing, Linda Parker, and many others for their ongoing administrative and logistical support of this study. We also recognize Janie Morrow at the National Institute of Standards and Technology for assistance with sessile drop analyses of the membranes. Pei Xu at the Colorado School of Mines provided additional support and analysis of membrane samples. We thank the U.S. Bureau of Reclamation for support throughout this project. Further, this project would not have been possible without the generous financial and equipment contributions from our cosponsors, including Hydranautics/Nitto Denko, APTwater, Air Products, TrojanUV, GE Water, the Clean Water Coalition, the City of Henderson, the City of Las Vegas, the Clark County Water Reclamation District, the Long Beach Water Department, and the West Basin Municipal Water District. We also thank our Technical Advisory Committee and Project Advisory Committee members for their constructive criticism and feedback throughout the project.

Principal Investigators

Benjamin D. Stanford, Ph.D., * *Southern Nevada Water Authority*
Aleksy N. Pisarenko, Ph.D., *Southern Nevada Water Authority*
Shane A. Snyder, Ph.D., † *Southern Nevada Water Authority*
R. David Holbrook, Ph.D, P.E., *National Institute of Standards and Technology*

* *Currently at Hazen and Sawyer, P.C.*

† *Currently at University of Arizona*

Research project team

Michael Arrasate, *City of Henderson*
Susanna Blunt, *Southern Nevada Water Authority*
Josephine Chu, *Southern Nevada Water Authority*
Saundy Cook, *City of Henderson*
Bruce Dacko, *City of Las Vegas Water Pollution Control Facility*
Shannon Ferguson, *Southern Nevada Water Authority*
Daniel Fischer, *City of Las Vegas Water Pollution Control Facility*
Richard Franks, *Hydranautics/Nitto Denko*
Benjamin Freeman, *Hydranautics/Nitto Denko*
Sujanie Gamage, *Southern Nevada Water Authority*
Naomi Jones, *Hydranautics/Nitto Denko*
Patrick Joyce, *Clark County Water Reclamation District*
Janie Holady, *Southern Nevada Water Authority*
Dana LaRance, *City of Henderson*
Jing Lin, *Southern Nevada Water Authority*
Erica Marti, *Southern Nevada Water Authority*
Douglas Mawhinney, *Southern Nevada Water Authority*
Steven Peck, *Hydranautics/Nitto Denko*
Keel Robinson, *APTwater*

LeAnna Risso, *Clark County Water Reclamation District*
Rebecca Trenholm, *Southern Nevada Water Authority*
Brett Vanderford, *Southern Nevada Water Authority*
Ricky Villalobos, *APTwater*
Yue Wang, *Southern Nevada Water Authority*
Dongxu Yan, *Southern Nevada Water Authority*

Technical Advisory Committee

Kevin Alexander and Silvana Ghiu, Ph.D., *Separation Processes, Inc.*
Jörg Drewes, Ph.D., *Colorado School of Mines*
Jan Schippers, Ph.D., *UNESCO-IHE Netherlands*

Participating Agencies

Air Products
APTwater
Clark County Water Reclamation District
City of Henderson
City of Las Vegas Water Pollution Control Facility
Colorado School of Mines
GE Water & Process Technologies
Hydranautics/Nitto Denko
Long Beach Water Department
Separation Processes, Inc.
Southern Nevada Water Authority
TrojanUV
UNESCO-IHE Netherlands
West Basin Municipal Water District

Project Advisory Committee

YuJung Chang, *HDR Engineering*
Saied Delagah, *Bureau of Reclamation*
Andrew Salveson, *Carollo Engineers*
Wyatt Won, *West Basin Municipal Water District*

Executive Summary

As worldwide human populations continue to rise and as clean water sources become more stressed from increased demand, alternative water sources must be made available to meet those demands. Freshwater drinking sources are a precious commodity and in many arid regions of the world can be scarce or completely unavailable. As continued population growth and expansion place heavy burdens on the available water supplies, utilities are examining innovative ways to stretch those supplies to ensure their ability to meet the demand for safe, clean, and sustainable drinking water. Among these options is water reclamation and reuse, either as potable or nonpotable water.

Membranes are a widely used technology for water reuse applications, especially reverse osmosis (RO) and nanofiltration (NF) membranes, largely because of their ability to reject dissolved organic matter (DOM), salts, chemical contaminants, and biological contaminants from the product (permeate) stream. RO membranes will reject up to 99.9% of DOM and salts, depending on the molecular weight cutoff of the membrane material. NF membranes can also provide reliable DOM removal rates of up to 98%, with some expected breakthrough of lower-molecular-weight fractions of DOM and salt. Even with some breakthrough of salts and lower-molecular-weight organics in NF membranes, both RO and NF membranes offer a robust barrier for contaminant removal in water reuse applications. However, membrane fouling due to DOM remains a significant concern, especially in water reuse applications where hydrophobic, aromatic, and protein-like biopolymers may dominate the total DOM in the water.

One of the major operational costs associated with RO and NF membrane systems is in the energy required to drive the water across the membrane. Membrane fouling can further exacerbate the energy demand by requiring higher feed pressures to meet production goals. Filtration performance will decrease over time as interstitial pore spaces become clogged and as particulate materials build up on the membrane surface. Fouling can result in the reduction of flux, water quality, and membrane operating efficiency, depending on the nature of the solute and of solute–membrane interactions. Fouling also impacts the frequency and duration of cleaning cycles, which is another source of increased energy and material costs. Some fouling has been partially mitigated by improvements in membrane design and engineering, though it is still the single largest obstacle to membrane operation.

Therefore, this multiyear study was designed to evaluate a novel approach of using oxidative technologies as a pretreatment for RO membrane feed water to address issues associated with organic fouling: instead of using oxidation as a final treatment step for system redundancy and removal of trace organic contaminants (TOrcs), the study was designed to investigate the use of ozone, ozone/peroxide, UV, and UV/peroxide, at bench and pilot scale, prior to membrane treatment in order to reduce the fouling associated with natural organic matter (NOM) while also achieving TOrc removal. If effective, the use of preoxidation could provide operations and maintenance (O&M) cost savings, including less pressure required to drive the membrane system over time and a greater life span for individual membranes within the system. Therefore, a cost analysis was also included in the study design.

The main hypothesis driving this study was that the application of oxidative processes upstream of RO membranes during treatment of water and wastewater for reuse applications could provide a benefit in minimizing fouling (specifically, *irreversible* fouling) associated with effluent organic matter (EfOM). The development of this hypothesis was driven in part by a conceptual reconfiguration of existing processes in California, where wastewater is pretreated by microfiltration (MF) or ultrafiltration (UF) membranes, followed by addition of antiscalant(s), acids for pH control, and chloramines for biofouling control, and then is treated by RO membranes and then by UV/peroxide for oxidation or photolysis of trace chemical contaminants, primarily 1,4-dioxane and *N*-nitrosodimethylamine (NDMA), in the product water. Thus, the treatment process of *microfiltration*→*reverse osmosis*→*UV/AOP* was rearranged to become *microfiltration*→*oxidation* (e.g., *ozone*, *ozone/peroxide*, and *UV/peroxide*)→*reverse osmosis* in order to ask three questions: (1) Can this reconfiguration still provide the advanced oxidation needed to remove TORCs? (2) Can this reconfiguration provide a benefit by controlling fouling associated with EfOM, thereby potentially minimizing membrane replacement costs and clean-in-place (CIP) events? and (3) Can this rearrangement provide a meaningful reduction in the amount of energy required to drive water across the RO membranes by minimizing EfOM fouling of the RO membranes?

Research Objectives

The specific research objective of this project was to investigate the potential for pilot-scale oxidative technologies placed upstream of membrane treatment to reduce the organic fouling of NF and/or RO membranes during drinking water treatment and reuse applications. Additionally, mechanisms associated with organic fouling with and without oxidative pretreatment were investigated along with relative energy costs associated with each technology.

On the basis of the literature review and working knowledge among the project team and TAC, the following hypotheses were to be tested:

1. Oxidation of water and wastewater by ozone, ozone/peroxide, and UV/peroxide will produce quantifiable changes in the polarity, reactivity, and optical properties of DOM (present as NOM in surface waters and as EfOM in wastewater effluents).
2. UV alone will have little appreciable impact on NOM and EfOM.
3. The changes in EfOM and NOM resulting from oxidation will change the rate and extent of organic fouling observed in RO membrane applications relative to waters that have not been oxidized.
4. Application of the oxidants upstream of RO membranes will not adversely impact the performance or integrity of the membranes.
5. By moving the oxidation step process typically reserved for RO permeate treatment (e.g., UV/peroxide) to the front of the RO membranes, a utility can achieve better membrane performance with less fouling, resulting in a net energy and operational cost benefit.
6. Oxidation processes applied upstream of RO membranes will produce a lower concentration of TORCs in the RO reject water (brine) than in a comparable system without oxidation and will lower the concentration of

TOrCs in the RO permeate to below detection or levels comparable with a typical RO membrane system followed by UV/peroxide treatment.

Study Overview

In order to address the hypotheses listed earlier and to assess the ability of oxidative pretreatment to reduce fouling in membrane systems adequately, several key components were required, including (1) access to multiple source waters, (2) access to pilot-scale and bench-scale membrane systems, (3) access to pilot-scale oxidation/advanced oxidation units, (4) the ability to characterize organic matter before, during, and after treatment, (5) microanalytical techniques to analyze surface composition and characteristics of fouled membranes, and (6) access to expertise from individuals in the membrane industry to guide the choice and operating parameters of membranes appropriate to the source waters. To address these issues, the approach for this study included experiments at three distinct locations using four different water qualities (Colorado River water [CRW], tertiary wastewater effluent, UF filtrate, and MBR filtrate), bench-scale membrane testing of each water and oxidation technology, and extended pilot-scale fouling studies at two wastewater locations. The project team also relied upon the microanalysis expertise provided by researchers at the National Institute of Standards and Technology, Colorado School of Mines, and the Hydraulics Analytical Laboratories. Although the specific equipment, materials, analytical techniques, and results will be described in the appropriate locations in this chapter and throughout the report, an overview of the results is presented here.

Major Study Findings

The results from this study provided compelling information regarding the benefits of ozone applied upstream of RO membranes for decreasing the aromatic, hydrophobic nature of EfOM and for providing a benefit toward minimizing organic fouling of membranes and for oxidation of TOrCs, which minimizes their presence in the RO permeate and in the brine stream with the exception of NDMA. The evidence regarding benefits in controlling membrane fouling was clearly observed in both the flat sheet and pilot-scale tests, though the difference in long-term operation, cleaning frequency, and biofouling potential could not be extrapolated from the pilot results. From a cost basis, there appear to be cases where ozone applied upstream of membranes could provide an operational and cost-savings benefit, though certainly that would need to be evaluated over a longer period for a given test water. The study results also indicated that the use of the MBR-RO and MBR-O₃-RO combined treatment system could allow for operation of the RO membranes at a higher flux than what is typically recommended by membrane manufacturers.

UV/peroxide preoxidation was not a viable alternative because of considerable long-term O&M costs, mostly as energy, that would be required to deliver a level of advanced oxidation required to impact fouling. Although some limited benefit was observed during the pilot test by using a UV dose at 1000 mJ/cm² with 4-mg/L peroxide addition, the overall operation of the system did not show a significant or sustained benefit from using UV/peroxide. A higher UV dose may be able to provide a greater benefit toward fouling control, but the capital and O&M costs for such a system do not appear to provide an attractive option for municipal water utilities.

In summary, the following points provide a brief overview of the hypotheses tested and their relevant results, including references to where the data can be found in this report.

1. *Oxidation of water and wastewater by ozone, ozone/peroxide, and UV/peroxide will produce quantifiable changes in the polarity, reactivity, and optical properties of DOM (present as NOM in surface waters and as EfOM in wastewater effluents).*

This hypothesis was strongly supported through the data collected throughout the project. Specific quantification of the impacts can be found in Chapter 3 of this report.

2. *UV alone will have little appreciable impact on NOM and EfOM.*

This hypothesis was also supported by the observations presented in Chapter 3 and based on EfOM in the UF and tertiary effluents from Water Reclamation Facility 2. Although there was an observable impact on the properties of EfOM, the required UV dose to provide an impact was well above typical UV advanced oxidation doses of about 400 mJ/cm².

3. *The changes in EfOM and NOM resulting from oxidation will change the rate and extent of organic (irreversible) fouling observed in RO membrane applications relative to waters that have not been oxidized.*

This hypothesis was consistently supported by the observations presented in chapters 4 (flat sheet membrane tests), 5 (MBR-O₃-RO pilot), and 6 (UF-O₃-RO pilot). Although promising in concept and even in practice for the experiments performed for this study, site-specific evaluation should be performed to determine whether the ozone preoxidation step would provide long-term cost savings and continued operational benefits for the full-scale facilities.

4. *Application of the oxidants upstream of RO membranes will not adversely impact the performance or integrity of the membranes.*

There were no observed adverse impacts to membrane integrity for any of the ozone preoxidation experiments. This finding largely stems from the fact that ozone was rapidly consumed in the MBR and/or UF filtrate and that therefore no residual ever made it to the membrane. Any future studies investigating the use of ozone as a preoxidant should consider the size of the ozone contactor to ensure that sufficient reaction time is allowed to avoid carryover of any dissolved ozone residual to the membrane surfaces.

The UV/peroxide preoxidation strategy appeared to have some adverse impact on the membrane surface that may have had to do with the presence of colloidal iron precipitate/scale on the membrane surface. Although the autopsy and wet tests did not indicate any leakage, the salt transport across the membrane was high enough to create some degree of doubt about the long-term viability of the UV/peroxide process when ferric chloride is used as a coagulant.

5. *By moving the oxidation step process typically reserved for RO permeate treatment (e.g., UV/peroxide) to the front of the RO membranes, a utility can achieve better membrane performance with less fouling, resulting in a net energy and operational cost benefit.*

From a capital expense perspective, systems treating more than 10 million gal of reuse water per day (mgd) can achieve comparable or even favorable costs by installing ozone in front of the RO membranes instead of UV/peroxide as a post-membrane treatment step. In some cases, and at low doses, ozone as a preoxidation strategy may provide a net energy and cost savings. However, this plan should be thoroughly evaluated for each location with a unique water quality–membrane pairing, and over a longer duration to determine impacts on membrane life and cleaning frequency. Further, if NDMA is a deciding factor on whether to place UV as a post-RO treatment step, then ozone may not be a viable strategy. This interplay of NDMA formation, RO performance, energy, and costs needs to be further evaluated before a solid recommendation can be made regarding the applicability of the process.

6. *Oxidation processes applied upstream of RO membranes will produce a lower concentration of TOrCs in the RO reject water (brine) than in a comparable system without oxidation and will lower the concentration of TOrCs in the RO permeate to below detection or levels comparable with a typical RO membrane system followed by UV/peroxide treatment.*

This hypothesis was strongly supported through the bench-scale and pilot-scale experiments with the TOrC data presented in Chapter 7. A preoxidation strategy with ozone lowered the concentration of all contaminants in both the reject and the permeate, with the exception of NDMA, which is only partially rejected by the RO membranes.

Recommendations

A highly effective pretreatment achieved by the biological processes and excellent filtration inherent in the MBR provided a low-fouling water that could be operated at a higher flux rate than typically recommended, especially when ozone is incorporated as a preoxidation strategy. In cases where membranes (other than the ESPA-2 membranes incorporated in this study) are used or where organic fouling is observed to be a problem with the particular water–membrane pairing, then ozone should definitely be evaluated as a possible pretreatment option. This idea may be particularly useful for facilities that either have only primary or nonnitrified secondary effluent (though the oxidation impacts on the character of the EfOM in nonnitrified waters need to be evaluated) or that receive their feed water from a separate wastewater treatment facility. It is recommended that future work focus on evaluating oxidative pretreatment on waters with minimal biological treatment, such as partial nitrification or biological oxygen demand removal only. Additional work should focus on determining strategies necessary for minimizing the formation of NDMA by ozone during preoxidation and/or chloramines used as a biocide in the RO membranes.

From a capital expense perspective, systems treating more than 10 mgd of reuse water can achieve comparable or even favorable costs by installing ozone in front of the RO

membranes instead of UV/peroxide as a post-membrane treatment step. In some cases, and at low doses, ozone as a preoxidation strategy may provide a net energy and cost savings. However, this plan should be evaluated for each location with a unique water quality and membrane pairing and over a longer duration to determine impacts on membrane life and cleaning frequency. Further, if NDMA is a deciding factor on whether to place UV as a post-RO treatment step, then ozone may not be a viable strategy. This interplay of NDMA formation, RO performance, energy, and costs needs to be further evaluated before a solid recommendation can be made regarding the applicability of the process.

Chapter 1

Introduction, Background, and Study Design

1.1 Introduction to Membranes and Water Reuse

As worldwide human populations continue to rise and as clean water sources become more stressed from increased demand, alternative water sources must be made available to meet those demands. Freshwater drinking sources are a precious commodity and, in many arid regions, can be scarce or completely unavailable. In areas where freshwater sources are available, the biological and/or chemical pollutant load may make the waters unsuitable for conventional drinking water treatment, adding to the scramble for potable water sources. Industrial, agricultural, and home uses all compete for the available water supplies.

According to the U.S. Department of Agriculture, 80% of water consumption in the United States is related to agricultural use (i.e., irrigation), but that number may be as high as 90% in several western states where droughts are common and water supplies are scarce (USDA, 2012). Such demands further stretch the resources available to a given population. As continued population growth and expansion in these arid and semi-arid areas place heavy burdens on the available water supplies, utilities are examining innovative ways to stretch water supplies to ensure their ability to meet the demand for safe, clean, and sustainable drinking water.

Not all end uses of potable water (e.g., industrial and agricultural) require the level of treatment necessary for human consumption. As such, many utilities in the United States and around the world have also been turning to the reuse of municipal wastewater, either directly or indirectly, to help meet this specific demand. In fact, recycled water is currently an indispensable fraction of numerous Western communities' water resource portfolio. Water reuse projects range from turf irrigation to recharge of groundwater supplies for drinking water (i.e., indirect potable reuse [IPR]). In the United States, potable reuse is becoming more widely accepted, though it has yet to achieve universal recognition as a potential part of the water supply portfolio. Although water reuse is a viable tool for utilities, it has yet to reach its full potential, in part because of public perceptions about the use of "sewage" for drinking water and a range of other misconceptions. Much of this opposition stems from the discovery of various pharmaceutically active compounds (PhACs), endocrine disrupting compounds (EDCs), and other trace contaminants in treated wastewater (S. A. Snyder et al., 1999; Ahel et al., 2000; S. A. Snyder et al., 2001; Aerni et al., 2004; Voutsas et al., 2006; Al-Rifai et al., 2007) and the potential impact that such compounds have on wildlife species (Brion et al., 2004; Gibson et al., 2005; Labadie and Budzinski, 2006; Brian et al., 2007). Furthermore, certain compounds such as caffeine, N,N-Diethyl-meta-toluamide (DEET), iopromide, and sulfamethoxazole have been shown to be highly pervasive in water systems and resistant to multiple treatment barriers (S. A. Snyder et al., 2007), though the health risk to humans from direct or indirect exposure to PhACs in water is quite low (S. Snyder et al., 2008; S. A. Snyder et al., 2010; Stanford et al., 2010; WHO, 2011). However, acceptance of IPR and of direct potable reuse remains dependent upon demonstrated removal of contaminants of concern during treatment and the use of multiple barriers to protect the public.

Conventional drinking water treatment processes typically involve treatment options such as coagulation, filtration (e.g., sand, activated carbon, and anthracite), and disinfection and are only moderately able to remove trace contaminants (S. A. Snyder et al., 2007; Benotti et al.,

2009b). More-advanced treatment options, including ozone, UV disinfection, advanced oxidation processes (AOPs) (e.g., UV/peroxide and ozone/peroxide), and membranes have been shown to be better suited for removal of PhACs and EDCs (Drewes et al., 2005; Drewes et al., 2007; Rosario-Ortiz et al., 2010; Pisarenko et al., 2012). Porous membranes such as microfiltration (MF) and ultrafiltration (UF) membranes are effective at mechanical separation of microbes and colloids by size exclusion, though they show only moderate removal of trace organic contaminants (TOCs) (S. A. Snyder et al., 2006; Yoon et al., 2006). Higher-rejection membrane systems, including nanofiltration (NF) and reverse osmosis (RO), offer the highest potential for removal of trace contaminants via a physical barrier capable of removing large and small molecules, depending on the properties of the membranes.

Membrane systems have been shown to be highly effective at removing trace contaminants, though even RO membranes are vulnerable to breakthrough of a few PhACs, EDCs, and other compounds such as *N*-nitrosodimethylamine (NDMA), bromide, and boron (W. Lee et al., 2007; S. A. Snyder et al., 2007; Steinle-Darling et al., 2007; Andrzejewski et al., 2008). However, state-regulated multibarrier approaches such as RO followed by UV/peroxide have allowed IPR projects to expand in areas such as California, where West Basin and Orange

County utilities have groundwater recharge/IPR systems in place. Membrane treatment plants are rapidly becoming an important source for potable or reuse water in areas of high population and/or with limited freshwater resources. In the last 10 years, the amount of potable water produced from RO membrane plants has increased dramatically, mostly as desalinated seawater in coastal populated areas (e.g., the United Arab Emirates, where as much as 98% of the water is from desalination plants, though not all of which are membrane-driven processes [Mohamed et al., 2005]). Additionally, the use of RO systems to treat wastewater is becoming viable in reuse applications as it can typically remove 90–95% of total dissolved solids (TDS). Furthermore, MF, UF, and membrane bioreactor (MBR) systems are being incorporated into wastewater treatment plants in order to improve the quality of water discharged from the plant (Radjenović et al., 2009). Such systems can be hybridized with RO membranes for an integrated reuse system (Tam et al., 2007). The main factors driving the increase in the production of potable or reuse water from membrane treatment plants have been demand and a decrease in operating cost. Once thought to be prohibitively expensive, the cost to produce potable or reuse water from membranes has declined to where the technology is now affordable in many settings and is often much more affordable than the alternative water production measures (e.g., desalination and long-distance pipelines).

One of the major operational costs associated with RO and NF membrane systems is in the energy required to drive the water across the membrane. Additionally, membrane fouling can further exacerbate that energy demand by requiring higher feed pressures to meet production goals. Membrane filtration performance tends to decrease over time as interstitial spaces become clogged and as particulate materials build up on the surface. Such fouling may be reversible or irreversible and may also be controlled through various strategies. Fouling in treatment applications is directly related to a corresponding rise in energy consumption due to the increased resistance and power required to drive water through the membrane (Yamamura et al., 2007b). Fouling also impacts the frequency and duration of cleaning cycles, another source of increased energy and material costs. Cleaning in place (CIP) is typically applied when normalized pressure is increased by 15% and acts to return operating pressures to lower levels by removing reversible foulants. Some fouling has been partially mitigated by improvements in membrane design and engineering, though it is still the single largest obstacle to membrane operation.

Thus, the objectives of this research study were to investigate the use of oxidation processes and AOPs for the mitigation of irreversible fouling and to compare the operational costs associated with the additional preoxidation treatment technology. For the sake of simplicity, most of the following review will focus on RO membrane operation and fouling unless specifically noted in the text. Each of the sections outlines the current state of knowledge with respect to fouling and fouling control, natural organic matter (NOM), effluent organic matter (EfOM), and the impact of oxidation on the dissolved organic matter (DOM, as a sum of NOM + EfOM).

1.2 Fouling and Options for Fouling Control in NF and RO Membranes

Membrane fouling is a critical parameter to be considered in RO membrane process design (Mulder et al., 2005). Both physically reversible fouling and physically irreversible fouling are factors impacting performance and must be taken into account in designing a membrane treatment system. Physically reversible fouling includes the buildup of particulate matter, scaling, and biological films on the membrane surface. Physically irreversible fouling involves the binding of compounds to the surface and interstitial spaces of the membrane and produces effects that cannot fully be reversed even after cleaning of the membranes. Membrane fouling is typically classified on the basis of fouling material and can be separated into several distinct categories (Vrouwenvelder et al., 2007; Al-Amoudi, 2010):

- Crystalline fouling resulting from the deposition of hardness scales or the precipitation of inorganic compounds of low solubility
- Scaling that is due to manganese(II) and iron(II) oxidation
- Particulate fouling resulting from the deposition of colloidal or particulate matter (inorganic or organic) on the membrane surface
- Organic fouling caused by DOM and humic substances
- Biofouling that is due to formation of biofilms on surfaces

The discussion of fouling here will be limited primarily to NF and RO applications except where otherwise noted.

1.2.1 Types of Fouling in NF and RO Membrane Applications

Crystalline Fouling. Inorganic compounds can cause membrane fouling when their concentrations in the region near the membrane surface exceed their respective solubility limits. This process results in deposition of scales of compounds such as BaSO_4 , CaSO_4 , and CaCO_3 (Al-Amoudi, 2010). Inorganic scale formation is typically more noticeable in the tail elements where the dissolved salts are concentrated in the brine stream prior to discharge.

Colloidal Fouling (Ning and Troyer, 2007; Tang et al., 2011): Colloids are fine particles in the size range of 1–1000 nm. This size range enhances their likelihood as membrane foulants. Unlike smaller particles, they cannot easily diffuse away from the membrane surface, and unlike larger particles, they cannot easily be removed by shear-induced diffusion at the membrane surface. Colloidal foulants can be either inorganic or organic in nature. Inorganic colloidal foulants tend to be rigid crystalline structures such as the commonly observed aluminum silicate minerals, iron (oxy)hydroxides, and elemental sulfur and, less frequently, aluminum oxides, manganese oxides, and metal sulfides. Some of these colloidal foulants can

form as a result of pretreatment steps, such as the formation of amorphous ferric or aluminum hydroxides that can occur when iron- or aluminum-based coagulants are applied during pretreatment upstream of the membrane. In addition, calcium phosphate colloids can act as foulants during membrane treatment of wastewater effluents. Organic colloidal foulants are flexible macromolecules, including polysaccharides, proteins, and other DOM (including fulvic and humic acids). The extent of colloidal fouling is affected by properties of the feed water, like the size, shape, conformation, and concentration of colloidal particles, as well as by solution pH, ionic strength, and presence of other interacting ions. Colloidal fouling is most prevalent under conditions in which the colloid is destabilized, e.g., high ionic strength, high colloid concentrations, and low pH. Membrane surface properties and operational conditions also influence colloidal fouling. Membranes that have rough surfaces, high surface charge, and hydrophobic characters are more prone to colloidal fouling. Colloidal fouling is also most likely to occur under operating conditions of high membrane flux.

Organic Fouling. DOM and related humic substances are ubiquitous in the environment and are important organic foulants. NOM and EfOM have been shown to be the predominant cause of physically irreversible fouling (Kimura et al., 2004; Yamamura et al., 2007a; Yamamura et al., 2007b). Most organic foulants are hydrophobic and carry a surface charge that can interact with the surface of the membrane in a manner that can either facilitate or deter accumulation (Zeman and Zydney, 1996; Mulder, 1997; Cheryan, 1998). Several studies have identified different subsets of DOM responsible for fouling, including hydrophobic fractions of NOM, hydrophilic fractions of NOM, and metal–NOM complexes (Shon et al., 2006; Gray et al., 2007; Her et al., 2007; Huang et al., 2007). Furthermore, both the size and the source of NOM can impact fouling (Kwon et al., 2005; Huang et al., 2007; Zhao et al., 2010a; Zhao et al., 2010b). Generally fouling by NOM is promoted by conditions of low pH, high divalent cation concentration (Ca and Mg), high ionic strength, and high foulant concentration (Al-Amoudi, 2010; Tang et al., 2011). EfOM tends to have properties different from those of surface water NOM; thus, it can lead to fouling behavior from organic matter in water reclamation applications different from that in drinking water applications. RO membrane fouling and decline in membrane performance over time as a result of fouling by EfOM have been observed during treatment of municipal wastewater effluents (Xu et al., 2010). Polysaccharides and proteins are the main components of EfOM, which can result in a much more hydrophilic character than observed in surface water NOM (Zhao et al., 2010a; Tang et al., 2011). Membrane fouling during reclamation of effluent has been found to be more severe in effluents that has gone through nitrification–denitrification than in nonnitrified effluent (Xu et al., 2010).

Biofouling. Biofouling results from the adhesion and growth of biofilms on the surfaces of membranes. Biofilms are assemblages of surface-associated microbial cells and extracellular polymeric substances (EPS) that are not removed by gentle membrane cleansing. These biofilms grow by using nutrients that are available in the feed water or in particles that have adhered to the membrane. Microorganisms present in all waters are capable of forming biofilms on almost any surface, and RO membranes have been shown to be able to be colonized by a large variety of bacteria, including *Pseudomonas*, *Corynebacterium*, *Bacillus*, *Arthrobacter*, *Mycobacterium*, *Acinetobacter*, *Cytophaga*, *Flavobacterium*, *Moraxella*, *Micrococcus*, *Serratia*, and *Lactobacillus* (Matin et al., 2011). Recent studies have suggested that *Sphingomonas* species play an important role in the structure and stability of membrane biofilms (Bereschenko et al., 2011).

1.2.2 Implications of Fouling in NF and RO Membranes

Fouling during membrane treatment can be a combination of several of these types of foulants. In membrane treatment of wastewater effluents for reclamation, organic fouling due to adsorption of hydrophobic EfOM, biofouling, inorganic scaling, and colloidal fouling have all been identified existing on membrane surfaces at the same time (Xu et al., 2010). Fouling can result in the reduction of flux, degradation of finished water quality, and lower membrane operating efficiency, which has significant consequences for the operation of membrane treatment facilities. The presence of a fouling layer increases the hydraulic resistance of the membrane and results in an increase in operating pressure to maintain a constant flux across the membrane. In addition, biofouling or particulate fouling can occur on feed spacers in spiral-wound membrane systems, leading to physical clogging of those spaces. Fouling can also exacerbate concentration polarization. As solutes are retained by the membrane, they accumulate in a layer near the membrane surface. In the presence of a foulant layer, the ability of these solutes to diffuse away from the membrane surface is hindered, leading to a higher concentration of these solutes near the membrane than in the bulk solution. This situation in turn increases the osmotic pressure at the membrane, resulting in increased operating pressure and a decrease in salt rejection causing a decline in water quality (Tang et al., 2011). The end result of these effects is increased costs due to increased energy demands, frequent chemical cleaning, and more frequent membrane replacement. The effects of fouling can be quantified by monitoring several parameters describing membrane performance. Fouling causes changes to measurable parameters such as pressure, flux, pressure drop across the feed/brine channel, and salt passage. However, regular fluctuations in operating conditions such as temperature, feed water TDS, recovery, and permeate flow can also cause changes in these same parameters. In order to assess the effects on these parameters due to fouling alone, it is necessary instead to calculate normalized pressure, normalized flux, normalized pressure drop across the feed/brine channel, and normalized salt passage, which can be used to compare system performance under different operating conditions.

There are several methods available to predict the fouling potential of a feed water. The silt density index (SDI) and modified fouling index (MFI) are techniques that are commonly used to determine colloidal fouling. However, these indices offer little information about the mechanisms of fouling (Tang et al., 2011). In addition, SDI and MFI poorly characterize the fouling potential of MF/UF-treated secondary effluent as RO feed waters as they cannot measure colloidal and soluble fouling components found in these waters (Park et al., 2006). However, more-recent work on an MFI-UF concept using membranes with pore sizes down to 10 kDa has been developed and shows promise for predicting colloidal fouling (Salinas-Rodriguez et al., 2009). Other potential fouling predictors are available, including methods for biofilm formation rate, membrane fouling simulation (calculation), and determination of organic carbon molecular weight by liquid chromatography with organic carbon detection, among others.

1.2.3 Control of Reversible Fouling in NF and RO Membranes

Membrane fouling is currently controlled in large part through the implementation of a variety of pretreatment systems designed to eliminate foulants before they can reach the membrane units (cartridge filtration and/or membrane filtration is most commonly used because of its ability to minimize the introduction of colloidal and particulate foulants to the membrane surface). Pretreatment units in use include the following:

- cartridge filtration (1–25 µm) MF/UF
- single and dual media filtration
- coagulation with sedimentation and filtration
- activated carbon filtration
- artificial recharge
- riverbank filtration
- beach/shore well filtration
- in-line coagulation to remove turbidity and microparticles during pretreatment to reduce fouling
- antiscalants and acids that can be applied to control scaling

Although scaling, biofilms, and particulate aggregation/matting can be controlled to some extent by prefiltration, the engineered cleaning processes and biological control processes may leave residual chemicals (e.g., antiscalants, disinfectants, etc.) that can impact permeate water quality. Further, some bacterial cells have been shown to survive passage through MF membrane pretreatment, enabling fouling of downstream RO membranes (Goosen et al., 2005) and forcing the use of consistent biological growth control measures.

Specifically, biofouling is typically controlled through pretreatment of feed water as well as through application of chemical agents such as monochloramine, peracetic acid, and 2,2-dibromo-3-nitripropionamide (DBNPA). Microbes may survive pretreatment processes such as coagulation, flocculation, filtration, and MF/UF and over time will colonize membrane surfaces or other surfaces within the membrane treatment system if a biocide is not applied. RO membranes have been shown to begin forming biofilms within 4 days and can form a mature biofilm layer on the entire membrane surface within 12 days (Bereschenko et al., 2011). In a biofilm, microbes are encased in an organic polymer matrix that provides some protection from chemical cleaning, meaning that chemical treatment of biofouled membranes is frequently ineffective for completely removing the biofilm (Flemming, 2002).

This failure to remove the remnants of established biofilms from surfaces during chemical treatment is the main reason that these treatments are unsuccessful at preventing further biofouling from occurring during RO membrane operation (Bereschenko et al., 2011). Microbial attachment and colonization of the remnants of the chemically treated biofilms occur immediately after the chemical addition ceases, and the regrowth of biofilms on membrane surfaces and feed-side space surfaces occurs rapidly (Bereschenko et al., 2011). Because the presence of incompletely removed biofilms provides ample attractive attachment surfaces, abundant nutrients from damaged cells, and an EPS matrix, the growth of biofilms can occur more rapidly on treated surfaces (within a week) than on fresh RO membranes, where comparable biofilms take 16 to 17 days to develop (Bereschenko et al., 2011). Other techniques for biofouling control have included membrane surface modifications (Goosen et al., 2005), using low linear flow velocity in lead elements, adapted feed spacer designs, and advanced cleaning strategies (Vrouwenvelder et al., 2011).

1.2.4 Control of Irreversible Fouling from NOM

During the past decade there have been extensive investigations of the reduction of fouling resulting from DOM, both in terms of pretreatment strategies including oxidation, coagulation, adsorption, and ion exchange (Holbrook et al., 2004; Haberkamp et al., 2007; Humbert et al., 2007) and in terms of improvements in interactions at the membrane surface, including better membrane materials, the use electrostatic exclusion, and optimization of hydrodynamic parameters based on flow regimen (Brant and Childress, 2002; Seidel and Elimelech, 2002; Bellona and Drewes, 2005; Huang et al., 2007; Vrouwenvelder et al., 2009).

Although the surface-based improvements are important in designing a membrane reuse system, the focus of the discussion in this report will be limited to investigations of pretreatment options.

Several studies have demonstrated that applying a coagulation process before UF membranes was very effective in fouling reduction (Holbrook et al., 2004; Jung et al., 2006; Haberkamp et al., 2007). The results have been attributed primarily to the precipitation of DOM and decrease in the molecular weight distribution of the DOM. Ferric iron has been shown to be an effective coagulant in reducing the amount of NOM and to alter the size distribution toward lower-molecular-weight compounds (Haberkamp et al., 2007). Ferrate, on the other hand, has been shown to provide both oxidation of trace contaminants such as EDCs (Y. Lee et al., 2008; Li et al., 2008) and removal of DOM through oxidation and coagulation (Lim and Kim, 2009). Ozone pretreatment and UV/TiO₂ photocatalysis at the bench scale have been shown to decrease the size and hydrophobicity of NOM and have shown promise for reduction of membrane fouling (Schechter and Singer, 1995; Nishijima et al., 2003; Wang et al., 2007; Gong et al., 2008; Huang et al., 2008), though this is not uniformly the case at bench- and full-scale operations (Her et al., 2007; Lee and Lee, 2007). Some studies have indicated that, as EfOM is broken down from larger, more hydrophobic molecules to smaller, more hydrophilic molecules, one might expect increased sorption due to the facilitated hydrogen bonding from the hydrophilic molecules (Gray et al., 2007; Her et al., 2007; Yamamura et al., 2008). However, preozonation has been shown elsewhere to reduce the fouling associated with organic matter in MBRs (Williams and Pirbazari, 2007), and its application as a control option for NOM/EfOM fouling in multiple membrane systems and configurations has been extensively reviewed elsewhere (Van Geluwe et al., 2011).

The difference between EfOM and surface water NOM may mean that pretreatment processes developed for drinking water RO systems may not be directly applicable to RO systems used for treating wastewater effluents (Zhao et al., 2010a). Additionally, membrane fouling is directly related to the flux and recovery used during water treatment (Zhao et al., 2010a). Thus, there is a need to develop monitoring and control strategies to manage irreversible fouling in water reuse applications and, possibly, to provide means of increasing membrane flux and recovery without negatively impacting membrane life, fouling, and cleaning frequency.

1.2.5 Hybridized Biological Treatment, Oxidation, and Membrane Separation Systems

Combinations of treatment technologies (e.g., biological removal in MBRs with oxidation upstream and RO downstream and ozone/ceramic membranes) have recently gained popularity for their ability to enhance removal of trace organic and inorganic contaminants, remove biodegradable dissolved organic carbon (BDOC), and reduce fouling in downstream RO and NF applications. For example, stand-alone MBR systems have been shown to be highly suitable for BDOC and trace contaminant removal (Cirja et al., 2007; Hu et al., 2007; Spring et al., 2007; Williams and Pirbazari, 2007; J. Lee et al., 2008; Radjenović et al., 2009), whereas combined MBR-RO hybridized systems are able to offer additional pretreatment for fouling control of RO systems (Tam et al., 2007; Dialynas and Diamadopoulos, 2009). Leiknes et al. proposed the oxidation-biofiltration-membrane (OBM) treatment concept for drinking water treatment by providing the additional benefit of oxidation in the process (Leiknes et al., 2005). The OBM process was shown to be effective at removal of NOM as well as of other micropollutants. The OBM process was able to remove total organic carbon (TOC) up to 95%, meaning 60% TOC removal by ozonation and 35% TOC removal by

biodegradation. A similar Korean study indicated that TOC and DOC removal of up to 50% and 30% respectively could be achieved under the optimized dose of O_3 and H_2O_2 upstream of a UF system (Jo, 2007). In seawater desalination, an ozone-MF-RO system was tested and researchers found that preozonation of the seawater was able to improve performance and reduce fouling of the hydrophobic MF membranes (Oh et al., 2009). However, when this system was tested with a hydrophilic MF membrane, additional fouling was observed, likely from the shift of larger, hydrophobic NOM to smaller, hydrophilic NOM caused by reaction with the ozone.

A recent review provides a good overview of some of the previously published studies investigating the impact of ozone on DOM and the implications for fouling control (Van Geluwe et al., 2011), though in general there are few cases of oxidation of MF, UF, or MBR permeates and even fewer cases where this has been tried in combination with RO membranes. In one study where UF- O_3 and O_3 -UF were examined for the treatment of cork-processing wastewater, the authors found that the UF- O_3 strategy had better efficiency in removal of organic matter (Benitez et al., 2008) because UF removed particulates and reduced the total ozone demand of the product water, thereby increasing the likelihood of a reaction between ozone and DOM. In another study, UV/peroxide was used in conjunction with RO membranes for the treatment of textile industry wastewater. In this case, UV + peroxide was shown to improve flux, reduce the SDI, and shift the molecular weight distribution of the DOM toward lower-molecular-weight compounds (Kang et al., 2003). Furthermore, both ozone and UV or UV/AOP applications prior to RO membranes may have desirable effects on biofouling control (Kim et al., 2009), though this prospect needs to be carefully balanced with the potential pitfalls mentioned in the following sections.

1.2.6 Potential Drawbacks to Preoxidation Strategies in Hybrid Treatment Systems

Although preoxidation has its merits in terms of membrane performance, operation, and life, oxidative processes such as ozone and UV/peroxide use may in fact produce a more biologically available form of organic matter, thereby providing a potential food source for microbes that survive the oxidation process and then attach to the membrane surface. On the one hand, BDOC and assimilable organic carbon (AOC) have both been shown to increase after various oxidative processes, including ozone, UV/peroxide, and other AOPs (Schechter and Singer, 1995; Yavich et al., 2004; Yasar et al., 2007; Metz et al., 2011). The presence of AOC and BDOC has been correlated to microbial regrowth in distribution systems (Escobar and Randall, 2001; Escobar et al., 2001) and could negatively impact membrane performance as microbial populations thrive on the BDOC and grow in numbers. On the other hand, it is not clear whether this will actually occur during normal operation. In the case of ozone, not all waters will produce a more biodegradable fraction of NOM after treatment (Yavich et al., 2004). Also, when AOPs are used instead of UV or ozone alone, albeit at high doses, regrowth may be completely stopped by the process (Yasar et al., 2007). As such, top experts in the field are sharply divided on whether preoxidation will hinder or help membrane performance.

A secondary issue re potential biofouling is the increased energy costs related to oxidation of the UF or MBR effluent: the higher DOC and concentrations of other dissolved constituents present in the RO feed water (as opposed to the RO effluent) may increase the ozone demand and decrease the UV transmission of that water. Post-RO oxidation is commonly used as a final safety measure and already adds an extra energy demand on the system beyond the membrane process itself. In the case of the Pascagoula, MS, drinking water treatment plant, RO membranes are used prior to ozonation and final chlorine disinfection. In the case of the Orange County, CA, wastewater reclamation project, RO treatment is followed by UV/peroxide, primarily for NDMA removal and final disinfection. Although these are effective means of providing safe and pleasant-tasting drinking water to the customers, it is unclear whether they are the most energy- and cost-efficient means of providing that water. A simple change in the order of treatment could provide the utilities with a net decrease in energy consumption due to reduced membrane fouling. However, such a change in operation order must be carefully balanced: any increase in energy required to obtain the desired oxidation effect should not outweigh the benefit of energy reduction and RO operation gained from the preoxidation strategy.

1.3 Summary and Study Overview

On the basis of information available at the time of proposal writing and the updates presented here, this study was designed to investigate a novel approach to using oxidative technologies in membrane-based drinking water and water reuse applications: instead of using oxidation as a final treatment step, this study investigated its use prior to membrane treatment in order to reduce the fouling associated with NOM. If effective, the use of preoxidation could provide a cost savings, including less pressure required to drive the membrane system over time and a greater life span for individual membranes within the system. Furthermore, although membrane systems have been shown to be highly effective at removing trace contaminants, even RO membranes are vulnerable to breakthrough of a few pharmaceuticals, EDCs, and other compounds such as NDMA, bromide, and boron (W. Lee et al., 2007; S. A. Snyder et al., 2007; Steinle-Darling et al., 2007; Andrzejewski et al., 2008). Thus, preoxidation should be able to convert bromide present in the source water to bromate (Orlandini et al., 1997; Wert et al., 2007), which is well rejected by membrane systems, thereby reducing the amount of undesirable bromine-containing compounds in the finished water (e.g., bromate or brominated disinfection by-products) (Gyparakis and Diamadopoulos, 2007) while also reducing the amount of other micropollutants common in reuse systems. A full description of the study objectives and design is provided in Chapter 2.

Chapter 2

Experimental Design and Analytical Methods

2.1 Project Approach and Experimental Design

This multiyear study was designed to evaluate the novel approach of using oxidative technologies as a pretreatment for RO membrane feed water to address issues associated with organic fouling: instead of using oxidation as a final treatment step for system redundancy and removal of TOrCs, the study was designed to investigate the use of ozone, ozone/peroxide, UV, and UV/peroxide at bench and pilot scale prior to membrane treatment in order to reduce the fouling associated with NOM while also achieving TOrC removal. If effective, the use of preoxidation could provide O&M cost savings including less pressure required to drive the membrane system over time and a greater life span for individual membranes within the system. Therefore, a cost analysis was also included in the study design.

2.1.1 Research Objectives

The specific research objective of this project was to investigate the potential for pilot-scale oxidative technologies placed upstream of membrane treatment to reduce the organic fouling of NF and/or RO membranes during drinking water treatment and reuse applications. Additionally, mechanisms associated with organic fouling with and without oxidative pretreatment were investigated along with relative energy costs associated with each technology.

On the basis of the literature review and the working knowledge among the project team and TAC, the following hypotheses were to be tested:

1. Oxidation of water and wastewater by ozone, ozone/peroxide, and UV/peroxide will produce quantifiable changes in the polarity, reactivity, and optical properties of DOM (present as NOM in surface waters and as EfOM in wastewater effluents).
2. UV alone will have little appreciable impact on NOM and EfOM.
3. The changes in EfOM and NOM resulting from oxidation will change the rate and extent of organic (irreversible) fouling observed in RO membrane applications relative to waters that have not been oxidized.
4. Application of the oxidants upstream of RO membranes will not adversely impact the performance or integrity of the membranes.
5. By moving the oxidation step process typically reserved for RO permeate treatment (e.g., UV/peroxide) to the front of the RO membranes, a utility can achieve better membrane performance with less fouling, resulting in a net energy and operational cost benefit.
6. Oxidation processes applied upstream of RO membranes will produce a lower concentration of TOrCs in the RO reject water (brine) than in a comparable system without oxidation and will lower the concentration of TOrCs in the RO permeate to below detection or levels comparable with a typical RO membrane system followed by UV/peroxide treatment.

2.1.2 Project Overview

In order to address the hypotheses listed earlier and to assess the ability of oxidative pretreatment to reduce fouling in membrane systems adequately, several key components were required, including (1) access to multiple source waters, (2) access to pilot-scale and bench-scale membrane systems, (3) access to pilot-scale oxidation/advanced oxidation units, (4) the ability to characterize organic matter before, during, and after treatment, (5) microanalytical techniques to analyze surface composition and characteristics of fouled membranes, and (6) access to expertise from individuals in the membrane industry to guide the choice and operating parameters of membranes appropriate to the source waters. To address these issues, the approach for this study included experiments at three distinct locations using three different water qualities (Colorado River water [CRW], secondary wastewater effluent, and MBR effluent), bench-scale membrane testing of each water and oxidation technology, and extended pilot-scale fouling studies at two wastewater locations. Although the specific equipment and materials will be described in the appropriate locations in this chapter and throughout the report, a list of the major equipment is provided here:

- Two side-by-side Sepa CF membrane cell holders for bench-scale flat sheet membrane systems (GE Osmonics, Minnetonka, MN; purchased from Sterlitech, Kent, WA)
- A HiPOx[®] unit (Applied Process Technology, Pleasant Hill, CA)
 - o Provided ozone and ozone/peroxide capabilities, 10-gal-per-min (gpm) flow rate
 - o Located at Drinking Water Treatment Plant 1 (DWTP 1) for initial flat sheet membrane testing
 - o Relocated to Water Reclamation Facility 1 (WRF 1) for pilot-scale membrane fouling studies
- A Hydranautics MBR (HYDRASub[®]; Hydranautics, Nitto/Denko, Oceanside, CA)
 - o Hollow-fiber vacuum-type polyvinylidene fluoride (PVDF) membranes
 - o Nominal pore size of 0.40 μm
 - o Located at WRF 1
 - o Fed with primary wastewater effluent
- A single RO membrane skid with parallel treatment trains
 - o 5-gpm permeate flow rate per train
 - o 35–50% recovery design capacity
 - o Single stage, six elements per train
 - o Located at WRF 1
- A Trojan UV Reactor (Trojan Technologies, London, ON, Canada)
 - o Located at WRF 2 for bench-scale and pilot-scale fouling studies
 - o Capable of 150-gpm flow rates and equivalent UV dose of 400 mJ/cm^2 to 4000 mJ/cm^2
 - o Injection ports for peroxide addition
 - o Capable of operation in UV or UV/AOP mode (TrojanUVPhox[®])
- Pilot-scale ozone system (Ozonix, Elmwood Park, NJ) consisted of generator and contactor at WRF 2, provided courtesy of a secondary project colocated at the WRF
- Pilot-scale UF system ZeeWeed 500d polymeric UF system (GE Water & Process Technologies, Trevose, PA) at WRF 2, provided courtesy of a secondary project colocated at the WRF

- Twin GE E4H-21K-DLX-60 RO membrane skids
 - o 15-gpm permeate flow rate
 - o 75% recovery design capacity
 - o Single stage, six elements
 - o Both located at WRF 2
- Membranes for all pilot-scale evaluation experiments were ESPA-2-4040 or ESPA-2-4040LD elements as noted throughout text.

Characterization of DOM was conducted at the Southern Nevada Water Authority laboratories as described elsewhere in this chapter and report. Techniques included size exclusion chromatography, three-dimensional fluorescence excitation–emission matrix spectroscopy (3D fluorescence or fluorescence EEM), “polarity rapid assessment methods” (PRAMs), and BDOC methods. Surface analysis of membrane samples was performed at three locations: the National Institute of Standards and Technology (NIST) lab in Gaithersburg, MD; the Advanced Water Technology Center at the Colorado School of Mines; and the Hydranautics facilities in Oceanside, CA. These characterization techniques include several types of electron microscopy (scanning electron microscopy [SEM] and environmental SEM [ESEM]) and confocal scanning laser microscopy. In addition, wet tests were performed at Hydranautics to assess the permeability and salt rejection of the new and used membranes.

The Technical Advisory Committee (TAC) for this study included Jörg Drewes (Colorado School of Mines), Jan Schippers (UNESCO-IHE Netherlands), and Kevin Alexander and Silvana Ghiu (Separation Processes, Inc.). The TAC provided feedback and guidance throughout the project on the approach, experimental design, technical parameters for pilot equipment selection and operation, data analysis, and review of project findings.

2.1.3 Project Approach

With the project team, TAC, and resources in place, the project was executed by using a multitiered approach to evaluating each of the technologies with the goal of finally selecting one mode of operation for each oxidative process (i.e., UV or UV/AOP and ozone or ozone/AOP) for pilot-scale evaluation at the water reuse sites. The overall approach to the project involved working through the following steps:

1. Select equipment, membranes, operational configurations, and test matrices based on discussion with the project team, TAC, and Project Advisory Committee (PAC).
2. Apply oxidation technologies to CRW and wastewater effluent to verify quantifiable changes in DOM.
3. Test three membranes with ozone and ozone/peroxide at various doses on CRW at high flux to verify that observable changes in fouling can occur; also use data to select membranes for further testing. All membrane tests were performed in parallel with one control water (no oxidation) and one oxidized water.
4. Install pilot equipment at wastewater treatment plants in preparation for pilot-scale membrane tests.
5. To determine optimal oxidant dose and selection (e.g., ozone vs. ozone/peroxide and UV vs. UV/peroxide), collect test waters in 200-gal vessels from pilot locations to measure changes in DOM and conduct fouling tests using flat sheet membranes.

6. Select “optimized” dose (based on minimal energy and chemical input to achieve observable difference in fouling in flat sheet tests) for pilot-scale evaluation.
7. Conduct pilot-scale tests at two facilities with two different oxidant combinations to observe differences in fouling and cleaning rates.
8. Use pilot-scale data to project energy implications and costs of the various treatment scenarios throughout all tests and at various stages of the treatment trains.

The project was divided into the following tasks, designed to support the overall project approach:

Task 1: Literature review and pilot setup: This project incorporated an ongoing literature review, including examination of recent conference proceedings, to determine the current state of knowledge of membranes and organic fouling control strategies.

Task 2: Evaluation of energy costs and ability of oxidative systems to modify and reduce natural organic matter: Each pilot-scale technology, ozone/peroxide (HiPOx[®]) and ozone alone, then UV/peroxide (TrojanUVPhox[®]) and UV alone, was assessed by using the aforementioned DOM characterization methods to determine the relationship between dose (i.e., energy consumed per volume of water treated) and the amount and nature of changes in DOM in the source water. Although similar work has been reported elsewhere (Wang et al., 2007; Gong et al., 2008; Huang et al., 2008), this work was a critical monitoring component of the project and was directly used to relate membrane performance over time to the ability of the pretreatment to remove or change DOM relative to energy consumption. Furthermore, each technology was evaluated side by side with the same source water, which provided a unique opportunity not realized in previously published studies. In addition to analysis for changes in DOM, destruction and/or formation of contaminants of concern (e.g., NDMA, bromate, and surrogate and indicator pharmaceuticals) was monitored for each bench-scale and pilot-scale evaluation test.

Subtask 2.1: Source water characterization and treatment doses: An important consideration in this preoxidation study was the dose of oxidant (e.g., ozone, peroxide, UV fluence) relative to current practices in drinking water treatment and water reuse systems. Using extreme doses of ozone or UV may provide a benefit of reducing membrane fouling, but such benefit could be at a substantial energy cost not recovered by the new treatment scheme. Therefore, this subtask focused on determining the most relevant dose of treatment for a given source water based on demand and/or current treatment practices.

Subtask 2.2: NOM characterization techniques: DOM was characterized extensively through multiple, complimentary techniques designed to provide insight into the size fractions, polarity, functional groups present, and bioavailability of the carbon. All preoxidation tests were accompanied by size exclusion chromatography (SEC) with UV light, fluorescence, and TOC detection (SEC/UV/fluorescence/TOC), 3D fluorescence, PRAM (Rosario-Ortiz et al., 2007a), and whole-water TOC analyses. Given the potential for preoxidation to increase the amount of BDOC, thereby potentially increasing the propensity for growth of microbes in the membrane system leading to biofouling. Limited BDOC testing was performed during this phase of the project.

Subtask 2.3: NDMA-FP, bromide/bromate speciation, and other contaminants: One of the advantages of UV technology is the ability to remove NDMA and NDMA precursors from water (Kruithof et al., 2007). This advantage is especially important in reuse applications

where the eventual chlorination and/or chloramination of the finished water (or RO feed) may result in more NDMA formation (Pehlivanoglu-Mantas et al., 2006). Furthermore, ozone and ozone/peroxide have been implicated in forming NDMA precursors and may in fact exacerbate the problem (Andrzejewski et al., 2008; Zhao et al., 2008; von Gunten et al., 2010), especially given that NDMA is only about 40 to 60% rejected by RO membrane systems (Steinle-Darling et al., 2007). Because such molecules are not typically rejected by RO systems, the impact that preoxidation may have on NDMA and its formation potential (FP), especially in water reuse systems, was a critical component for monitoring. To support this view, NDMA destruction and NDMA-FP tests were performed on all waters tested before and after oxidation. Similarly, the conversion of bromide to bromate during ozonation was monitored during this study, even though bromate is entirely rejected by RO (Gyparakis and Diamadopoulos, 2007). The oxidation and removal of TOrCs were also monitored throughout the study at various locations within the treatment processes.

Task 3: Bench-scale evaluation of membrane fouling: In order to have more control of the source water, flow rates, recycle volumes, and other experimental conditions used for the evaluation of oxidation to reduce fouling, laboratory membrane experimentation was first performed at the bench scale. The initial testing from Task 2 provided the project team with a matrix of operational parameters and outcomes in terms of DOM speciation and microcontaminant concentration/removal, speciation, and FP. This matrix was used to determine the range of operational doses of oxidants for testing with the flat sheet membrane systems. From that matrix, the bench-scale flat sheet membrane tests were used to assess organic fouling at the bench scale and to further define the operational parameters for testing at pilot scale.

Although the preoxidation of water was conducted at pilot scale, both treated and nontreated (control) waters were collected in 200-gal tanks to be run side by side with bench-scale flat-sheet membrane cells (GE Osmonics). Initially, three types of membranes (ESPA-2 [Hydranautics] plus FL and NE-70 [Woongjin Chemical, Seoul, Korea]) were tested for each preoxidation test with CRW. Of the three membranes, the ESPA-2 was selected for further use at pilot scale because of its widespread use in water reuse applications.

Task 4: Pilot-scale evaluation: Each of the tasks leading up to Task 4 provided information regarding performance and evaluation of each technology with the intent of choosing two optimized preoxidation processes to use as the treatments of choice for the pilot membrane system. Here, an MBR-RO and MBR-O₃-RO pilot study was conducted at WRF 1, while a UF-RO and UF-O₃-RO pilot study was conducted at WRF 2. The pilot-scale evaluation was designed to allow the project team to investigate the membrane system performance with respect to energy input, fouling, and membrane life side by side using the same source water. Further, TOrCs and bromate along with other traditional water quality parameters were monitored for each system.

Task 5: Preparation of the final report: Significant findings of the study are summarized and outlined in the final report. General recommendations on using preoxidation to control organic fouling of RO membranes are provided.

2.2 Overview of Analytical Methods

Explanations and details of many of the analytical techniques and experimental methods are provided in context throughout this report. However, a few techniques are described here for

ease of reference and to avoid distraction in subsequent chapters where the results are the focus of the information presented.

2.2.1 Dissolved Organic Matter Characterization Techniques

Sample absorbance at 254 nm was measured by using Perkin-Elmer Lambda 45 UV-VIS Spectrometer, consistent with Standard Method 5910 B. Specific UV absorbance (SUVA) ($L \cdot m^{-1} \cdot mg^{-1}$) was calculated on the basis of Equation 1.1:

$$SUVA = TOC/UV_{254} \cdot 100 \quad (1.1)$$

2.2.1.1 Polarity Rapid Assessment Method

Assessment of relative changes in the polarity of DOM were performed by using a previously published method (Rosario-Ortiz et al., 2007a). Use of PRAM does not require modifications to the water matrix (e.g., pH and ionic strength changes), therefore providing a representation of DOM as it is found in the environment. PRAM allows monitoring the changes in the retention coefficients (RCs) of hydrophobic (C_{18}), hydrophilic (Diol), and anionic (NH_2) moieties of the DOM, thus theoretically allowing one to assess the impacts of various treatments on changes in relative polarity of various fractions of DOM.

2.2.1.2 Size Exclusion Chromatography/UV/Fluorescence/Total Organic Carbon

SEC was performed by using a previously published method (Rosario-Ortiz et al., 2007b). It was performed by using an Agilent 1100 LC system (Palo Alto, CA) with a Toyopearl HW-50 S 250×20 -mm column (Tosh Biosciences, Grove City, OH) and Agilent 1100 diode array detector (Palo Alto) set at 254 nm. A secondary fluorescence detector (Agilent) was used to monitor emission at 450 nm based on excitation at 370 nm. The mobile phase consisted of a phosphate buffer (0.028 M) adjusted to a pH of 6.8. The flow rate of 1.0 mL/min was used. Data were collected and analyzed by using Agilent ChemStation software (Version A.10.01). The sample injection volume was set at 1.8 mL to avoid preconcentrating the samples.

2.2.1.3 Total Organic Carbon Analysis

For DOC/TOC analysis, samples were collected in a glass vial and were acidified to a pH of <3 with hydrochloric acid and were filtered through a 0.20- μ m-pore-size hydrophilic polypropylene filter (GHP Acrodisk, Pall Life Sciences). A Shimadzu (Shimadzu Scientific Instruments, Carlsbad, CA) TOC/total nitrogen analyzer was used for quantification.

2.2.1.4 3D Fluorescence Excitation–Emission Matrix Spectroscopy

Fluorescence EEMs were developed by using a PTI fluorometer (Birmingham, NJ) for the data acquisition and were processed by MatLab (Natick, MA). A modified Fluorescence regional integration (FRI) method described elsewhere (Chen et al., 2003) and the Fluorescence Index (FI) (McKnight et al., 2001) were used to assess changes in DOM. The EEM spectra were corrected for the Raman scatter by subtracting the emission of the blank and were corrected for inner-filter effect, following a previously described method (MacDonald et al., 1997). The EEM spectra were also normalized by the integrated area of the water Raman peak at 397 nm to account for changes in excitation lamp intensity and/or slit width adjustments from day-to-day measurements. Briefly, samples were placed in four-sided quartz cuvettes (1 cm \times 1 cm) and were exposed to various wavelengths of light ranging from 240 nm to 470 nm, with discrete exposures occurring in 5-nm increments (“excitation” wavelength). Excitation and emission slit widths were typically set at 2 nm. An orthogonal detector then measured the resulting fluorescence (“emission” wavelengths, measured from 280 nm to 580 nm) that occurred for each discrete excitation wavelength.

Thus, each individual excitation wavelength produced a spectrum of emissions that were measured and compiled into a 3D EEM. Corrections for variability in intensity of excitation light were applied during acquisition by using a reference detector. Corrections for the emission intensity based on the detector's sensitivity and losses along the optical path were applied by using the manufacturer's correction factors.

The quantification of subtle differences in the EEMs involved the use of FRI (Chen et al. 2003). The concept of FRI is based on using specific regions of the EEM to identify (and quantify) specific components of organic matter that may be present in a given water sample. In the Chen et al. (2003) study, EEMs were divided into five regions. However, because of differences in instrumentation and observed differences in EEM outputs, we reduced the number of regions from five to three, operationally defined as described in Table 1.1 and Figure 2.1 consisting of a microbial by-product/biopolymer region, fulvic-like substances, and humic-like substances. To avoid any bias from excitation wavelength ($E[\lambda]$), a boundary for the integration regions at $[E(\lambda) - 15 \text{ nm}]$ was used. Similarly, to avoid any bias from the second order of the excitation wavelength, an upper boundary of $[2 \times E(\lambda) - 15 \text{ nm}]$ was used. For the sake of brevity, two major inferences can be made on the basis of work by Chen et al. (2003): first, hydrophobic compounds tend to have higher aromatic carbon content. Aromaticity is associated with a greater amount of region-specific fluorescence. Thus, changes in FRI (and the sum of the regional volumes, Φ_T) provided a basis for quantifying changes in aromaticity (and hydrophobicity) of the organic matter in the sample. Second, FRI can be used to determine the relative contribution of types of organic matter to the overall composition of the wastewater sample, as indicated by specific regions. Thus, as the relative distribution of organic material components changes between regions, one can assess the impact that a given treatment may be having on the quality of the organic matter. Such observations may be useful for relating membrane fouling to treatment techniques/doses.

Table 1.1. Delineation of Fluorescence Regional Integration Volumes

Region ID	Excitation/Emission Range	Description
Region I	EX _{240 to 300} /Em _{280 to 390}	Microbial by-products, proteins, biopolymers
Region II	EX _{240 to 300} /Em _{390 to 580}	Fulvic-like compounds
Region III	EX _{300 to 470} /Em _{300 to 580}	Humic-like

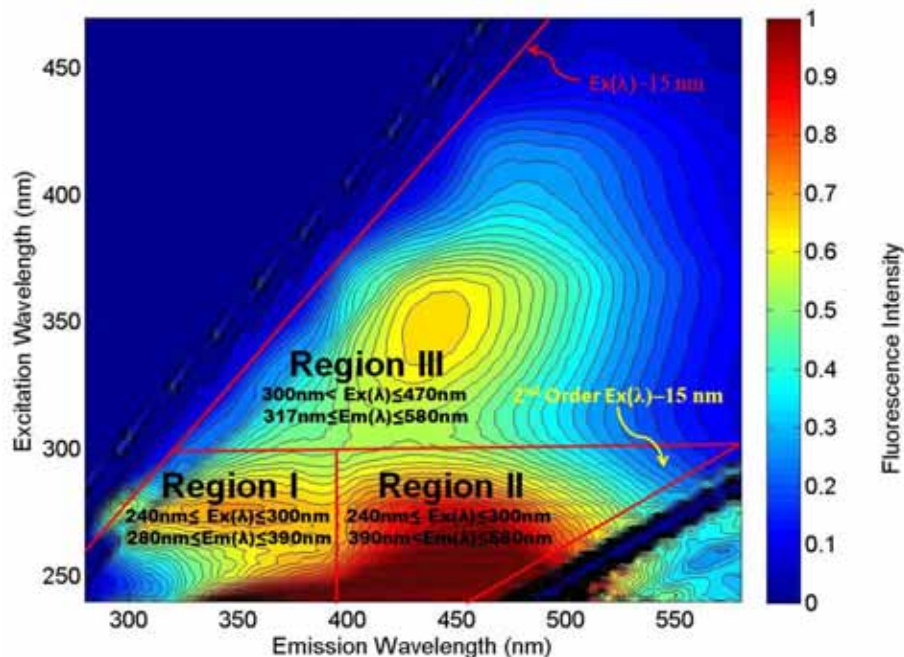


Figure 2.1. A fluorescence EEM image, with outlined boundaries for integration regions and data collection.

2.2.1.4 Biodegradable Dissolved Organic Carbon Analysis

For DOC and BDOC determinations, a Shimadzu TOC analyzer was used. BDOC was determined by spiking sample aliquots with Polyseed inoculum and incubating at 30 °C for 5 to 7 days. The BDOC was determined as the difference between initial and final DOC, resembling a previously published method (Khan et al., 2005). The inoculum was prepared by dissolving a biological oxygen demand (BOD) nutrient buffer pillow (product no. 1416066; Hach, Loveland, CO) in 300 mL of Milli-Q water in a capped bottle and by shaking contents vigorously for 1 min to ensure dissolution of nutrients. Following this, one Polyseed capsule (No. 2918700 [manufactured by Interlab]; Hach) was added into the BOD nutrient reagent. The solution of BOD nutrient buffer and Polyseed was stirred for 1 h. The solution was used within 6 h of preparation and was prepared fresh for each analysis. Water samples to be inoculated were stored at 4 °C and were used within 24 h of collection from the source. Aliquots of the water sample were filtered through a 0.45-μm- or 0.2-μm-pore size filter that had been previously rinsed with 250 mL of Milli-Q water. Sodium thiosulfate was added at 6 mg/L to neutralize any disinfection residual (from ozonation and/or chloramination). Sodium acetate standard was used for a positive control. To prepare sodium acetate solution, 25 μL of 1.0 M sodium acetate solution was added to 500 mL of BOD water sterilized with a 0.2-μm-pore-size filter before use. For inoculation and incubation, autoclaved, nonsilanized amber glass bottles were used. Per 40 mL of water sample, 1 mL of seed solution (inoculum) was added and gently mixed. A “control” sample with no inoculum added was incubated alongside. An inoculated sodium acetate sample for comparison was also prepared. The first DOC measurement was performed on a sample aliquot collected right after addition of the inoculum. Samples were incubated at 30 °C for 5–7 days on a gently moving shaker (~100 rpm). To preserve samples for DOC analysis, 20 mL of sample at the time points of 0 and 5 days was collected in a glass vial containing 150 μL of 2 N HCl and stored at 4 °C until analysis.

2.2.2 Trace Organic Contaminant and Inorganic Constituent Analyses

2.2.2.1 Pharmaceuticals and Personal Care Products

Samples were collected in 40-mL glass amber bottles containing 40 mg of sodium azide (preservative) and were transported on ice to the laboratory for analysis. Analysis of trace contaminants was determined on the basis of a previously published rapid on-line solid phase extraction (SPE) and liquid chromatography–tandem mass spectrometry (LC-MS/MS) (Trenholm et al., 2009). Briefly, sample extraction and analysis of 1.5 mL were performed by using a Symbiosis (Spark Holland, Emmen, The Netherlands) automated SPE system, coupled to an API4000 QTRAP (ABSCIEX, Framingham, MA) mass spectrometer. Oasis HLB cartridges were used for the on-line SPE. Separation was performed by using a Luna C₁₈ column (Phenomenex, Torrance, CA) and with a mobile phase consisting of 5 mM ammonium acetate in deionized (DI) water:methanol gradient. All samples were analyzed by using positive electrospray ionization and MS/MS or by using multiple-reaction monitoring. Quantitation was performed by using isotope dilution.

2.2.2.2 Nitrosamine Analysis

For NDMA analysis, samples were collected in 1 L amber bottles containing 1.0 g of sodium azide and 80 mg of sodium thiosulfate (for quenching any residual chlorine). NDMA quantitation was performed by using a gas chromatography–MS/MS (Saturn 2000, Varian, now Agilent, Santa Clara, CA) system and isotope dilution, using a method developed at the Southern Nevada Water Authority laboratories (Holady et al., 2012). NDMA standards were purchased from Ultra Scientific (Kingstown, RI), and isotopically labeled NDMA was purchased from Cambridge Isotope Laboratories (Andover, MA). For evaluating NDMA FP, samples were collected from the pilot system and were spiked with preformed monochloramine before storage for 10 days at room temperature based on a previously published method (Mitch and Sedlak, 2004). Blank samples of DI water were always below the method reporting limit for NDMA and did not yield any measurable NDMA during the 10-day FP test. A stock solution of monochloramine was prepared by rapidly mixing sodium hypochlorite into ammonium chloride solution following a method described previously (Kumar and Margerum, 1987). Sodium hypochlorite, 10–14 wt % free available chlorine (FAC), was obtained from VWR (Radnor, PA) and was standardized by using iodometric titration prior to use. Ammonium chloride, 99%, was obtained from Sigma-Aldrich (St. Louis, MO).

2.2.2.3 Bromide and Bromate

Bromate was determined by using EPA method 302 or 317. Bromide was determined by using EPA method 300.

2.2.2.4 Dissolved Ozone

Dissolved ozone was measured by using the indigo method (4500-Ozone-B; *Standard Methods*, 1998) and a Hach D-2000, UV/Vis spectrometer (Hach, Loveland, CO). Potassium indigotrisulfonate was obtained from Sigma-Aldrich (St. Louis, MO); potassium monobasic phosphate, ACS grade, was obtained from Fisher (Thermo Fisher Scientific, Waltham, MA). Concentrated phosphoric acid was obtained from JT Baker (Avantor Performance Materials, Phillipsburg, NJ).

2.2.2.5 Peroxide

A Hach Model HYP-1 Hydrogen Peroxide Test Kit (as H₂O₂) was used to measure hydrogen peroxide.

2.2.2.6 Inorganic Water Constituents

Analysis of inorganic water constituents was performed by each water reclamation facility's lab according to standard methods.

2.2.3 Membrane Autopsy and Surface Analyses

Membrane autopsy included examination of the exterior and interior of the membrane elements prior to and after disassembly and dissection. The visual inspection for manufacturing flaws or damage from use or handling included the following:

- Brine seal
- Hard shell (fiberglass outer wrap)
- Antitelescoping device (ATD)
- Glue lines
- Surfaces with deposits of scale or organic growth and any unusual features

The elements were then disassembled to inspect the internal components and to obtain samples for further analysis. The inspection of internal components included the following:

- Measurement of membrane effective area
- Dye test using Rhodamine B solution to diagnose membrane surface damage
- Integrity of glue lines
- Examination of membrane leafs, feed spacers, and permeate carriers

Membrane samples were then taken from the elements for determination of the membrane fouling, including the following:

- Scanning electron microscopy (SEM) coupled with energy dispersive spectroscopy (EDS) to observe and identify fouling and scaling on membrane surface.
- Contact angle measurement with sessile drop and captive bubble methods to identify membrane hydrophobicity.
- Quantification of membrane foulants and scalants by extraction methods followed by elemental analysis using an inductively coupled plasma (ICP) spectrometer, ion chromatography, and TOC analyzer, as well as using EEMs to measure proteins and humic acids.

2.2.3.1 Environmental Scanning Electron Microscopy

SEM provides direct observation of a sample, including membrane morphology and the fouling layer. The SEM in combination with EDS enables analysis of the elemental composition of a grain, a spot, or a whole area being imaged by the SEM. It provides detailed information on the size, shape, structure, and chemical composition of membrane material and foulants. SEM-EDS may also be used to characterize a very thin fouling layer, such as microbiological fouling, membrane scaling, or membrane degradation and defects.

Conventional SEM often requires sample preparation, such as coating with a thin layer of gold, carbon, or other material in order to reduce membrane surface charge. This process may cause artifacts during membrane characterization when membrane samples are completely dried. For all analyses completed by the Colorado School of Mines, environmental SEM (ESEM) was used to study the nonconductive materials, RO membranes, without a need for coating with carbon or gold. ESEM enables one to observe membrane structure from a low magnification of $\times 17$ to a magnification of $\times 30,000$. For microscopy analysis performed at

the Colorado School of Mines, an FEI Quanta 600 environmental scanning electron microscope with a Princeton Gamma-Tech Prism EDS (Hillsboro, OR) was used. For microscopy analysis performed at NIST in Gaithersburg, MD, the electron microscopy images of fixed (1% formalin), completely air-dried, and gold sputter-coated membrane samples were taken on a Quanta 200 environmental scanning electron microscope (FEI, Inc., Hillsboro, OR). All ESEM images were acquired in high vacuum mode with an electron beam energy of 20 keV. Image scan speed and contrast were varied to optimize image quality.

2.2.3.2 Confocal Microscopy

Although the confocal microscopy results were inconclusive in this study, the method is listed here if needed for reference information: samples (approximately 0.3 cm²) were excised from the membrane via core sampler and were placed in a light microscope mounting well; at least three samples were obtained for each membrane. 4',6-Diamidino-2-phenylindole (DAPI) nucleic acid stain (Invitrogen, Eugene, OR) was used to compare bacterial colony density findings among membrane samples. Confocal laser scanning microscopy images were obtained on a TCS SP5/DM6000 from Leica by using an HCX PI Apo oil immersion 63× coverslip corrected objective. A 405-nm diode laser was used as the excitation source and the emission bands were set to 440 nm to 480 nm (DAPI). Electronic zoom functions between ×1 and ×6 were used as needed.

2.2.3.3 Sessile Drop Analyses

A NIST-built goniometer system was used to conduct the static sessile drop measurements. This system consists of a motor-driven syringe pump, motorized stage, and optical microscope (Zeiss) with a 5× objective to capture images of liquid–solid interfaces. Images are captured with a camera and with the ImagePro software package, which is also used to measure the contact angle. Figure 2.2 provides a sample image from the goniometer at NIST. For contact angle analysis performed at the Colorado School of Mines, the membrane specimens were measured with a Ramé-hart Standard Goniometer Model 200-00 (Surface Science Instrument, Landing, NJ) by using the sessile drop and captive bubble methods. Computerized goniometer systems combining digital optics and shape recognition programs can accurately measure the contact angle of membranes. An example imageA sample image from the goniometer of water placed on the membrane surface is shown in Figure 2.2, with a contact angle drawn in for illustrative purposes. For the sessile drop contact angle method for the dry membrane samples, 10 measurements were performed and the average was taken. In addition, the captive bubble contact angle method was performed on wet membrane samples, as an alternative to the sessile drop method, while using three measurements.



Figure 2.2. Image from sessile drop method using water on a fouled membrane surface.

2.2.3.4 *Quantitative Measurements of Organic and Inorganic Substances in the Fouling Layer*

Membranes with measured sizes (50 cm²) were obtained from each membrane element for foulant extraction. They were cut into small pieces; soaked in 100 mL of DI water, 100 mL of 0.8 M HNO₃, or 0.1 M NaOH; and then ultrasonicated for 120 min in a typical laboratory sonication bath. Six common anions (fluoride, chloride, bromide, phosphate, sulfate, and nitrate) extracted with DI water and NaOH solutions were analyzed by ion chromatography (Model ICS-90; Dionex, Sunnyvale, CA). Thirty-three elements in the extracts with DI water and HCl solutions were analyzed by an ICP optical emission spectrometer (Optima 3000; PerkinElmer Inc., Waltham, MA). Organics extracted from the three solutions were quantified with a TOC analyzer (GE, Sievers 900 TOC analyzer with autosampler). Samples were also analyzed for organic compound classification by using UV radiation (DU 800 UV Spectrometer; Beckman Coulter, Brea, CA) in conjunction with a spectrofluorometer (FluoroMax-4; HORIBA Jobin Yvon, Edison, NJ). Protein and humic- or fulvic-like substances were analyzed by using EEM spectroscopy. EEM spectroscopy was used to determine the presence of protein-like and humic-like matter in water. Fluorescence intensity for protein-like organic matter was quantified at an emission wavelength of 330 nm and an excitation wavelength of 270 nm. Humic matter (humic and fulvic acids) intensities were quantified at emission wavelengths of 420 and 450 nm and at excitation wavelengths of 350 and 250 nm, respectively. These specific wavelengths for this particular set of samples varied slightly, perhaps because of high iron content in the water that could interfere with the spectroscopy instrument. The base extracted samples and the DI water extracted samples were run without dilution through the instrument. All samples were diluted to levels suitable for analysis for the different analytical instruments. The virgin membrane sample was used as a blank for all extraction analysis.

2.2.4 *Determination of the UV Dose at the Pilot-Scale UV/H₂O₂ Reactor*

The UV skid at WRF 2 was operated at 15- to 20-gpm feed flow, with 17 of 32 lamps working at 60% power. In order to verify the effective UV dose (fluence) delivered during continuous pilot operation, the project team used atrazine as a chemical actinometer. Atrazine has been well characterized in previously reported studies, with a known quantum yield (Φ_λ) of 0.046 and molar absorptivity coefficient (ϵ_λ) of 3860 L•mol⁻¹•cm⁻¹ at 254 nm (Canonica et al., 2008). Atrazine undergoes a direct photodegradation following first-order kinetics. A fluence-based rate constant, k' , can be determined by plotting $\ln(C/C_0)$ versus UV dose in millijoules per square centimeter. However, k' can also be calculated on the basis of Equation 1.2:

$$k' = \Phi_\lambda \cdot \epsilon_\lambda \cdot \ln(10)/U_\lambda \quad (1.2)$$

Where U_λ is the energy carried by 1 mol of photons at specific wavelength λ , at 254 nm this equates to 47,528 J/E (Bolton and Stefan, 2002). The project team utilized a bench-scale collimated beam apparatus and used a UV radiometer to supplement determination of atrazine degradation studies in pilot-scale operation. Various correction factors that are specific to the water quality (mainly absorbance at specific wavelength) and to the UV apparatus were determined on the basis of previously reported methodology (Bolton and Stefan, 2002) and were applied for accurate estimation of the target UV dose.

The project team operated the UV skid at different flow rates while continuously spiking atrazine. Samples were collected immediately before the inlet to the UV skid and after UV treatment at an interval equal to approximate hydraulic retention time (HRT), on the basis of the feed flow. Samples were analyzed by using a modified LC-MS/MS method to determine

change in atrazine concentration, UV_{254} absorbance, fluorescence, and DOC. The average UV_{254} absorbance for all influent samples ($n = 7$) was 0.1034 ± 0.0006 (0.6% relative standard deviation), so UV transmittance at 254 nm (UVT) was consistent during the entire experiment. Figure 2.3 shows the experimentally determined, fluence-based rate constant. According to the literature values for the quantum yield and molar absorptivity constant, $k' = 8.7 \cdot 10^{-4} \text{ cm}^2/\text{J}$, so there is reasonable agreement between the two rate constants. Figure 2.4 shows the fluence determined by radiometer- versus actinometry-based ones with a slope of 1.09, indicating that the UV fluence determined by the two methods is within 10% error.

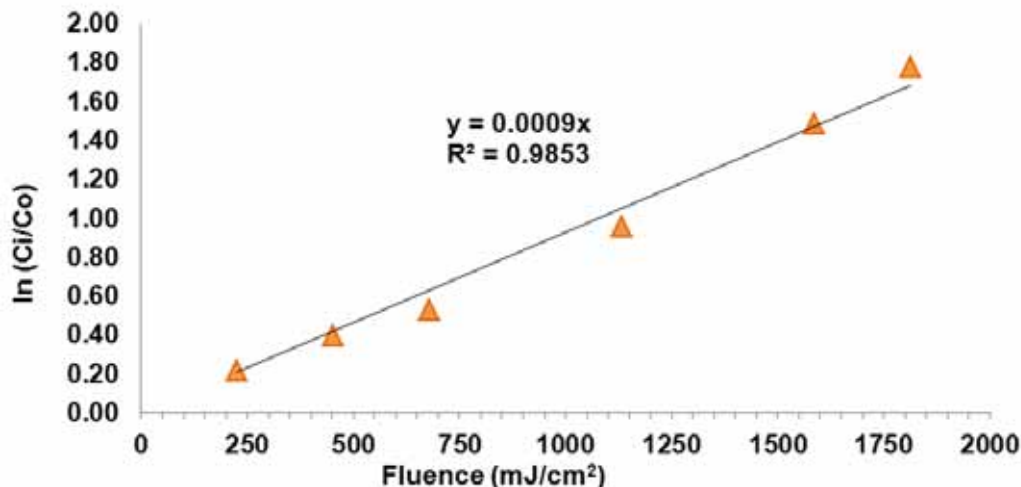


Figure 2.3. A plot of atrazine concentration, as $\ln(C_i/C_o)$ vs. fluence (UV dose), as determined by radiometer measurements.

In general the agreement between the radiometer-based estimation and the actual photochemical transformation of atrazine was quite reasonable, enabling the project team to use the experimentally determined value of the fluence-based rate constant of $k' = 9.0 \cdot 10^{-4} \text{ cm}^2/\text{J}$ to calculate the effective UV dose at various feed flows to the UV skid. Figure 2.5 provides a plot of UV dose versus the feed flows.

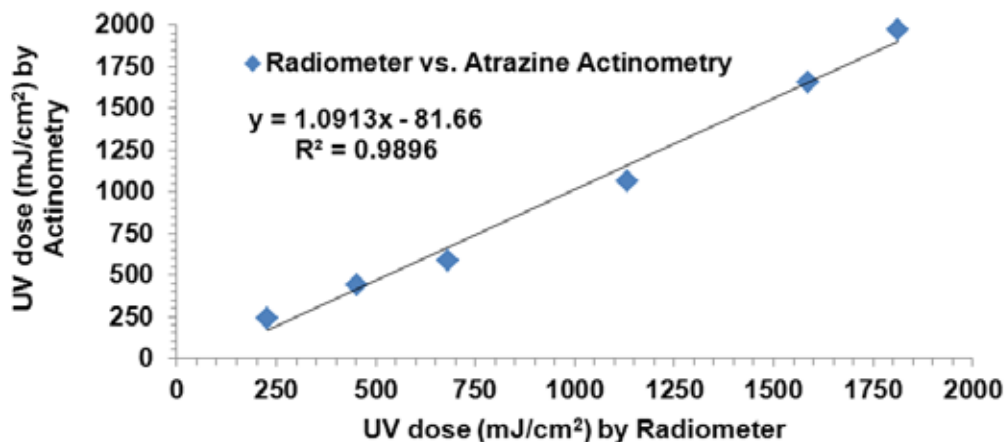


Figure 2.4. A plot of UV dose determined by actinometry vs. radiometer measurements.

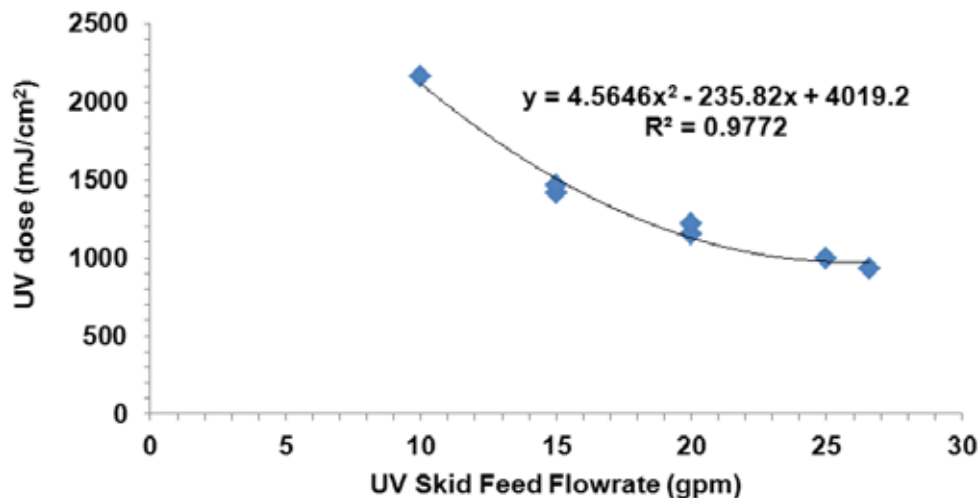


Figure 2.5. A plot of UV dose values determined by actinometry vs. the feed flow to the UV skid running with 17 active lamps at 60% power.

Because the feed flow to the UV skid has been observed to vary between 17 and 20 gpm on the basis of temperature and UF filtrate tank level (effect of automatic scaling of UF filtering capacity based in changes in transmembrane pressure [TMP]), the project team estimated that the UV dose used for the continuous testing of the UV/H₂O₂ pretreatment to RO ranged from 1100 to 1300 mJ/cm².

The remainder of this report contains the data, analysis, and conclusions based on the methodology outlined in this chapter. Where needed, additional analytical information and methods are described in the context of the chapters.

Chapter 3

Oxidation Impacts on Dissolved Organic Matter

3.1 Chapter Overview

This chapter of the report includes information regarding the characterization of the changes in NOM and EfOM after treatment with various preoxidation strategies (ozone, ozone/peroxide, UV, and UV/peroxide). Both NOM and EfOM have been shown to be the predominant cause of physically irreversible fouling and are ultimately responsible for the decline in membrane performance over time (Kimura et al., 2004; Yamamura et al., 2007a; Yamamura et al., 2007b). Different subsets of organic matter may be responsible for fouling, including hydrophobic fractions, hydrophilic fractions, and metal–organic matter complexes (Shon et al., 2006; Gray et al., 2007; Her et al., 2007; Huang et al., 2007). Furthermore, both the size and the source of organic matter can impact fouling (Kwon et al., 2005; Huang et al., 2007). Thus, the purpose of this subtask was to investigate and quantify the transformations occurring in the bulk NOM and EfOM as a result of oxidation. Although many of the data presented were collected in parallel with the membrane fouling experiments, they are presented independently in this chapter to demonstrate the impacts of oxidation on organic matter and to provide information for later discussion as it pertains to membrane fouling. This chapter also provides the basis for evaluating and understanding the oxidant doses used in each of the experiments and pilot plant studies.

Characterization of DOM described in this chapter is focused on using such techniques as molecular spectroscopy, molecular polarity assessment, and SEC employing various detectors. General descriptions of various analytical methods are provided in Chapter 2. The bulk of experiments in the project involved using UV absorbance measurements and fluorescence EEM spectroscopy as indicators of the oxidation effects. Another emphasis was made on the quantification of differences in the fluorescence EEM spectra. Two widely accepted methods for quantification of differences in EEMs include FRI and FI (McKnight et al., 2001; Chen et al., 2003). First, hydrophobic compounds tend to have a higher aromatic carbon content that is associated with a greater amount of region-specific fluorescence. Thus, changes in FRI (and the sum of the regional volumes, Φ_T) provide a basis for quantifying changes in aromaticity (and hydrophobicity) of the organic matter in the sample. Second, FRI can be used to determine the relative contribution of types of organic matter to the overall composition of EfOM or NOM. Thus, as the relative distribution of organic material components changes between regions, one can assess the impact that a given treatment may be having on the quality of the organic matter. Such observations may be useful for relating membrane fouling to treatment techniques and doses.

Although more information can be obtained from the entire EEM by using FRI, the concept of a single-point FI may also prove useful in interpreting NOM and EfOM characterization data. In its original development, FI was used to identify external (allochthonous) inputs of NOM to watersheds and internal (autochthonous) microbial inputs (e.g., sewage waste) of organic matter to watersheds. The FI is operationally defined as the ratio of the peak intensity at Ex_{340}/Em_{450} to Ex_{340}/Em_{500} . Typically, FIs of ~ 1.9 indicate microbially derived fulvic acids, whereas FIs of ~ 1.4 indicate terrestrially derived fulvic acids. In other words, waters with higher FI values tend to be more closely related to a wastewater-like character. More

important, the FI has been correlated to aromaticity; thus, a higher FI indicates a higher proportion of aromatic carbons than does a lower FI. Thus, one would expect more hydrophobic molecules and a greater fouling potential at a higher FI than at a lower FI.

3.2 Experimental Setup

Background water quality parameters were measured according to standard methods. Water quality parameters for representative MBR filtrate (from WRF 1), tertiary effluent from WWTP (from WRF 2), UF filtrate (from WRF 2), and CRW (from DWTP 1) are provided in Table 3.1.

Table 3.1. Water Quality Parameters for MBR Filtrate and Colorado River Water

	MBR Filtrate (mg/L)	UF Filtrate (mg/L)	Tertiary Effluent (mg/L)	CRW (mg/L)
Calcium	74	100	N/A	78
Magnesium	31	39	N/A	27
Sodium	160	190	N/A	94
Potassium	22	18	N/A	6.2
Total phosphorus	0.2	0.2	N/A	N/A
Ammonia-N	<0.5	<0.5	<0.5	<0.5
Barium	0.045	0.039	N/A	0.14
Strontium	1.2	1.3	N/A	N/A
Bromide	0.10	0.17	0.15	0.09
Alkalinity (as CaCO ₃)	99	83	123	138
Sulfate	250	359	N/A	248
Chloride	180	238	N/A	88
Fluoride	0.74	0.73	N/A	0.34
Nitrate-N	13.8	13.0	14.0	0.60
Boron	0.31	0.36	N/A	N/A
Silica	12.5	11.0	M	7.5
TDS	1100	1050	1050	625
pH	7.3	7.2	6.9	8.1
Temp	26–33 °C	24–30 °C	24–30 °C	14–19 °C
TOC	6.0	5.4	7.2	2.6
UV ₂₅₄ (cm ⁻¹)	0.125	0.118	0.130	0.036
Coliforms (MPN/100 mL)	<5	N/A	N/A	N/A
Turbidity	<0.1	<0.1	0.1	<0.5 NTU
SDI	<3–6	<3–6	>6	<3

The CRW had a lower DOC of 2.6 mg/L; however, it had a relatively high alkalinity. The MBR and UF filtrates were typically fully nitrified and partially denitrified (and equivalent to a full-scale tertiary effluent) with a DOC of 5.1 to 6.5 mg/L, UV₂₅₄ of less than 0.130, and turbidity of less than 0.10 NTU as indicated in Table 3.1.

The initial stage of this study examined the impact of ozone and ozone/peroxide on the surface water samples and then on the MBR filtrates, comparing them with control samples collected without oxidation. Ozone and ozone/peroxide oxidation was performed on site by using a HiPOx[®] pilot skid (APTwater, Pleasant Hill, CA) operating at a flow rate of 10 gpm with an ozone dose of 1.5, 3, 6, or 10 mg/L, allowing for a total of 6 min of contact time. When added, peroxide was dosed at a molar ratio of 0.5:1 with ozone. In addition bench-scale ozone and ozone/peroxide spike experiments were conducted at the DWTP 1 laboratories by using water collected and transported from the pilot locations. Batch ozone solutions were prepared and oxidation tests were performed as described elsewhere (Wert et al., 2009). Dissolved ozone was measured by using the indigo method with modifications described elsewhere (Wert et al., 2009).

The effect of various UV dose and UV/H₂O₂ doses on tertiary effluent and UF filtrate from WRF 2 was evaluated by using the pilot-scale TrojanUVPhox[®] and a bench-scale collimated beam apparatus. UV dose (fluence) was determined by using chemical actinometry and described in Chapter 2.

3.3 Results and Discussion

3.3.1 Oxidation Impacts on NOM in Colorado River Water

Because of the low TOC concentration of the CRW, ozone typically persisted beyond the 6 min of contact time in the HiPOx[®] reactor and therefore had to be quenched with sodium thiosulfate to ensure uniform handling and contact times. The raw CRW has been well characterized with an ozone demand varying from 0.6 to 0.8 mg/L and UVT of about 88%. Figure 3.1 shows ozone decay curves in CRW at various applied ozone doses. When peroxide was added to form an AOP, no sodium thiosulfate was needed to quench the residual as the ozone was rapidly consumed by the peroxide.

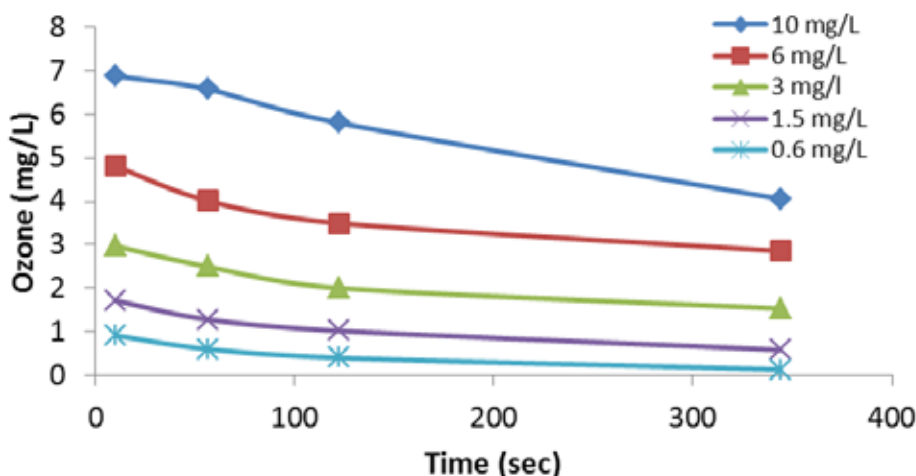


Figure 3.1. Ozone demand/decay curve for Colorado River water.

3.3.1.1 Associated Changes in UV Absorbance and Fluorescence

Table 3.2 lists the measured changes in the UV absorbance, DOC, and SUVA as a result of various ozone and ozone/peroxide doses. As the ozone dose increased, the UV₂₅₄ and UV₂₈₀ decreased, likely an indicator of reductions of chromophoric functional groups of the NOM

matrix. These changes are also reflected by corresponding decreases in SUVA as a general decrease in the aromaticity of the NOM, even though no significant changes were observed in the DOC values. Similarly, Figure 3.2 shows that the fluorophoric regions of the NOM were also impacted by ozone and ozone/peroxide, providing additional evidence that the NOM became less aromatic after oxidation.

Table 3.2. Change in Specific UV Absorbance for Ozone- and Ozone/Peroxide-Treated Samples

Sample Water	O ₃ Dose (mg/L)	O ₃ :H ₂ O ₂ (Mol Ratio)	UV ₂₅₄ (cm ⁻¹)	UV ₂₈₀ (cm ⁻¹)	DOC (mg/L)	SUVA (L m ⁻¹ mg ⁻¹)
CRW	0	(no H ₂ O ₂ added)	0.042	0.026	2.2	1.9
CRW	1.5	(no H ₂ O ₂ added)	0.041	0.015	2.2	1.9
CRW	3	(no H ₂ O ₂ added)	0.033	0.015	2.1	1.6
CRW	1.5	0.5	N/A	N/A	N/A	N/A
CRW	3	0.5	0.033	0.013	2.1	1.6

Note. N/A = not analyzed.

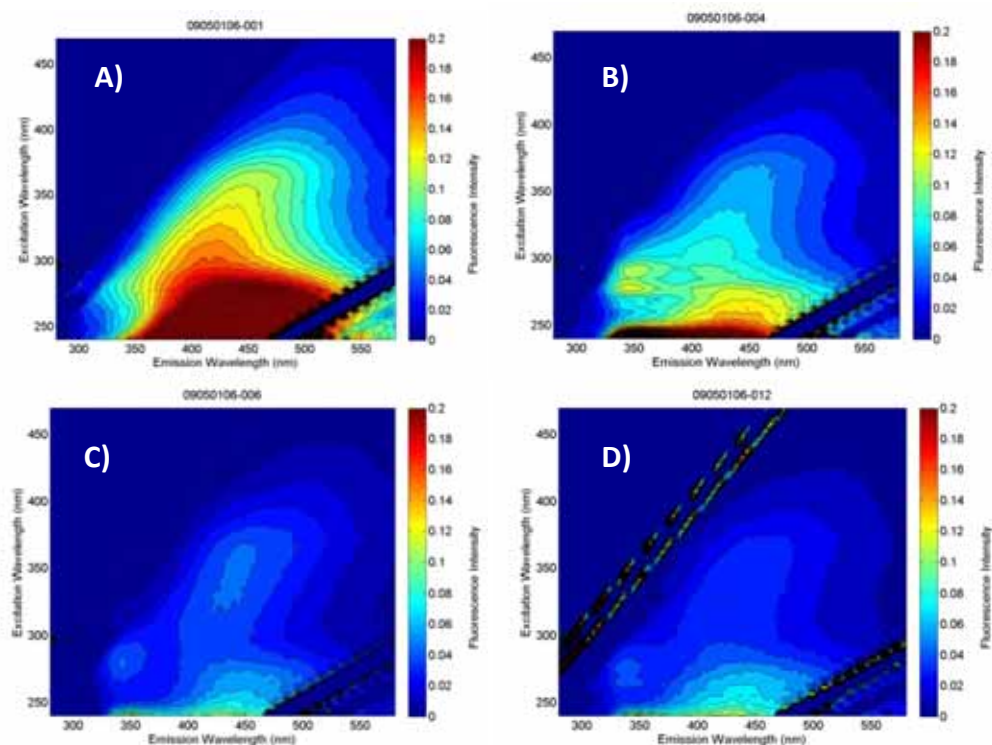


Figure 3.2. Fluorescence EEM spectra for (A) raw Colorado River water, (B) after 1.5-mg/L O₃ and 0.5-mg/L H₂O₂, (C) after 3-mg/L O₃ and 1.1-mg/L H₂O₂, D) after 3 mg/L.

3.3.1.2 Size Exclusion Chromatography and Polarity Rapid Assessment Method Analysis of Colorado River Water Treated with Ozone and Ozone/Peroxide

To investigate changes in the NOM, SEC paired with UV and fluorescence detectors was used. Selected SEC-UV/FL chromatograms for samples exposed to various ozone and

ozone/peroxide doses are shown in Figure 3.3. Although both UV_{254} and fluorescence decrease as a function of the ozone and ozone/peroxide doses, the SEC analysis can be used to demonstrate which molecular weights are affected by ozone and/or hydroxyl radicals. However, because both UV_{254} and fluorescence decline, detection of subtle changes in the molecular weight distribution is difficult. In other words, when using optical detectors to detect shifts in molecular weight distribution based on changes that also impacted the optical properties of the material, the detector might not “see” the resulting transformed molecules. As such, these results were not able to provide conclusive evidence for changes in the molecular weight distribution due to ozone or ozone/peroxide. However, it may be concluded that the both ozone and ozone/peroxide do impact NOM across all the molecular weights containing chromophoric and fluorophoric functional groups, and therefore it should be expected that some change in molecular weight will have also occurred. Additional analysis by SEC with a sensitive on-line DOC detector would be necessary to confirm changes in molecular weight.

PRAM also was used to determine if measurable changes in the polarity of NOM occur because of ozone and ozone/peroxide. However, because of the relatively low UV_{254} of the raw water (0.042) (Table 3.2) and its significantly reduced absorbance after treatment with ozone or ozone/peroxide, the results from PRAM analysis were too variable to make any conclusions about changes in the polarity of NOM.

3.3.1.3 Summary of Oxidation Impacts on NOM in Colorado River Water

Reductions of UV absorbance and fluorescence EEM intensities that were due to ozone and ozone/peroxide reactions with CRW NOM were observed. These effects were attributed to loss of chromophoric and fluorophoric functional groups in the NOM. Furthermore, a decrease in the SUVA was observed as evidence of decrease in the overall aromaticity of the NOM during oxidation. Data were not available regarding any changes in molecular weight distribution of the oxidized NOM versus that of the raw water NOM.

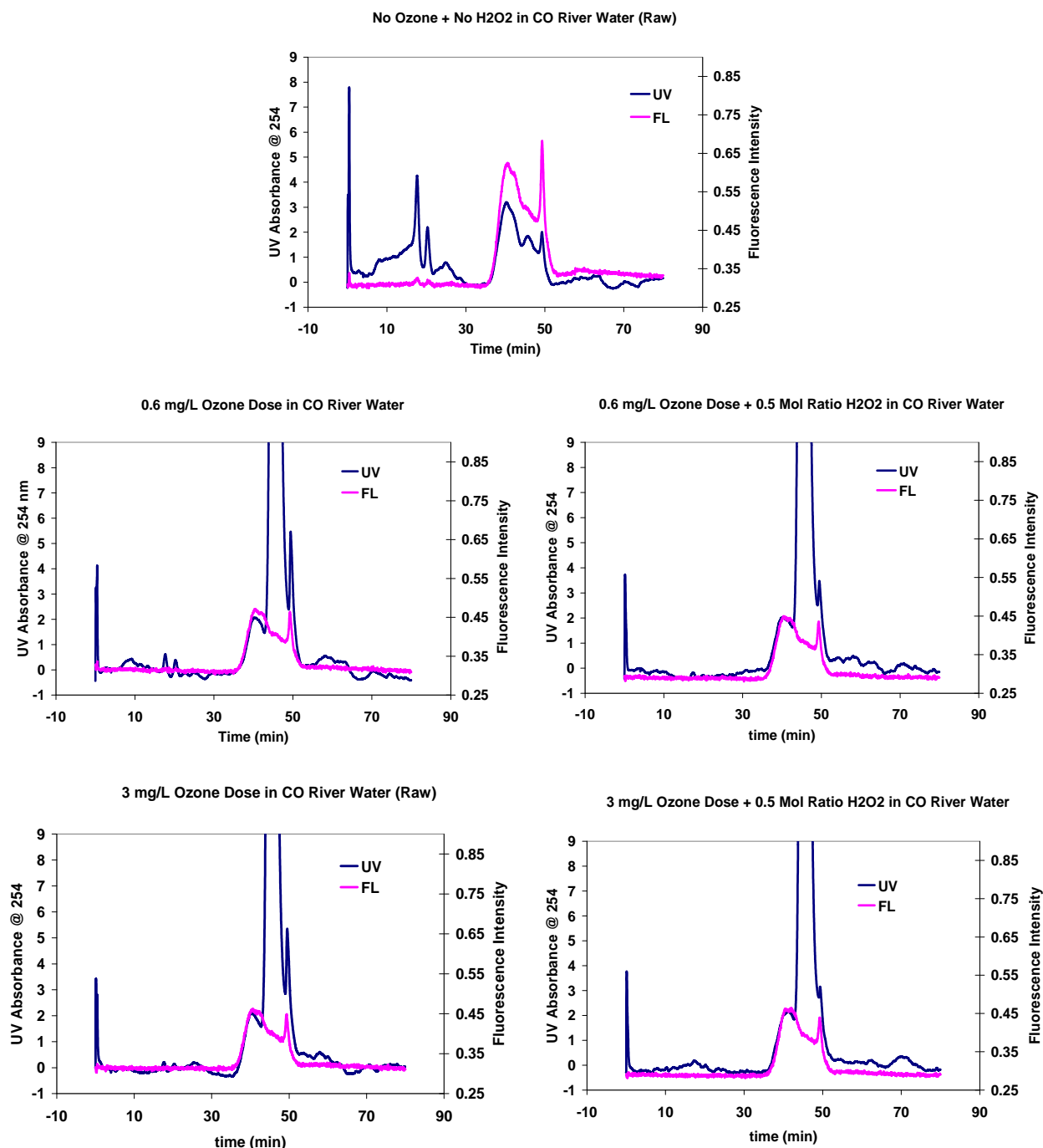


Figure 3.3. Size exclusion chromatography/UV/fluorescence data for Colorado River water samples.

3.3.2 Oxidation Impacts on EfOM in Tertiary Effluent from Water Reclamation Facility 2

The preliminary investigation of oxidation on the reduction of RO membrane fouling during bench-scale flat sheet experiments from WRF 2 relied on the use of tertiary effluent treated by the pilot UV skid at various UV dose and hydrogen peroxide doses. Changes in UV₂₅₄,

fluorescence, and TOC were measured during these tests. A relatively high UV fluence of approximately 2300 mJ/cm² resulted in a small decrease of total fluorescence volume under the EEM by 20%, although UV₂₅₄ was reduced by only 3% (EEMs shown in Figure 3.4). With the addition of hydrogen peroxide at approximately the same UV dose, the total fluorescence was substantially decreased, as shown in Figure 3.4. These changes may reduce aliphatic, chromophoric/fluorophoric regions of organic matter, potentially indicating a shift toward more-polar, lower-molecular-weight organic matter.

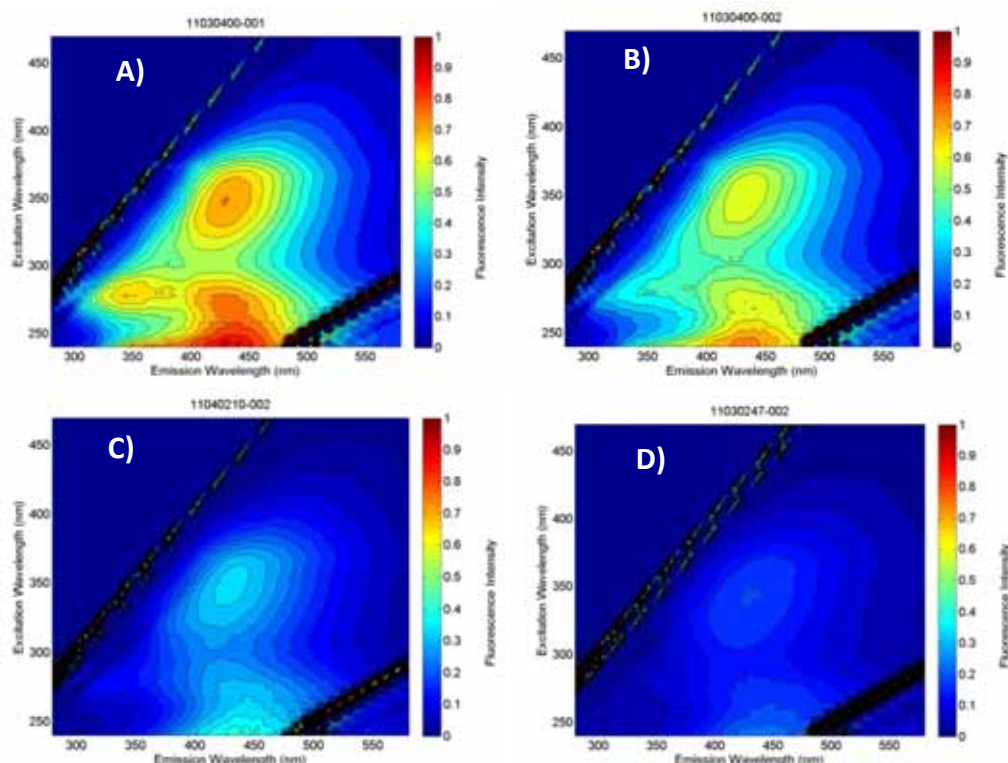


Figure 3.4. Fluorescence EEM spectra of (A) tertiary effluent, (B) tertiary effluent treated with a UV dose of 2300 mJ/cm² (UV dose is approximate), (C) tertiary effluent treated with a UV dose of 1900 mJ/cm² and 7-mg/L H₂O₂, (D) tertiary effluent treated with a UV dose of 2500 mJ/cm² and 10-mg/L H₂O₂.

3.3.3 Oxidation Impacts on EfOM in UF Filtrate

Impacts of ozone, UV, and UV/H₂O₂ on EfOM were investigated by using UF filtrate and UF feed (ozone only). In addition to pilot-scale testing, a series of bench-scale experiments were performed at various UV doses.

3.3.3.1 Effects of Ozone on EfOM in UF Filtrate

Ozone demand decay in UF filtrate

The UF feed and filtrate waters were collected in plastic carboys (5 L) at WRF 2 and were transported back to the Southern Nevada Water Authority laboratory, where they were cooled to 4 °C. Ozone testing was completed within 7 days of sample collection. On the day of testing, samples were allowed to warm to 25 °C prior to ozone dosing. Hydrogen peroxide, when used, was dosed at a 0.7-mol ratio (excess peroxide) to ensure complete reaction with

ozone. Bulk water quality parameters were independently measured by standard methods by the WRF 2 laboratory, as shown in Table 3.3.

Table 3.3. Bulk Water Quality Parameters for UF Feed and Permeate

Water Quality Parameter	UF Feed	UF Filtrate
Fecal coli (MPN/100 mL)	7900	<2.0
Total coli (MPN/100 mL)	13,000	110
<i>E. coli</i> (MPN/100 mL)	7900	<2.0
TSS (mg/L)	5.6	<5
TDS (mg/L)	1160	1180
TOC (mg/L)	7.1	5.7
Ortho PO ₄ (mg/L)	0.076	0.074
Total PO ₄ (mg/L)	0.265	0.12
Total alkaline (mg/L [CaCO ₃])	133	130
Chloride (mg/L)	—	237
SO ₄ (mg/L)	—	380
Fluoride (mg/L)	0.73	0.74
Bromide (mg/L)	0.23	<0.20
NH ₃ -N (mg/L)	0.11	0.09
NO ₂ -N (mg/L)	<0.100	<0.100
NO ₃ -N (mg/L)	13.8	13.8
TN (mg/L)	14	14
Turbidity (NTU)	1.66	<1.0

Ozone decay curves for UF feed and filtrate are shown in Figure 3.5. Contrary to conventional wisdom, the ozone demand/decay rates were slightly higher in the UF filtrate than in the feed water. This observation does not appear to be explained by the differences in the water quality parameters (e.g., nitrite and alkalinity). To confirm that the ozone decay was in fact higher in the UF filtrate, a second set of experiments were performed. The ozone decay curves for UF feed and filtrate are shown in Figure 3.6.

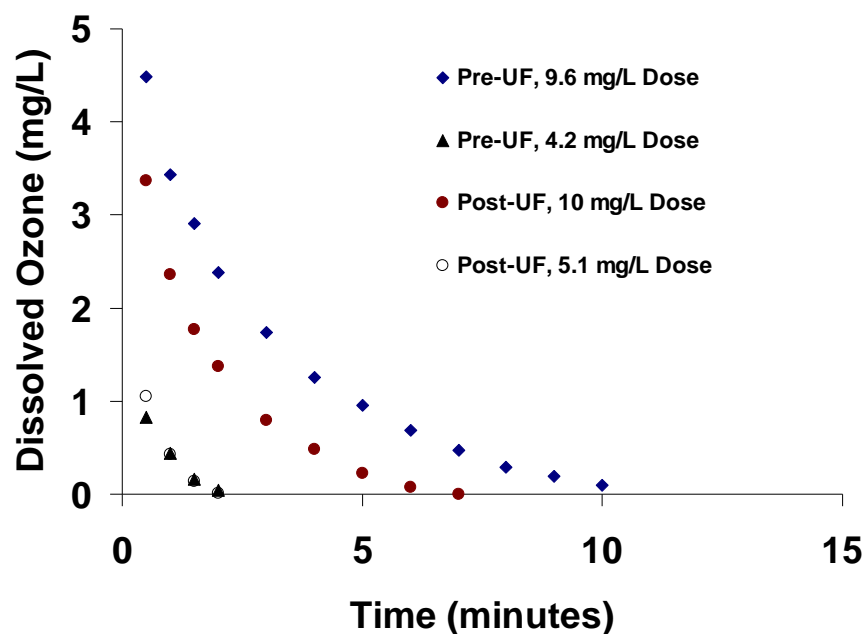


Figure 3.5. Ozone decay curves in the UF feed ("Pre-UF") and filtrate ("Post-UF") from Test 1.

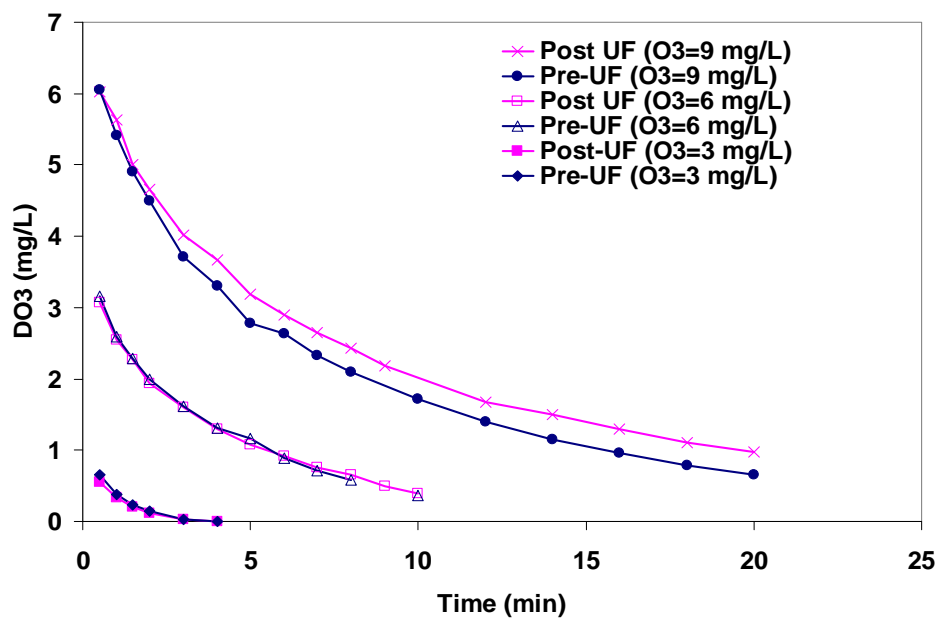


Figure 3.6. Ozone decay curves in UF feed and UF filtrate at various ozone doses (Test 2).

The ozone demand of the UF feed and filtrate waters was indistinguishable in the 3-mg/L and 6-mg/L ozone-dosed samples, although at the 9-mg/L dose, one observes again that the filtrate exerted a slightly higher ozone demand than did the feed water. These data are contrary to conventional wisdom, which states that UF filtrate should have a lower ozone demand than the unfiltered water. However, the results of two separate sets of data reported here (Figure 3.5 and Figure 3.6) would indicate that this assumption does not universally hold true.

Associated Changes in UV Absorbance and Fluorescence

Separate sample aliquots of the ozonated samples were collected to determine the changes in UV_{254} and UV_{280} of water samples, the DOC concentration, and SUVA ($SUVA = DOC/UV_{254} \times 100$) with results shown in Table 3.4. As can be seen from the data presented in Table 3.4, increasing the ozone dose decreased the UV_{254} , DOC content, and SUVA of the sample. The decrease in UV_{254} was likely due to the loss of the aromatic nature (i.e., loss of chromophores) of the EfOM present in the sample (dissolved ozone is an electrophile and rapidly attacks conjugated pi bonds and other electron-rich sites). The loss of aromaticity likely correlates to a change in polarity of the EfOM as indicated by the decreasing SUVA values. Higher SUVA values are indicative of more-reactive organic material, a greater abundance of aromatic carbons, and a higher tendency of the organic matter to be removed by coagulation (Archer and Singer, 2006a; Archer and Singer, 2006b). The observed changes in UVA provide a basis for the establishment of a correlation between the decrease in UVA and applied ozone dose. Such a correlation may be useful for future ozone application control devices that rely on changes in UVA to trigger changes in applied dosages.

Table 3.4. Changes in UV_{254} and UV_{280} of UF Feed and UF Filtrate When Treated with Various Doses of Ozone

Type	Treatment	DOC (mg/L)	UV_{254} (cm^{-1})	UV_{280} (cm^{-1})	SUVA ($L\ m^{-1}\ mg^{-1}$)
UF feed	No ozone	6.5	0.118	0.088	1.8
UF feed	1.5-mg/L O_3	6.3	0.098	0.063	1.6
UF feed	3-mg/L O_3	6.2	0.082	0.047	1.3
UF feed	6-mg/L O_3	6.0	0.067	0.037	1.1
UF feed	9-mg/L O_3	5.8	0.054	0.030	0.9
UF filtrate	No ozone	6.4	0.110	0.084	1.7
UF filtrate	1.5-mg/L O_3	6.4	0.090	0.057	1.4
UF filtrate	3-mg/L O_3	5.6	0.075	0.044	1.3
UF filtrate	6-mg/L O_3	5.2	0.058	0.032	1.1
UF filtrate	9-mg/L O_3	4.8	0.048	0.028	1.0
Filter blank	N/A	<0.2	<.002	<.002	N/A

Figure 3.7 shows a plot of natural log of UV_{254} versus applied ozone dose. A decrease in fluorescence that was due to ozone was also observed in both UF feed and UF filtrate, as shown by Figure 3.8.

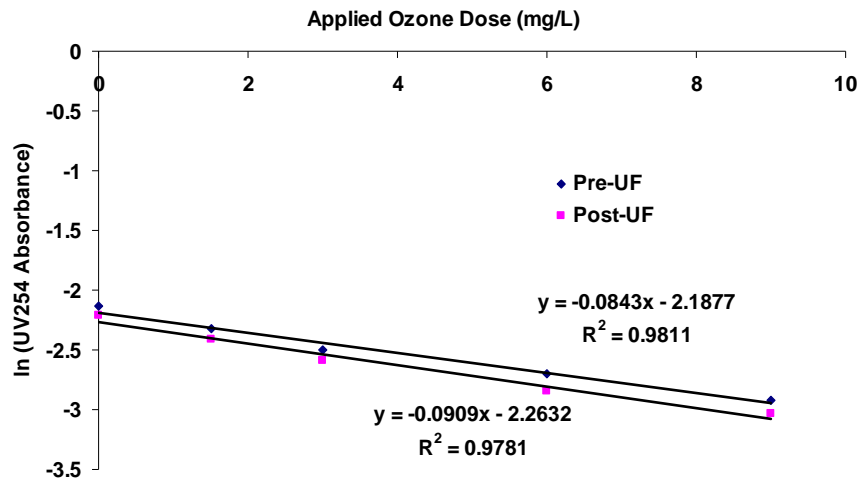


Figure 3.7. UV₂₅₄ plotted versus applied ozone dose in UF feed (pre-UF) and UF filtrate (post-UF).

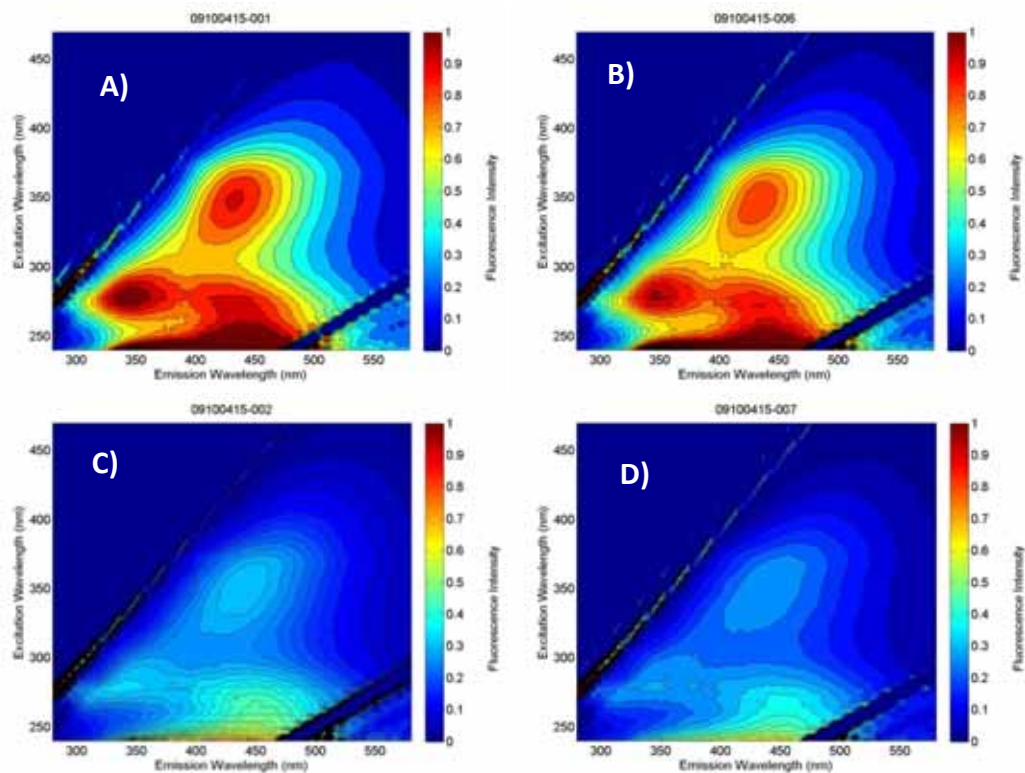


Figure 3.8. Fluorescence EEM spectra of (A) UF feed (without ozone), (B) UF filtrate (without ozone), (C) UF feed with 1.5-mg/L ozone, and (D) UF filtrate with 1.5-mg/L ozone.

Although the EEM spectra show an immediately observable difference between the ozone doses, there is little observable difference between the UF feed and UF filtrate, as can be seen from the EEM integration results presented in Table 3.5. In addition to the decrease of

fluorescence in all regions, a reduction of the FI (indicating less-aromatic, less-hydrophobic EfOM) is also evident. These changes in EfOM have implications for the reduction in fouling observed in the flat sheet membrane tests and described later in Chapter 4.

Table 3.5. Fluorescence Regional Integration UF Feed UF Filtrate Treated with Various Doses of Ozone

Description	I	II	III	Φ_T	FI
UF Feed	12235	13304	5782	31322	1.69
UF Feed -1.5 mg/L O ₃	4666	6141	2552	13359	1.42
UF Feed -3.0 mg/L O ₃	1941	3303	1454	6699	1.38
UF Feed -6.0 mg/L O ₃	1489	1655	742	3886	1.37
UF Feed -9.0 mg/L O ₃	132	783	431	1346	1.33
UF Filtrate	11587	12507	5364	29458	1.72
UF Filtrate -1.5 mg/L O ₃	4180	5372	2243	11795	1.42
UF Filtrate -3.0 mg/L O ₃	1757	2983	1344	6084	1.36
UF Filtrate -6.0 mg/L O ₃	286	1186	605	2077	1.34
UF Filtrate -9.0 mg/L O ₃	111	645	370	1125	1.36

Size Exclusion Chromatography and Polarity Rapid Assessment Method Analysis of UF Filtrate Treated with Ozone

To investigate changes in the EfOM, SEC paired with UV and fluorescence detectors was used. Overlaid SEC-UV chromatograms for UF filtrate samples exposed to various ozone doses are shown in Figure 3.9. Figure 3.10 shows chromatograms for the same samples obtained with a fluorescence detector.

As was similar for SEC results of the CRW ozone tests, a reduction in both UV₂₅₄ and in fluorescence signal was observed as a function of the ozone dose. The results of SEC analysis demonstrate which molecular weights were affected by ozone and/or hydroxyl radicals; however, they do not provide evidence for changes in the molecular weight distribution. Rather, they demonstrate that a loss of chromophoric and fluorophoric functional groups occurred across all the molecular weights in EfOM.

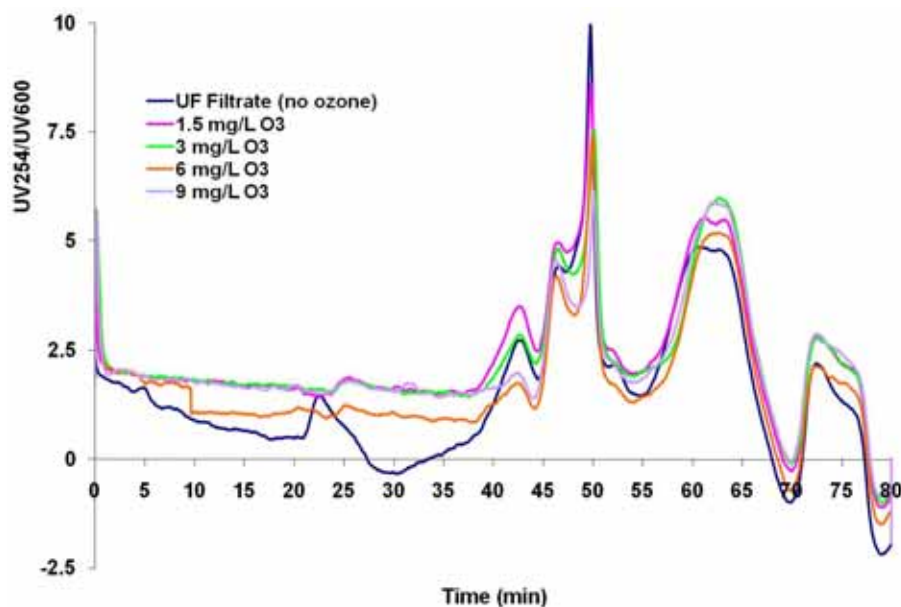


Figure 3.9. Overlaid size exclusion chromatography–UV chromatograms for UF filtrate at various ozone doses.

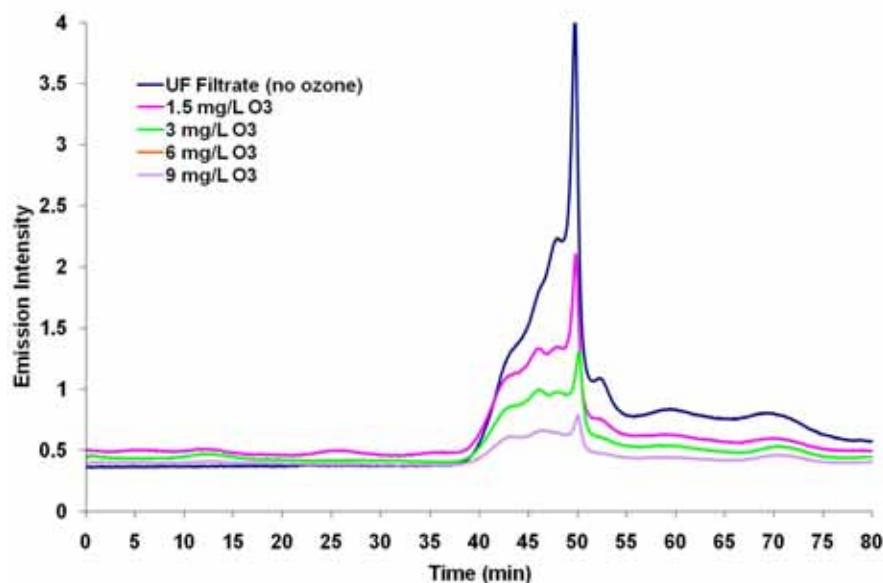


Figure 3.10. Overlaid size exclusion chromatography–fluorescence chromatograms for UF filtrate treated with various ozone doses.

Figure 3.11 shows PRAM data related to changes in the RCs of hydrophobic (C_{18}), hydrophilic (Diol), and anionic (NH_2) moieties of the EfOM. Rather than a specific reduction in a particular fraction, a general decrease in all of fractions was observed. Thus, these results may indicate that oxidation was impacting various fractions of EfOM but did not provide quantitative changes in the relative polarity of EfOM before and after oxidation.

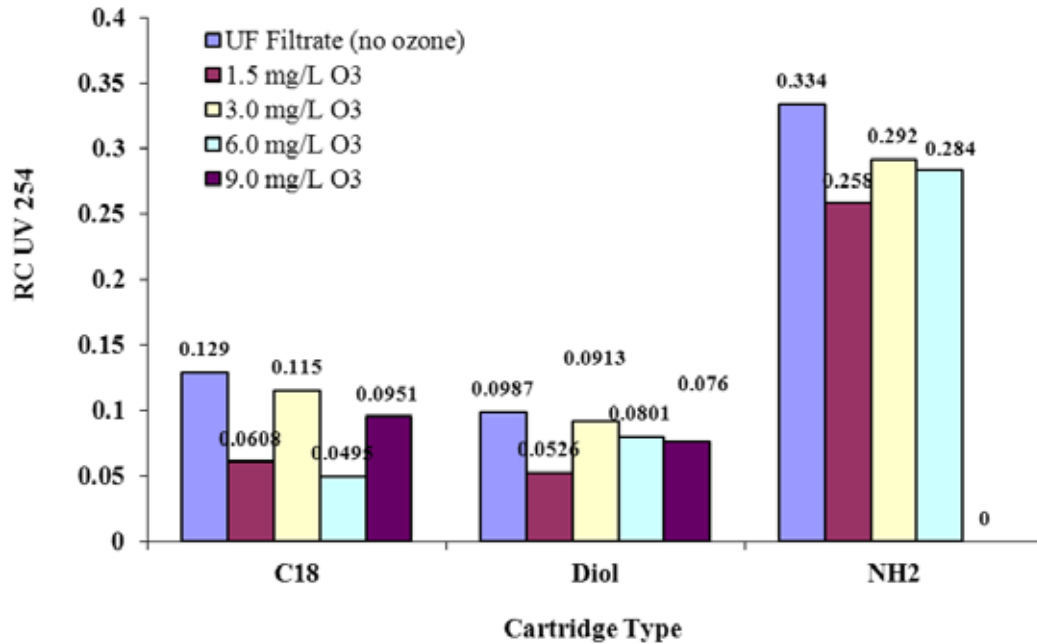


Figure 3.11. Polarity rapid assessment method analysis results for UF filtrate treated with various ozone doses.

3.3.3.2 Effects of UV and UV/H₂O₂ on EfOM UF Filtrate

To support continuous operation of the UF-UV/H₂O₂-RO train at WRF 2, investigation of the UV and UV/H₂O₂ impacts on EfOM was supplemented with a bench-scale collimated beam reactor setup, described in Chapter 2. These experiments evaluated UV doses of 400 and 1000 mJ/cm² with and without addition of hydrogen peroxide. Table 3.6 shows changes in the UV₂₅₄ and SUVA for bench-scale and pilot-scale UV experiments with and without the use of hydrogen peroxide, whereas Table 3.7 shows the results of FRI and FI.

Table 3.6. Changes in UV₂₅₄ of UF Filtrate When Treated with Various Doses of UV and UV/H₂O₂

Source Water	UV Dose (mJ/cm ²)	H ₂ O ₂ Dose (mg/L)	UV ₂₅₄ (cm ⁻¹)	DOC (mg/L)	SUVA (L·m ⁻¹ ·mg ⁻¹)
UF-F bench scale	0	0	0.100	5.0	2.0
UF-F bench scale	400	0	0.091	5.1	1.8
UF-F bench scale	400	5	0.084	5.0	1.7
UF-F bench scale	400	10	0.082	5.0	1.6
UF-F bench scale	1000	0	0.085	5.1	1.7
UF-F bench scale	1000	5	0.073	5.0	1.5
UF-F bench scale	1000	10	0.067	4.8	1.4
UF-F pilot scale	0	0	0.102	5.1	2.0
UF-F pilot scale	1000	5	0.081	4.9	1.7

Table 3.7. Fluorescence Regional Integration of Samples from UF Filtrate Treated with Various UV and UV/H₂O₂ Doses

	UV Dose	UV/H ₂ O ₂ Dose	I	II	III	Φ _T	FI
UF-F bench scale	0	0	10,737	14,135	5353	30,226	1.65
UF-F bench scale	400	0	13,745	15,912	5868	35,525	1.58
UF-F bench scale	400	5	8380	12,922	4882	26,183	1.55
UF-F bench scale	400	10	6259	11,203	4383	21,844	1.54
UF-F bench scale	1000	0	10,140	14,707	5647	30,494	1.56
UF-F bench scale	1000	5	5537	10,521	4099	20,157	1.51
UF-F bench scale	1000	10	3719	8169	3230	15,118	1.48
UF-F pilot scale	0	0	9182	12,438	4862	26,482	1.64
UF-F pilot scale	1000	5	6865	9564	3845	20,274	1.58

These results indicate that quantifiable impacts on EfOM through UV and UV/H₂O₂ can be achieved, albeit at relatively high UV doses. The addition of hydrogen peroxide strongly affected the overall effectiveness of UV treatment on the EfOM matrix. On the basis of the fluorescence results, a UV/AOP of 400 mJ/cm² and 10 mg/L appeared to provide impacts on the EfOM similar to those provided by a UV/AOP condition of 1000 mJ/cm² and 5 mg/L, as highlighted in Figure 3.12.

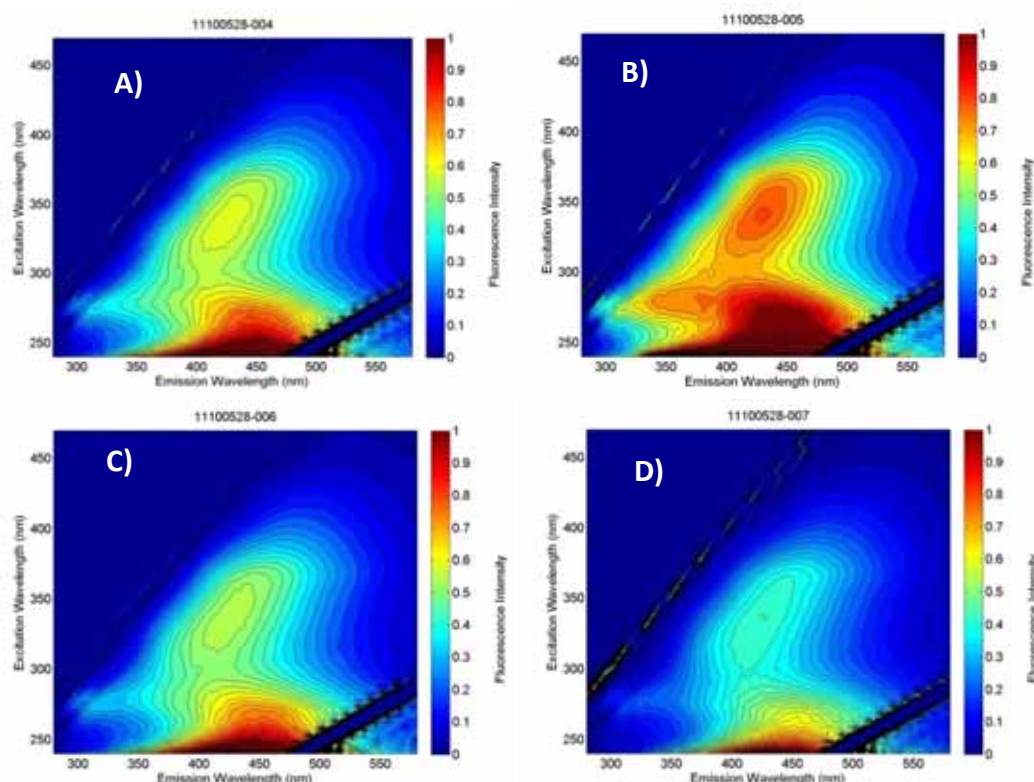


Figure 3.12. Fluorescence EEM spectra of (A) UF filtrate after 400 mJ/cm² and 10-mg/L H₂O₂; (B) UF filtrate after 1000 mJ/cm² (no H₂O₂); (C) UF filtrate after 1000 mJ/cm² and 5-mg/L H₂O₂; (D) UF filtrate after 1000 mJ/cm² and 10-mg/L H₂O₂.

3.3.4 Oxidation Impacts on EfOM in MBR Filtrate

3.3.4.1 Ozone Demand/Decay Study of MBR Filtrate

Ozone demand tests on the MBR filtrate were conducted by using the HiPOx[®] pilot skid, which is equipped with multiple sample ports allowing an operator to collect samples representing water samples with unique residence time. The residence times were calculated on the basis of feed flow and pipe(s') diameters. The ozone residual was measured by using the indigo method that was described previously (Wert et al., 2009). Figure 3.13 shows the ozone demand decay curve for the MBR filtrate, although Table 3.8 shows changes in UV₂₅₄ and UV₂₈₀ during various ozone/hydrogen peroxide treatments. Both ozone and ozone/peroxide treatments were effective at reducing the UV₂₅₄ and SUVA, indicating a decrease in aromaticity of the EfOM. The observed changes in UVA allow for the establishment of a correlation between the decrease in UVA and applied ozone dose. Figure 3.14 shows a plot of natural log of UV₂₅₄ versus applied ozone dose.

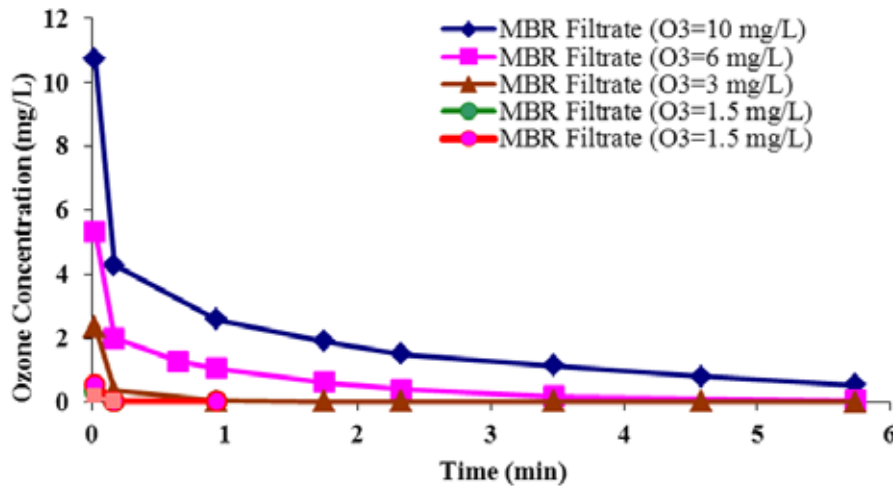


Figure 3.13. Ozone decay curves in MBR filtrate at various ozone doses.

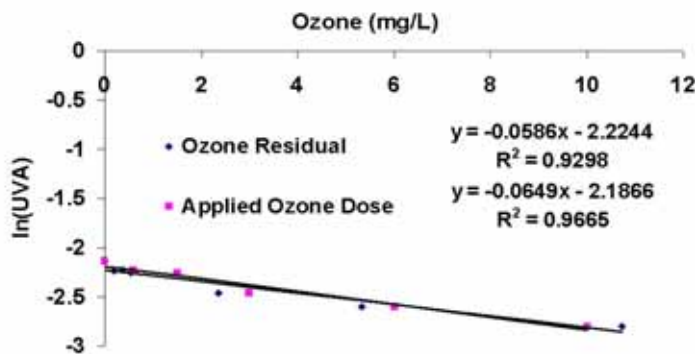


Figure 3.14. UV₂₅₄ plotted versus measured ozone residual and applied ozone dose.

Table 3.8. Changes in UV₂₅₄ and UV₂₈₀ of MBR Filtrate Treated with Various Doses of Ozone and Hydrogen Peroxide

Sample	Ozone Dose (mg/L)	H ₂ O ₂ Dose (mg/L)	DOC (mg/L)	UV ₂₅₄ (cm ⁻¹)	UV ₂₈₀ (cm ⁻¹)	SUVA (L·m ⁻¹ ·mg ⁻¹)
MBR influent	0	0	35.0	0.377	0.279	1.1
MBR filtrate	0	0	5.8	0.112	0.083	1.9
MBR filtrate	0.6	0	6.0	0.100	0.072	1.7
MBR filtrate	0.6	0.2	6.5	0.121	0.089	1.9
MBR filtrate	1.5	0	6.0	0.096	0.067	1.6
MBR filtrate	1.5	0.5	6.5	0.110	0.078	1.7
MBR filtrate	3	0	6.0	0.086	0.057	1.4
MBR filtrate	3	1.1	6.5	0.091	0.060	1.4
MBR filtrate	6	0	6.1	0.072	0.045	1.2
MBR filtrate	6	2.1	6.4	0.076	0.048	1.2
MBR filtrate	10	0	6.1	0.072	0.045	1.2
MBR filtrate	10	3.5	6.3	0.060	0.032	0.9

For the sake of brevity, the fluorescence data are summarized in tabular format on the following page. The FRI results and changes in FI are shown in Table 3.9. As was similar for results presented in earlier sections, the sum of the integrated volumes, Φ_T , and individual regions of the EEMs decreases with an increase in oxidation treatment, indicating less-aromatic and less-hydrophobic EfOM after oxidation.

Table 3.9. Fluorescence Regional Integration on MBR Filtrate Treated with Various Doses of Ozone and Hydrogen Peroxide

Sample	Ozone Dose (mg/L)	H ₂ O ₂ Dose (mg/L)	I	II	III	Φ_T	FI
MBR influent	0	0	27,681	19,587	6370	53,638	1.34
MBR filtrate	0	0	9378	12,691	4920	26,988	1.34
MBR filtrate	0.6	0	6501	8332	2922	17,755	1.33
MBR filtrate	0.6	0.2	7444	10,030	3979	21,454	1.34
MBR filtrate	1.5	0	5682	7410	2643	15,734	1.26
MBR filtrate	1.5	0.5	5844	7821	2943	16,608	1.31
MBR filtrate	3	0	4028	5568	2058	11,654	1.21
MBR filtrate	3	1.1	3252	5067	2014	10,332	1.24
MBR filtrate	6	0	1936	3489	1366	6791	1.22
MBR filtrate	6	2.1	1425	3351	1416	6192	1.25
MBR filtrate	10	0	948	2564	969	4481	1.23
MBR filtrate	10	3.5	655	2084	947	3686	1.35

3.3.4.2 Size Exclusion Chromatography Analysis of MBR Filtrate Treated with Ozone and Ozone/Peroxide

The overlaid chromatograms for MBR filtrate treated with various ozone and ozone/peroxide doses are shown in Figure 3.15. As reported in previous sections, the associated decrease in UVA that was due to oxidation resulted in an overall decrease of the peak intensity of all the

peaks as shown in Figure 3.15. The overall decrease in UVA did not provide the basis for drawing any firm conclusions about changes in the distribution of molecular weight of the EfOM based on visual inspection (shorter retention time = higher molecular weight; longer retention time = lower molecular weight).

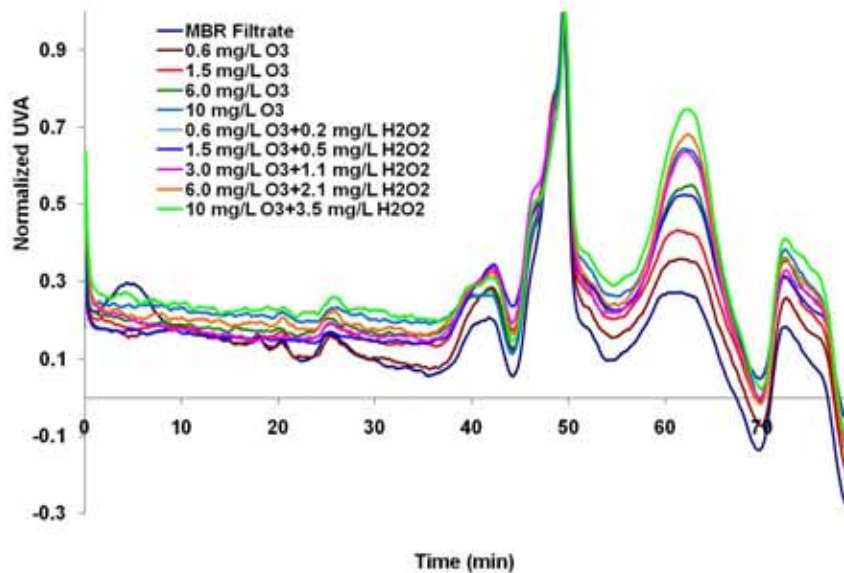


Figure 3.15. Size exclusion chromatography–UV overlaid chromatograms for MBR filtrate samples treated with various ozone and ozone/hydrogen peroxide doses.

However, using a concept demonstrated by Gregory V. Korshin from the University of Washington (personal communication, unpublished data), a mathematical basis for interpreting the SEC chromatograms was attempted. The individual peak heights from the chromatogram can be normalized by the most intense peak, for example, thereby allowing one to evaluate proportional changes in the rest of the peaks. Similarly, changes in the relative ratios of the chromatographic peaks can be normalized to the highest-molecular-weight peak (e.g., retention time = 42 min in Figure 3.15), or the data can be normalized to the lowest-molecular-weight peak (e.g., retention time = 72.5 min in Figure 3.15). By presenting the data in this manner, it is easier to show the trends in the molecular weight distribution of the EfOM before and after oxidation. Figure 3.16 and Figure 3.17 show trends in molecular weight during oxidation of EfOM by ozone and ozone/peroxide.

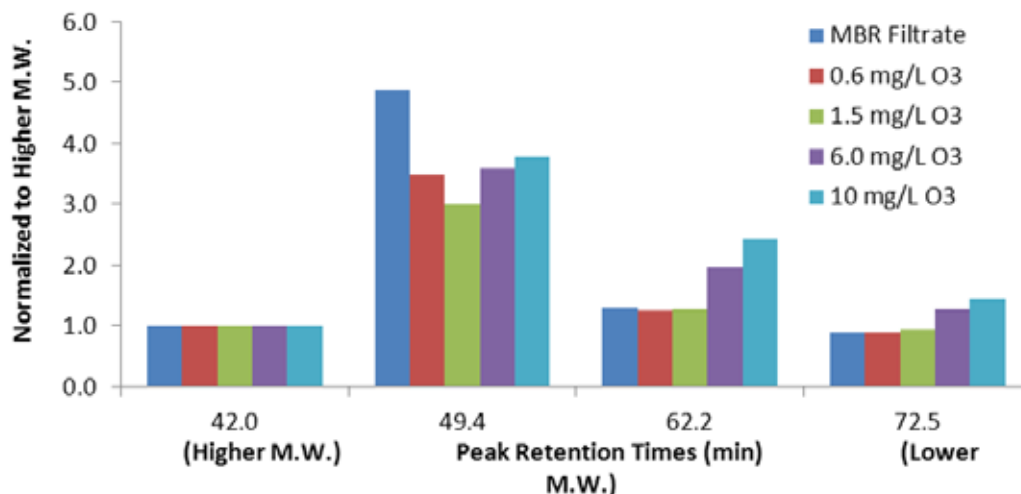


Figure 3.16. (Ozone alone) Overlaid size exclusion chromatography–UV chromatograms normalized by higher-molecular-weight peak at 42 min for MBR filtrate samples treated with various ozone doses.

Note: M.W.=molecular weight.

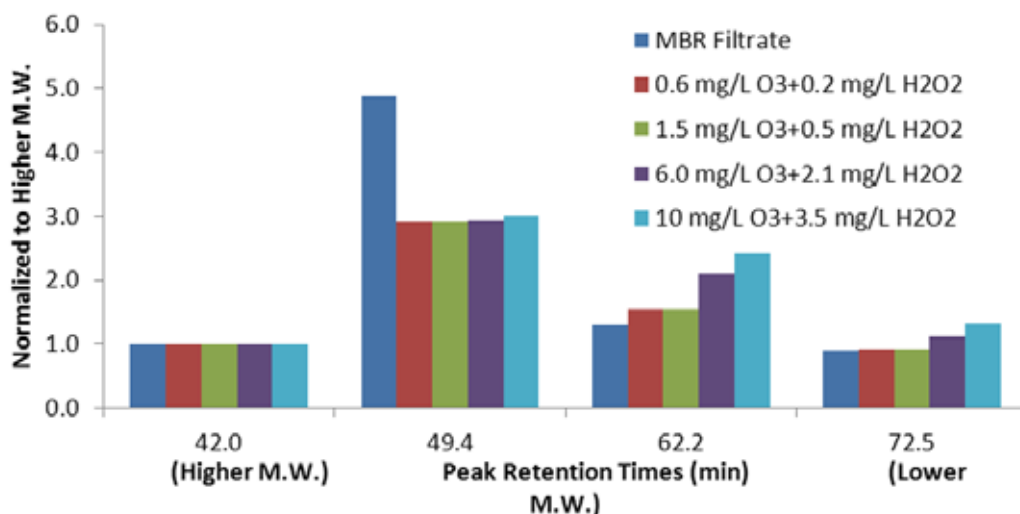


Figure 3.17. (Ozone + peroxide) Overlaid size exclusion chromatography–UV chromatograms normalized higher-molecular-weight peak at 42 min for MBR filtrate samples treated with various ozone/hydrogen peroxide doses.

Note: M.W.=molecular weight.

The results shown in Figure 3.16 and Figure 3.17 indicate an increase in lower-molecular-weight fractions (peaks at 62.2 min and 72.5 min) at higher ozone and ozone/hydrogen peroxide doses. Similarly, the data shown in Figure 3.18 and Figure 3.19 indicate a decrease in the higher-molecular-weight fractions (represented by peaks at 42 min and 49.4 min) at higher ozone and ozone/hydrogen peroxide doses. Although these data were not truly indicative of changes in molecular weight distribution of EfOM resulting from ozone or ozone/peroxide addition, the results did provide some insight into and possible support of the hypothesis that oxidation breaks up the higher-molecular-weight DOM, creating smaller, less-aromatic material.

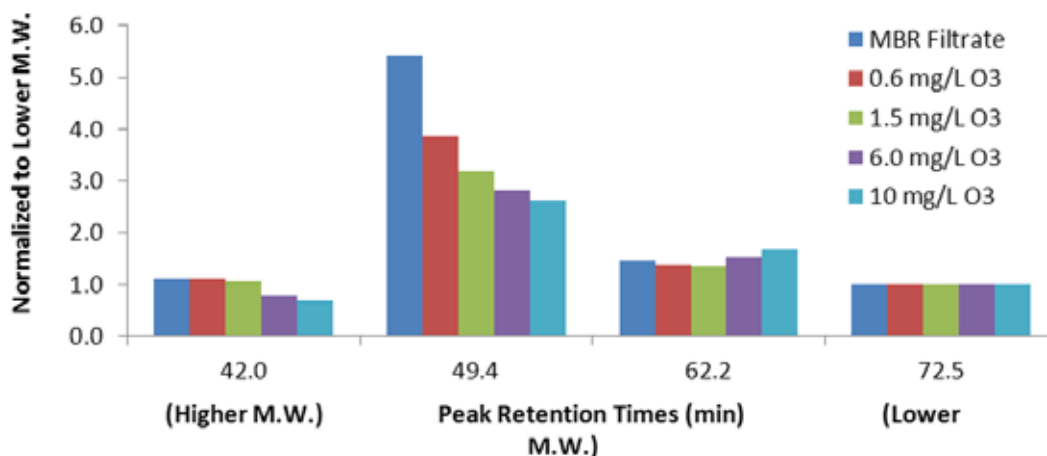


Figure 3.18. Overlaid size exclusion chromatography–UV chromatograms normalized by lower-molecular-weight peak at 72.5 min for MBR filtrate samples treated with various ozone doses.
Note: M.W.=molecular weight.

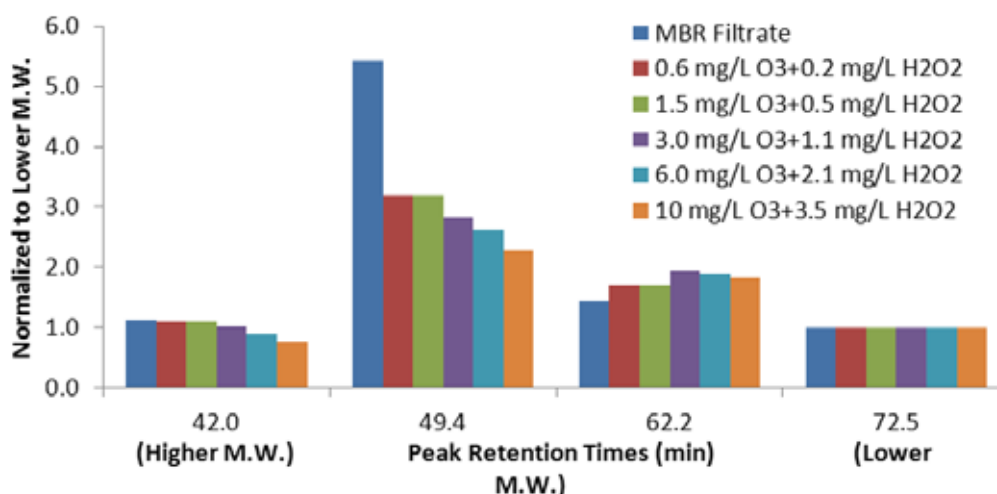


Figure 3.19. Overlaid size exclusion chromatography–UV chromatograms normalized by lower-molecular-weight peak at 72.5 min for MBR filtrate samples treated with various ozone/hydrogen peroxide doses.
Note: M.W.=molecular weight.

Further efforts to investigate molecular weight changes during oxidation of EfOM were made by using the SEC–TOC method. Figure 3.20 shows a size exclusion chromatogram of the MBR influent (primary effluent) and MBR filtrate samples made by using an on-line TOC detector. Significant transformations in both molecular weight and molecular functionality occurred during the biological treatment of the MBR. Note there also was reduction in the DOC concentration between the MBR influent (DOC = 40 mg/L) and MBR filtrate (DOC = 5.7 mg/L). With such a drastic change in DOC, the changes in the molecular weight distribution can easily be seen in Figure 3.20. However, when the MBR filtrate was treated with an ozone of 6.0 mg/L (O₃:DOC ~ 1.0), the changes in the molecular weight distribution, as shown by Figure 3.21, still are not easily discerned, even when one used the on-line TOC detector.

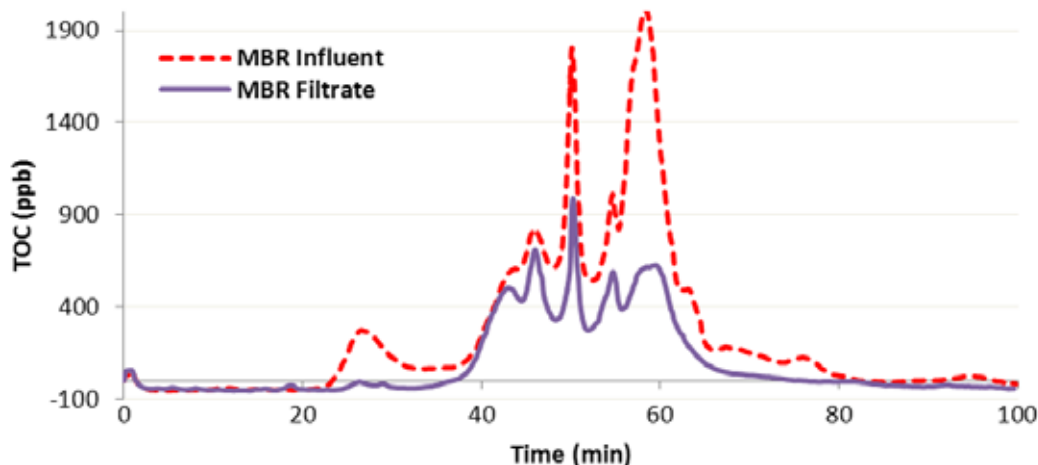


Figure 3.20. Size exclusion chromatogram with TOC detector of MBR influent and effluent samples.

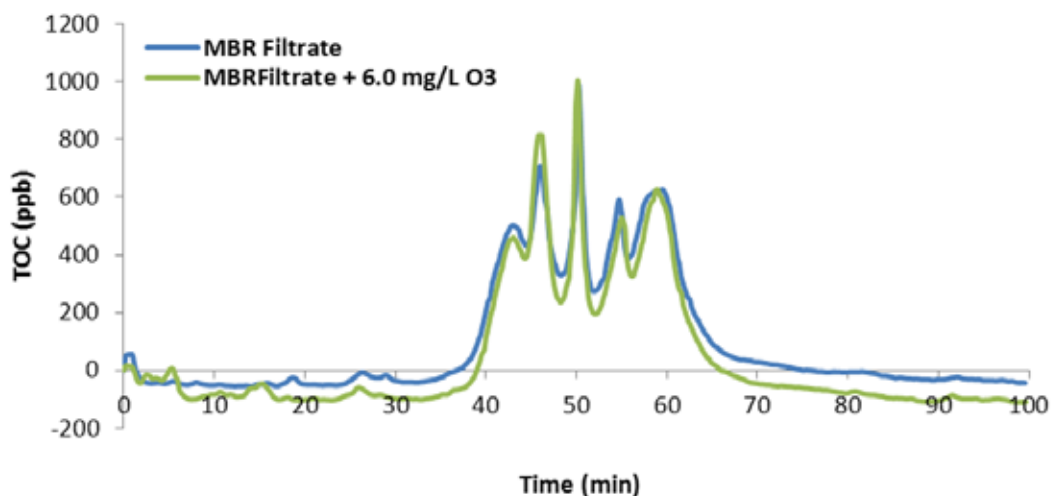


Figure 3.21. Size exclusion chromatogram with TOC detector of MBR effluent without and with ozone spiked at 6 mg/L (O_3 :TOC ~ 1.0).

In contrast to the SEC–UV analysis employed through the study, which showed a decrease in intensity of all of the peaks because of oxidation, SEC–TOC analysis did not reveal any additional information to support conclusive changes in molecular weight distribution. Thus, further improvements in the SEC methods as well as in sample preparation methods are needed in order to advance the knowledge of transformations occurring during oxidation of EfOM.

3.3.4.3 *Changes in Biodegradable Dissolved Organic Carbon in MBR Filtrate Due to Ozone and Ozone/Peroxide*

It has been reported that ozonation may result in an increase in AOC by about 0.1 mg/L (Ramseier et al., 2011). To investigate this, a BDOC method was employed on the various waters. Initially, control MBR filtrate samples (no ozone added) were spiked with sodium acetate as a surrogate for readily biodegradable organic compounds and were incubated at 30 °C over 28 days to validate the method. As indicated by Figure 3.22, in most of the tested

samples, the BDOC level reached a plateau after 5 days of incubation. However, for determination of BDOC values greater than 3.0 mg/L, an incubation time of at least 7 days was needed. The precision of the measurements was nominally ± 0.1 mg/L (based on the method's reporting limit), and thus differences in BDOC results of <0.3 mg/L were deemed not to be significant by using the current method. On the basis of work by Ramseier et al. (2011), this limitation may have created a situation where smaller changes in BDOC were not detected. Table 3.10 provides a summary of BDOC results from MBR filtrate samples treated with various ozone and ozone/hydrogen peroxide doses. Based on the variability in the data and changes in BDOC that was due to oxidation of less than 0.3 mg/L, the results were inconclusive. The use of BDOC can be effective for monitoring the biostability of the MBR filtrate. However, because of the current method's relatively high method reporting limit, the use of only a BDOC measurement may overestimate the relative biostability of the MBR filtrate. Other parameters such as AOC or a more precise BDOC method may need to be monitored as well.

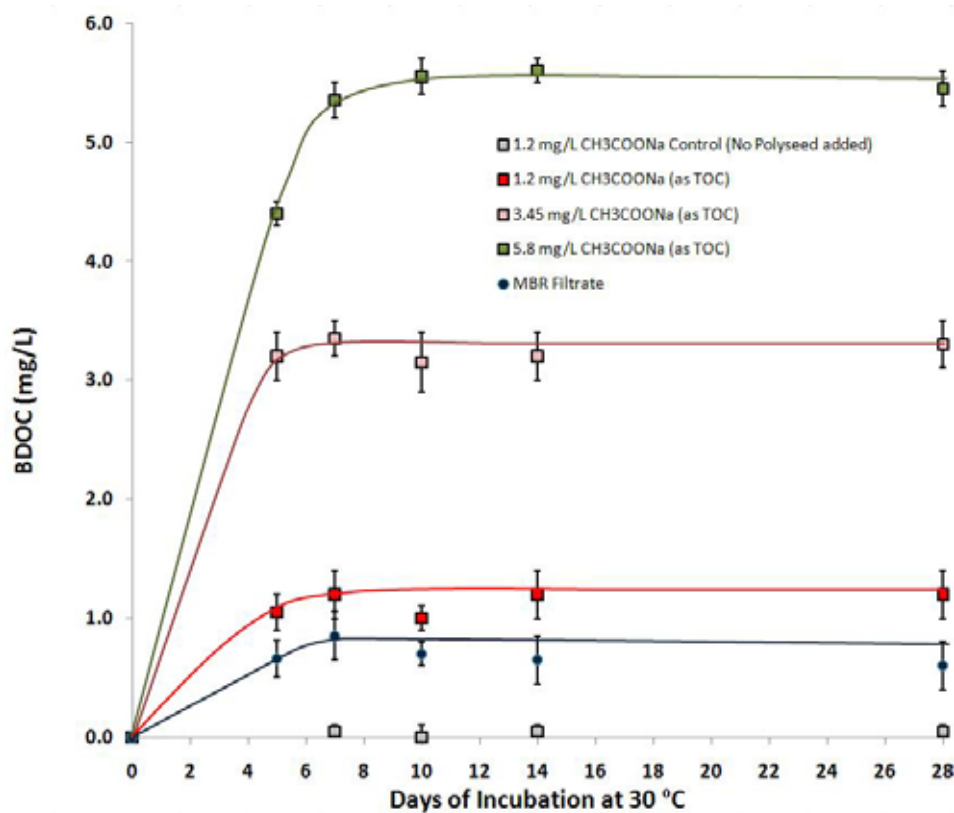


Figure 3.22. Biodegradable dissolved organic carbon over time in control samples spiked with sodium acetate and MBR filtrate.

Note; Error bars are based on duplicate sample.

Table 3.10. Summary of Biodegradable Dissolved Organic Carbon Results for MBR Filtrate Samples Treated with Various Ozone and Ozone/Hydrogen Peroxide Doses

Ozone Dose (mg/L)	H ₂ O ₂ Dose (mg/L)	BDOC ₅ (mg/L)
0.0	0.0	0.8
0.0	0.0	0.6
0.6	0.0	0.7
0.6	0.2	0.7
1.5	0.0	0.7
1.5	0.5	0.8
3.0	0.0	0.9
3.0	1.1	1.0
6.0	0.0	0.8
6.0	2.1	0.8
10.0	0.0	1.0
10.0	3.5	0.9
Mean		0.81
SD		0.12
Relative SD		15.3

3.4 Conclusions

Reductions in UV_{Ae} and fluorescence EEM volume as a result of ozone and ozone/peroxide reactions with DOM were observed and documented. These effects were attributed to loss of chromophoric and fluorophoric functional groups in the DOM. Furthermore, a decrease in SUVA provided additional evidence of decreases in the overall aromaticity of the DOM during oxidation. Results from PRAM were inconclusive on whether the polarity of DOM constituents was significantly affected during oxidation, though this result likely stems from the measurement being based on optical (UVA) properties of the DOM that were shown to change after oxidation. Having a measurement independent of optical properties of DOM would greatly improve the ability to detect changes in polarity and molecular weight distribution as a result of oxidation. Similarly, SEC showed that oxidation impacts various molecular weights of DOM, though precise changes in molecular weight distribution could not be determined because of limitations of the current analytical methods.

The established relationship between UV₂₅₄ and applied ozone dose for a specific water provides a useful tool for back-calculating what the ozone dose may have been during an operational period when the dissolved ozone levels were not monitored. In other words, for a given water, one should be able to determine the relationship (equation) of ozone dose to UV₂₅₄ under controlled conditions and should then be able to use UV₂₅₄ during normal operation to back-calculate the actual (applied) ozone dose at any given time. The project team used this concept to monitor the consistency of the ozone treatments throughout the pilot process. Similarly, UV/peroxide treatments reduced UV₂₅₄ and fluorescence, thus allowing monitoring of consistency of the UV oxidation. Appendix B shows results from monitoring changes in absorbance and fluorescence during the pilot testing of the project.

Chapter 4

Bench-Scale Evaluation of Preoxidation Impacts on RO Membrane Fouling

4.1 Chapter Overview

The purpose of the bench-scale portion of this project was to demonstrate the feasibility and effect of applying ozone, ozone/peroxide, UV, and UV/peroxide upstream of RO membranes as a means of controlling organic fouling during reuse applications. The changes observed in the organic matter (EfOM and NOM) described in Chapter 3, even at low ozone doses, indicated that there was an observable reduction in the aromaticity (and hydrophobicity) of the organic matter and a smaller proportion of biopolymers such as proteins and microbial by-products, all of which have been implicated in membrane fouling (Cho et al., 1998; S. Lee et al., 2005; Yoon et al., 2005; Shon et al., 2006). From an energy perspective, the implication of the effect on EfOM from low ozone doses without peroxide could be indicative of a potential process improvement with minimal energy inputs. An ideal RO membrane pretreatment process would be able to improve operational performance, minimize fouling, and minimize the pressure (energy) required to maintain a constant flux over time. Thus, the membrane fouling tests were started with low ozone and ozone/peroxide doses and were then compared with control water (no ozone) and higher ozone doses as a proof of concept and to determine the range of operating conditions for the pilot-scale tests described in later chapters.

4.2 Experimental Setup

4.2.1 Flat Sheet Membrane Test System

Two side-by-side GE Osmonics Sepa-CF cross-flow membrane flat sheet cell holders were used to process the raw and oxidized test waters. The effective membrane area in the membrane unit was 140 cm². The membrane selected for this study was the ESPA-2 membrane, generously provided by Hydranautics. All experiments were operated in batch mode whereby all the retentate and permeate were returned to the feed water reservoir at ambient temperature, which was monitored and recorded throughout the test. Prior to introduction of the test water, each membrane was equilibrated under pressure (approximately 100–160 psi) overnight by using laboratory-grade (DI) water chilled with an immersion chiller to 20 °C (Thermo Scientific). At the end of the equilibration period, the feed line was switched to the test water and the pressure was adjusted to achieve the desired permeate flow rate of 6 to 10 mL/min, depending on the water quality and the expected duration of the fouling experiment. During preliminary testing for the CRW tests, the membrane cells were operated under constant pressure and variable flux conditions. However, the configuration was changed to operate under constant flux, as this is typically how a real-world RO treatment plant would operate. All of the results reported later for CRW, MBR filtrate, UF filtrate, and tertiary-filtered/UV-treated tests were obtained from constant flux and variable pressure conditions. The retentate flow rate was adjusted to 1000 to 4700 mL/min and permeate fluxes were adjusted to a constant flux of 12 to 25 gal per sq ft per day (gfd) (flux was consistent between cells for each experiment). Each membrane test was allowed to continue for up to a maximum of approximately 200 h, depending upon the

severity of observed fouling (as measured by the increase in pressure required to maintain the desired flux). The permeate flow rate was measured volumetrically and feed pressure was adjusted to maintain constant flux for a given experiment. In all cases, conductivity, TDS, oxidation-reduction potential (ORP), pH, and temperature were measured for both the system feed and permeate in order to monitor membrane integrity. Data from flat sheet membrane tests were transformed by using specific flux for surface water and temperature-corrected specific flux (TCSF, J in Equation 4.1) by using Equations 4.1 through 4.6, consistent with previously published methods (Xu et al., 2006).

$$TCSF, J = \frac{Flux \times TCF}{NDP} \quad (4.1)$$

$$Flux = \frac{Q \text{ (gpd)}}{Area \text{ (ft}^2\text{)}} \quad (4.2)$$

$$TCF = e^x \quad (4.3)$$

$$x = 2700 \times \left(\frac{1}{Ta + 273.15} - \frac{1}{298.15} \right) \quad (4.4)$$

$$NDP = \frac{P_f + P_c}{2} - P_{osmotic} \quad (4.5)$$

$$P_{osmotic} = (C_f - C_p) \times 0.01 \quad (4.6)$$

Where J is calculated by dividing specific flux (permeate volume per membrane area) by the net driving pressure (NDP); TCF = the temperature correction factor. Equations 4.3 and 4.4 detail calculation of the temperature correction factor, where T_a is water temperature in degrees Celsius during each measurement and where 2700 is a correction factor for polyamide-type membrane. Calculated TCSF, J and normalized J/J_o were monitored during the tests. The NDP in pounds per square inch is calculated by using Equation 4.5, where P_f is the feed pressure, P_c is the concentrate (reject) pressure, and $P_{osmotic}$ is the osmotic pressure. Osmotic pressure in pounds per square inch is calculated by using the difference in the concentration of salts (milligrams per liter) between feed and permeate multiplied by an approximation factor (0.01).

4.2.2 Application of Preoxidation Technologies for Flat Sheet Tests

For the ozone and ozone/peroxide tests, a series of doses and combinations were applied to CRW prefiltered through 5- μ m-pore size cartridge filters at DWTP 1 and through MBR filtrate from WRF 1 by using a HiPOx[®] reactor skid, with ozone-to-dissolved organic carbon ratios of approximately 0.25 to 1.75. It should be noted that, for CRW tests, because of the likelihood of ozone residual persisting beyond the 6 min of contact time in the HiPOx[®] reactor, calcium thiosulfate was added at the end of the reactor to quench any residual ozone. Furthermore, conductivity (and TDS), pH, ORP, and temperature were monitored for all tests to ensure that the integrity of the RO membranes had not been compromised during the tests from any residual ozone or chlorine that might have been present. For each test, the control water (no preoxidation) was collected shortly before (within 30 min) the ozone-treated water was collected. Thus, for any given test, one ozone dose would be tested against one paired control water sample. Flat sheet membrane tests were commenced no later than 48 h after collection of the waters.

Tertiary effluent from the full-scale facility WRF 2 and pilot-scale UF filtrate were used for investigation of the UV and UV/peroxide in bench-scale flat sheet testing. A pilot-scale UV reactor was run at various flow rates and power to produce various test scenarios. A working solution of 1 to 2% hydrogen peroxide and a variable flow chemical feed pump were used to spike the water prior to the inlet of the reactor. Test waters were collected in 65-gal batch tanks and were transported to the laboratory testing at DWTP 1. The test waters were spiked

with monochloramine at 2 to 6 mg/L as Cl₂ (formed in situ by dosing the 65 gal batch tanks with sodium hypochlorite followed by ammonium chloride) to control biological activity and maintained at above 2 mg/L as Cl₂ throughout the duration of the test (any residual hydrogen peroxide was consumed by addition of sodium hypochlorite). These flat sheet membrane tests were typically commenced several hours after collection of the waters.

4.3 Data from Flat Sheet Tests

4.3.1 Colorado River Water Tests

The results from the fouling tests using CRW are summarized later in Table 4.1 as paired tests (one control + one ozone or ozone/peroxide run simultaneously by using the same batch of source water). As observed from the change in specific flux shown in Table 4.1 as % change, ozone treatment and ozone/peroxide treatment of CRW were able to provide a better control of flux decline than the raw CRW alone (“control”) in these flat sheet tests. Although any of the ozone doses tested appeared to offer a potential fouling benefit over the control waters, there was much less noticeable difference between the 1.5-mg/L and the 3-mg/L ozone doses. As a proof-of-concept test, the CRW results supported the hypothesis that preoxidation would significantly reduce the rate of fouling of RO membranes during tests with wastewaters from MBR and UF filtrates and with tertiary effluent at WRF 1 and WRF 2.

Table 4.1. Comparison of Changes in Specific Flux (SF) after i Hours of Operation (SF_i), Targeted Flux, Initial Pressure (P₀), and Initial Specific Flux (SF₀) for Colorado River Water

Pair	Source Water/Experiment	Targeted Flux (gfd)	P ₀ (psi)	SF ₀ (gfd/psi)	SF _i (gfd/psi)	% Change	Time (i, h)
A	CRW + 1.5 mg/L O ₃	25	280	0.089	0.089	0%	71
A	CRW –Control A	25	290	0.086	0.027	-69%	65
B	CRW + 3-mg/L O ₃	25	240	0.100	0.100	0%	71
B	CRW –Control B	25	340	0.074	0.053	-28%	71
C	CRW + 3-mg/L O ₃	25	380	0.066	0.051	-23%	65
C	CRW + 1.5-mg/L O ₃	25	300	0.083	0.052	-37%	65
D	CRW + 3-mg/L O ₃ /H ₂ O ₂	25	280	0.089	0.066	-26%	72
D	CRW + 1.5-mg/L O ₃ /H ₂ O ₂	25	200	0.130	0.020	-85%	72

Note: % Change = $-(SF_0 - SF_i)/SF_0 \times 100$.

Source: Data originally printed by Stanford et al., 2011; reprinted by permission of Taylor & Francis.

Limited qualitative surface analysis of the fouled membranes from the CRW flat sheet membrane tests were analyzed at NIST in Gaithersburg, MD. For these analyses, flat sheet membranes were recovered from the cell holder, cut into 2-cm × 2-cm swatches, placed in laboratory-grade water, and shipped to NIST. Details of analysis are provided in Chapter 2.

Figure 4.1 shows ESEM images of a virgin ESPA-2 membrane and two other membranes after fouling experiments with CRW control and CRW + 3-mg/L ozone, indicating an obvious visual difference in the severity of fouling between the non-ozone-treated water and the ozonated water. Sessile drop analysis was also performed on the fouled membranes with results presented in Figure 4.2. Here, the three liquids (water, formamide, and diiodomethane) were used to assess the relative hydrophobicity of a membrane surface (Brant and Childress,

2002). Although the data indicate a noticeable, measurable change in the hydrophobicity of the membrane surface after fouling (for both ozone and control waters), they are inconclusive with respect to the quantifiable differences between treatments.

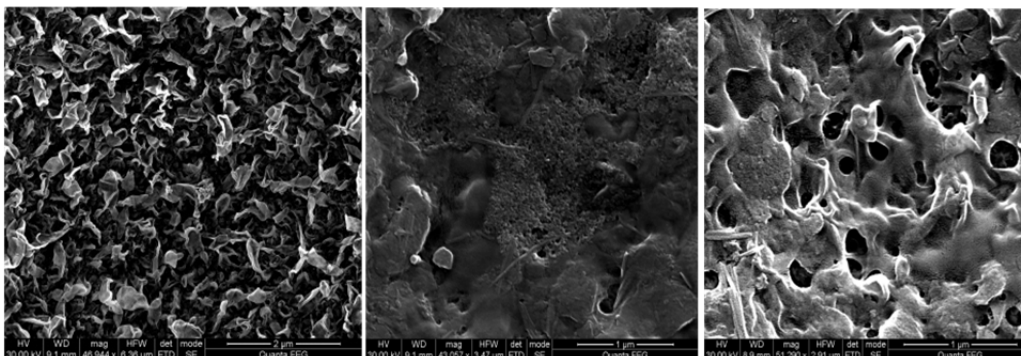


Figure 4.1. ESEM images from left to right: Virgin ESPA-2 membrane, ESPA-2 after 72-h fouling test with Colorado River water, and ESPA-2 membrane after 72-h fouling test with Colorado River water + 3-mg/L ozone.

Source: Data originally published by Stanford et al., 2011; reprinted by permission of Taylor & Francis.

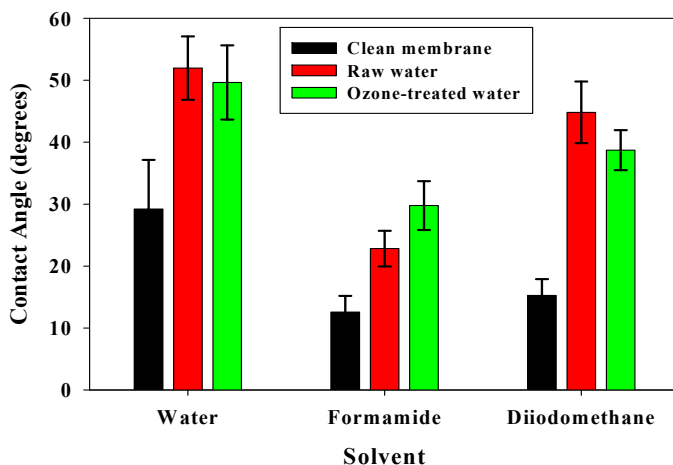


Figure 4.2. Contact angle measurements for clean and fouled ESPA-2 membranes (3-mg/L ozone dose and raw Colorado River water).

Note: The increased contact angle for fouled membranes vs. clean membrane indicates organic fouling and specific changes in membrane surface properties.

Although the sessile drop analysis was inconclusive, the ESEM and flat sheet membrane data pointed toward observable differences in membrane fouling, with and without oxidation as well as between oxidant doses. Thus, the preliminary results appeared to further support the hypothesis that oxidation can provide a benefit in reducing membrane fouling and were justification to move forward with additional flat sheet testing.

4.3.2 MBR Filtrate Pretreatment with Ozone and Ozone/Peroxide Tests (WRF 1)

The results from the fouling tests using MBR filtrate are summarized in Table 4.2 as paired tests (one control + one ozone or ozone/peroxide run simultaneously using the same batch of

source water); curves showing change in normalized temperature-corrected flux (J/J_0) over time are shown in Figures 4.3 through 4.5. As observed from the change in specific flux in Table 4.2, ozone and ozone/peroxide were able to provide a better control of flux decline than the raw MBR alone (“control”). Further, none of the preoxidation strategies resulted in changes in salt rejection different from those observed in the control waters, indicating that membrane performance or rejection was not adversely affected (data not shown).

The difference in flux decline between the 1.5-mg/L and 6-mg/L ozone doses is less apparent (Pair F), though the curves appear to be offset from each other (Figure 4.4). Although there did appear to be somewhat less flux decline in the 6-mg/L ozone dose than in the 1.5-mg/L ozone dose, both RO systems were able to operate for 100 h (6 mg/L) and 80 h (1.5 mg/L) prior to experiencing greater than 20% change in specific flux, as is also indicated by a similar decrease in the normalized TCSF shown by Figure 4.4. In contrast to this, the MBR filtrate control and 3-mg/L ozone + peroxide dose experienced a 20% loss of flux decline within 20 to 30 h (“E” and “G” in Table 4.2; also Figures 4.3 and 4.5). Given that this result was unexpected, the test was repeated (and verified) a second time, including swapping the pump and cell holders to ensure no bias was present between the two feed systems and monitoring chloramine residual to ensure ample biofouling control. It is hypothesized that the ozone + peroxide system did not perform as well as the ozone alone because of the competition reactions between ozone/EfOM and ozone/peroxide. A recent review by van Geluwe et al. noted that the addition of hydrogen peroxide resulted only in modest improvement for removal of DOC, which highlighted the significance of direct ozone and DOM reactions in waters with DOC of >3.0 mg/L (Van Geluwe et al., 2011).

Table 4.2. Comparison of Changes in Specific Flux (SF) after i Hours of Operation (SF_i), Targeted Flux, Initial Pressure (P₀), and Initial Specific Flux (SF₀) for MBR Filtrate (MBR-F)

Pair	Source Water/Experiment	Targeted Flux (gfd)	P ₀ (psi)	SF ₀ (gfd/psi)	SF _i (gfd/psi)	% Change	Time (i, h)
E	MBR-F + 3-mg/L O ₃	12, 18	130	0.150	0.140	-7%	69
E	MBR-F + 3-mg/L O ₃ /H ₂ O ₂	12, 18	130	0.150	0.072	-52%	69
F	MBR-F + 6-mg/L O ₃	18	180	0.081	0.071	-12%	72
F	MBR-F + 1.5-mg/L O ₃	18	80	0.220	0.190	-14%	72
G	MBR-F + 3-mg/L O ₃	18	130	0.129	0.099	-23%	52
G	MBR-F	18	170	0.118	0.032	-73%	52

Note: % Change = $-(SF_0 - SF_i)/SF_0 \times 100\%$.

Source: Data originally published by Stanford et al., 2011; reprinted by permission of Taylor & Francis.

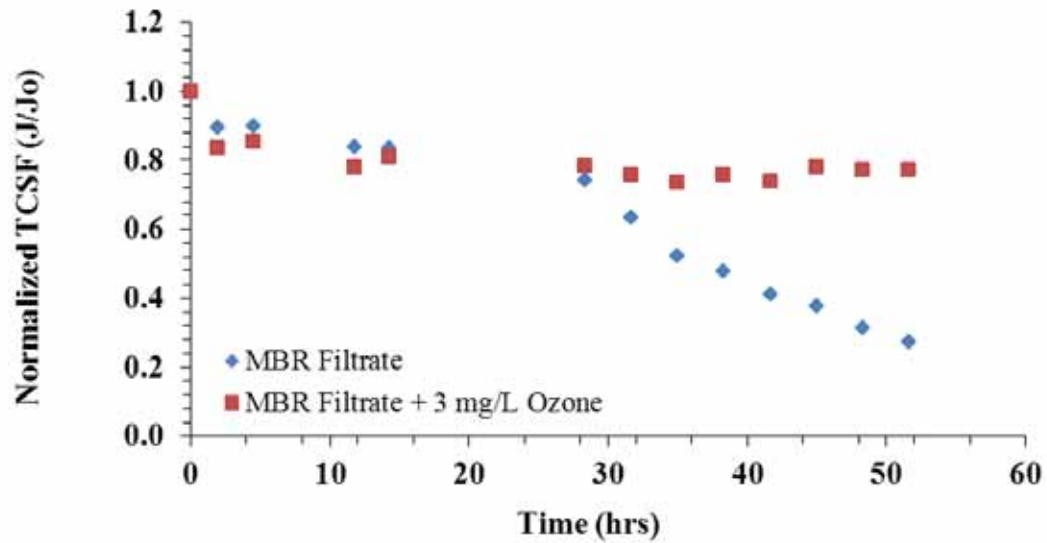


Figure 4.3. Change in normalized TCSF (J/J_0) in RO flat sheet tests using MBR filtrate and MBR filtrate + 3-mg/L ozone.

Source: Data originally published by Stanford et al., 2011; reprinted by permission of Taylor & Francis.

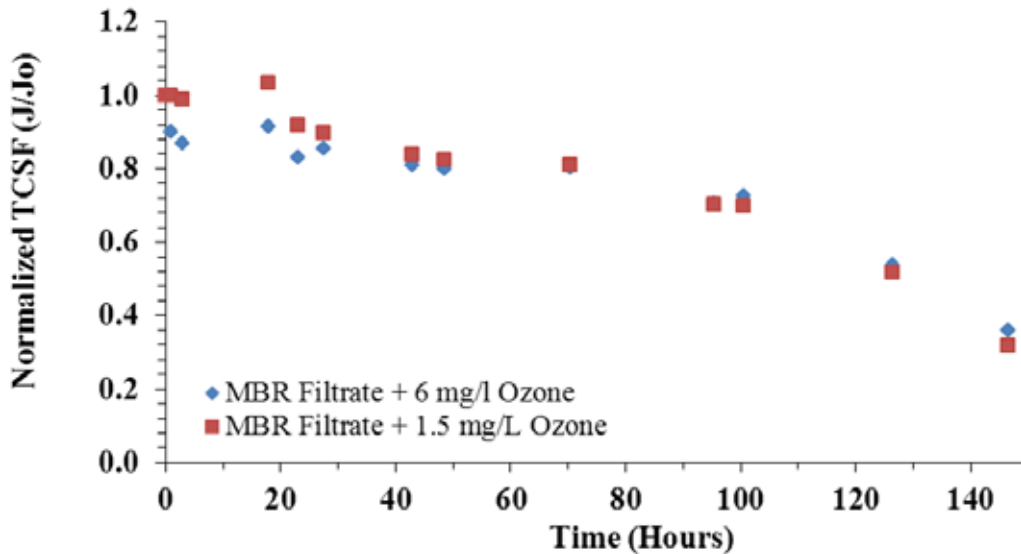


Figure 4.4. Change in normalized TCSF (J/J_0) in RO flat sheet tests using MBR filtrate treated with 1.5-mg/L ozone and 6-mg/L ozone.

Source: Data originally published by Stanford et al., 2011; reprinted by permission of Taylor & Francis.

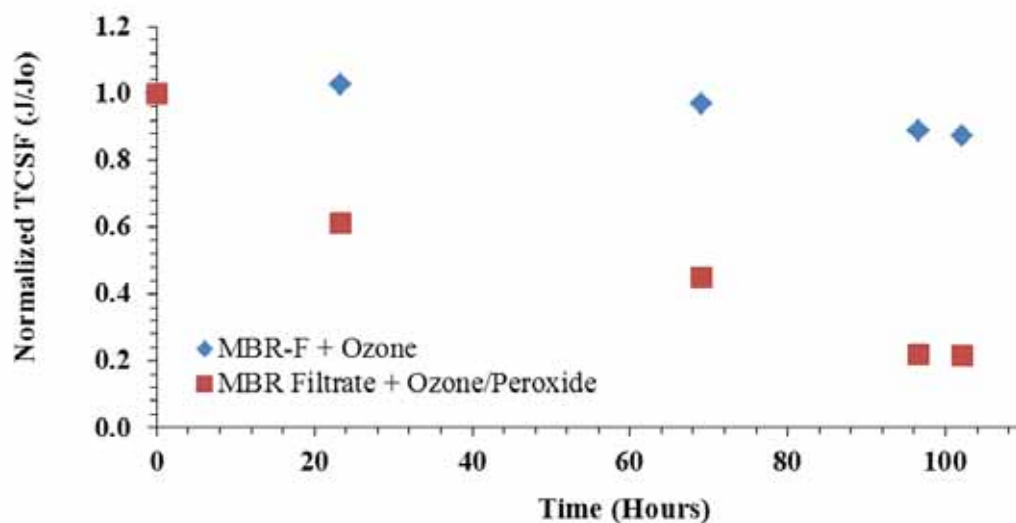


Figure 4.5. Change in normalized TCSF (J/J_0) in RO flat sheet tests using MBR filtrate treated with 3-mg/L ozone and 3-mg/L ozone + peroxide (0.5-mol ratio).

Source: Data originally published by Stanford et al., 2011; reprinted by permission of Taylor & Francis.

In comparison to ozone, the ozone/peroxide treatment in MBR filtrates resulted in a greater rate of flux decline than in the ozone-treated water. Thus, for the MBR filtrate used in this study, it was concluded that using ozone treatment at O_3 :DOC of approximately 0.50 (~3.0 mg of O_3 /L) resulted in the best method for minimizing organic fouling of RO membranes. Although this result indicates that peroxide may not be beneficial at low-ozone doses for filtrates tested in this study, it is not clear whether that relationship would continue at higher ozone/peroxide doses. Also, although reduced fouling was observed at ozone doses of 1.5 and 3.0 mg/L, using a higher ozone dose of 6.0 mg/L (O_3 :DOC ~ 1.0) did not result in additional reduction of the fouling. This finding may imply that preoxidation at a lower ozone dosing of O_3 :DOC of 0.50 may be sufficiently effective to reduce the organic fouling of RO membranes.

4.3.3 Tertiary Effluent and UF Filtrate Pretreatment with UV and UV/Peroxide Tests (WRF 2)

Additional flat sheet tests were performed on tertiary effluent and UF filtrate from WRF 2, with and without UV or UV/peroxide pretreatment. As observed in Chapter 3, UV alone had very little impact on EfOM and UV peroxide required high UV fluence to achieve the magnitude of impact observed with ozone. Thus, the initial flat sheet tests with UV and UV/peroxide were performed at high UV doses to determine whether low-dose testing would be necessary. Table 4.3 provides a summary of various UV and UV/peroxide treatments.

Table 4.3. Comparison of Changes in Specific Flux (SF) after i Hours of Operation, Targeted Flux, Initial Pressure (P₀), and Initial Specific Flux (SF₀) for Tertiary Effluent and UF Filtrate from WRF 2 Treated under Various UV and UV/Peroxide Conditions

Pair	Source Water/Experiment	Flux (gfd)	P ₀ (psi)	SF ₀ (gfd/psi)	SF _i (gfd/psi)	% Change	Time (i, h)
A	Tertiary effluent (control)	18	80	0.269	0.117	-57%	120
A	Tertiary effluent + UV (~ 2300 mJ/cm ²)	18	80	0.268	0.122	-55%	120
B	Tertiary effluent (control)	18	92	0.267	0.099	-63%	123
B	Tertiary effluent + UV (~ 5500 mJ/cm ²)	18	95	0.255	0.074	-71%	123
C	Tertiary effluent (control)	18	72	0.285	0.091	-68%	117
C	Tertiary effluent + UV/peroxide (~ 1900 mJ/cm ² + 7 mg/L H ₂ O ₂)	18	75	0.285	0.169	-41%	117
D	Tertiary effluent (control)	18	90	0.249	0.093	-63%	118
D	Tertiary effluent + UV/peroxide (~ 2500 mJ/cm ² + 10 mg/L H ₂ O ₂)	18	85	0.268	0.156	-42%	118
E	Tertiary effluent (control)	18	96	0.239	0.081	-66%	116
E	Tertiary effluent + UV/peroxide (~ 5500 mJ/cm ² + 10 mg/L H ₂ O ₂)	18	92	0.248	0.171	-31%	116
F	UF filtrate	18.5	75	0.272	0.219	-20%	190
F	UF filtrate + UV/peroxide (1000 mJ/cm ² /4.0 mg/L H ₂ O ₂)	18.5	80	0.257	0.190	-26%	190

Note: % Change = $-(SF_0 - SF_i)/SF_0 \times 100$.

Source: Data originally published by Pisarenko et al., 2011; reprinted by permission of International Desalination Association.

As the UV dose was increased from 2500 to approximately 5500 mJ/cm², the fouling was further reduced in contrast to the increase in ozone dose, where only slight improvement was observed (Table 4.3). However, using a less intensive UV/peroxide treatment at a UV dose of 1900 mJ/cm² provided a similar reduction in fouling. This finding potentially indicates that even a lower UV dose with addition of hydrogen peroxide may be effective at reducing the fouling. Without the addition of hydrogen peroxide, a UV-only treatment at similar doses did not introduce any significant benefit in reducing the fouling rate. Figure 4.6 shows overlaid changes in normalized permeate flux over time for the experiments with tertiary effluent with various UV and UV/peroxide treatments and UF filtrate with and without UV/peroxide at a more realistic UV dose of 1000 mJ/cm² and H₂O₂ dose of 4 mg/L (results also shown in Table 4.3).

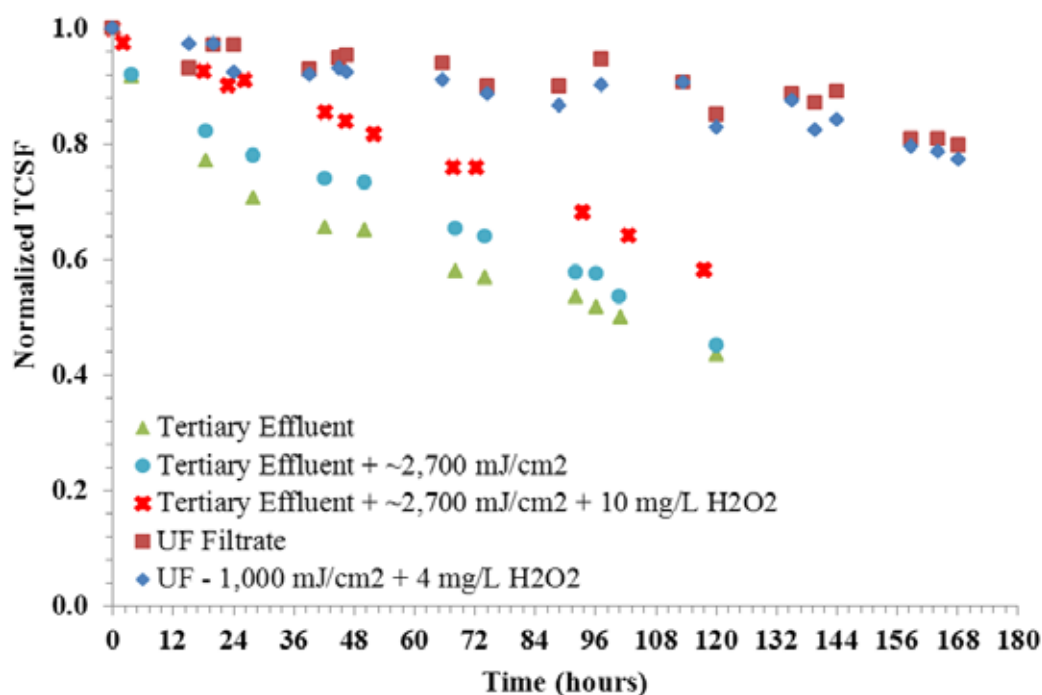


Figure 4.6. Overlaid changes in normalized RO permeate flux (J/J_0) over time for tertiary effluent with various UV and UV/peroxide treatments and UF filtrate with and without UV/peroxide preoxidation.

The results shown in Table 4.3 and Figure 4.6 indicate that UV/H₂O₂ can be an effective means of reducing RO fouling at higher UV doses. A 1000-mJ/cm² dose with 4-mg/L H₂O₂ gave no no observable benefit. However, because of the high energy requirements for delivering doses of even 400 mJ/cm², it was decided that the pilot study should be conducted at the 1000-mJ/cm² dose with a 4-mg/L H₂O₂ pretreatment as a compromise between typical conditions and observed fouling benefits at the higher UV doses.

In contrast to the tertiary filtered effluent from WRF 2, which consisted of full-scale secondary effluent from activated sludge treatment undergoing dual medium filtration, the UF water was able to show a noticeable reduction in the fouling rate compared to tertiary filtration, as seen in Figure 4.6. Not surprisingly, the observed benefits of membrane filtration as pretreatment to RO were correlated with associated reduction in SDI values. Where SDI values for tertiary effluent were typically too high to get a measurement based on 15, 10, or 5 min of testing and 500 mL of volume, the UF filtrate typically had SDI₁₅ values of <6 (results for SDI tests on the UF filtrate are shown in Appendix A, Table A-39). Thus, the combination of UF + 1000 mJ/cm² UV with 4-mg/L peroxide was used for the pilot-scale evaluation.

4.4 Results Summary and Conclusions

Results from the short-term, flat sheet testing indicated that both ozone- and ozone/peroxide-treated waters, even at the lowest ozone dose of 1.5 mg/L, fouled the membranes less than did the MBR filtrate and surface control waters tested in this study, although both treated and control waters maintained consistent levels of salt rejection throughout the tests. The results presented here indicated the potential benefit of ozone as a preoxidation step for the waters tested in this study using the flat sheet membrane setup. Although the results indicate the peroxide may not have been a beneficial addition at low ozone doses for the filtrates tested in

this study, it is not clear whether that relationship would be present at higher ozone and ozone/peroxide doses. On the basis of the flat sheet results, it was decided that ozone doses in the range of 1.5 mg/L to 3 mg/L would be tested during the pilot-scale experiments. Oxidation by a relatively high UV dose of approximately 5500 mJ/cm², without the addition of hydrogen peroxide, did not provide any benefit in reducing fouling of RO membranes. With the addition of peroxide, the UV treatments showed significant impact on EfOM, as reflected by changes in fluorescence and by reduction of RO membrane fouling. Similar reductions in fouling were observed when approximate UV doses of 1900 and 2500 mJ/cm² were used. However, it was observed that UF filtrate and a slightly more realistic UV dose of 1000 mJ/cm² and 4.0-mg/L H₂O₂ did not prove to be an effective means to reduce organic fouling, though the addition of UF improved fouling control over the tertiary-treated wastewater. The ineffectiveness of this pretreatment condition in reducing the fouling rate was not surprising, given the relatively low impact on EfOM at this UV dose as reported in Chapter 3.

From an energy perspective, choosing the lowest possible ozone dose or UV/peroxide treatment dose (additional tests are planned for the future) may provide a benefit in terms of lower overall energy consumption and potentially reducing cleaning and life cycle costs of the membranes. Thus, for pilot-scale tests an ozone dose of 1.5 to 3.0 mg/L without addition of hydrogen peroxide was chosen. Even though a UV dose of 1000 mJ/cm² is already relatively high in terms of energy, this condition was selected for pilot-scale testing as a compromise between the typical UV dose for AOP (400 mJ/cm²) and the observed benefits in fouling that occur after a dose of 2000 mJ/cm².

Chapter 5

Pilot-Scale Evaluation of the MBR-O₃-RO System at Water Reclamation Facility 1

5.1 Chapter Overview

The results from the bench-scale experiments and pilot-scale EfOM characterization showed that ozone can have a significant impact on the character of the organic matter and on the fouling rate of RO membranes. However, for bench-scale work, only a small area of RO membrane was used to test whether preoxidation had any effect on membrane fouling. Using a small surface area enabled the modification of the permeate flux in order to speed up or slow down fouling. The downside of this technique is that permeate flux conditions were more extreme than would be expected at pilot scale in order to force fouling to occur during the proof-of-concept tests. Therefore, this study was designed to incorporate pilot-scale evaluation of the process to determine if the bench-scale results were still observable at pilot scale and to provide a basis for understanding the larger feasibility of the preoxidation process. The general operating conditions for the pilot were based on the established industry experience in RO treatment (described in this chapter) with an operating flux of 14 gfd to mimic the lead elements in a full-scale system based on the pilot's 10-gfd conditions. This chapter describes the MBR-O₃-RO pilot conducted at Water Reclamation Facility 1 (WRF 1).

5.2 Description of MBR-O₃-RO Pilot-Scale Equipment

Primary wastewater from the Las Vegas Valley at WRF 1 was pumped to a pilot-scale HYDRASub® MBR system (Hydranautics) for further biological nutrient removal and filtration (described in Section 5.2.1). The MBR filtrate was collected in a 300-gal equalization tank and then was fed directly to a pilot-scale HiPOx® system (APTwater) for ozone or ozone/peroxide addition via a feed pump. The HiPOx® system was used in this study because it has received California Department of Public Health Title 22 certification for disinfection in wastewater and water reuse applications. The feed flow to the HiPOx® was split into two trains: one train bypassing ozone treatment—listed as “RO Train 2” (also referred to as the control)—and ozonated MBR filtrate—listed as “RO Train 1.” The pilot-scale RO skid (Hydranautics) was set up to run on two parallel trains, with an optional second stage. For this project both trains ran in parallel on single arrays of four to six ESPA-2-LD-4040 elements. The pilot equipment photographs are shown in Figure 5.1, although Figure 5.2 shows the process layout of the RO trains.

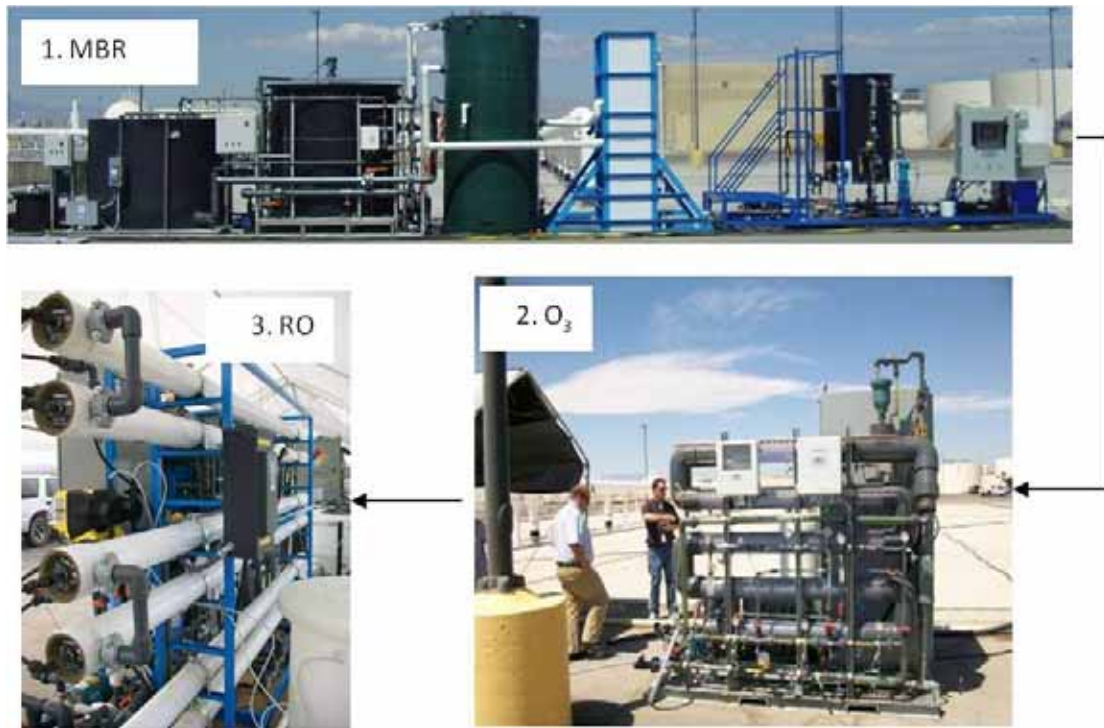


Figure 5.1. Photographs of MBR setup, HiPOx[®], and RO at WRF 1 (series of aeration and anoxic tanks in top panel; HiPOx[®] unit, bottom right panel; RO unit, bottom left panel).

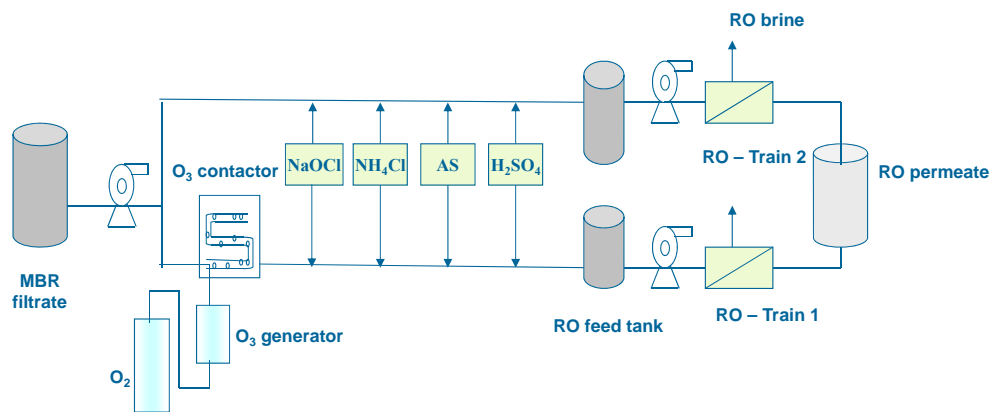


Figure 5.2. Process layout of MBR-RO and MBR-O₃-RO treatment trains.

Note: AS=antiscalant.

5.2.1 Description of MBR Equipment

The MBR pilot skid used hollow-fiber vacuum-type PVDF membranes with a reinforced core, an outer diameter of 2.8 mm, and a nominal pore size of 0.40 μm . According to the manufacturer's specifications, the PVDF membrane should have a high tensile strength and good chemical (particularly sodium hypochlorite) tolerance. The fibers had a dual layer coating of PVDF on the central reinforced core. The pilot unit contained a fine screen, an anoxic tank, an aerobic tank, a membrane tank, and a filtrate tank and full automation via programmable logic controller (PLC). There were two membrane modules placed inside the

membrane tank, but they were operated as a single component (no difference between the modules).

For this project, the MBR was operated at a mixed liquor suspended solids (MLSS) concentration of approximately 8000 mg/L, a solid retention time (SRT) of 12 days, and an HRT of 4 h. A process flow diagram (PFD) of the MBR system is shown in Figure 5.3. Typical operating parameters for the MBR pilot are shown in Table 5.1, whereas typical values for biological oxygen demand/chemical oxygen demand (BOD/COD), ammonia, and phosphorus in MBR feed and filtrate are shown in Table 5.2.

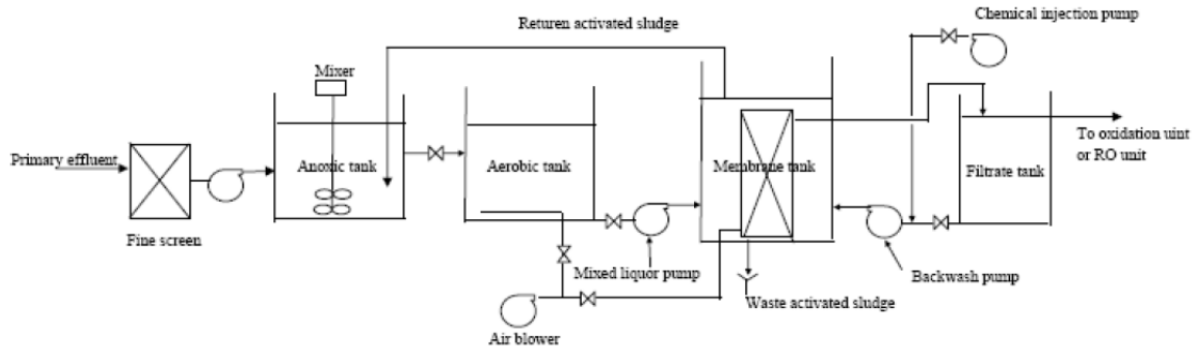


Figure 5.3. Process flow diagram of Hydranautics MBR and wastewater treatment skid.

Table 5.1. Typical Operating Parameters for Hydranautics MBR Pilot System

MBR Pilot	Parameter	Value	Unit
Fine screen	Opening	1	mm
Anoxic tank	Vol	1750	gal
	HRT	1.8	h
Aerobic zone	Total aerobic vol	3900	gal
	Total HRT	4.1	h
	SRT	12	days
	F:M ratio	0.1	kg of BOD/day/kg of MLSS
Membrane module 1	Membrane area	1345	ft ²
	Nominal pore size	0.40	μm
	Design flux @ 25 °C	19.6	gfd
Membrane module 2	Net flow	18.7	gpm
	Membrane area	807	ft ²
	Design flux @ 25 °C	19.6	gfd
	Net flow	6.2	gpm
Filtrate tank	TMP	2–4	psi
	Vol	300	gal

Table 5.2. Typical MBR Feed and Filtrate Water Quality for BOD/COD, Ammonia, and Phosphorus Removal

Parameter	Unit	MBR Feed	MBR Filtrate
COD	mg/L	200	<20
BOD	mg/L	100	<2
NH ₄	mg/L N	25	<0.1
TKN	mg/L N	36	<1.0
NO ₃ ⁻	mg/L N	<0.2	8.5
NO ₂ ⁻	mg/L N	<0.2	<1.0
Total P	mg/L	2.5	<1.0
Ortho P	mg/L	1.4	<0.5
UV ₂₅₄	cm ⁻¹	>0.3	<0.15
UV ₂₈₀	cm ⁻¹	>0.2	<0.12
Turbidity	NTU	>5	<0.1
DOC	mg/L	35	6.0

5.2.2 Description of HiPOx[®] Equipment

The HiPOx[®] pilot unit was capable of operating in a variety of modes and configurations, at flow rates of 10 to 25 gpm, and at ozone doses of up to 15 mg/L. The pilot was fed by using either liquid oxygen feedstock or high-purity (99.9%) oxygen gas to generate up to 10% ozone in dry gas. A concentrated hydrogen peroxide solution (34%) was purchased from EnviroTech Chemical Services (Modesto, CA), diluted to a 1 to 2% working solution, and injected immediately before ozone injection in the HiPOx[®] reactor during ozone/peroxide tests. In addition to the injection ports and static mixers, the HiPOx[®] pilot contained a 60-gal pipeline contactor with numerous sampling ports that allow sample collection at hydraulic residence times ranging from 0 to 5.5 min at a flow rate of 10 gpm. Ozone doses were applied at approximately 1.5 to 2 mg/L and 3.0 to 4.0 mg/L for two separate extended pilot-scale tests.

5.2.3 Description of RO Equipment

The pilot-scale RO skid (Hydranautics) was designed with parallel treatment trains by using ESPA-2-LD-4040 RO membranes. The operating parameters were determined by using IMS Design Software (IMSdb3 v.28; Hydranautics) in order to achieve an average flux of 14 gfd and a beta value of less than 1.2, consistent with the lead elements of a full-scale design of a 4:2 membrane array with seven elements per vessel and a recovery of 85%. Thus, the pilot skid was operated at 52% recovery by using a single array of six elements in order to mimic the lead elements of the full-scale system. The feed water was adjusted to pH 6.8 by using 50% sulfuric acid (Brenntag, Las Vegas, NV) and was spiked with bulk sodium hypochlorite (obtained from the wastewater treatment plant) and food-grade ammonium chloride (99%) (Brenntag) to form residual monochloramine. The residual monochloramine was measured frequently using a N,N-diethyl-p-phenylenediamine (DPD) test kit and maintained in the range of 2 to 6 mg/L as Cl₂. An antiscalant agent, Pretreat Plus (KingLee, San Diego, CA), was used based on a dose recommended by the manufacturer of 8 mg of the product per L in the RO concentrate. A PFD of the skid is shown in Figure 5.4; note that the optional second-stage vessel was not used in this project.

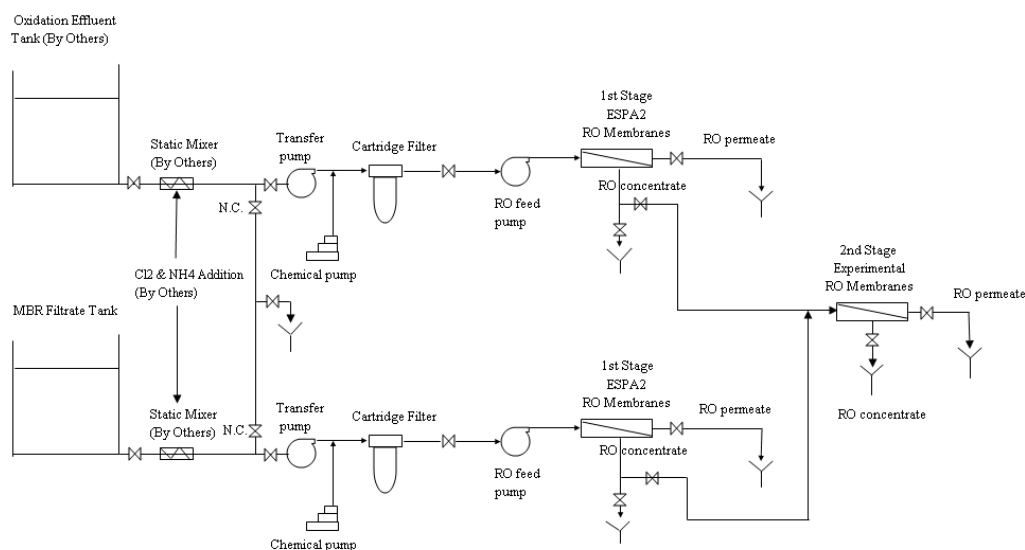


Figure 5.4. Schematic of Hydranautics twin RO system.

Note: System was operated by using two first stages in parallel, though the second stage was not used for this study.

The feed, reject, and permeate pressures; feed/permeate conductivity; temperature; and pH were recorded during each pilot visit. Periodic SDI measurements were also collected during various phases of the study by using a portable SDI-2000 test kit (Applied Membranes, Inc., Vista, CA). The water quality of the feed, concentrate, and permeate was tested periodically. Table 5.3 shows the target parameters and frequency. The feed pressures were adjusted manually by using the variable frequency drive on the RO pumps to maintain permeate flow and the recovery constant.

Table 5.3. Selected Analysis for RO Grab Samples and Frequency

Sampling Parameter(s)	Unit	Freq
TDS	mg/L	2/mo
TSS	mg/L	2/mo
Ca ²⁺ , Mg ²⁺ , Na ⁺ , K ⁺ , NH ₄ ⁺ , Ba ²⁺ , Sr ²⁺	mg/L	2/mo
Cl ⁻ , F ⁻ , NO ₂ ⁻ , NO ₃ ⁻ , SO ₄ ²⁻ , PO ₄ ³⁻ , TP,		
TN	mg/L	2/mo
Silica	mg/L	2/mo
Alkalinity	mg/L	2/mo
TOC	mg/L	2/mo
SDI		2/mo

Recorded operational data were input into ROData (ROData; Hydranautics) to determine various parameters such as NDP or the net force to drive the water across the membrane surface, specific flux, temperature correction factor (using 25 °C as reference), TCSF, STCn, and normalized differential pressure (dPn). In addition, changes in normalized TCSF (J/J_o) and % decrease in TCSF ($[1 - J/J_o] \times 100\%$) were plotted by using MS Excel 2010.

5.3 Results and Discussion

As previously stated, the intent of the project was to conduct the entire pilot-scale evaluation under the 14-gfd conditions for a 3000-h pilot test. Although there was significant difference in fouling between the control and the ozone-treated process trains (~10% difference in TCSF) after 2500 h, there was not as much fouling as had been expected. The test was extended through 3000 h to complete the planned testing schedule; then it was decided to increase the flux to see if a forced fouling could occur under more-challenging conditions. To force fouling, the flux was increased several times, with the hope to observe significant fouling and to evaluate further how preoxidation affected the cleaning frequency of the two trains. The results from each testing phase are outlined in sections later, beginning with the 3000 h of Phase I testing. A routine analysis of RO samples as well as of MBR filtrate and ozone effluent was established. A complete water quality log is provided in appendices A–C.

5.3.1 Phase I: 14-gfd Conditions

The RO pilot run at 14 gfd commenced on March 3, 2010, with six ESPA-2-LD-4040 elements per train, running at 52% recovery and 4.7 gpm of permeate flow and an accumulated 3000 h of run time by July 19, 2010. Table 5.4 shows the operating parameters for the RO pilot.

Table 5.4. 14-gfd RO Operating Parameters for 1 × 6 Array

Operating Parameter	Unit	Value
Feed flow rate	gpm	9.0
Permeate flow rate	gpm	4.7
Concentrate flow rate	gpm	4.3
Filtrate flux	gfd	14.1
Feed pressure	psig	99–141
Feed water temp	°C	22.2–34.6
Recovery	%	52

The operating data were entered into the Hydranautics tracking spreadsheet for calculation of various parameters such as specific flux and dP and to monitor for salt breakthrough in the event of any membrane integrity problems. Temperature corrections were used for calculation of TCSF and were plotted versus run time. Figure 5.5 shows the TCSF for the two treatment trains, with ozone showing a modest benefit over the control. Figure 5.6 provides details on the percent change in the TCSF decline between the two systems. The red dashed line represents a marker of 15% flux decline, at which point a membrane CIP event would typically be performed in a full-scale system.

Note that although the control water briefly crested over the 15% flux decline during early operation (Figure 5.6), the decision was made not to perform a CIP unless significant additional fouling was observed. Because the performance remained stable and slightly below the 15% line through approximately 2500 h, the project team decided not to perform a CIP. The MBR-O₃-RO train had also lost approximately 5% of initial flux during the first 2500 h, though. In total, the difference between the two trains was 10%, indicating that even at this flux the ozone pretreatment resulted in a smaller flux loss.

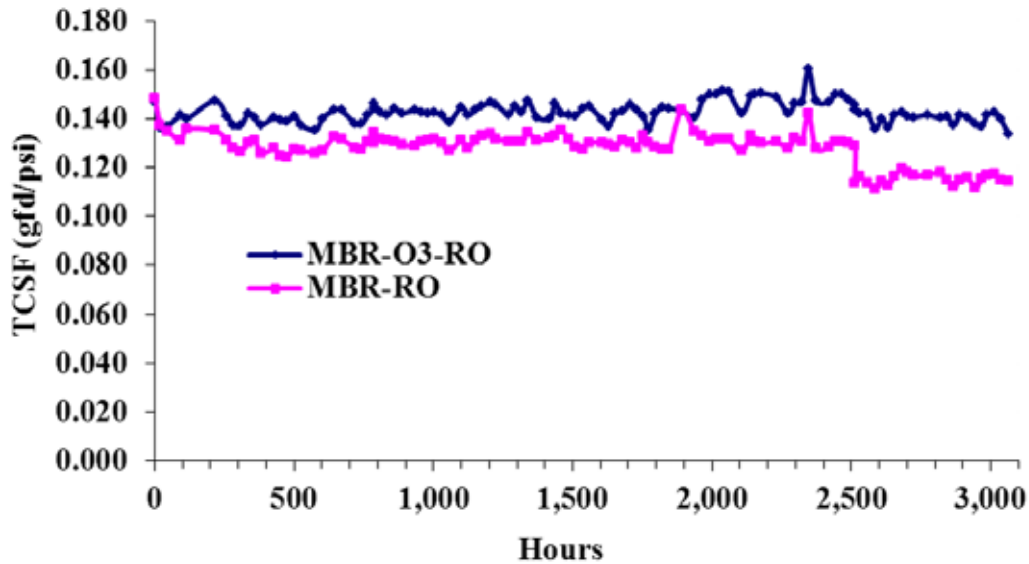


Figure 5.5. Changes in temperature-corrected specific flux (TCSF) (gfd/psi) for the two treatments under 14-gfd conditions.

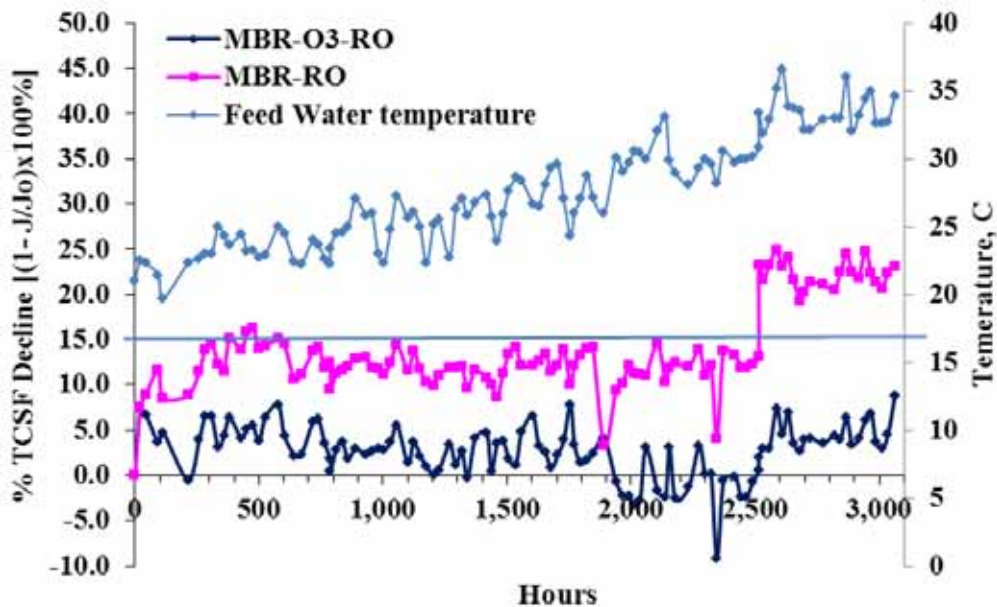


Figure 5.6. Changes in temperature-corrected specific flux (TCSF) decline (%) for the two treatments under 14-gfd conditions.

After approximately 2500 h, a significant jump in TCSF decline was observed for both systems, though this jump was worse for the control treatment train. It was noted that the water temperature also increased during this time, which was accompanied by a series of shutdowns. However, once the pilot operation was resumed, the flux decline did not get progressively worse. Figure 5.7 shows changes in STCn, and Figure 5.8 shows changes in dP over the run time. As summer temperatures set in, the normalized STCn increased (Figure 5.7). Both trends represent predictable behavior with higher feed water temperature. There were no marked changes in dP for either train during the loss in TCSF (at approximately 2500 h).

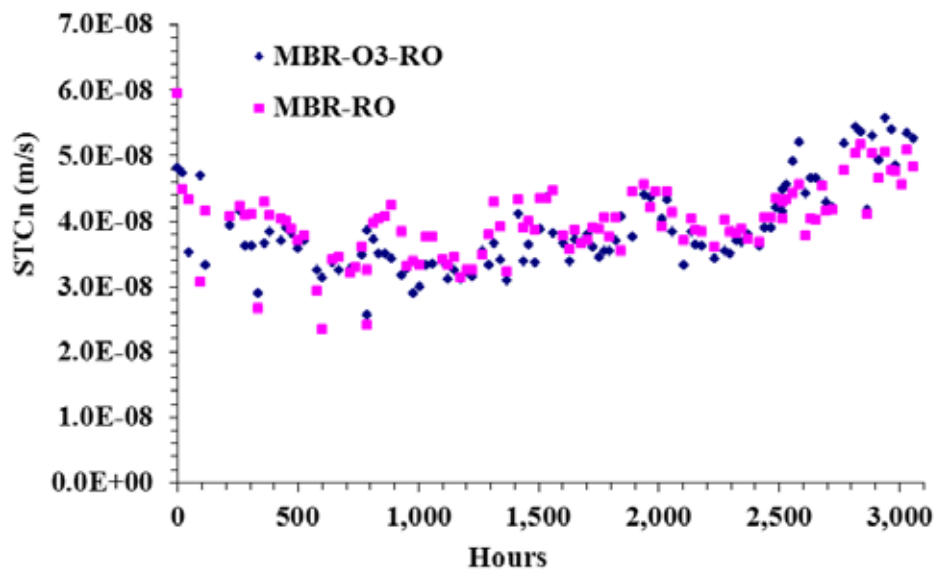


Figure 5.7. Changes in normalized salt transport coefficient (STCn) for the two treatments under 14-gfd conditions.

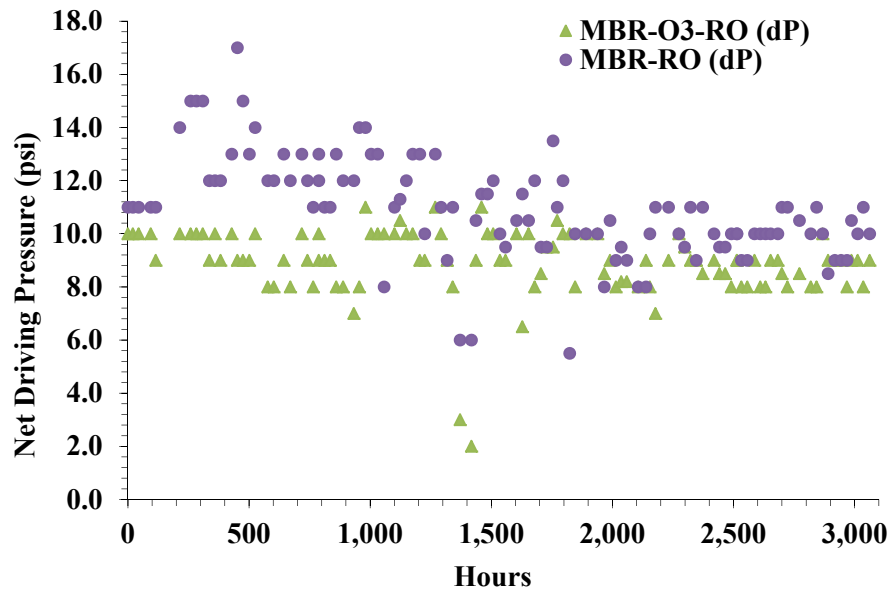


Figure 5.8. Changes in differential pressure (dP) for the two treatments under 14-gfd conditions.

Because of the relative stability of the system during the pilot testing, it was decided that, after the first phase of testing, a challenge test would be attempted whereby the recovery of the system was maintained at approximately 52% but the flux would be increased to 15.5 gfd and then to 16.9 gfd. Because of the uncertainty over the relative rate of fouling at 15.5 gfd versus 14.1 gfd, it was decided not to perform a CIP before attempting the 15.5 gfd challenge test. However, if significant fouling was observed after a few weeks of running at 15.5 gfd (i.e., if the membranes were “crashing”), then a CIP was planned.

5.3.2 Phase II: 15.5-gfd Conditions

In order to increase the flux to 15.5 gfd, a higher feed flow was used for the same 1×6 array of RO elements. Table 5.5 shows the updated operating parameters used for this phase of the study. Changes in TCSF are shown in Figure 5.9 for both trains.

Table 5.5. 15.5-gfd RO Operating Parameters for 1×6 Array

Operating parameter	Unit	Value	
Feed flow rate	gpm	9.9	
Filtrate flow rate	gpm	5.2	
Concentrate flow rate	gpm	4.8	
Filtrate flux	gfd	15.5	
Feed pressure	psig	111–151	
Feed water temp	°C	28.3–35.4	
Recovery	%	52	

Element	Wt %	At %
C	75.63	82.06
N	07.16	06.66
O	10.50	08.55
S	06.44	02.62
Cl	00.27	00.10
Matrix	Correction	ZAF

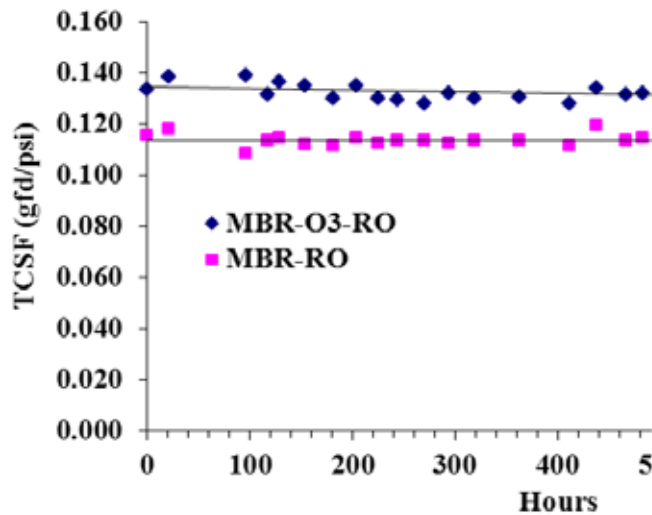


Figure 5.9. Changes in temperature-corrected specific flux TCSF (gfd/psi) for the two treatments under 15.5-gfd conditions.

The MBR-O₃-RO pilot completed 728 h at 15.5 gfd with no significant changes in TCSF for the two treatment trains beyond what was observed in Phase I. Thus, it was decided to step-up the flux to 17 gfd for Phase III. To achieve the 17-gfd flux test parameters, the project team removed the fourth RO membrane element from both trains, reducing the total number of elements to five. However, prior to the inception of Phase III, the removed elements were sent to Hydranautics, where surface characterization tests were performed. Results from SEM and energy dispersive X-ray (EDAX) analysis of the clean ESPA-2 membrane surface are shown in Figure 5.10.

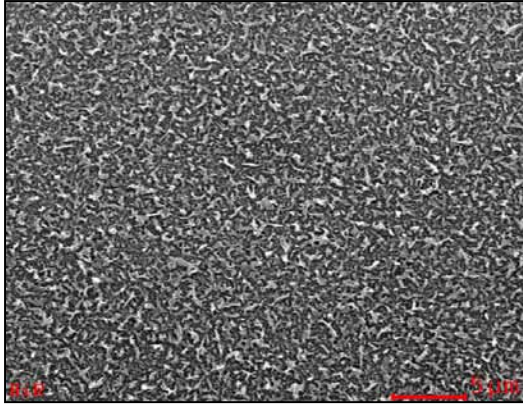
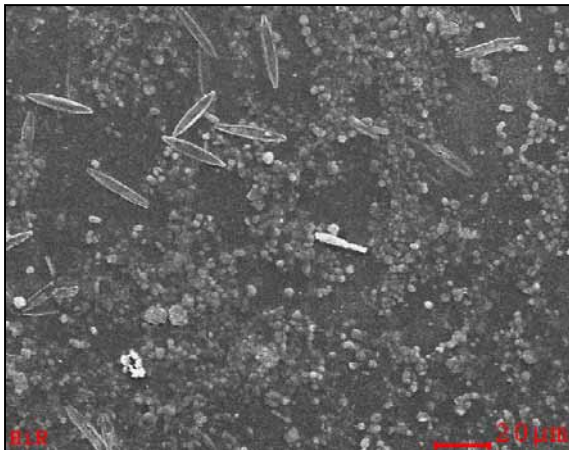


Figure 5.10. SEM image (the scale bar in red is for 5 μm) of a clean ESPA-2 membrane (left image) and a table generated from EDAX analysis.

Source: Courtesy of Hydranautics

A sample was taken from each autopsied membrane element and was exposed to HCl. Neither sample produced bubbles upon exposure to HCl, indicating that the presence of carbonate precipitants was very low or absent on these samples. Upon EDAX analysis, however, it became apparent that the two elements had very different foulant characteristics. According to the analyst at Hydranautics, the fourth element of train 1 (MBR-O₃-RO) had thin foulant covering most of the surface, but there were also significant clean areas. The thin foulant layer had diatom-like particles at 30 μm and many paired cells (Figures 5.11 and 5.12). Crystals and phosphorus were not seen on this sample. Because the foulant layer was thin, some of the carbon, oxygen, nitrogen, and sulfur seen on scans could have come from polysulfone under the foulant.



<i>Element</i>	<i>Wt %</i>	<i>At %</i>
C	69.29	76.25
N	07.68	07.24
O	16.81	13.88
Na	00.34	00.20
Si	00.33	00.15
S	05.11	02.11
Cl	00.44	00.17
Matrix	Correction	ZAF

Figure 5.11. SEM image (the scale bar in red is for 20 μm) of Train 1 (MBR-O₃-RO) membrane (left image) and a table generated from EDAX analysis.

Source: Courtesy of Hydranautics

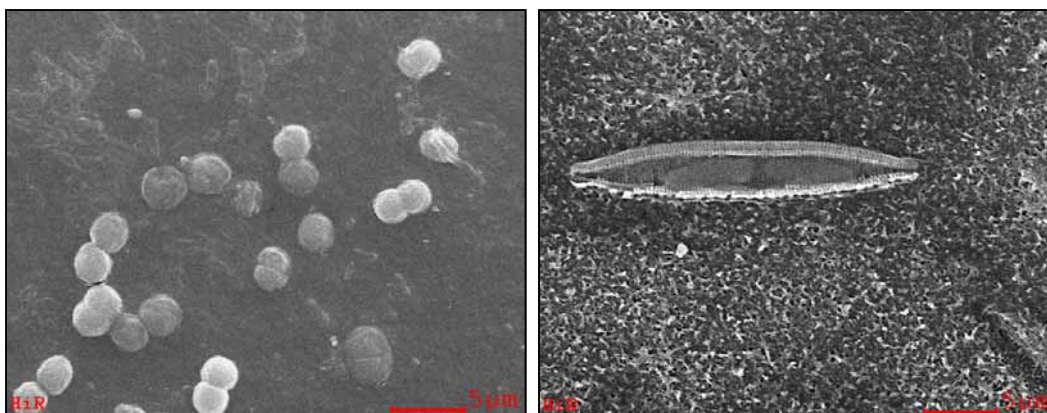
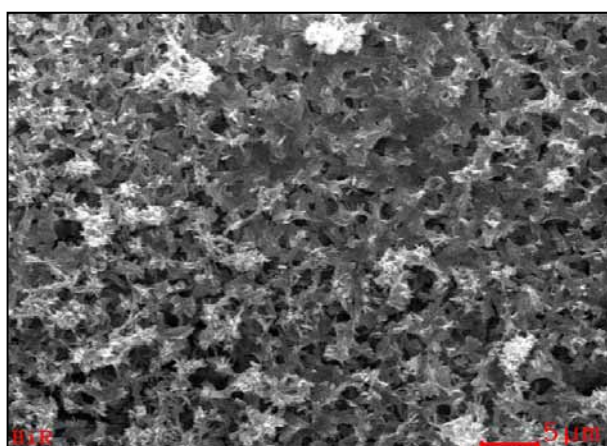


Figure 5.12. SEM image (the scale bar in red is for 5 μm) of Train 1 (MBR-O₃-RO) membrane showing paired cells (left image) and a diatom (right image) at higher magnification. Source: Courtesy of Hydranautic.

Regarding the control train, the analysis indicated that the fourth element of train 2 (MBR-RO) had crystals containing phosphorus covering most of the surface. Figure 5.13 shows the composition and appearance of a subsection of the surface. There could be carbon and sulfur in the foulant layer of scan 2, but the carbon and sulfur also could have been from the polysulfone membrane under the foulant. No cell types were seen on the surface.



Element	Wt %	At %
C	29.29	40.13
N	05.37	06.31
O	35.82	36.85
Na	02.00	01.43
Mg	04.59	03.10
Al	05.67	03.46
P	14.30	07.60
S	00.37	00.19
Cl	00.00	00.00
Ca	01.45	00.60
Fe	01.14	00.34
Matrix	Correction	ZAF

Figure 5.13. SEM image (the scale bar in red is for 5 μm) of Train 2 (MBR-RO) membrane showing paired cells (left image) and a diatom (right image) at higher magnification. Source: Courtesy of Hydranautics

These results are preliminary; however, they are somewhat unexpected: some scaling observed on Train 2 (no ozone) and biofouling on Train 1 (ozone). The project team hypothesizes that much of this finding may be attributed to the frequent shutdowns during summer resulting in partial drying of the concentrate in the vessels. The project team made all efforts to address the shutdowns as quickly as possible and to flush both trains with RO permeate to prevent the vessels from drying during downtime and to minimize any potential fouling and/or scaling.

5.3.3 Phase III: 17-gfd Conditions

For Phase III testing, the flux was increased to 17 gfd by removing the fourth element from the 1×6 array as previously mentioned. Thus, the lead three elements were exposed to a higher flux, whereas the same flux conditions with recovery of 52% as with Phase I and II testing were used. Table 5.6 shows the operating parameters used in this phase.

Table 5.6. 17-gfd RO Operating Parameters for 1×5 Array

Operating Parameter	Unit	Value
Feed flow rate	gpm	9.1
Filtrate flow rate	gpm	4.7
Concentrate flow rate	gpm	4.4
Filtrate flux	gfd	16.9
Feed pressure	psig	110–199
Feed water temp	°C	20.2–36.1
Recovery	%	52

5.3.3.1 17-gfd Test Run A

Piloting at 17 gfd commenced on July 29, 2010. Figure 5.14 shows changes in TCSF. Although stable during the initial operation period, after approximately 385 h of run time, mechanical failures were encountered on the MBR skid, temporarily stopping the RO piloting work. During the downtime, the project team performed a high-pH and a low-pH CIP, consistent with the Hydranautics Technical Bulletin 107, Cleaning Solutions 1, 3. In addition the RO elements were flushed with a 1% (w/w) sodium bisulfate solution to inhibit any biofouling during storage.

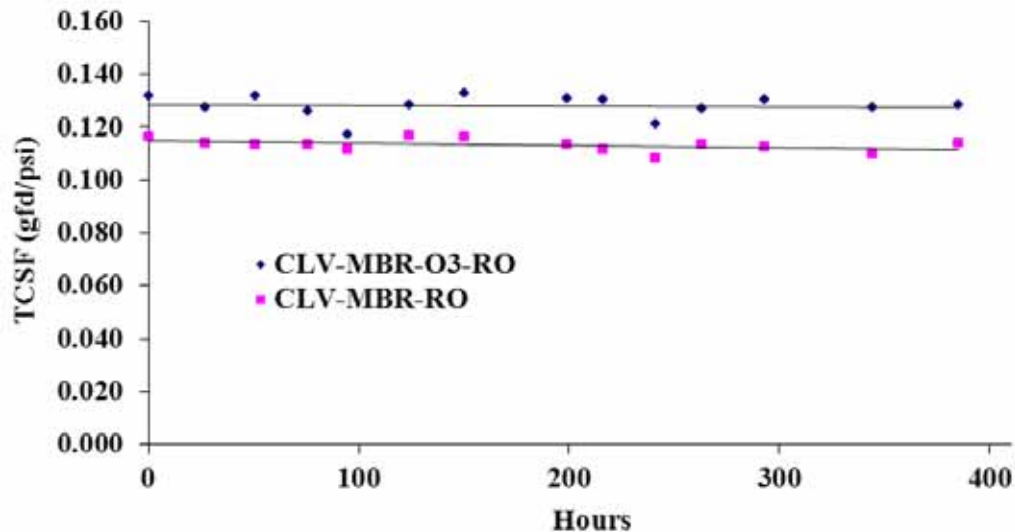


Figure 5.14. Changes in temperature-corrected specific flux TCSF (gfd/psi) for the two treatments under 17-gfd conditions.

Note: CLV = City of Las Vegas

On February 28, 2011, both trains were restarted (time 0 in Figure 5.15). Although the TCSF was similar to what was observed during 2010 testing (Figure 5.14), both trains ran at higher

feed pressure then previously, whereas the dP in Train 1 was double that of Train 2 at 25 psi (Figures 5.15 and 5.16). In order to rule out any adverse effects of prolonged storage, the project team carried out a high-pH CIP again and restarted the piloting at 17 gfd on March 23, 2011 (at approximately 190 h on Figure 5.15). After conduct of high-pH CIP, the feed pressure was lowered for both trains; however, rapid fouling was observed (Figure 5.15).

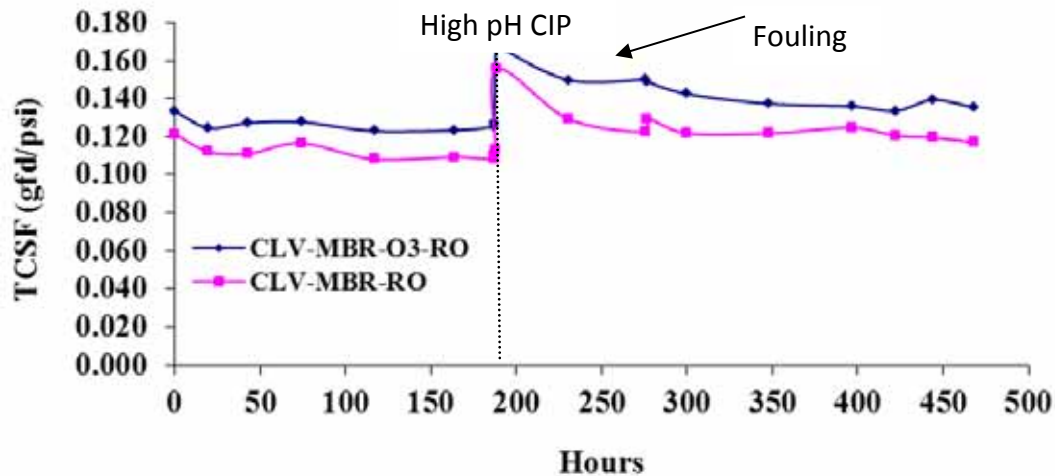


Figure 5.15. Change in in temperature-corrected specific flux (TCSF) for CLV pilot system for the 17-gfd testing at restart on February 28, 2011.

Note: CLV= City of Las Vegas

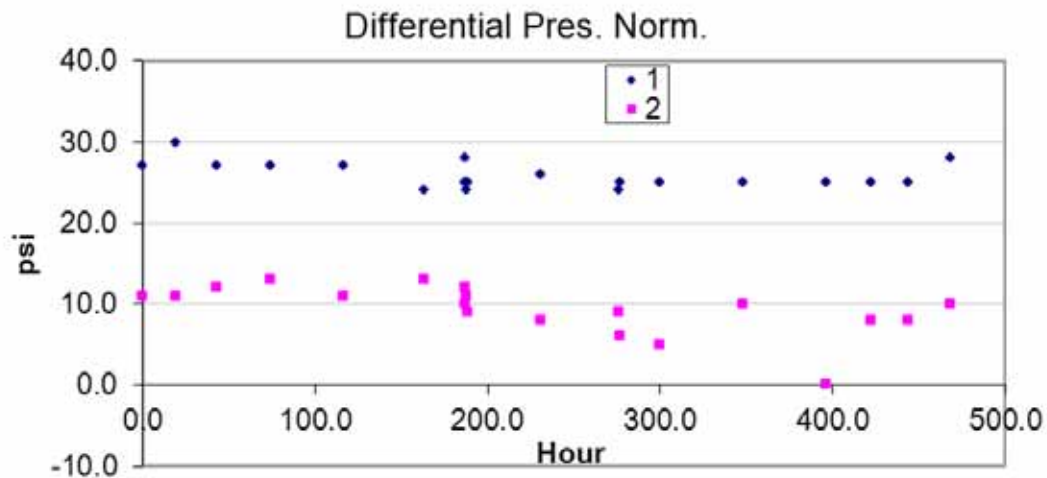


Figure 5.16. Change in differential pressure for CLV pilot system for the 17-gfd testing at restart on February 28, 2011 (1 = MBR-O₃-RO Train; 2 = MBR-RO Train).

Note: CLV = City of Las Vegas

After further troubleshooting and uncertainty regarding the fouling of elements, the project team decided to remove and autopsy the used elements prior to proceeding with Phase IV. The fouled elements were sent to Hydranautics for further analysis. The wet testing of the elements indicated that some fouling had occurred. Table 5.7 shows results of factory testing and retesting performed in late April 2011. It is interesting to note that the lead element on

the control train (MBR-RO, Train 2) had lost significant permeability whereas the tail element on Train 1 showed some signs of scaling.

Table 5.7. Wet Tests of the Lead and Tail Elements from MBR-RO Treatment Trains at 17 gfd

	Factory-Tested Membranes		Fouled Membranes	
	Salt Rejection (%)	Production (GPD)	Salt Rejection (%)	Production (gpd)
MBR-O ₃ -RO				
Lead	99.7	1949	99.7	1942
Tail	99.6	2052	99.8	1536
MBR-RO				
Lead	99.7	1915	99.9	1449
Tail	99.6	2039	99.8	1772

Figure 5.17 illustrates the process of opening the elements. Figure 5.18 captures the individual leaves and sampling scheme. Visually, the autopsied lead/tail elements appeared very “clean,” and thus it was decided to sample three rectangular pieces of membrane from a single leaf No. 4 across the length of the element (Figure 5.18).



Figure 5.17. Photographs illustrating the process of opening the RO elements.



Figure 5.18. Photographs illustrating the process of sampling RO elements for microscopy analysis.

Some areas of the membranes samples collected for microscopy analysis were also subjected to HCl testing for the presence of carbonates. All samples showed very limited bubbling from exposure to acid, indicating that the carbonates were very scant or absent. In addition, all membrane samples appeared to have very little foulant on the surface. Figure 5.19 shows an

SEM image (left) and a table of elemental composition from EDAX analysis of a clean ESPA-2 membrane as a reference (the scale bar in red is for 5 μm).

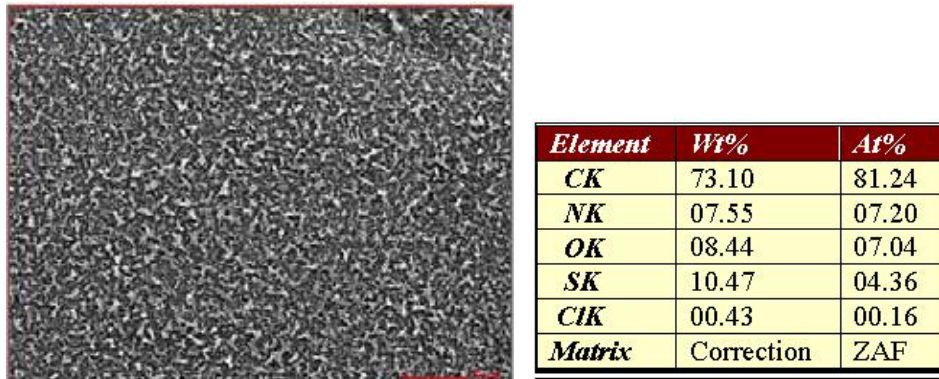


Figure 5.19. SEM image at $\times 3000$ (the scale bar in red is for 5 μm) of a clean ESPA-2 membrane (left image) and a table generated from EDAX analysis.

Source: Courtesy of Hydranautics

Figures 5.20 and 5.21 show SEM and EDAX summaries of the lead elements from the two trains. These samples did not appear to have any signs of fouling, whereas the elemental composition closely matched that of a clean membrane sample shown by Figure 5.19.

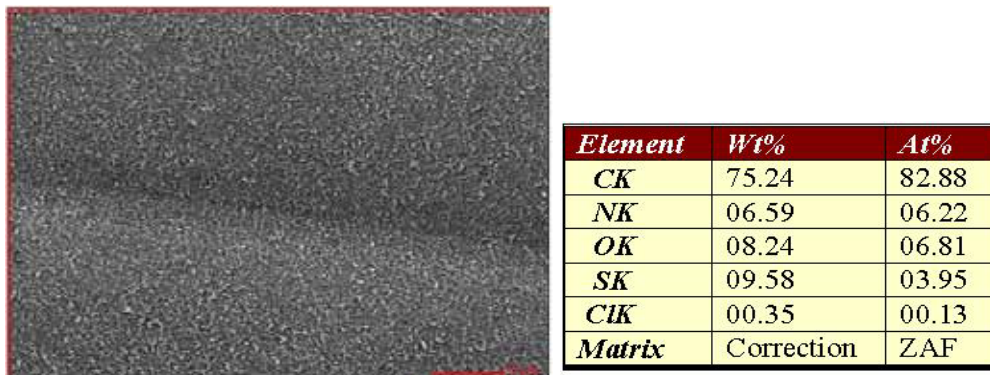
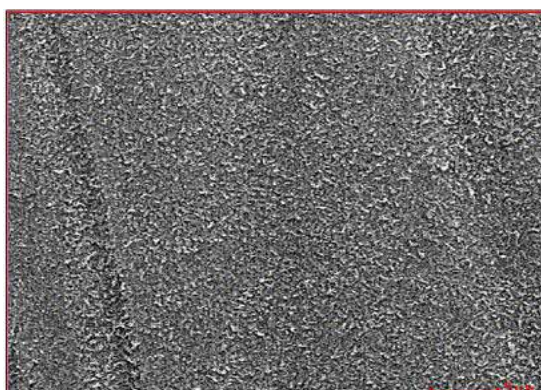


Figure 5.20. SEM image at $\times 3000$ (the scale bar in red is for 5 μm) of a sample of MBR-O₃-RO lead element (left image) and a table generated from EDAX analysis.

Source: Courtesy of Hydranautics



<i>Element</i>	<i>Wt%</i>	<i>At%</i>
<i>CK</i>	74.82	82.24
<i>NK</i>	07.12	06.71
<i>OK</i>	08.77	07.24
<i>SK</i>	08.91	03.67
<i>CIK</i>	00.38	00.14
<i>Matrix</i>	Correction	ZAF

Figure 5.21. SEM image at ×3000 (the scale bar in red is for 5 μm) of a sample of MBR-RO lead element (left image) and a table generated from EDAX analysis.

Source: Courtesy of Hydranautics

Similarly, the microscopy analysis of the tail elements, shown in Figures 5.22 and 5.23 of the two trains, did not indicate any significant fouling or scaling. On the basis of these results, it was concluded that no fundamental differences were observed between the two treatment trains, even though the wet testing data listed in Table 5.7 suggested some fouling and/or scaling. The SEM analysis also showed that all of the tested samples had unusual scratches (examples can be seen from Figures 5.22 and 5.23). The scratches did not resemble those sometimes seen when brine spacer moves relative to a membrane surface. There were sharply defined narrow lines with embossed and, in spots, gouged polyamide layer. There were also wide areas where it could be seen that something had rubbed the surface, causing wider areas of minor embossing. There was no apparent directionality to the lines (i.e., indicative of specific flow patterns and abrasion). Some of the brine spacer lines had dents characteristic of embedded particles. However, the foulant from membrane element no. 6 from train 1 that was received in a vial had very small particles that did not appear to be large enough to contribute to the scratches on the membrane. Thus, the exact cause of observed scratches could not be identified.



<i>Element</i>	<i>Wt%</i>	<i>At%</i>
<i>CK</i>	73.47	81.59
<i>NK</i>	07.02	06.68
<i>OK</i>	08.67	07.23
<i>SK</i>	10.45	04.35
<i>CIK</i>	00.39	00.15
<i>Matrix</i>	Correction	ZAF

Figure 5.22. SEM image at ×40 (the scale bar in red is for 200 μm) of a sample of MBR-O₃-RO tail element (left image) and a table generated from EDAX analysis.

Source: Courtesy of Hydranautics

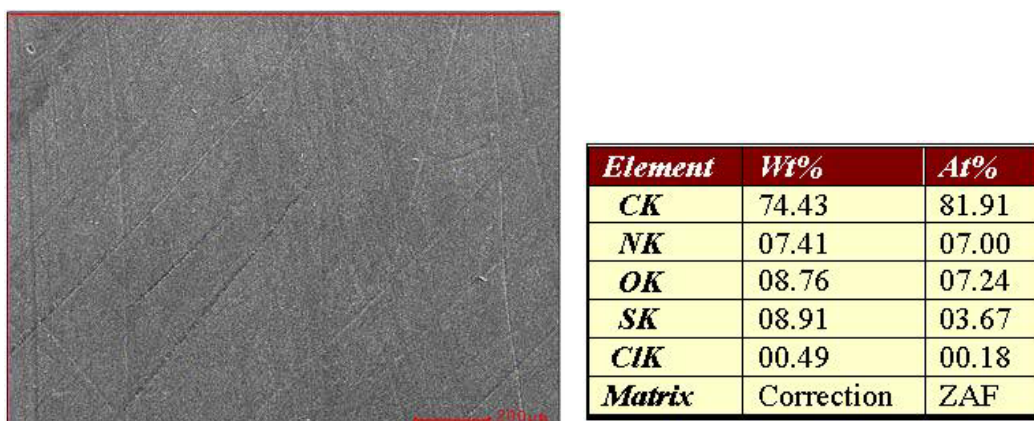


Figure 5.23. SEM image at $\times 80$ (the scale bar in red is for 200 μm) of a sample of MBR-RO tail element (left image) and a table generated from EDAX analysis.

Source: Courtesy of Hydranautics

On further analysis of the pilot equipment, the project team was able to determine that at least two pressure gauges had failed, which may have been the cause for the consistently high dP observed on Train 1 as shown in Figure 5.16. All four pressure gauges (feed/reject on each train) were replaced, and an additional set of dP gauges was installed to provide some redundancy in monitoring changes in pressures.

5.3.3.2 17-gfd Test Run B

With a new set of elements in place (courtesy of Hydranautics), the RO pilot accumulated nearly 2000 h of additional testing, with the data summarized in Figure 5.24. Some initial fouling was observed on control Train 2 (MBR-RO). In a manner nearly identical to the Phase I testing, the ozone pretreatment train showed less flux decline than did the control train. However, after approximately 800 h, some unexpected loss in flux was observed on train 1 (ozone). After a series of troubleshooting exercises and CIPs, the problem was linked to a faulty check valve on a sulfuric acid feed line, resulting in some corrosion during shutdowns. The project team also observed some odd concentration for aluminum in the concentrate of Train 1 (refer to Appendix A: April–September 2011).

The project team attempted to recover the flux on Train 1 with a series of low- and high-pH cleanings (Hydranautics Technical Bulletin 107, Cleaning Solutions 1, 3) but did not succeed. To resolve this problem, RO elements Nos. 1, 2, and 6 on Train 1 were replaced with retested elements from a previous run, in order to match the flux on MBR-RO train (Train 2). The project team also performed additional high-pH CIP cleaning on both trains because Train 2 had lost $>15\%$ of the TCSF (Figures 5.25 and 5.26).

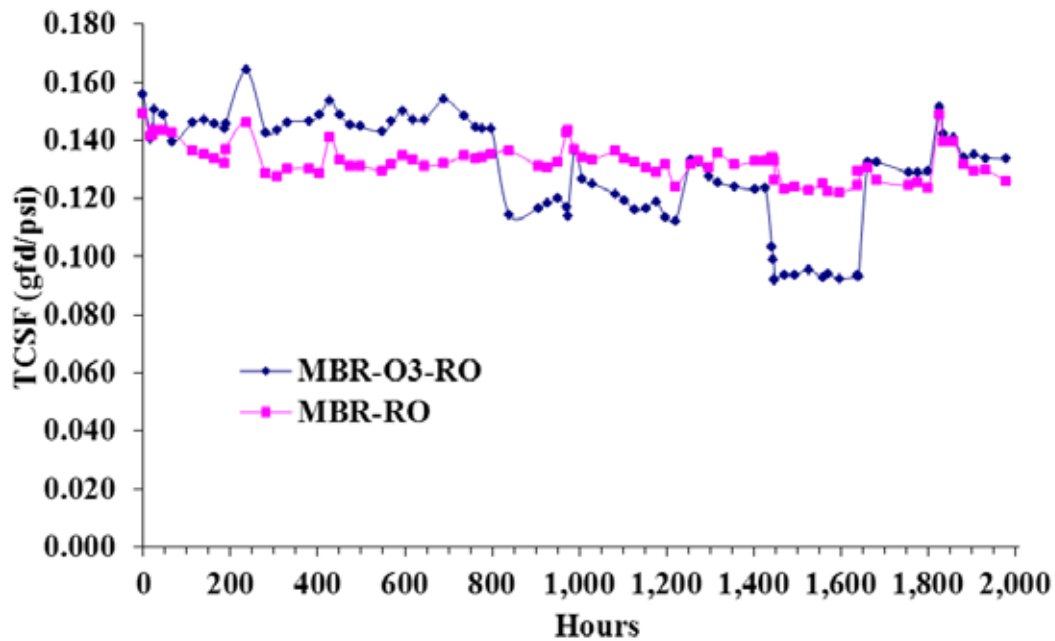


Figure 5.24. Change in temperature-corrected specific flux (TCSF) for CLV pilot system for the 17-gfd testing with new elements.
Note: CLV = City of Las Vegas

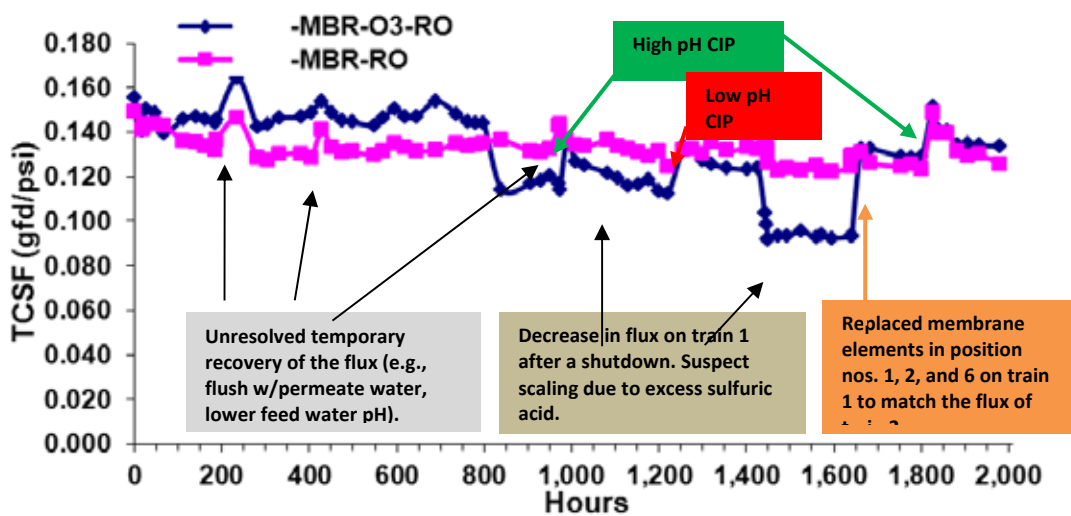


Figure 5.25. Changes in temperature-corrected specific flux (TCSF) for the MBR-RO trains over time for 17-gfd conditions.

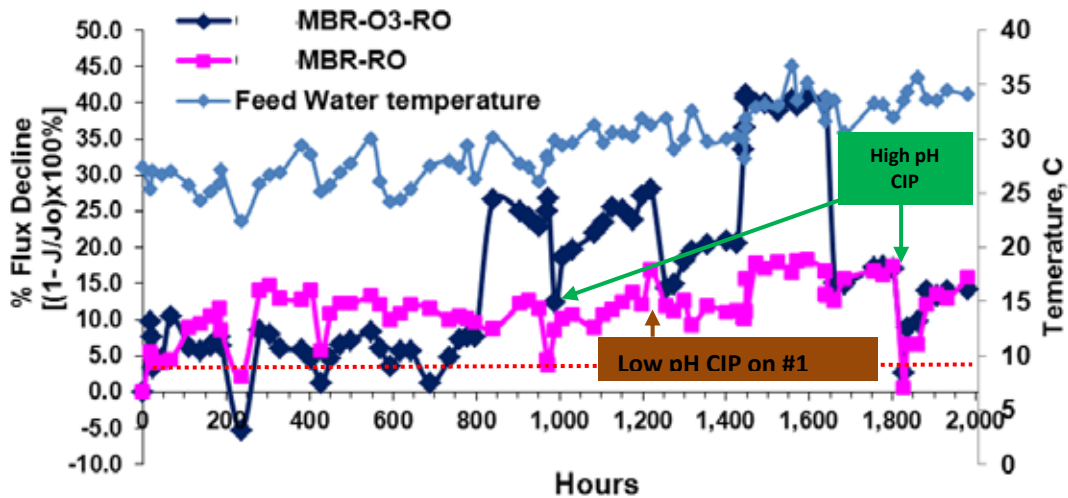


Figure 5.26. Changes in % temperature-corrected specific flux decline for the MBR-RO trains over time for 17-gfd conditions.

Following the CIP, both trains were restarted under 17-gfd conditions to verify the efficacy of the cleaning procedure. After CIP, and at approximately 2000 h of total run time (September 1, 2011), the project team increased the flux to 19-gfd conditions by removing the third element from each train in order to challenge the system and potentially force fouling. This task was done to further evaluate the effects of preoxidation on the cleaning frequency.

5.3.4 Phase IV: 19-gfd conditions

Table 5.8 lists the operating parameters for the RO pilot under 19-gfd conditions. Figure 5.27 shows changes in TCSF over the run time for both trains, Figure 5.28 shows changes in percentage of TCSF decline, and Figure 5.29 shows normalized TCSF and the percent difference between the two trains.

Table 5.8. 19-gfd RO Operating Parameters for 1 × 4 Array

Operating Parameter	Unit	Value
Feed flow rate	gpm	8.2
Filtrate flow rate	gpm	4.3
Concentrate flow rate	gpm	3.9
Filtrate flux	gfd	19.4
Feed pressure	psig	122–243
Feed water temp	°C	18.6–35.0
Recovery	%	52

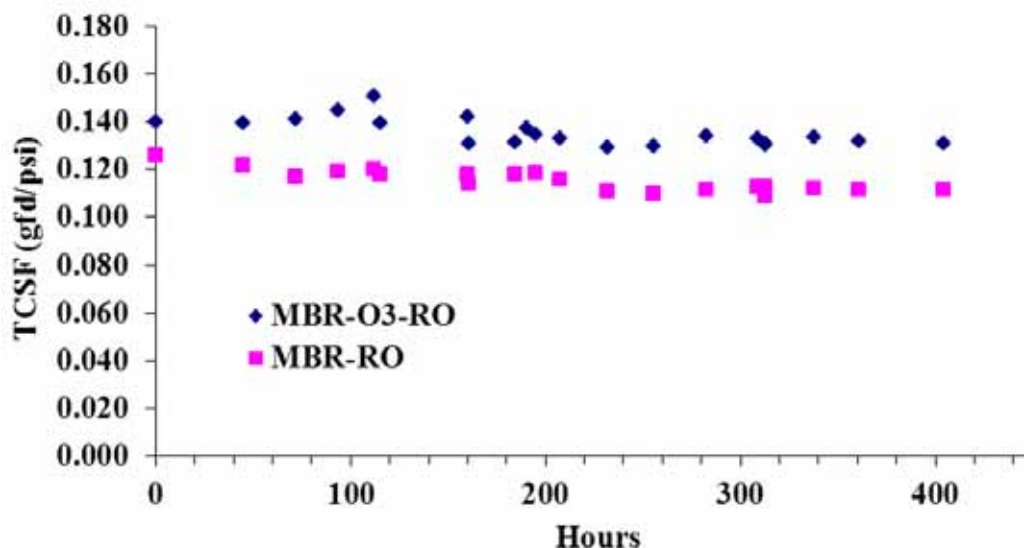


Figure 5.27. Changes in temperature-corrected specific flux (TCSF) for the MBR-RO trains over time for 19-gfd conditions.

Despite the encountered mechanical failures and setbacks, the results after an >400-h run time at 19 gfd show that there was an observable difference in the fouling. The data presented in Figures 5.28 and 5.29 show that, on the basis of changes in normalized TCSF for the two trains and a calculated percent difference in TCSF over run time, the fouling rate was higher on the control, nonozonated train. The MBR-RO control train showed a cumulative loss in TCSF of 12%, whereas the MBR-O₃-RO lost only 6%.

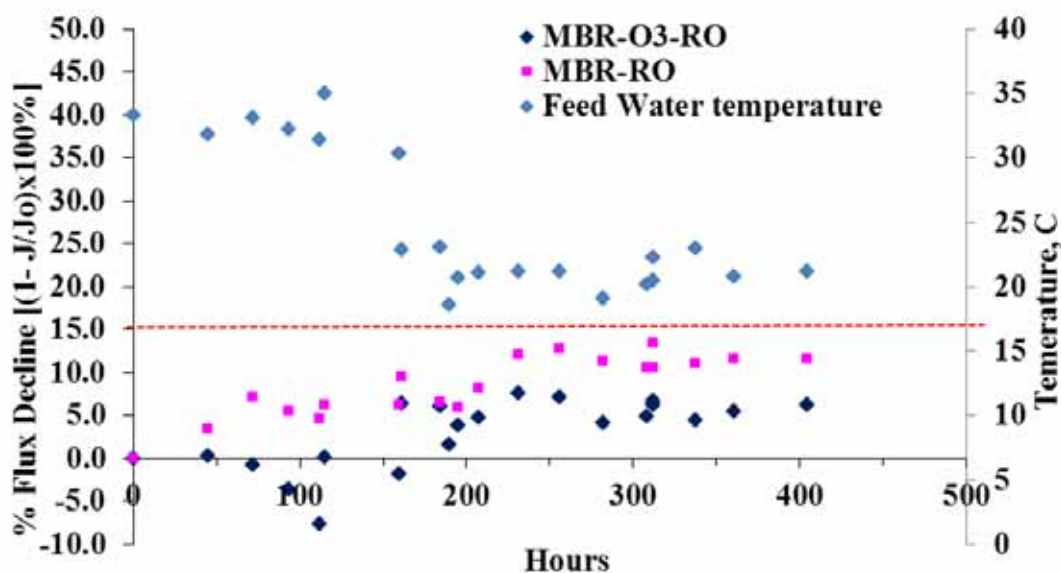


Figure 5.28. Changes in temperature-corrected specific flux for the MBR-RO trains over time for 19-gfd conditions.

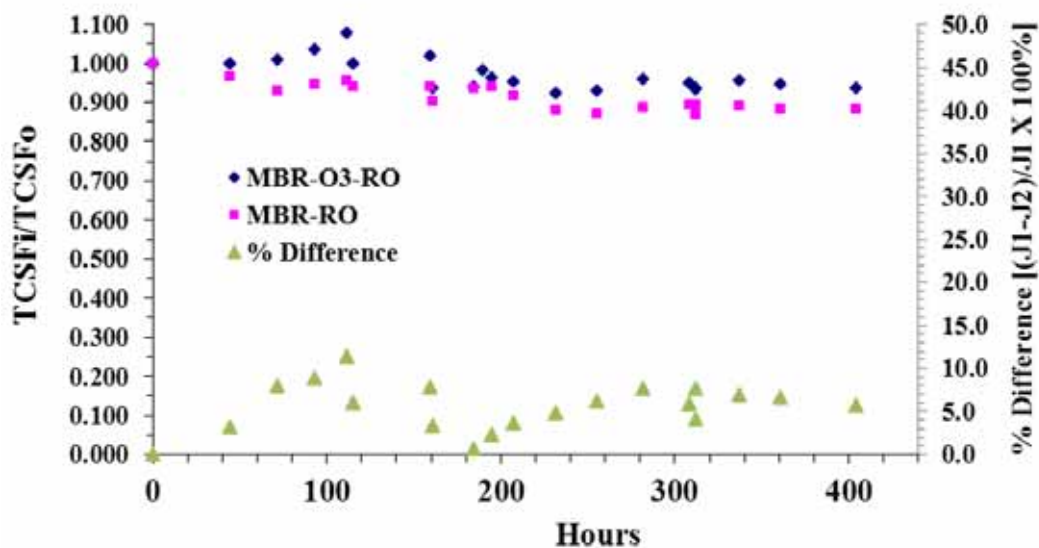


Figure 5.29. Changes in normalized temperature-corrected specific flux TCSF and % difference for the MBR-RO trains over time for 19-gfd conditions.

At the end of the tests, the project team collected the lead (No. 1) and tail (No. 6) elements for surface characterization. The results of microscopy analysis are presented in the following section. Table 5.9 lists the results from wet testing of the elements (courtesy of Hydranautics). The lead and tail elements of the MBR-O₃-RO train lost only 11% and 8% in permeability, whereas the MBR-RO lead and tail elements lost 37% and 43%, respectively. In contrast, a cumulative loss in TCSF of 12% for the MBR-RO train and of only 6% for MBR-O₃-RO was observed. The maximum design recovery of these RO elements is 20% (per single element), whereas the pilot-scale test was conducted with an average water recovery of 13% per element; this discrepancy is hypothesized to be the main reason why the magnitudes of TCSF loss and individual elements' permeability loss are different. In any case, decrease in both parameters could be significant for the life cycle of the membranes during long-term use without an ozone preoxidation step.

Table 5.9. Wet Tests of the Lead and Tail Elements from MBR-RO Treatment Trains at 19 gfd

Substance	Factory-Tested Membranes		Fouled Membranes	
	Salt Rejection (%)	Production (GPD)	Salt Rejection (%)	Production (GPD)
MBR-O ₃ -RO				
Lead	99.7	1957	99.7	1735
Tail	99.8	1628	99.8	1492
MBR-RO				
Lead	99.6	2177	99.7	1368
Tail	99.6	2199	99.8	1263

5.3.5 End-of-Study Microscopy Analysis and Discussion

The objectives of the final investigation were to characterize membrane fouling of the RO elements taken from the pilot-scale test run by describing the types and extent of foulants after using a suite of advanced analytical techniques (methods described in Chapter 2). Surface analysis of the lead and tail elements from the WRF 1 pilot study was performed at the Colorado School of Mines. In accordance to methods described in Chapter 2, membrane samples were analyzed by using ESEM for nonconductive materials. The results from various analysis are summarized in the following subsection. A complete list of supporting data and images is presented in Appendix D (D-4), whereas specific supporting data for the interpretation and conclusions outlined in this section are referenced accordingly.

5.3.5.1 Visual Inspection of the RO Elements

Table D-1 summarizes the inspection of the exterior of the membrane elements. Brine seal, hard shell (fiberglass outer wrap), and ATDs were not visibly defective. The glue lines of the eight membrane elements were all in good condition. No visible defects were observed.

Table D-2 summarizes the inspection of the interior of the membrane elements. All membrane elements consisted of 10 membrane leaves. The glue lines of all the membrane leaves were well sealed and in good condition. All permeate carriers and permeate sides of the membrane leaves were very clean. The fouling layer was for the most part randomly distributed on membrane feed surfaces; there was not a noticeable difference between the feed and brine ends. Fine black particulates, with particles ranging in size from 1 to 10 mm, were observed on all sheets of all elements except for the tail element of the MBR-O₃-RO train. This element had an orange coating on all layers, especially when the surface was disturbed as the sheets were moved during examination. The active layer on a few of the sheets also had many fine black lines ranging from 1 to 3 cm long, mostly in a pattern diagonal to the feed and brine ends that looked like scratch marks. For all elements, the imprint of the feed spacers on the membrane was visible by darker spots and clean lines.

Dye testing showed that none of the membrane elements experienced mechanical damage (Table D-3). After Rhodamine B was applied to the active layer, the support layer was completely clean for all of the element samples, indicating that no leakage occurred.

5.3.5.2 Surface Hydrophobicity/Hydrophilicity

Table 5.10 summarizes the contact angle measurement results of the different membranes from both tests. The range of values for the sessile drop method was quite large, as is reflected by standard deviations of 3.2° to as high as 9.3°. For some of the samples, the values seemed to ascend or descend along the sample length, whereas for most the distribution was random. The virgin membrane was significantly more hydrophilic than any of the fouled membranes, with an average angle of 14.6°.

Table 5.10. Contact Angle Measurements for MBR-RO Treatment Trains at 19 gfd

Pretreatment Used	Position	Sessile Drop	
		Mean	SD
Virgin ESPA membrane		14.6	3.3
MBR-RO	Lead	41.5	5.2
	Tail	47.4	9.3
MBR-O ₃ -RO	Lead	46.4	9.3
	Tail	40.8	3.2

All membrane samples exhibited different levels of increase in hydrophobicity as a result of adsorption of transphilic and hydrophobic organics, scaling, and biofouling. The comparisons of the contact angle results between the two trains do not definitively indicate that oxidation as a pretreatment method significantly impacted the hydrophobic foulant layers because of large variability in the measurements.

5.3.5.3 Quantitative Measurements of Organic and Inorganic Substances in Fouling Layer

An acid solution is typically used to extract inorganic foulants, whereas a caustic solution is commonly used to remove organic foulants and silica. However, it should be noted that, even if sonication is applied, the method may still not be able to extract all foulants and scalants from the fouling layer. This is because the fouling layer consists predominantly of inorganic compounds and because precipitations of metal hydroxides prevent the extraction process from occurring completely.

Results of the TOC extraction with various solvents are shown in Table 5.11. The concentration of TOC was highest for the samples extracted with base and lowest for those extracted with acid. The greatest TOC concentration was obtained from elements of the MBR-RO train rather than from MBR-O₃-RO. An exception was with an acid extraction of the lead element of the MBR-O₃-RO train showing a higher TOC than did the lead element of the MBR-RO train.

In addition to the TOC measurements, the DI extracted solutions were analyzed by using the fluorescence EEM, described in Chapter 2. The EEMs should be consistent with the TOC analysis, as both examine the organic constituents of the extracted foulants. Table 5.12 shows a summary of the fluorescence analysis, whereas EEM images are presented in Appendix D Table D-4.

Table 5.11. TOC Analysis (in mg/cm² of Membrane Surface) for MBR-RO Trains

Pretreatment	Lead/Tail Element	DI Water Extraction	0.1 M NaOH Extraction	0.8 M HNO₃ Extraction
MBR-RO	Lead	0.0028	0.0039	0.0003
	Tail	0.0072	0.0049	0.0024
MBR-O ₃ -RO	Lead	0.0020	0.0035	0.0017
	Tail	0.0033	0.0041	0.0012

Table 5.12. Fluorescence Analysis of Foulant Extraction of MBR-RO Trains

Pretreatment	Lead/Tail	Protein-Like Substance Peak Intensity (Emission/Excitation)	Humic- and Fulvic-Like Substance 1 Peak (Intensity)	Humic- and Fulvic-Like Substance 2 Peak (Intensity)
Extraction with DI water:				
	Lead	0.21 (345/280)	none	none
MBR-RO	Tail	0.06 (335/277)	0.01 (460/350)	none
	Lead	0.02 (325/285)	0.01 (400/300)	none
MBR-O ₃ -RO	Tail	0.08 (335/277)	none	none

The lead element of the MBR-RO train had higher intensity of the protein-like peak than did the MBR-O₃-RO counterpart. However, the tail elements of both trains showed similar levels of the protein-like peak. This finding may indicate that ozone treatment can reduce biofouling in the lead element. An increase of peak intensity in the tail elements would indicate insufficient operational control of biofouling in both trains (e.g., insufficient chloramine residual).

The ICP analysis (Appendix D, Table D-4) demonstrated that DI water extracted higher chloride concentrations for each sample. Chloride levels were higher on all lead elements than on tail elements. On average, chloride levels were lower in the MBR pretreated samples. Nitrate, on the other hand, was highest in concentration in the MBR-O₃ samples. Fluoride, phosphate, and sulfate were not present above detection limits for any of the membrane elements. The ICP analysis showed that the membranes pretreated by MBR-O₃ had approximately twice as much iron buildup as did the control train.

5.3.5.4 Scanning Electron Microscopy and Energy-Dispersive X-Ray Spectroscopy Examination of Membrane Surface

Table 5.13 provides a summary of the ESEM/EDS analysis as well as observations made regarding the biofouling based on results described in preceding sections. Supporting images are compiled in Appendix D. Figure D-1 shows a series of ESEM images and EDS results of the virgin membranes. Figure D-2 shows ESEM/EDS results for the lead element of the MBR-RO train, whereas Figure D-3 shows results for the tail element of the same train. Figures D-4 and D-5 show ESEM/EDS results for the lead and tail elements of the MBR-O₃-RO train, respectively.

Table 5.13. Summary of the ESEM and EDS Characterization Results of MBR-RO Trains

Analysis	Virgin Membrane	MBR-RO		MBR-O ₃ -RO	
		Lead	Tail	Lead	Tail
ESEM/EDS	Smooth membrane surface, the major elements are C, O, S.	Heterogeneous thin fouling layer; numerous diatoms, algae, and Al-silicate particles on membrane surface. Broken hollow-fiber pieces were found on MBR-RO and MBR-O ₃ -RO lead elements. This finding means hollow-fiber membranes might be damaged and resulted in breakthrough of large particles to RO membranes	More homogeneous thin fouling layer; the fouling layer is of more organic nature and fewer particles. There are CaSO ₄ and Al-silicate particles on membrane surface	Heterogeneous thin fouling layer; Al-silicate particles on membrane surface. Broken hollow-fiber pieces were found on MBR-RO and MBR-O ₃ -RO lead elements. This finding means HF membranes might be damaged and resulted in breakthrough of large particles to RO membranes	More homogeneous thin fouling layer. The fouling layer is of more organic nature and fewer particles. There are CaSO ₄ and Al-silicate particles, on membrane surface
Biofouling —protein analysis	None	The protein concentration is higher in the tail element than in the lead element.		The protein analysis indicates less biofouling in the lead element than in the tail element.	

Notes: No significant visual difference between MBR-RO and MBR-O₃-RO.

Major differences between the lead and tail membrane elements are noted with underlined text.

The lead elements of both trains also contained pieces of broken hollow fibers. The lead element MBR-RO train contained a thin foulant layer heterogeneous in nature. Numerous diatoms were also observed. The fouling layer in the tail element was more homogeneous and more of organic nature than was the MBR-RO lead element. In contrast, the surface of the lead element of the MBR-O₃-RO train was smoother and cleaner. However, some bacteria and some Al-silicate and CaSO₄ particles, with small amounts of Na, K, and Cl, also were present. The fouling layer was more severe in the tail element and had more similar small particles. In summary, elements from both trains showed signs of scale, biofouling, and organic fouling, especially in the tail elements. The lead element of the MBR-O₃-RO train appeared cleaner than that of the MBR-RO control, which correlated with a smaller amount of extracted foulant as determined by TOC and fluorescence analysis.

5.4 Conclusions

Although not as significant as the bench-scale test results, the pilot-scale results observed at WRF 1 indicate a modest improvement in the performance of RO membranes with the use of ozone as a pretreatment step, though it is not clear whether this finding is related directly to organic fouling. However, the improvement in performance was observed during multiple phases of testing and under different flux conditions. The lack of clarity concerning the potential benefit of ozone as a pretreatment step may be due to the already effective pretreatment achieved by the biological treatment of the MBR. In fact future work should focus on evaluating oxidative pretreatment on waters with minimal biological treatment, such as partial nitrification or BOD removal only.

The results from Chapter 3 showed that the effects of preoxidation on EfOM molecular weight distribution and polarity are difficult to measure and quantify. Nevertheless, the pilot-scale results indicate that there can be benefits from preoxidation. It was observed that the initial flux decline that occurs within 100–150 h of commencement of operation was typically 5 to 10% less for the MBR-O₃-RO train than for the MBR-RO control. This difference was stable throughout most of the test period. At 14 gfd, this difference was monitored out to 2500 h. At 17 gfd, this difference seemed to vary; however, it was observed until other problems were encountered. At 19 gfd, both trains showed loss during 420 h of run time. The MBR-RO control train showed a cumulative loss in TCSF of 12%, whereas the MBR-O₃-RO lost only 6%. Surface analysis of the lead and tail elements and extractions of the foulant layer showed that both trains had signs of organic fouling, scale, and biofouling. The lead element of MBR-O₃-RO appeared to be the cleanest of all based on ESEM and EDS analysis as well, as it contained less TOC and fewer protein-like substances than did the lead element of the MBR-RO train. However, the contact angle measurements did not yield definitive differences in the hydrophobicity of the foulant layer, thus not allowing testing of the hypothesis that ozone pretreatment resulted in a thinner and less hydrophobic foulant layer. However, on the basis of results of the operating parameters and permeability retests, the MBR-O₃-RO train was found to maintain a greater permeability than did the MBR-RO control, indicating a potential long-term benefit of ozone in lengthening the useful life of membrane elements.

Chapter 6

Pilot-Scale Evaluation of the UF-O₃-RO and UF-UV/H₂O₂-RO System at Water Reclamation Facility 2

6.1 Chapter Overview

The initial flat sheet membrane test results at high UV fluence (Chapter 4) clearly showed promise for both ozone and UV/peroxide treatment as strategies to control flux decline in RO membranes. In the case of ozone, realistic doses of 1.5 to 3.0 mg/L were found to be effective for fouling control. Similarly, preliminary tests at high UV doses showed promise that UV/peroxide may also be effective at impacting EfOM and reducing the fouling rates of flat sheet membranes used during the bench-scale tests. However, when a more reasonable (though still high) UV fluence of 1000 mJ/cm² and H₂O₂ dose of 4 mg/L for 18.5-gfd conditions were used, the bench-scale flat sheet testing showed no significant difference between the fouling rate of the control water (UF filtrate) and that of UF-UV/H₂O₂ train. The project team also recognized that UV doses (chemical actinometry based) higher than 1000 mJ/cm² may not be practical for most utilities. Thus, even though 1000-mJ/cm² conditions did not appear to have much impact on fouling at bench scale, the unlikely use of doses higher than 1000 mJ/cm² dictated a maximum dose of 1000 mJ/cm² for the pilot. To test these conditions and whether UV/peroxide may be a useful option for organic fouling control, the pilot was operated at a flux of 14 gfd to mimic the lead elements in a full-scale system based on 10-gfd conditions. This chapter describes the UF-UV/H₂O₂-RO plus a short UF-O₃-RO pilot conducted at WRF 2.

6.2 Description of UF-UV/H₂O₂-RO and UF-O₃-RO Pilot-Scale Equipment

For the wastewater tests, a primary-treated wastewater from the Las Vegas Valley at WRF 2 was treated by using a pilot-scale Zenon Ultrafiltration (UF) ZeeWeed 500 polymeric system (GE Water & Process Technologies, Trevose, PA), operated by the WRF staff. The UF filtrate was collected in an 1800-gal equalization tank and then was fed directly to a pilot-scale contactor, where ozone gas was fed from an Ozonia[®] system (Ozonia, Elmwood Park, NJ). The UF filtrate was then split into two parallel trains: one train bypassing ozone or UV/peroxide treatment (UF-RO train, also referred to as the control) and one passing through the ozone contactor or the UV/peroxide skid, both referred to as UF-O₃-RO or UF-UV/H₂O₂-RO, respectively. Twin GE E4H-21K-DLX-60 RO membrane skids (provided with support from GE Water) with six elements per vessel were used during the pilot tests. The pilot-scale RO skids were set up to run on a single array of six ESPA-2-4040 RO elements. The pilot equipment photographs are shown in Figure 6.1, whereas Figure 6.2 shows a more detailed process layout of the UF-RO trains.

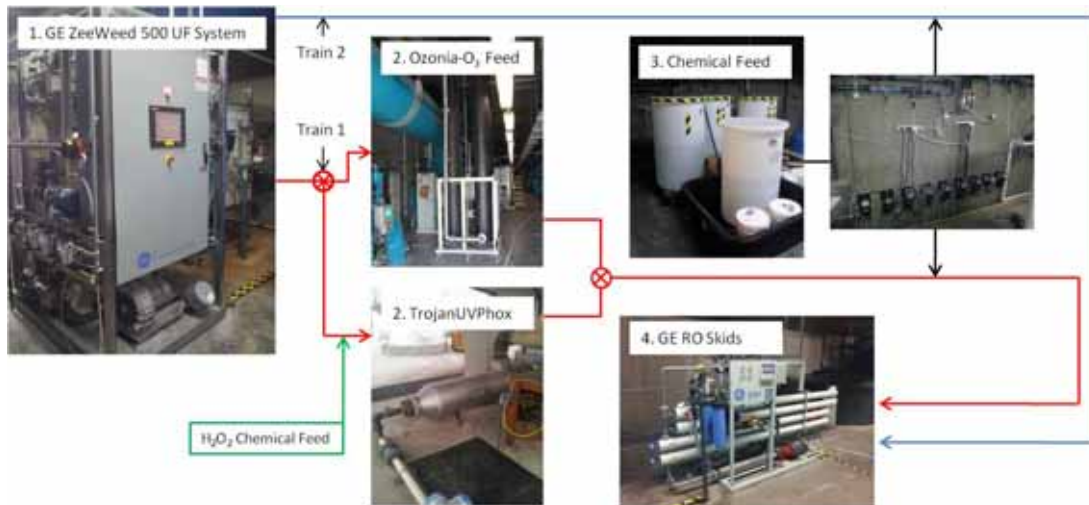


Figure 6.1. Photographs of UF, Ozonia, TrojanUVPhox®, chemical feed, and RO systems at WRF 2.

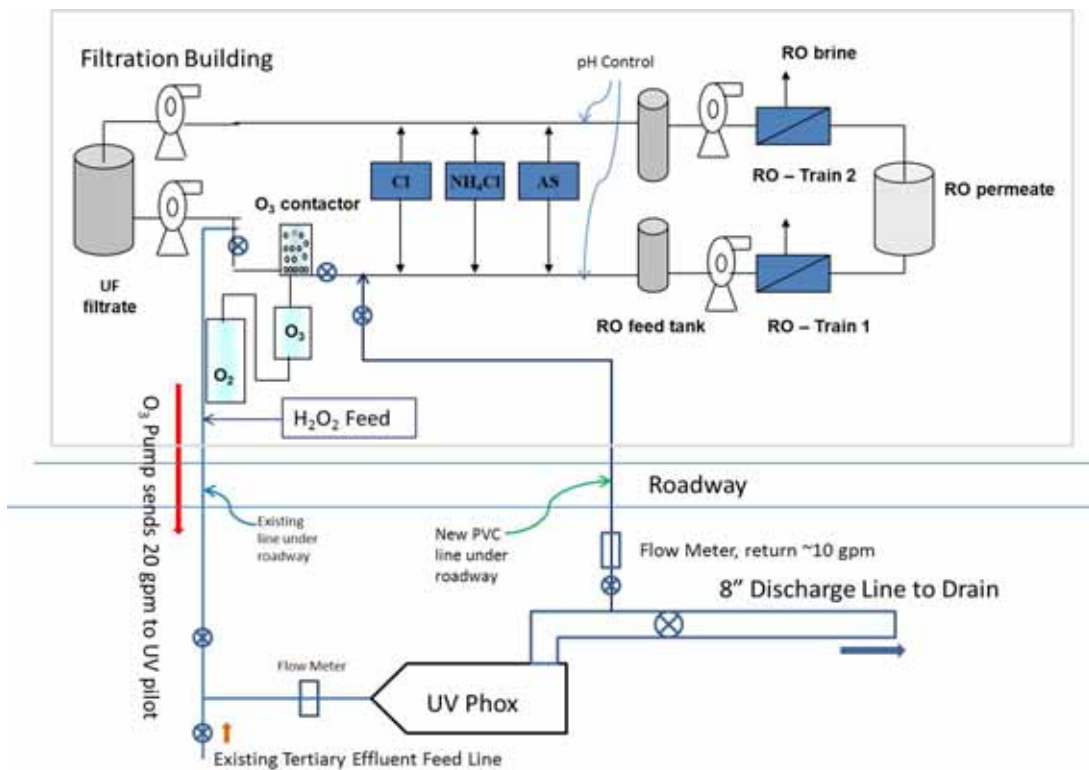


Figure 6.2. Process layout of UF-RO, UF-O₃-RO, and UF-UV/H₂O₂-RO treatment trains.

Note: AS = antiscalant agent

6.2.1 Description of UF Equipment

A selection of typical water quality parameters for the UF feed and filtrate is shown by Table 6.1. The UF system was used by the staff at WRF 2 to evaluate phosphorus removal (as direct filtration after ferric or alum addition) and for disinfection of secondary effluent. The

feed to the UF system was first treated with a coagulant to enhance phosphorus removal and to optimize the fouling of the membranes. Initially, aluminum sulfate was used, which was later switched to ferric chloride.

Table 6.1. Typical UF Feed and Filtrate Water Quality for Phosphorus Removal

Parameter, Unit	UF Feed	UF Filtrate
TSS, mg/L	5.6	<5
TDS, mg/L	1160	1180
TN, mg/L N	14	14
NO ₂ ⁻ , mg/L N	<0.100	<0.100
NO ₃ ⁻ , mg/L N	13.8	13.8
Total PO ₄ ³⁻ , mg/L	0.265	0.12
Ortho PO ₄ ³⁻ , mg/L	0.076	0.074
UV ₂₅₄	<0.15	<0.13
UV ₂₈₀	<0.12	<0.10
Turbidity, NTU	1.66	<0.1
TOC, mg/L	7.1	5.7

6.2.2 Description of Ozonia[®] Equipment

The Ozonia system was designed and operated to deliver a dose of 4–6 mg/L of ozone in the UF filtrate.

6.2.3 Description of TrojanUVPhox[®] UV Equipment

The TrojanUVPhox[®] pilot (Trojan Technologies, London, ON, Canada; UVPhox[®] = UV Photolysis and UV Oxidation) was an optically and hydraulically optimized UV reactor with the capacity for hydrogen peroxide addition (UV/H₂O₂) upstream. With respect to the proposed research, the TrojanUVPhox[®] was used to assess pilot-scale UV and UV/H₂O₂ following different pretreatment options. The reactor contained 32 low-pressure mercury lamps, which could be turned on or off (and removed) individually. The reactor volume was 9.6 ft³ or 71.8 gal. For these tests, the reactor was reconfigured such that 15 lamps were disconnected and removed and that the total power was lowered to only 60%. At a projected 20-gpm feed flow rate, the estimated UV fluence by the manufacturer was at 1400 mJ/cm².

6.2.4 Description of the RO Equipment

Two separate pilot-scale RO skids (GE Water, Minnetonka, MN) were used for this study, with a 1 × 6 array of ESPA-2-4040 RO membranes. The pilot skids were operated at 54.5% recovery using a single array of six elements. The feed water was adjusted to pH 6.8 by using 50% sulfuric acid (Brenntag) and was spiked with bulk sodium hypochlorite (obtained from the wastewater treatment plant) and food-grade ammonium chloride, 99% (Brenntag), to form residual monochloramine. The residual monochloramine was measured frequently by using a DPD test kit and maintained in the range of 2–6 mg/L as Cl₂. An antiscalant, Pretreat Plus (KingLee), was used on the basis of a dose recommended by the manufacturer of 8 mg of the product/L in the RO concentrate. The feed, reject, and permeate pressures, feed/permeate conductivity, temperature, and pH were recorded during each pilot visit. Periodic SDI measurements were also taken during various phases of the study by using a portable SDI-2000 test kit (Applied Membranes, Inc.). The water quality of the feed, concentrate, and

permeate was tested periodically. Table 6.2 shows the target parameters and frequency of measurements. The feed pressures were adjusted manually by using a throttle valve to maintain a constant permeate flow and product recovery.

Table 6.2. Selected Analysis for RO Pilot Grab Samples and Frequency

Sampling Parameter	Unit	Freq
TDS	mg/L	2/mo
TSS	mg/L	2/mo
Ca ²⁺ , Mg ²⁺ , Na ⁺ , K ⁺ , NH ⁴⁺ , Ba ²⁺ , Sr ²⁺	mg/L	2/mo
Cl ⁻ , F ⁻ , NO ²⁻ , NO ³⁻ , SO ⁴⁻ , PO ⁴⁻ , TP, TN	mg/L	2/mo
Silica	mg/L	2/mo
Alkalinity	mg/L	2/mo
TOC	mg/L	2/mo
SDI		2/mo

Recorded operational data were input into ROData (ROData; Hydranautics) to determine various parameters such as NDP or the net force to drive the water across the membrane surface, specific flux, the temperature correction factor (using 25 °C as reference), TCSF, STCn, and dPn. In addition, changes in normalized TCSF (J/J_o) and % decrease in TCSF ($[1 - J/J_o] \times 100\%$) were plotted by using MS Excel 2010.

6.3 Results and Discussion

The initial pilot testing of the UF-O₃-RO and UF-RO treatment trains encountered problems with the alum coagulation that could not be switched until the completion of a concurrent fathead minnow study (U.S. Fish and Wildlife Project 200610002.1) at the same location. Upon completion of that project, the coagulant agent was switched to ferric chloride. The results later are summarized by each phase where either ozone or UV/H₂O₂ pretreatment to RO is discussed. After a switch to ferric chloride, the operating flux of the UF-RO and UF-UV/H₂O₂-RO trains was increased in order to attempt to force significant fouling (similar to the pilot evaluation in Chapter 5) and to evaluate how preoxidation affected the cleaning frequency of the two trains. A routine analysis of RO samples as well as of UF filtrate and ozone or UV/H₂O₂ effluent was established. A complete water quality log is provided in Appendices 1–3.

6.3.1 Phase I: 14-gfd Conditions for UF-RO and UF-O₃-RO Trains

The RO pilot run at 14 gfd and using ozone as the preoxidant commenced on April 16, 2010, with six ESPA-2-4040 elements per train, at 54.5% recovery and 4.8 gpm of permeate flow, and ran intermittently through February 26, 2011. Table 6.3 shows the operating parameters for the RO pilot. Whereas ozone showed less initial flux decline than did the control train (similar to observations made at WRF 1), each of the tests resulted in massive flux decline for both trains. After the various phases of testing with ozone pretreatment, it could not be decisively concluded that ozone reduced organic fouling because aluminum scaling was suspected to have caused the rapid flux decline in each of the tests. Figure 6.3 shows the observed changes in TCSF over the test period.

Table 6.3. 14-gfd RO Operating Parameters for 1 × 6 Array

Operating Parameter	Unit	Value
Feed flow rate	gpm	8.8
Permeate flow rate	gpm	4.8
Concentrate flow rate	gpm	4.0
Filtrate flux	gfd	13.6
Feed pressure	psig	91–225
Feed water temp	°C	21.4–30.0
Recovery	%	54.5

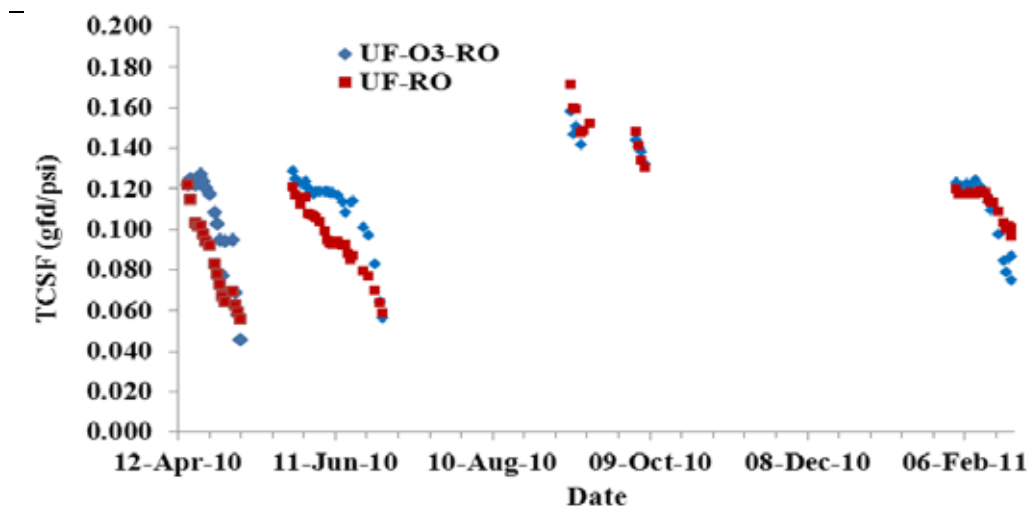


Figure 6.3. Changes in temperature-corrected specific flux (TCSF) (gfd/psi) for the UF-RO and UF-O3-RO treatments at 14 gfd during Phase I.

A high-pH CIP was conducted between several of the tests, as seen by the successful recovery of initial TCSF, shown in Figure 6.3. Rapid fouling or scaling occurred quickly each time after a system restart and could not be controlled by the pretreatment options employed during this phase of testing. On the basis of these projections for the water quality of the UF filtrate, it was not necessary to adjust the RO feed pH from 7.0 to 6.8. However, the dissolved aluminum concentration was <0.1 mg/L in the feed and 0.13 mg/L in the concentrate. Aluminum solubility at a pH between 6.8 and 7.8 is between 0.01 and 0.04 mg/L, which means that the RO feed water was likely already supersaturated with aluminum, explaining the gelatinous layer that was observed on the membranes during later autopsy (see later).

The project team collected lead and tail RO elements from each train for autopsy and preliminary microscopy analysis. Table 6.4 lists the results of factory testing and retests performed in late April 2011, courtesy of Hydranautics. The wet testing of the elements indicated that some fouling and significant scaling of the tail elements had occurred.

Table 6.4. Wet Tests of the Lead and Tail Elements from UF-RO Pilots

	Factory		Retest	
	Rejection and GPD		Rejection and GPD	
Lead	99.5	1710	99.62	1511
Tail	99.6	1644	99.33	869

UF-RO	Factory		Retest	
	Rejection and GPD		Rejection and GPD	
Lead	99.5	1866	99.66	1418
Tail	99.6	1912	99.31	700

Membrane sample swatches were also excised and prepared for SEM analysis. Portions of the membranes were exposed to hydrochloric acid for visual examination of potential effervescence (indicating a possible carbonate-based scale). None of the samples bubbled in the presence of HCl, so carbonate salts were likely uncommon or absent. There were no bacteria observed on any of the samples. Some crystals were seen on the tail end elements that are typically rarely seen during RO microscopy analysis. The brine spacer lines of the tail end samples had patches of foulant that had higher silicon content than did the surrounding foulant. A few dark, soot-like particles were observed on the feed end samples but covered very little (qualitative observation only) of the surface. Sample areas away from the brine spacer lines showed the presence of aluminum in the membranes from both trains. Figure 6.4 and Figure 6.5 show SEM images and elemental composition (with aluminum as the predominant cation) of the UF-O₃-RO and UF-RO membrane samples, revealing scale crystals and the presence of aluminum.

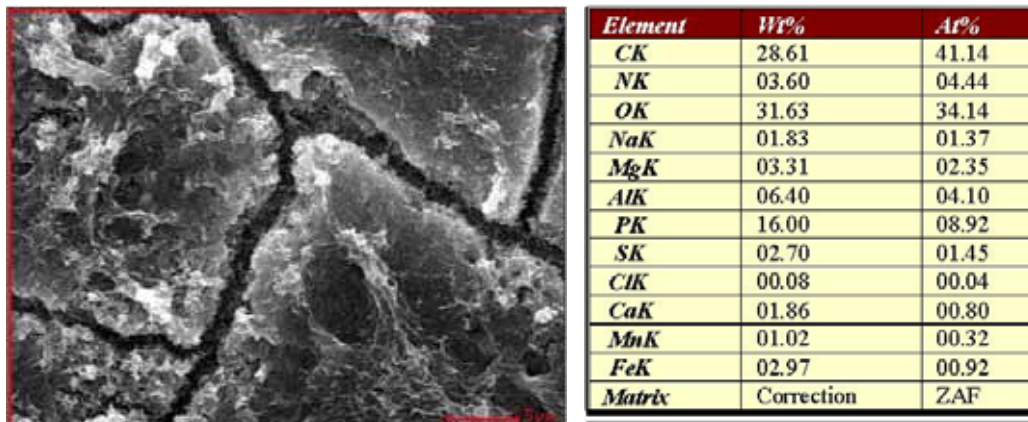


Figure 6.4. SEM image at ×3000 (the scale bar in red is for 5 μm) of a sample of UF-O₃-RO tail element (left image) and a table generated from EDAX analysis.

Source: Courtesy of Hydranautics

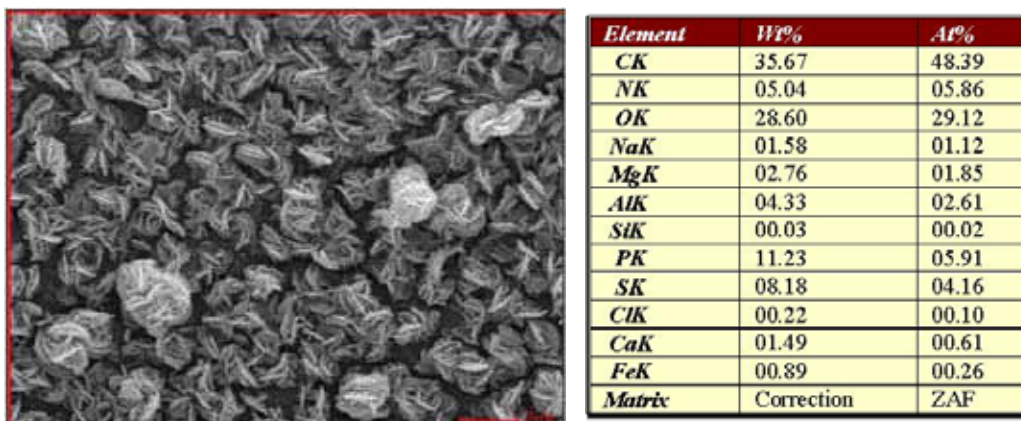


Figure 6.5. SEM image at $\times 6000$ (the scale bar in red is for 2 μm) of a sample of UF-RO tail element (left image) and a table generated from EDAX analysis.

Source: Courtesy of Hydranautics

6.3.2 Phase II: 14-gfd Conditions for UF-RO and UF-UV/H₂O₂-RO Trains

After the staff at WRF 2 was able to discontinue the use of alum, instead switching to ferric chloride, the project team started piloting the UF-UV/H₂O₂-RO trains with a new set of ESPA-2-4040 elements at a flux of 14 gfd (permeate flow = 4.8 gpm, concentrate flow = 4.0 gpm, recovery of 54.5%) on July 27, 2011. Hydrogen peroxide was fed ahead of the UV reactor at 3.0–4.0 mg/L, whereas the UV reactor was configured to run on a 20-gpm feed flow, with 17 lamps at 60% power. The project team verified the UV dose by conducting experiments with chemical actinometry. It was determined that the effective UV dose varied in the range of 1100–1300 mJ/cm² because of slight variations in the UV skid feed flow. Although slightly above the 1000-mJ/cm² target, this was the lowest possible UV dose that could be achieved while maintaining a continuous operation of both trains.

Figure 6.6 shows changes in TCSF for the two treatment trains, whereas Figure 6.7 shows the percent TCSF decline over the same run time. Similar to previous observations in the flat sheet tests and pilot-scale tests from WRF 1, the control (nonoxidized) train had an initial drop in TCSF of 24% and stabilized after 50 h of run time, whereas the oxidized train maintained steady operation. Interestingly, the nonoxidized train (CCWRD-UF-RO) began to regain flux after 400 h of operation. This result was somewhat unexpected because there were no changes in the operating conditions of the pilot during this time. The UF-UV/H₂O₂-RO train (also referred to as Train 1) showed a cumulative flux decline of 20% over 2200 h of run time, whereas the UF-RO train (Train 2 or control) had shown an initial flux decline of 24% (after 36 h) but only a net cumulative flux decline of 10% over the 2200 h of run time. The project team suspects that the accompanying increase in the normalized salt passage (Figure 6.8) was an indication of membrane deterioration occurring on both trains (and could explain the increase in flux observed for the control treatment train).

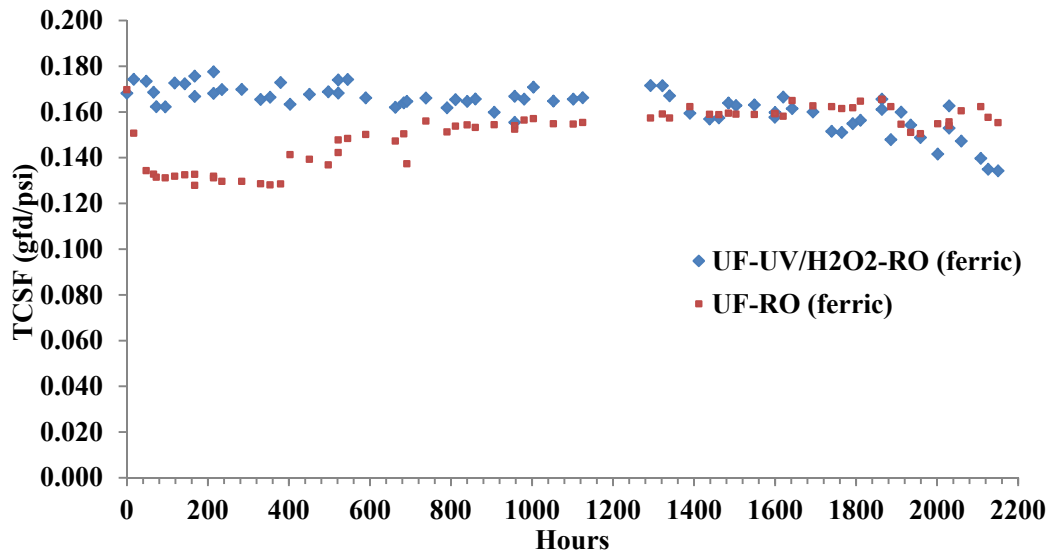


Figure 6.6. Changes in temperature-corrected specific flux (TCSF) (gfd/psi) for the UF-RO and UF-UV/H₂O₂-RO trains under 14-gfd conditions.

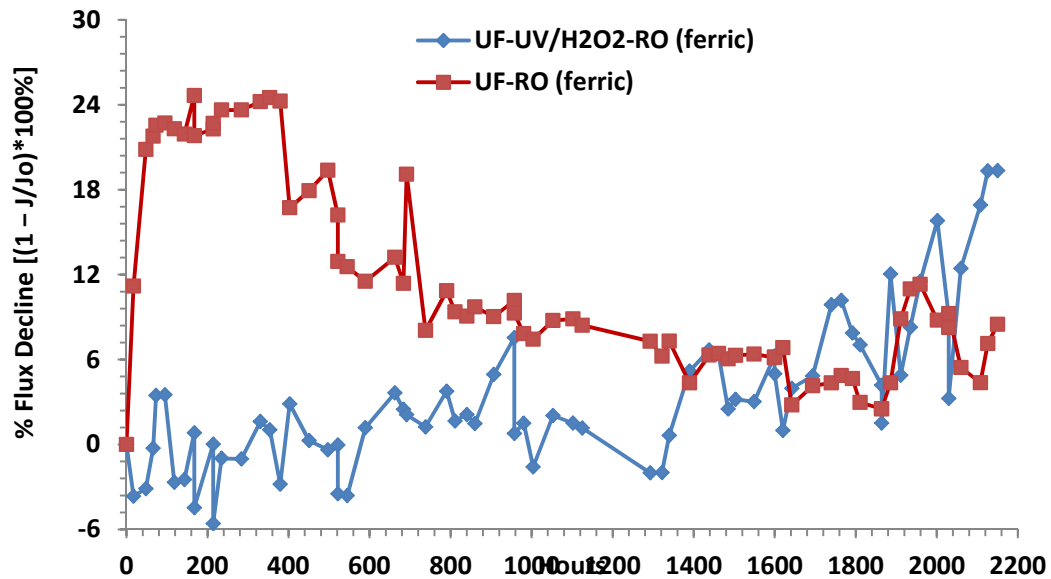


Figure 6.7. Changes in percentage of temperature-corrected specific flux decline for the UF-RO and UF-UV/H₂O₂-RO trains under 14-gfd conditions.

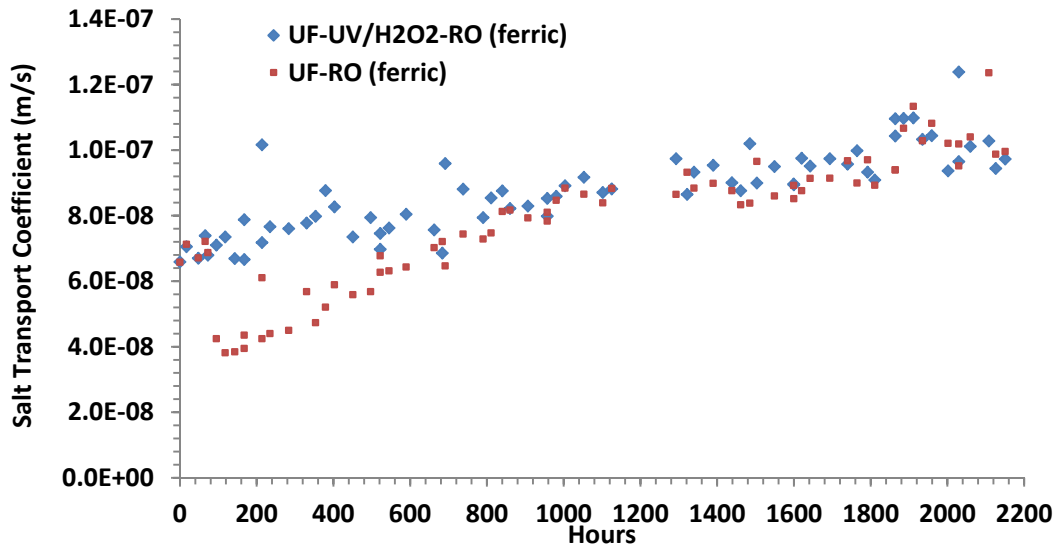


Figure 6.8. Changes in normalized salt transport coefficient for the UF-RO and UF-UV/H₂O₂-RO trains under 14-gfd conditions.

A larger dP was observed on the UF-UV/H₂O₂-RO train (Train 1, RO system no. 1), whereas the UF-RO train dP across the RO membranes remained stable as shown in Figure 6.9. The project team suspects that significant iron oxide scale was attributed to decreasing performance by Train 1. This observation was made by comparing cartridge filters between the two trains replaced after approximately 1900 h of run time. The cartridge filters from Train 1 showed heavy brown-orange deposits, whereas the Train 2 cartridge did not, as is indicated in Figure 6.10.

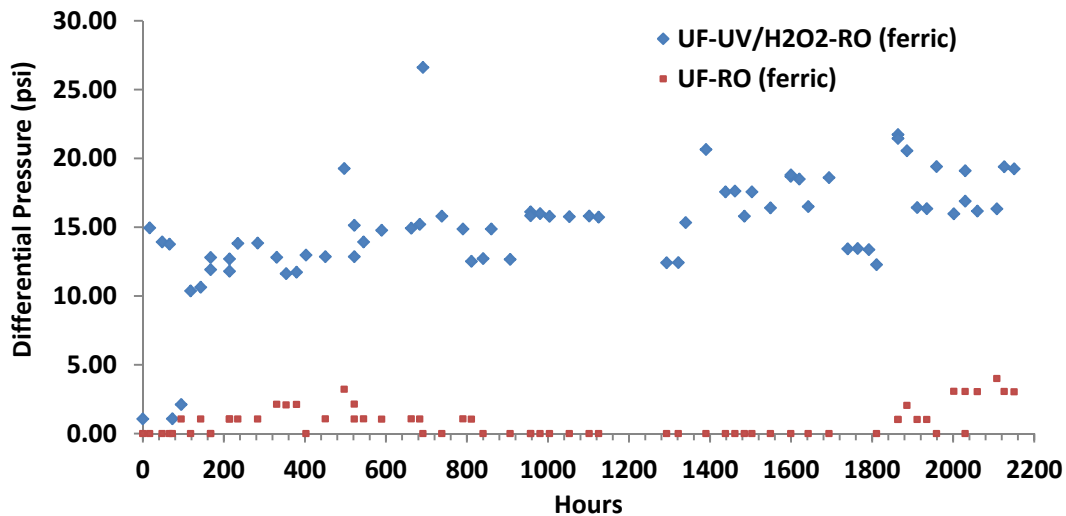


Figure 6.9. Changes in differential pressure for the UF-RO and UF-UV/H₂O₂-RO trains under 14-gfd conditions.



Figure 6.10. Photograph of cartridge filters from UF-UV/H₂O₂-RO (Train 1) and UF-RO (Train 2) trains under 14-gfd conditions.

Further review of the water quality log showed that iron was present at levels as high as 0.08 mg/L in the feed of Train 1 and Train 2 (Appendix A). Some of this iron was likely in the form of Fe(II) (as an impurity in the ferric chloride coagulant), which was oxidized by UV/H₂O₂ to insoluble forms. It was also hypothesized that some reduction of iron and manganese occurred during anaerobic/anoxic treatment, leading to soluble—for example, Fe(II) and Mn(II)—forms and thus not affecting the performance of the control train (without UV/H₂O₂ oxidation).

6.3.2 Phase III: 15.5-gfd Conditions for UV/H₂O₂ Pretreatment

After Phase II testing, a CIP was performed on both trains (at high pH to remove organics and then at low pH to remove suspected metal oxide scale) to return the membranes to their initial operating conditions. In order to try to force organic fouling to occur (further probing the efficacy of the UV/peroxide pretreatment concept), the flux was increased to 15.5 gfd by using a higher feed flow for the same 1 × 6 array of RO elements. Table 6.5 shows the operating parameters used for this phase of the study. Piloting at 15.5 gfd commenced on December 8, 2011, and continued through January 9, 2012. To mitigate iron oxide scale, the feed pH was adjusted to 6.5 by using sulfuric acid for the remainder of the pilot. Figure 6.11 shows changes in TCSF, and Figure 6.12 shows the percent TCSF decline over the same run time.

Table 6.5. 15.5-gfd RO Operating Parameters for 1 × 6 Array

Operating Parameter	Unit	Value
Feed flow rate	gpm	9.1
Permeate flow rate	gpm	5.5
Concentrate flow rate	gpm	4.6
Filtrate flux	gfd	15.5
Feed pressure	psig	112–137
Feed water temp	°C	22.0–24.6
Recovery	%	54.5

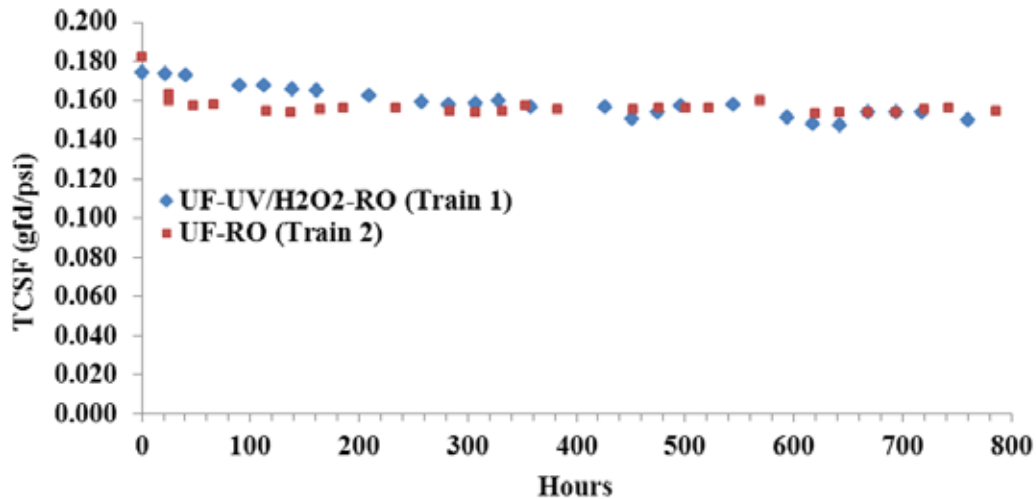


Figure 6.11. Changes in temperature-corrected specific flux (TCSF) (gfd/psi) for the UF-RO and UF-UV/H₂O₂-RO trains under 15.5-gfd conditions.

As can be seen from Figure 6.11 and Figure 6.12, the nonoxidized (control) train had an initial drop in TCSF of 15% during the first 100 h of run time, whereas the UF-UV/H₂O₂-RO train had a gradual cumulative loss of about 15% after 760 h of operation. As previously noted, these results indicate that the UV/H₂O₂ offers some benefit to preserving the initial loss of flux experienced by the control train, though the difference in flux decline could not be maintained after continuous operation.

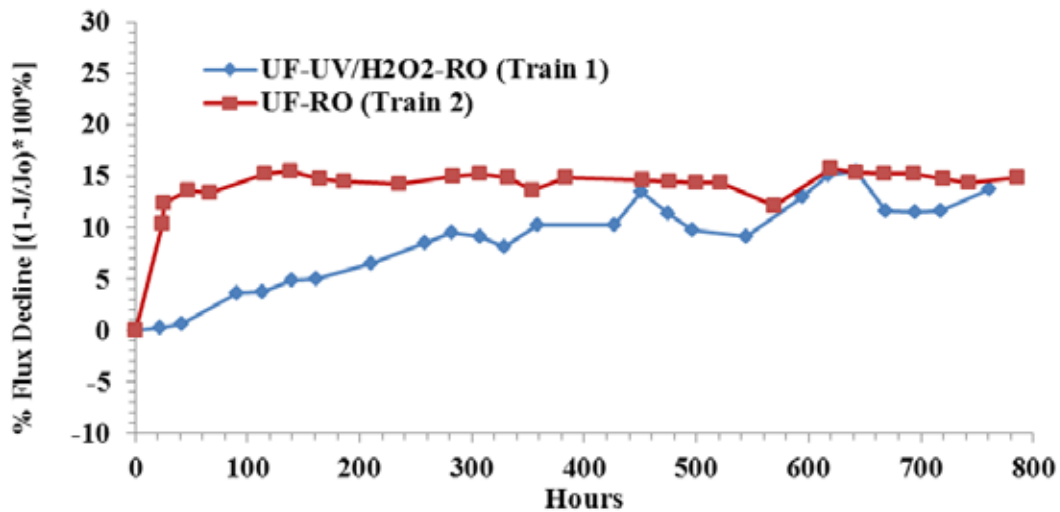


Figure 6.12. Changes in percentage of temperature-corrected specific flux decline for the UF-RO and UF-UV/H₂O₂-RO trains under 15.5-gfd conditions.

The STCn and normalized dP remained stable for the UF-RO train; however, an increase in the dP was observed for the UF-UV/H₂O₂-RO train, as can be seen from Figure 6.13.

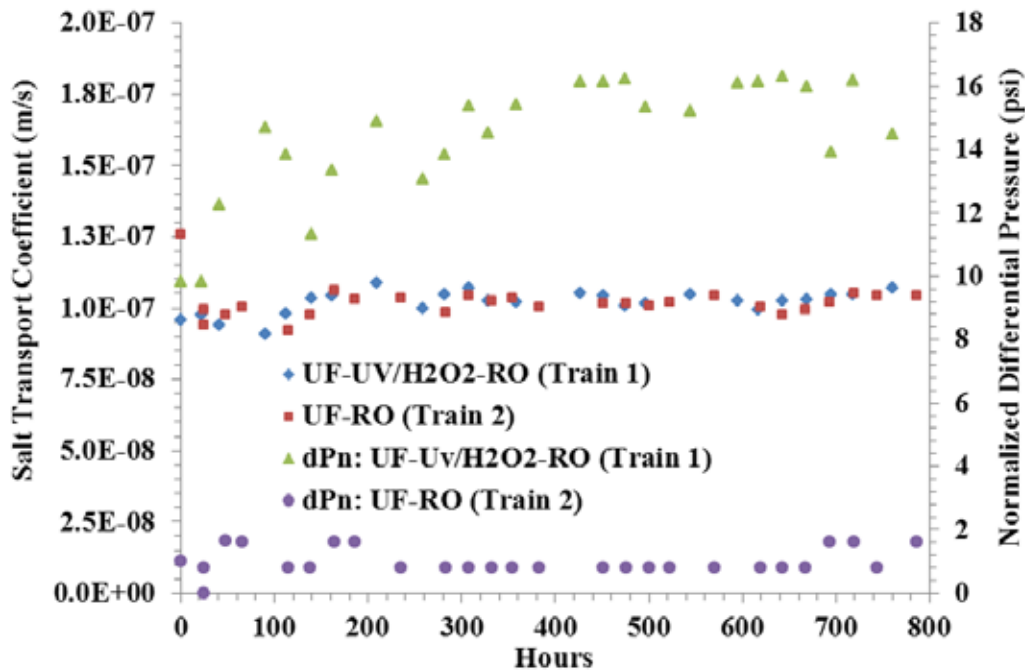


Figure 6.13. Changes in normalized salt transport coefficient and normalized differential pressure (dPn) for the UF-RO and UF-UV/H₂O₂-RO trains under 15.5-gfd conditions.

The project team collected lead and tail RO elements from each train for microscopy analysis. Table 6.6 shows the results of factory testing and retesting performed in January 2012, courtesy of Hydranautics. The wet testing of the elements indicated that some fouling and loss of salt rejection had occurred. Consistent with Figure 6.12, the results from Table 6.6 show that the UF-RO had a slightly larger loss in permeability of 19% versus 13% for the lead element of the UF-UV/H₂O₂-RO train.

Table 6.6. Wet Tests of the Lead and Tail Elements from UF-RO and UF-UV/H₂O₂-RO Trains

	Factory (Rejection and GPD)		(Retest Rejection and GPD)	
Lead	99.6	2273	99.6	1973
Tail	99.5	1843	99.5	1786
UF-RO	Factory (Rejection and GPD)		(Retest Rejection and GPD)	
Lead	99.6	2216	99.5	1805
Tail	99.5	1934	99.5	1759

6.3.4 End-of-Study Autopsy and Microscopy Analysis

The objectives of the final investigation were to characterize membrane fouling of the RO elements taken from the pilot-scale tests regarding the identification of foulants and the extent of fouling using a suite of advanced analytical techniques (methods described in Chapter 2). Surface analysis of the lead and tail elements from the WRF 2 pilot study was performed at the Colorado School of Mines. In accordance with methods described in Chapter 2, membrane samples were analyzed by ESEM for nonconductive materials, without coating with carbon or gold to minimize any artifacts associated with this sample preparation. The results from various analysis are summarized in a subsection later. A complete list of

supporting data and images is presented in Appendix D (D-4), whereas specific supporting data for the interpretation and conclusions outlined in this section are referenced accordingly.

6.3.4.1 Visual Inspection of the RO Elements

Appendix Table D-1 summarizes the inspection of the exterior of the membrane elements. The brine seal, hard shell (fiberglass outer wrap), and ATDs were not visibly defected. The lead and tail elements from the UF-UV/H₂O₂-RO train were covered with an orange coating, visible on the hard shell, on both ATDs, and within the plastic carrier. The glue lines of the membrane elements were all in good condition. No visible defects were observed.

Appendix Table D-2 summarizes the inspection of the interior of the membrane elements. All membrane elements consisted of 10 membrane leaves. The glue lines of all the membrane leaves were well sealed and in good condition. All permeate carriers and permeate sides of the membrane leaves were very clean. The observed fouling layer was for the most part homogeneously or randomly distributed on membrane feed surfaces; there was no a noticeable difference between the feed and brine ends. The lead and tail elements from the UF-UV/H₂O₂-RO train had a prevalent orange coating on all layers. Fine black particulates, with particles ranging in size from 1 to 10 mm, were observed on all sheets of all elements. The lead element from the UF-RO train had a few clusters of black particulate about 1 cm in diameter on one of the sheets. The tail element from the UF-RO train had some orange coating on the top sheet of the element. The lead element from the UF-RO train had significantly less orange coating. For all elements, the imprint of the feed spacers on the membrane was visible by darker spots and clean lines.

Dye testing showed that none of the membrane elements experienced mechanical damage (Table D-3). After the Rhodamine B dye was applied to the active layer, the support layer was found to be completely clean for all of the element samples, indicating that no leakage occurred.

6.3.4.2 Surface Hydrophobicity/Hydrophilicity

Table 6.7 summarizes the contact angle measurement results of the different membranes from both tests. The range of values for the sessile drop method was large, as is reflected by standard deviations of 2.0 to as high as 4.6°. For some of the samples, the values seemed to ascend or descend along the sample length, whereas for most, the distribution was random. The captive bubble method had a lower standard deviation, but initial measurements were more difficult to perform because there was slippage for many of the samples. The air bubble would not adhere to the membrane surface; rather, it would slide and float to the surface of the bath. For each sample, the correct alignment was selected and from there the measurement was taken until consistent angles were measured.

All of the samples were hydrophilic or moderately hydrophobic under both tests, ranging from approximately 22° to approximately 35°. The virgin membrane was extremely hydrophilic, with an average angle of 14.6°, which is significantly more hydrophilic than any of the fouled membranes. The captive bubble method was not effective for the virgin sample because the air bubbles would not adhere to the membrane surface.

During wastewater treatment, all membranes exhibited different levels of increasing hydrophobicity as a result of adsorption of transphilic and hydrophobic organics, scaling, and biofouling. The two most hydrophilic membrane samples found in both the sessile drop and the captive bubble methods were those from the UF-RO train. The mean contact results for the UF-UV/H₂O₂-RO membranes were statistically different (higher), despite large standard

deviations. Thus, the UV/peroxide treatment train actually had more hydrophobic active layers than did the UF-RO train.

Table 6.7. Contact Angle Measurements for UF/RO Treatment Trains at 15.5 gfd

Pretreatment of:	Lead/Tail	Sessile Drop		Captive Bubble	
		Mean	SD	Mean	SD
Virgin ESPA membrane		14.6	3.3	Not measurable	
UF-UV/H ₂ O ₂ -RO	Lead	34.1	4.6	42.3	1.7
	Tail	35.4	3.4	41.5	0.9
UF-RO	Lead	25.8	4.6	31.7	2.9
	Tail	21.6	2.0	31.2	1.1

6.3.4.3 Quantitative Measurements of Organic and Inorganic Substances in Fouling Layer

Results of the TOC extraction with various solvents are shown in Table 6.8. As a reminder, an acid solution is typically used to extract inorganic foulants, whereas caustic solution is commonly used to remove organic foulants and silica. However, it should be noted that, even if sonication is applied, the method may still not be able to extract all foulants and scalants from the fouling layer. This is because the fouling layer consists predominantly of inorganic compounds and because precipitations of metal hydroxides prevent the extraction process from occurring completely.

Table 6.8. TOC Analysis (as mg/cm² of Membrane Surface) for UF-RO Trains

Pretreatment	Lead/Tail Element	DI Water Extraction	0.1 M NaOH Extraction	0.8 M HNO ₃ Extraction
UF-UV/H ₂ O ₂ -RO	Lead	0.0047	0.0037	0.0017
	Tail	0.0029	0.0045	0.0010
UF-RO	Lead	0.0003	0.0027	-0.0003
	Tail	0.0017	0.0019	-0.0001

The highest TOC concentration was for the samples extracted with base and was lowest for those extracted with acid. The lead elements sometimes had lower TOC concentration, although for certain samples the opposite was true. The lead element of the membranes with UF-UV/H₂O₂ pretreatment seemed to have a greater TOC concentration than did the tail element for both the DI water extraction and the acid extraction method. For the base extraction, the elements from the UF-RO train showed higher levels of TOC on the lead sample than on the tail sample. The lowest TOC concentration was observed for the elements from the UF-RO train.

The results from fluorescence analysis, presented by Table 6.9, show higher peak intensity of the protein-like substances for the UF-UV/H₂O₂-RO train. Supporting fluorescence EEM images are presented in Appendix D, Table D-4. In addition, the metals analysis by ICP-OES (Appendix D, Table D-6) confirmed that the membranes pretreated with UF-UV/H₂O₂ exhibited much higher iron content than did the elements from the UF-RO train. Given these results, it is likely that the UF-UV/H₂O₂-RO train suffered from heavier organic fouling due to coprecipitation of iron species.

Table 6.9. Fluorescence Analysis of Foulant Extraction of UF-RO Trains

Pretreatment	Lead/Tail	Protein-Like Substance Peak Intensity (Em/Ex)	Humic- and Fulvic-Like Substance 1 Peak (Intensity)	Humic- and Fulvic-Like Substance 2 Peak (Intensity)
Extraction with DI Water:				
UF-UV/H ₂ O ₂ -RO	Lead	0.15 (344/277)	None	None
	Tail	0.12 (345/275)	None	None
UF-RO	Lead	0.08 (350/280)	None	None
	Tail	0.03 (360/275)	None	None

6.3.4.4 *Scanning Electron Microscopy (SEM) and Energy Dispersive X-Ray Spectroscopy (EDS) Examination of Membrane Surface*

Table 6.10 provides a summary of the ESEM/EDS analysis as well as observations made regarding the biofouling based on results described in preceding sections. Supporting images are compiled in Appendix D. Figure D-1 shows a series of ESEM images and EDS results of the virgin membranes. Figure D-6 shows ESEM/EDS results for the lead element of the UF-RO train, whereas Figure D-7 shows results for the tail element of the same train. Figure D-8 and Figure D-9 show ESEM/EDS results for the lead and tail elements of the UF-UV/H₂O₂-RO train, respectively.

The membrane surface of the tail elements was much cleaner than the lead elements, with some Fe-based precipitates and organically based particles for both trains. Heterogeneous fouling was formed on the membrane surface of the lead elements. The fouling layer was thicker on the lead element of the UF-UV/H₂O₂-RO train as a combination of biofouling and iron precipitates. In addition some iron-containing particles with small amounts of silicate and calcium phosphate were also observed.

Table 6.10. Summary of the ESEM and EDS Characterization Results of UF-RO Trains

Analysis	Virgin Membrane	UF-RO		UF-UV/H ₂ O ₂ -RO	
		Lead	Tail	Lead	Tail
ESEM/EDS	Homogeneous membrane surface, flower-like surface features evenly distributed; the major elements are C, O, S.	Heterogeneous thin fouling layer, some areas having significant biogrowth; numerous bacterial cells and Al-silicate, Ca- and Fe-based particles observed on membrane surface.	Very clean membrane surface; the fouling layer is of more organic nature and has fewer Fe-based precipitates.	Heterogeneous fouling layer, some areas having very thick fouling layer with biogrowth and Fe-based precipitates on membrane surface.	Heterogeneous fouling layer, membrane surface is cleaner than the lead element; the fouling layer is combination of biofouling and Fe-based precipitates.
Biofouling —protein analysis	None	The protein analysis indicates biofouling in the lead element and less than in the tail element.		The protein analysis indicates biofouling in the lead element and less than in the tail element.	

Note: Major differences between the lead and tail membrane elements are noted with underlined text.

6.4 Conclusions

The project team could not decisively conclude that ozone applied at WRF 2 in the UF filtrate reduced organic fouling because heavy aluminum scaling occurred on both trains despite scale control by the addition of an antiscalant. Once the coagulant was switched to ferric chloride and the UV/peroxide testing was commenced, the UV/H₂O₂ treatment offered some benefit in preserving the flux initially, similar to what was observed in the ozone tests at WRF 1 and summarized in Chapter 5. However, this effect was lost after continuous operation. Despite efforts to minimize scaling (e.g., pH adjustment of the feed to 6.5 and addition of antiscalant agent), the heaviest iron scaling was actually found on the lead element of the UF-UV/H₂O₂-RO train, as shown by ESEM/EDS analysis, characterization of the foulant layer, and an associated steady decline in the TCSF with a steady increase of dP. Overall, the results from this pilot-scale study showed that heavy iron-based deposits were accompanied with organic fouling and biofouling occurring on the lead element of the UF-UV/H₂O₂-RO train, thus negating any benefit from oxidative pretreatment. This finding is significant as it shows that, despite potential benefits that can be realized from preoxidation for organic fouling control, preoxidation may increase scaling potential, leading to higher dP increases and more-heterogeneous fouling, where coagulant use is required for UF or MF membrane operation.

Chapter 7

Preoxidation Impacts on Trace Organic Contaminant (TOC) Concentrations

7.1 Introduction and Background

The primary objective of this portion of the study was to evaluate TOC fate and transport at each of the test facilities (WRF 1, WRF 2, and DWTP 1) in CRW and through each stage of the various pilot- and bench-scale water reuse tests. The efficacy of both ozone and ozone/peroxide was monitored to evaluate NDMA destruction, direct NDMA formation, NDMA FP, and the destruction of other TOCs (e.g., pharmaceuticals and personal care products) at DWTP 1 and WRF 1. Likewise, similar experiments were conducted on the UV/peroxide system at WRF 2. In order to narrow the scope of this aspect of the project, a subset of the numerous compounds detected in previous occurrence studies was selected for evaluation. The indicator compounds were selected on the basis of their magnitude and frequency of occurrence in water and wastewater (S. A. Snyder et al., 2007), various physical/chemical characteristics, and resulting susceptibility to treatment (Ternes et al., 2002; Westerhoff et al., 2005; S. A. Snyder et al., 2007) and ease of analytical methods (Trenholm et al., 2009). Because bromate formation has historically been the most significant concern related to the use of ozone in water treatment (Orlandini et al., 1997; Wert et al., 2007), bromate was also monitored during the study. With respect to the advanced treatment trains, the project team also evaluated the integration of this technology as a possible pretreatment to an RO membrane system to minimize transport of trace contaminants and consequent impacts on the RO permeate. In this way, this technology was broadly evaluated for its application in reuse applications.

Various oxidation processes using substances such as ozone, ozone/peroxide, UV/H₂O₂, and nonthermal plasma have been reported to be effective in oxidizing TOCs (Rosenfeldt and Linden, 2004; S. A. Snyder et al., 2007; Benotti et al., 2009a; Wert et al., 2009; Gerrity et al., 2010; Rosario-Ortiz et al., 2010; Gerrity et al., 2011), but these processes are not equally able to remove all compounds. For example, one of the advantages of UV/H₂O₂ is the ability to remove NDMA and NDMA precursors in water (Kruithof et al., 2007) via photolysis and hydroxyl radical (\bullet OH) oxidation. This process may be especially important in reuse applications where the eventual chlorination and/or chloramination of the finished water may result in more NDMA formation (Pehlivanoglu-Mantas et al., 2006). In contrast, ozone and ozone/peroxide have been implicated in direct formation of NDMA during oxidation of dimethylamine and may in fact exacerbate NDMA concerns (Andrzejewski et al., 2008). Furthermore, Schmidt and von Gunten reported direct NDMA formation due to oxidation of *N,N*-dimethylsulfamide by ozone in natural waters (Schmidt and Brauch, 2008; von Gunten et al., 2010). Despite the direct formation of NDMA, ozonation has been shown to be extremely effective in reducing FP, which is the formation of NDMA following chloramination.

Therefore, assuming direct NDMA formation can be controlled in ozone or ozone/peroxide applications, the preoxidation of water intended for RO membrane treatment may provide the ancillary benefit of notably reduced breakthrough of contaminants through the RO

membranes and improved quality of the RO concentrate. This portion of this report addresses the experiments and data collected throughout the project at each of the pilot facilities.

7.2 Experimental Methods and Equipment

7.2.1 Drinking Water Treatment Plant 1, Colorado River Water Tests

For the drinking water tests, CRW from Lake Mead, NV, was used as the source water for the pilot-scale HiPOx[®] and bench-scale RO membrane testing. The ozone dose was controlled by adjusting oxygen flow and generator power and by monitoring the percent ozone in the dry gas for the following doses: 0.6, 1.5, 3.0, 6.0, and 10.0 mg/L; peroxide addition is described in Chapter 5. The transfer efficiency was typically high (>95%), so the applied ozone dose was approximately equal to the transferred ozone dose. The bench-scale RO testing consisted of using two identical GE Osmonics Sepa-CF cross-flow membrane flat sheet cell holders to process the raw and oxidized waters by applying a protocol previously described in Chapter 3.

A description of the HiPOx[®] reactor is provided in Chapter 5. However, for the CRW tests the reactor was installed at DWTP 1. The CRW received at the pilot plant was prechlorinated (0.8 mg of free chlorine/L) by the local water utility to control Quagga mussel growth in the intake structures. The experimental water initially contained a free chlorine residual less than 0.2 mg/L, but the water was also recirculated for 24 h in a 3000-gal batch tank to remove residual chlorine. The feed water also passed through a 5- μ m-pore-size cartridge filter prior to filling the tank. A recirculation rate of 10 gpm allowed for complete turnover of the batch tank nearly five times in the 24-h period. At the end of 24 h, a spike solution of the analytes dissolved in laboratory-grade water was added to the batch tank, and the water was recirculated for an additional 24 h. The analytes were not dissolved in a solvent in order to prevent the introduction of potential \cdot OH scavengers. Control samples were collected at the beginning and end of the experiments to evaluate consistency in the target compound concentrations.

7.2.2 Water Reclamation Facility 1, MBR-O₃-RO Tests

Full details of the WRF 1 MBR-O₃-RO pilot can be found in Chapter 5. Ozone doses of 0.6 to 10 mg/L were applied in a manner consistent with that described in Section 7.1.1.

7.2.3 Water Reclamation Facility 2, UF-UV/Peroxide/RO Tests

Full details of the WRF 2 UF-UV/peroxide-RO pilot can be found in Chapter 5. UV fluence of 400 mJ/cm² and 1000 mJ/cm² and peroxide doses of 0–10 mg/L were tested to simulate realistic UV/AOP treatment trains.

7.2.4 Analytical Methods

Analytical methods were applied as described in Chapter 2 with the following addition: in the NDMA destruction experiments with MBR filtrate, an NDMA spike solution was fed into the HiPOx[®] with an in-line static mixer. As mentioned previously, the NDMA was dissolved in water to prevent the introduction of any solvents that would contribute to \cdot OH-scavenging. For the CRW NDMA destruction experiment, NDMA was spiked at 2300 ng/L into a 3000-gal tank. Ozone doses of 0.6, 1.5, 3, 6, and 10 mg/L were used with and without excess hydrogen peroxide at a 0.7-mol ratio to evaluate NDMA destruction. For the CRW TOrC destruction experiment, selected organic compounds were spiked into the batch tank at approximately 1000 ng/L, except for tris(2-carboxyethyl)phosphine (TCEP) and tris(1-

chloro-2-propyl)phosphate (TCPP), which were spiked at approximately 5000 ng/L. For the WRF 1 NDMA destruction experiment, an NDMA spike solution designed to provide a working concentration of 30 ng/L in the test water was dosed into the feed line of the HiPOx[®] with an in-line mixer. For WRF 2, an NDMA spike solution designed to provide a working concentration of 300 ng/L in the test water was dosed into the feed line of the UV reactor at a variable flow rate to accommodate test conditions at various UV doses. In both cases (WRF 1 and WRF 2), the actual NDMA concentration was measured in the reactor influent to obtain the starting concentration (C_0). For the TOrC destruction experiments in MBR (WRF 1) and UF (WRF 2) filtrate tests, changes in the ambient TOrC concentrations were monitored during various ozone and UV/peroxide dose conditions.

7.2.5 Energy Calculations for Contaminant Destruction

The electrical energy-per-order (EEO) values were determined by plotting $\ln(C/C_0)$ versus energy, consistent with previously described methods (Benotti et al., 2009a; Gerrity et al., 2010). The energy required to generate 1 g of O_3 was assumed to be 0.01232 kWh. Hydrogen peroxide cost was assumed as \$0.68/kg (Rosenfeldt et al., 2006). Through use of an electrical energy cost of \$0.07 per kWh, the cost of hydrogen peroxide addition was converted to units of energy per unit volume of treated wastewater. This additional energy cost was factored into calculation of EEO values for the ozone/peroxide process. The cost of pumping or pressurization was not considered in this calculation as it will vary from process to process. For determination of electrical energy consumption by UV, lamp power rating was divided by the flow rate to achieve a particular UV fluence and converted to kWh/m³. The cost of hydrogen peroxide was also added (where applicable). The EEO values were then similarly determined by plotting $\ln(C/C_0)$ versus energy, consistent with methods described earlier.

7.3 Experimental Results

7.3.1 Background Water Quality Data

Water samples were analyzed at the WRF 1, WRF 2, or DWTP 1 laboratory for background water quality parameters according to standard methods. Representative MBR filtrate (WRF 1), UF filtrate (WRF 2), and CRW (DWTP 1) water quality parameters are provided in Table 7.1. Analysis of inorganic water constituents was performed by the water reclamation facility's lab according to standard methods. The CRW had a lower DOC of 2.6 mg/L; however, it had a relatively high alkalinity. The MBR and UF filtrates were typically fully nitrified, partially denitrified, and equivalent to a full-scale tertiary effluent with a DOC of 5.1 to 6.5 mg/L, UV_{254} of less than 0.130, and turbidity of less than 0.2 NTU as indicated in Table 7.1.

Table 7.1. Water Quality Parameters for MBR Filtrate and Colorado River Water

Constituent	Concentrations (mg/L) or Other Values for:		
	MBR Filtrate	UF Filtrate	CRW
Calcium	74	100	78
Magnesium	31	39	27
Sodium	160	190	94
Potassium	22	18	6.2
Total phosphorus	0.2–2.0	0.2	N/A
Ammonia (as N)	<0.5	<0.5	N/A
Barium	0.045	0.039	0.14
Strontium	1.2	1.3	N/A
Bromide	0.1	0.17	0.085
Alkalinity, as mg of CaCO ₃ /L	99	83	138
Sulfate	250	359	248
Chloride	180	238	88
Fluoride	0.74	0.73	0.34
Nitrate (as N)	13.8	13.0	0.60
Boron	0.31	0.36	N/A
Silica	12.5	11.0	7.5
TDS	865–1200	1032–1150	625
pH	7.3–7.6	7.2–7.6	8.1
Temp	26–33 °C	24–30 °C	14–19 °C
TOC	5.8–6.5	5.1–6.3	2.6
UV ₂₅₄	0.11–0.13	0.091– 0.126	0.036
Coliforms	<5 MPN/100 mL	N/A	N/A
Turbidity (NTU)	<0.2	<0.2	<0.5
SDI	<3–6	<3–6	<3

Given the focus on contaminant oxidation/photolysis of this chapter, Table 7.1 is supplied for quick reference to the water quality parameters for the waters where oxidation is occurring. However, for the larger context, the water quality parameters through the entire pilot systems (WRF 1 and 2) are also of importance. Therefore, the relevant data for the feed, filtrate, and permeate waters from the MBR-O₃-RO (WRF 1) and UF-UV/peroxide-RO (WRF 2) facilities can be found in Chapters 5 and 6.

7.3.2 TOrC Removal/Oxidation from Colorado River Water with Ozone and RO Treatment

7.3.2.1 NDMA Removal in CRW

The data from the CRW NDMA destruction tests are summarized in Figure 7.1. All replicate samples and controls were reproducible with a relative error of less than 6.3% based on duplicate samples. As expected, ozone alone had little impact on the removal of NDMA

(12% removal at 10 mg of O₃/L). However, ozone with peroxide achieved a similar level of destruction with significantly less ozone (12% removal at 1.5 mg of O₃/L + 0.5 mg of peroxide/L and 46% removal at 10 mg of O₃/L + 3.5 mg of peroxide/L). These levels of degradation are consistent with the low second-order ozone ($k_{O_3} = 5.3 \times 10^{-2} \text{ M}^{-1} \text{ s}^{-1}$) and •OH ($k_{\bullet OH} = 4.6 \times 10^8 \text{ M}^{-1} \text{ s}^{-1}$) rate constants for NDMA (C. Lee et al., 2007b).

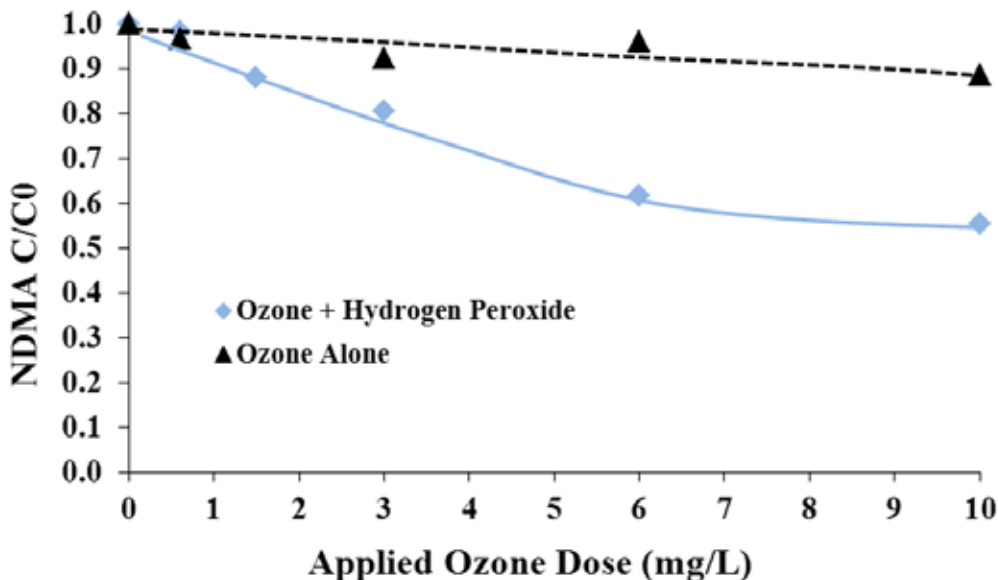


Figure 7.1. Removal of NDMA by ozone and ozone/peroxide in spiked Colorado River water.
Source: A similar version of this figure was presented in Pisarenko et al. (2012).

7.3.2.2 TOrC Removal in CRW

Experiments with TOrCs showed similar removal trends for ozone and ozone/peroxide, although most of the compounds were more amendable than NDMA to ozone oxidation, as shown by Table 7.2 and Table 7.3. As expected, the two flame retardants (TCEP and TCPP) were considerably more resistant to oxidation than were the other compounds. Both compounds have been reported to have a modest second-order rate constant with hydroxyl radical (TCEP = $5.6 \times 10^8 \text{ M}^{-1} \text{ s}^{-1}$ and TCPP = $7.0 \times 10^8 \text{ M}^{-1} \text{ s}^{-1}$) versus an estimated rate constant with ozone of $<10 \text{ M}^{-1} \text{ s}^{-1}$ (Pocostales et al., 2010). These tests were performed in CRW with pH of 8.1. Previously it has been shown that decomposition of ozone in basic aqueous solutions produces hydroxyl radicals (Staehelin and Hoigné, 1982; Tomiyasu et al., 1985), which supports the observed degradation of these flame retardant compounds with ozone only. The addition of peroxide expedited the formation of •OH and yielded greater removal of many compounds than did ozone alone.

Table 7.2. Percentage Removal of TOrCs by Ozone in Colorado River Water at Various O₃:DOC Ratios

Contaminant	Percentage Removal				
	O ₃ :DOC =	O ₃ :DOC =	O ₃ :DOC =	O ₃ :DOC =	O ₃ :DOC =
	0.23 (0.6 mg/L)	0.58 (1.5 mg/L)	1.15 (3 mg/L)	2.31 (6 mg/L)	3.85 (10 mg/L)
Carbamazepine	>99.2	>99.2	>99.2	>99.2	>99.2
Trimethoprim	>99.1	>99.1	>99.1	>99.1	>99.1
Atenolol	98.0	>99.0	>99.0	>99.0	>99.0
Primidone	77.7	86.7	95.2	98.6	>99.0
Dilantin	74.1	82.5	93.5	98.3	>99.0
Meprobamate	42.7	57.3	71.8	83.6	91.6
Atrazine	41.3	54.5	69.2	83.9	91.2
TCPP	22.7	13.7	30.7	37.8	71.9
TCEP	20.7	19.0	23.3	27.6	51.7

Table 7.3. Percentage Removal of TOrCs by Ozone + Peroxide in Colorado River Water at Various O₃:DOC Ratios

Contaminant	Percentage Removal				
	O ₃ :DOC =	O ₃ :DOC =	O ₃ :DOC =	O ₃ :DOC =	O ₃ :DOC =
	0.23 (0.6 mg/L)	0.58 (1.5 mg/L)	1.15 (3 mg/L)	2.31 (6 mg/L)	3.85 (10 mg/L)
Carbamazepine	>99.2	>99.2	>99.2	>99.2	>99.2
Trimethoprim	>99.1	>99.1	>99.1	>99.1	>99.1
Atenolol	96.2	>99.0	>99.0	>99.0	>99.0
Dilantin	91.2	98.6	>99.0	>99.0	>99.0
Primidone	83.6	97.8	>99.0	>99.0	>99.0
Meprobamate	66.4	83.6	95.6	>99.0	>99.0
Atrazine	55.5	74.4	89.6	97.1	>99.0
TCEP	31.0	25.9	25.0	37.9	60.9
TCPP	29.7	31.7	24.7	43.8	73.7

7.3.2.3 TOrC Removal in CRW through RO and O₃-RO

In addition to the oxidation experiments earlier, several hundred gallons of spiked CRW—with ozonation (3 mg/L) and without ozonation—was collected for flat sheet testing with ESPA-2 RO membranes (see Chapter 4 for details on experimental setup). The feed water and RO permeate samples were then analyzed for the various target compounds to evaluate the effects of ozone pretreatment on subsequent RO processes, including RO breakthrough. The removal of all TOrCs through the RO membrane was >95% for the raw/control water; however, with the exception of TCEP and TCPP, TOrCs were detected at reportable concentrations in this RO permeate (Table 7.4). In contrast, none of the target compounds was detected at reportable concentrations in the RO permeate with preozonation. Therefore, the use of preozonation in the CRW matrix does lower the concentration of the contaminants in the permeate and, by mass balance, could also be expected to minimize the concentration of TOrCs in the retentate.

Table 7.4. Summary of the Effects of RO (ESPA-2) and Preozonation on TOrC Concentration (ng/L)

Analyte	Spiked CRW	Spiked CRW-RO Permeate (No Ozone)	Spiked CRW +3-mg/L O ₃	Spiked CRW-O ₃ -RO Permeate (3 mg/L O ₃)
Carbamazepine	800	16	<10	<10
Trimethoprim	760	16	<10	<10
Atenolol	780	25	<25	<25
Dilantin	930	19	77	<10
Primidone	1000	24	70	<10
Meprobamate	860	23	290	<10
Atrazine	820	19	290	<10
TCEP	4100 ^a	<200	5000 ^a	<200
TCPP	3100	<200	2500	<200

^aThe precision of these measurements was ± 1000 ng/L (based on dilution factor and MRL).

7.3.3 TOrC Removal/Oxidation Through MBR, Ozone, and RO Treatments at WRF 1

7.3.3.1 TOrC Removal by MBR, Ozone, Ozone/Peroxide, and RO

TOrCs were measured in hydraulically linked MBR influent and filtrate samples. As expected, the MBR achieved significant reductions in the target compounds that are susceptible to biotransformation and biodegradation (e.g., naproxen, ibuprofen, and gemfibrozil) (Figure 7.2) consistent with previous work (S. A. Snyder et al., 2006). However, the more biologically recalcitrant compounds, including sulfamethoxazole, TCEP, DEET, primidone, and dilantin, were persistent in the filtrate. In general, ozone alone in the MBR filtrate accomplished removal of most compounds to below detection limits. For easily oxidized compounds in wastewater such as carbamazepine, trimethoprim, and diclofenac, the ozone/peroxide process did not provide additional removal benefits compared to ozone alone. For persistent compounds such as DEET and TCEP, the addition of hydrogen peroxide achieved only marginal improvements in the oxidation of these contaminants, as shown in Table 7.5 and Table 7.6. This observation is likely due to the AOP inherent in a high EfOM-ozone system, thereby negating the need for addition of peroxide to promote hydroxyl radical formation (Buffle et al., 2006; Nöthe et al., 2009; S. Lee et al., 2010; Pocostales et al., 2010).

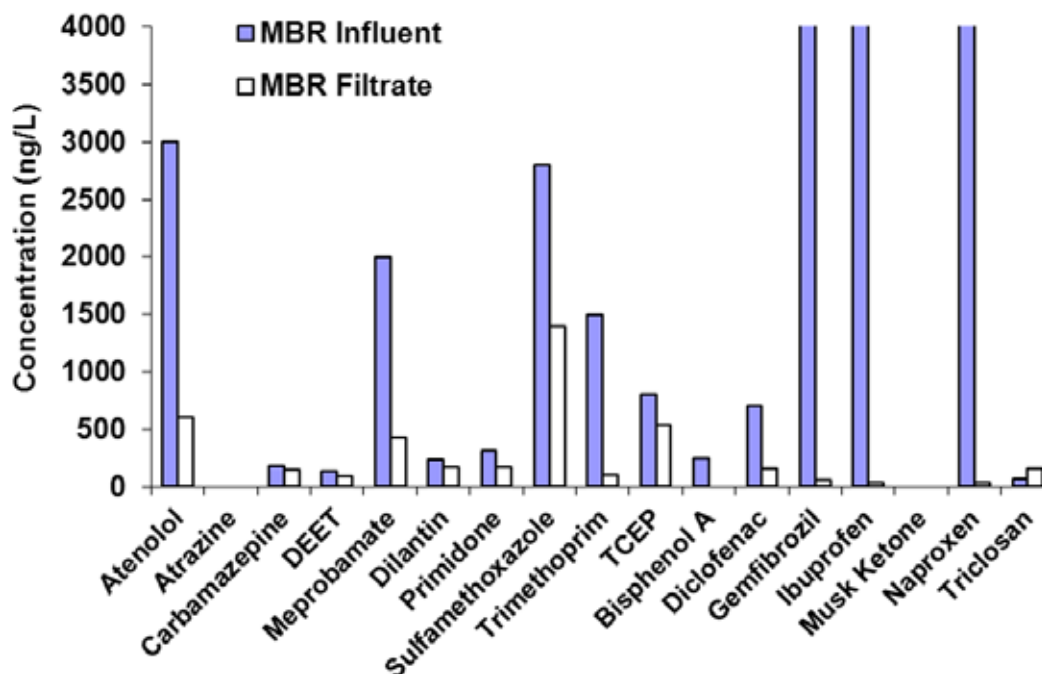


Figure 7.2. Concentration of TOxCs through MBR treatment at WRF 1.

Note that concentrations of gemfibrozil (5200 ng/L), ibuprofen (30,000 ng/L), and naproxen (29,000 ng/L) extend beyond the y axis range shown here.

Table 7.5. Percentage Removal of TOxCs by Ozone in MBR Filtrate at Various O₃:DOC Ratios

Contaminant	Percentage Removal				
	O ₃ :DOC = 0.10 (0.6 mg/L)	O ₃ :DOC = 0.25 (1.5 mg/L)	O ₃ :DOC = 0.5 (3 mg/L)	O ₃ :DOC = 1.0 (6 mg/L)	O ₃ :DOC = 1.7 (10 mg/L)
TCEP	0.0	0.0	8.3	11.9	17.4
Meprobamate	0.0	10.5	16.2	27.0	54.3
Primidone	0.0	1.2	30.9	58.5	83.2
Dilantin	0.0	13.9	39.2	67.1	92.9
DEET	0.0	18.8	38.8	64.7	>99.0
Atenolol	0.0	0.0	18.3	>99.0	>99.0
Sulfamethoxazole	21.4	70.0	90.7	>99.0	>99.0
Ibuprofen	0.0	0.0	13.3	>99.0	>99.0
Carbamazepine	20.0	72.0	>99.0	>99.0	>99.0
Trimethoprim	44.0	84.0	>99.0	>99.0	>99.0
Gemfibrozil	55.0	N/A	>99.0	>99.0	>99.0
Naproxen	47.0	61.6	>99.0	>99.0	>99.0
Diclofenac	65.6	>99.0	>99.0	>99.0	>99.0
Triclosan	>99.0	>99.0	>99.0	>99.0	>99.0

Table 7.6. Percentage Removal of TOrCs by Ozone + Peroxide in MBR Filtrate at Various O₃:DOC Ratios

Contaminant	Percentage Removal				
	O ₃ :DOC = 0.10 (0.6 mg/L)	O ₃ :DOC = 0.25 (1.5 mg/L)	O ₃ :DOC = 0.5 (3 mg/L)	O ₃ :DOC = 1.0 (6 mg/L)	O ₃ :DOC = 1.7 (10 mg/L)
TCEP	0.0	0.0	4.6	17.4	21.1
Meprobamate	7.6	10.6	21.2	45.5	74.2
Primidone	0.0	0.0	23.8	67.6	89.0
DEET	9.1	20.0	47.3	74.5	>99.0
Dilantin	8.3	16.7	50.0	80.4	>99.0
Atenolol	0.0	7.1	49.3	95.9	>99.0
Sulfamethoxazole	7.1	68.9	95.7	98.6	>99.0
Ibuprofen	6.1	18.4	38.8	>99.0	>99.0
Diclofenac	9.9	83.0	>99.0	>99.0	>99.0
Trimethoprim	16.7	69.3	>99.0	>99.0	>99.0
Carbamazepine	22.7	61.4	>99.0	>99.0	>99.0
Naproxen	7.9	51.7	>99.0	>99.0	>99.0
Gemfibrozil	23.1	34.6	>99.0	>99.0	>99.0
Triclosan	92.6	>99.0	>99.0	>99.0	>99.0

In addition to monitoring the removal of these contaminants during oxidation, changes in the RO concentrate and permeate were determined by calculating the mass balance among RO feed, permeate, and concentrate. The feed and permeate samples were analyzed for the various target compounds, but the RO concentrate levels were determined on the basis of the 52% recovery of the RO pilot. Without preozonation, RO breakthrough was observed only for carbamazepine (Table 7.7), thereby indicating that the pilot-scale RO skid was effective in achieving the reporting limits for the target compounds. The use of preozonation with 1.5-mg/L ozone reduced carbamazepine breakthrough to the reporting limit of the assay. Further, on the basis of the mass balance calculations, the RO concentrate is expected to contain significantly lower concentrations of TOrCs than would be expected from a system with no preoxidation.

Table 7.7. Removal of TOrCs (ng/L) by MBR, Ozone, and RO

Contaminant	Results with No Preoxidation				Results with 1.5-mg/L Ozone Preoxidation		
	MBR Influent	MBR Filtrate	RO Permeate	RO Concentrate	Ozone Effluent	RO Permeate	RO Concentrate ^a
Atenolol	3000	950	<25	1980	950	<25	1310
Carbamazepine	180	150	110	313	42	<10	88
DEET	130	85	<25	177	69	<25	144
Diclofenac	700	160	<25	333	<25	<25	<25
Dilantin	240	170	<10	354	27	<10	354
Gemfibrozil	5200	161	<10	335	N/A	<10	250
Ibuprofen	30,000	49	<25	100	48	<25	100
Meprobamate	2000	545	<10	1140	488	<10	979
Naproxen	29,000	121	<25	251	46	<25	104
Primidone	310	170	<10	354	170	<10	417
Sulfamethoxazole	2800	1400	<25	2920	420	<25	875
TCEP	800	540	<200	1130	540	<200	1200
Triclosan	67	160	<25	333	<25	<25	<25
Trimethoprim	1500	100	<10	210	16	<10	33
Atrazine	<10	<10	<10	N/A	<10	<10	N/A
Bisphenol A	250	<50	<50	N/A	<50	<50	N/A
Musk ketone	<100	<100	<100	N/A	<100	<100	N/A

^aNote that the values listed for contaminants in the RO concentrate are based on mass balance.

Similarly, transport of TOrCs through RO trains was monitored during routine testing of water quality parameters after approximately 190 h of operation at 19 gfd, O₃:DOC ~ 0.5 and 52% recovery. These data are shown in Table 7.8. Train 1 corresponds to MBR-O₃-RO, whereas Train 2 corresponds to the MBR-RO treatment train. Here, TOrCs were monitored not only in the feed and permeate but also in the concentrate/brine, thereby adding further validity to the calculated concentrations in Table 7.7. The results shown in this table demonstrate the relative differences in the water quality of the concentrates between the two trains and highlight the benefits of preoxidation in minimizing TOrC concentration in concentrates and potential breakthrough into RO permeate.

Table 7.8. Transport of TOxCs and Bromate Through MBR-RO Trains

Constituent (ng/L)	Train 1: MBR-O ₃ -RO			Train 2: MBR-RO		
	Feed	Permeate	Concentrate ^a	Feed	Permeate	Concentrate ^a
Atenolol	<25	<25	<25	420	<25	850
Atrazine	<10	<10	<10	<10	<10	<10
Bisphenol A	<50	<50	<50	<50	<50	160
Carbamazepine	<10	<10	<10	140	<10	370
DEET	<25	<25	<25	30	<25	62
Diclofenac	<25	<25	<25	<25	<25	600
Dilantin	60	<10	130	330	<10	670
Gemfibrozil	<10	<10	<10	240	<10	520
Ibuprofen	29	<25	44	110	<25	250
Meprobamate	190	<10	380	360	<10	780
Musk ketone	<100	<100	<100	<100	<100	<100
Naproxen	<25	<25	<25	280	<25	750
Primidone	48	<10	130	210	<10	410
Sulfamethoxazole	<25	<25	<25	990	<25	3100
TCEP	310	<200	710	290	<200	790
Total nitrogen	16	1.0	29	16	0.9	31
Triclosan	<25	<25	<25	<25	<25	<25
Trimethoprim	<10	<10	<10	79	<10	220
Bromate	<0.005	<0.001	0.006	<0.005	<0.001	<0.005
Bromide	0.040	<0.020	0.078	0.041	<0.020	0.080
TOC	6.0	<0.20	12	6.1	<0.20	13
UV ₂₈₀	0.045	0.006	0.084	0.086	0.004	0.179
UV ₂₅₄	0.099	0.029	0.158	0.138	0.022	0.264

^aNote that the RO concentrate values are based on actual measured contaminant concentrations.

7.3.3.2 Impact of Ozone and Ozone/Peroxide on NDMA Occurrence and Transport

Of concern during water reuse applications is the removal of NDMA through a given process, driven in large part by California's Title 22 regulations and potential future EPA regulations on drinking water contaminants. In addition, the formation of bromate by ozone processes may be of further concern when potable reuse is considered and when ozone is used in bromide-containing waters. Table 7.9 lists data regarding changes in the concentrations of NDMA, bromide, and bromate at various ozone and ozone/peroxide doses. Ironically, in the control sample, direct formation of NDMA (6–9 ng/L) was observed in the MBR filtrate treated with ozone and ozone/peroxide. Even at a higher ozone dose of 10 mg/L (O₃:DOC = 1.7) with the addition of hydrogen peroxide, net NDMA destruction was not observed.

Table 7.9. Direct NDMA and Bromate Formation from Ozone and Ozone/Peroxide of MBR Filtrate

Source	Ozone Dose	H ₂ O ₂ Dose	NDMA
Water	(mg/L)	(mg/L)	(ng/L)
MBR filtrate	0.0	0.0	30.5 ± 2.5
MBR filtrate	1.5	0.0	32
MBR filtrate	1.5	0.5	28
MBR filtrate	3.0	0.0	40
MBR filtrate	3.0	1.1	37
MBR filtrate	6.0	0.0	40
MBR filtrate	6.0	2.1	38
MBR filtrate	10.0	0.0	37
MBR filtrate	10.0	3.5	42
RO permeate	0.0	0.0	16
RO permeate	10.0 ^a	0.0	18

^aOzone pretreatment to RO pilot.

This direct NDMA formation was re-evaluated during separate experiments (Table 7.10) resulting in NDMA formation of 13 to 33 ng/L. In addition, the formation of 36 to 48 ng/L also was observed in bench-scale ozonation experiments with secondary effluent samples from WRF 2 (Table 7.10). These results indicate that direct formation of NDMA is reproducible regardless of the wastewater and ozone system source and that there may be variable factors responsible for NDMA formation during ozonation of wastewater. The formation of NDMA during ozonation has recently been reported elsewhere (Hollender et al., 2009; Zimmermann et al., 2011). These results indicate a potential direct path to NDMA formation from reactions of unknown precursors with ozone and/or ·OH in wastewaters. Without additional screening for factors and precursors, it is not yet clear what precursor material may be responsible for this ozone-mediated formation of NDMA. Other compounds that form NDMA during reactions with ozone have been summarized elsewhere (Nawrocki and Andrzejewski, 2011). However, additional research is necessary to determine the exact precursors and reaction pathways responsible for direct NDMA formation during ozonation of wastewaters.

Table 7.10 also summarizes the NDMA-FP results from the MBR-ozone pilot tests. As indicated, both ozone and ozone/peroxide provided significant reductions in NDMA FP (for consequent chloramination). Because ozone and ozone/H₂O₂ generally provide similar overall ·OH exposure in wastewater when sufficient reaction time is provided, the H₂O₂ addition is often unnecessary for ozone to qualify as an AOP, as indicated by similar reductions in TOxCs and NDMA-FP during use of ozone and ozone/peroxide.

Table 7.10. Direct NDMA Formation by Ozone (Day 0) and NDMA Formation Potential (Day 10–Day 0)

Source Water	O ₃ Dose (mg/L)	H ₂ O ₂ Dose (mg/L)	Day 0 ^a (ng/L)	Day 10 (ng/L)	NDMA-FP ^b (ng/L)
MBR filtrate	0.0	0.0	4.3	1600	1596
MBR filtrate	1.5	0.0	21	160	139
MBR filtrate	1.5	0.5	18	150	132
MBR filtrate	6.0	0.0	31	78	47
MBR filtrate	6.0	2.1	33	84	51
MBR filtrate	10.0	0.0	30	70	40
MBR filtrate	10.0	3.5	29	74	45
RO permeate	0.0	0.0	2.9	7.2	4
RO permeate	10.0 ^c	0.0	13	12	None
WRF 2 sec. ^d effluent	0.0	0.0	<2.5	590	590
WRF 2 sec. effluent	3.55	0.0	48	230	182
WRF 2 sec. effluent	3.55	1.3	45	230	185
WRF 2 sec. effluent	7.1	0.0	42	150	108
WRF 2 sec. effluent	7.1	2.5	36	140	104

^aDay 0 refers to ambient concentrations or direct formation of NDMA from ozonation.

^bNDMA-FP refers to Day 10 (after addition of preformed chloramine)–Day 0.

^cPilot-scale ozonation

^dsec.= secondary

In addition to NDMA removal, the impact of ozone and ozone/peroxide treatment on NDMA-FP was also evaluated. Because NDMA is hydrophilic ($\log K_{ow} = -0.57$), has a low pK_a of <1 (C. Lee et al., 2007a), and low molecular weight (74.08 g/mol), NDMA is poorly rejected by polyamide RO membranes (Steinle-Darling et al., 2007; Plumlee et al., 2008), which is a significant issue in water reuse applications. NDMA rejection or breakthrough for the current study is described in Table 7.9. Although preozonation achieves significant reductions in NDMA-FP, the direct formation during ozonation, subsequent formation during chloramination, and only partial rejection by RO highlight the potential concern for this contaminant in water reuse applications and the importance of multiple barriers in IPR treatment trains.

7.3.3.3 Impact of Ozone and Ozone/Peroxide on Bromide and Bromate

Bromate formation was generally not a problem (<10 µg/L) for the waters tested in this study as the bromide concentration in the MBR filtrate was typically 0.1 mg/L, which was insufficient to induce significant bromate formation during ozonation. However, in recognition of the issue, when bromide was spiked to approximately 0.4 mg/L, bromate exceeded 10 µg/L for applied ozone doses higher than 3.0 mg/L. At a dose of 10 mg/L (O₃:DOC ratio of 1.7), as much as 42 to 50 µg of bromate/L was formed. However, as indicated by the results in Table 7.11, bromate was not detected in the RO permeate samples above 10 µg/L. This finding highlights an additional benefit of the RO system, which is very effective at bromate rejection.

Table 7.11. Direct Bromate Formation from Ozone and Ozone/Peroxide of MBR Filtrate

Source Water	Concentration			
	Ozone (mg/L)	H ₂ O ₂ (mg/L)	Bromide (mg/L)	Bromate (mg/L)
MBR filtrate	0.0	0.0	0.423	<0.001
MBR filtrate	1.5	0.0	0.424	<0.010
MBR filtrate	1.5	0.5	0.435	<0.010
MBR filtrate	3.0	0.0	0.427	<0.010
MBR filtrate	3.0	1.1	0.442	<0.010
MBR filtrate	6.0	0.0	0.414	0.010
MBR filtrate	6.0	2.1	0.437	<0.010
MBR filtrate	10.0	0.0	0.404	0.042
MBR filtrate	10.0	3.5	0.416	0.050
RO permeate	0.0	0.0	<0.020	<0.001
RO permeate	10.0 ^a	0.0	0.043	<0.010

^aOzone pretreatment to RO pilot.

7.3.4 TOrC Removal/Oxidation through UF, UV/Peroxide, and RO Treatments at WRF 2

7.3.4.1 TOrC Removal by UF, UV/Peroxide, and RO Transport

Removal of TOrC by UV/peroxide was investigated by using a bench-scale UV apparatus, as described in Chapter 2. This was done because of limitations of pilot setup and availability of necessary flows to allow testing of lower UV doses. As previously described in Chapter 2, the UV dose of the pilot-scale UV reactor was separately determined by using a spike solution of atrazine. Similar UV exposures were carried out by using a bench-scale UV reactor to cross-validate UV fluence determination by actinometry and radiometry. Table 7.12 shows percent TOrC removal achieved during various UV and UV/peroxide doses. Compounds susceptible to direct photolysis, such as sulfamethoxazole, were effectively removed. However, compounds resistant to UV and oxidation such as TCEP were not significantly removed even at 1000 mJ/cm² and 10 mg of hydrogen peroxide/L. In contrast to ozone, UV/peroxide may require further refinement in pretreatment (e.g., to improve UV transmission of the feed water) to allow similar effectiveness at removing TOrCs.

Table 7.12. Percentage Removal of TOrCs by UV/Peroxide in UF Filtrate in Bench-Scale UV Experiments

Constituent	UV Fluence (mJ/cm ²)/Peroxide (mg/L)					
	400/0	400/5	400/10	1000/0	1000/5	1000/10
Atenolol	0.0	38.7	58.1	16.1	64.5	86.5
Carbamazepine	12.5	51.9	70.6	31.3	84.4	92.5
DEET	2.0	33.0	50.0	7.0	58.0	>75.0
Diclofenac	>83.3	>83.3	>83.3	>83.3	>83.3	>83.3
Dilantin	46.9	63.8	77.7	78.5	>92.3	>92.3
Gemfibrozil	9.5	42.9	>52.4	23.8	>52.4	>52.4
Meprobamate	1.1	18.9	30.0	4.4	36.7	60.0
Naproxen	>3.8	>3.8	>3.8	>3.8	>3.8	>3.8
Primidone	6.7	40.0	52.7	20.0	64.7	83.3
Sulfamethoxazole	68.2	72.4	81.2	93.5	96.1	97.8
TCEP	8.7	-8.7	0.0	0.0	8.7	4.3
Triclosan	>44.4	>44.4	>44.4	>44.4	>44.4	>44.4
Trimethoprim	8.5	40.7	59.3	18.6	72.9	>83.1

In pilot-scale tests, samples were grabbed from the feed and permeate lines of each RO train. These results are presented in Table 7.13. In general, similar removals were observed between the bench-scale and pilot-scale tests (Table 7.12 and Table 7.13). It is interesting that atenolol was detected in the RO permeate of Train 2 (UF-RO), which is a surprising finding because the molecular weight of atenolol is 266 Da and thus should be well rejected by an RO membrane.

Table 7.13. Removal of TOrCs by UV/Peroxide and RO in UF Filtrate in Pilot-Scale Tests

Constituent	UV Fluence (mJ/cm ²)/Peroxide (mg/L)			
	0/0 UF Filtrate	0/0 RO Permeate	1000/5 UF Filtrate	1000/5 RO Permeate
Atenolol	310	40	170	<25
Carbamazepine	150	<10	76	<10
DEET	110	<25	62	<25
Diclofenac	180	<25	<25	<25
Dilantin	130	<10	22	<10
Gemfibrozil	16	<10	<10	<10
Meprobamate	920	<10	710	<10
Naproxen	<25	<25	<25	<25
Primidone	160	<10	83	<10
Sulfamethoxazole	2000	<25	190	<25
TCEP	240	<200	240	<200
Triclosan	68	<25	<25	<25
Trimethoprim	49	<10	27	<10

The transport of TOrCs through the UF, UV/peroxide, and RO pilot skids was further evaluated at WRF 2 after the pilot had been in operation for approximately 90 h (after CIP) at 15.5 gfd and 54% recovery. These results are shown by Table 7.14. Train 1 corresponds to UF-UV/peroxide-RO and Train 2 to the UF-RO treatment train. The UF feed was sampled at approximately the same time as RO samples (feed, concentrate, and permeate); however, it was not precisely hydraulically linked and represents a typical water quality of secondary wastewater that was fed to the pilot plant for use during this study.

Table 7.14. Transport of TOxCs and Bromate Through UF-RO Trains

Location Sub Location	Unit	UF	Train 1: UF-UV/Peroxide-RO			Train 2: UF-RO		
		Feed ^a	Feed	Permeate	Concn	Feed	Permeate	Concn
Atenolol	ng/L	310	240	<25	460	380	<25	780
Atrazine	ng/L	<10	<10	<10	<10	<10	<10	<10
Bisphenol A	ng/L	<50	100	<50	<50	96	<50	310
Carbamazepine	ng/L	100	38	<10	140	110	<10	310
DEET	ng/L	110	74	<25	170	120	<25	260
Diclofenac	ng/L	140	<25	<25	<25	86	<25	230
Dilantin	ng/L	120	14	<10	34	120	<10	270
Gemfibrozil	ng/L	15	11	<10	27	22	<10	49
Ibuprofen	ng/L	<25	<25	<25	<25	<25	<25	<25
Meprobamate	ng/L	800	640	<10	1400	790	<10	1800
Musk ketone	ng/L	<100	170	<100	<100	<100	<100	<100
Naproxen	ng/L	<25	<25	<25	<25	<25	<25	26
Primidone	ng/L	150	76	<10	180	130	<10	320
Sulfamethoxazole	ng/L	1300	78	<25	170	1200	<25	2300
TCEP	ng/L	270	230	<200	620	290	<200	690
Triclosan	ng/L	65	<25	<25	<25	<25	<25	<25
Trimethoprim	ng/L	94	52	<10	110	85	<10	200
Total nitrogen	mg/L	11	12	1.4	24	12	1.1	24
TOC	mg/L	6.6	5	<0.20	11	5.2	<0.20	11
Bromate	mg/L	<0.001	<0.005	<0.001	<0.005	<0.005	<0.001	<0.005
Bromide	mg/L	0.15	0.07	<0.020	0.103	0.077	<0.020	0.107
UV ₂₈₀	/cm	0.091	0.053	0.003	0.112	0.065	0.002	0.142
UV ₂₅₄	/cm	0.119	0.083	0.012	0.160	0.101	0.010	0.207

^aUF feed (secondary wastewater) is not hydraulically linked to Train 1 and Train 2 and represents typical values.

7.3.4.2 Effects of UV/Peroxide on Bromate and NDMA Removal in UF Filtrate

As expected, the UV and UV/peroxide treatments were much more effective for NDMA destruction than were the ozone and ozone/peroxide systems. A UV dose of 400 mJ/cm² achieved 0.93-log removal, which was slightly better than with the addition of peroxide, as shown by Table 7.15. At a UV dose of 1000 mJ/cm², NDMA was removed by at least 1.48 logs with or without addition of peroxide. This result is to be expected, as the dominant removal mechanism for nitrosamines is through photolysis rather than through reaction with hydroxyl radicals (Kruithof et al., 2007). No significant formation of bromate was observed during all UV and UV/peroxide tests. UV/peroxide treatment also reduced the NDMA FP, results shown by Table 7.16.

Table 7.15. NDMA Destruction and Bromate Formation from UV/Peroxide Treatment of UF Filtrate (UF-F)

Source Water	UV Fluence (mJ/cm ²)	H ₂ O ₂ Dose (mg/L)	NDMA (ng/L)	NDMA (log[C/Ci])	BrO ₃ (mg/L)
UF-F bench scale	0	0	305	0	<0.001
UF-F bench scale	400	0	36	-0.93	<0.001
UF-F bench scale	400	5	38	-0.90	<0.001
UF-F bench scale	400	10	44	-0.84	<0.001
UF-F bench scale	1000	0	<10	-1.48	<0.001
UF-F bench scale	1000	5	<10	-1.48	<0.001
UF-F bench scale	1000	10	<10	-1.48	<0.001
UF-F pilot scale	0	0	320	0	<0.001
UF-F pilot scale	1000	5	12	-1.43	<0.001
RO permeate	0	0	<25	N/A	<0.001
RO permeate	1000	5	<25	N/A	<0.001

Table 7.16. Impact of UV/Peroxide on NDMA Formation Potential in UF Filtrate (UF-F)

Source Water	UV Fluence (mJ/cm ²)	H ₂ O ₂ Dose (mg/L)	Day 0 ^a (ng/L)	Day 10 (ng/L)	NDMA-FP ^b (ng/L)
UF-F bench scale	0	0	305	790	485
UF-F bench scale	400	0	36	470	434
UF-F bench scale	400	5	38	340	302
UF-F bench scale	400	10	44	270	226
UF-F bench scale	1000	0	<10	350	350
UF-F bench scale	1000	5	<10	170	170
UF-F bench scale	1000	10	<10	100	100
UF-F pilot scale	0	0	320	760	440
UF-F pilot scale	1000	5	12	280	268
RO permeate	0	0	<25	<25	<25
RO permeate	1000	5	<25	<25	<25

^aDay 0 refers to changes in spike concentration of NDMA from UV/peroxide. UF-F, UF filtrate.

^bNDMA-FP refers to day 10 (after addition of preformed chloramine)–day 0.

7.4 Implications of Findings

Table 7.17 provides a summary of the removal of trace contaminants at various O₃:DOC ratios and the calculated EEO (kilowatt-hours per cubic meter-log) values for surface water and wastewater, including the embedded energy in peroxide. As expected, the EEO values are lower for the removal of TOrCs in CRW than in wastewater (WRF 1), likely because of the presence of higher organic matter content and ozone scavenging in the wastewater matrix than in the surface water matrix. Similar trends in the EEO values were recently reported elsewhere (Katsoyiannis et al., 2011). In addition, comparable EEO values for sulfamethoxazole and atrazine are reported in the current study. However, for NDMA, that study reported EEO values of 0.5 kWh/m³ and 0.9 kWh/m³ per 90% removal (same as kilowatt-hours per cubic meter-log) by using ozone treatment of surface and wastewater, respectively. As shown by Table 7.17, in CRW the EEO for NDMA for ozone was 2.608 kWh/m³-log and for ozone/peroxide was 0.603 kWh/m³-log. This disagreement is substantial for the two studies; however, in both cases the NDMA removal to 90% due to ozone was not shown and the EEO values are based on extrapolation, thereby increasing the uncertainty in determination of these values. Because NDMA has a relatively low rate constant describing the reaction with ozone, significantly higher EEO values for ozone could be expected over the ozone/peroxide.

Table 7.17. Electrical Energy per Order (EEO) of TOrC Removal by Ozone (O₃) and Ozone/Peroxide (O₃/H₂O₂) in CRW and MBR Filtrate, Sorted by Ozone-Based EEO in MBR Filtrate

Contaminant	MBR Filtrate		CRW	
	EEO (O ₃) (kWh/m ³ -log)	EEO (O ₃ /H ₂ O ₂) (kWh/m ³ -log)	EEO (O ₃) (kWh/m ³ -log)	EEO (O ₃ /H ₂ O ₂) (kWh/m ³ -log)
Triclosan	<0.010	0.037	N/A	N/A
Diclofenac	0.022	0.051	N/A	N/A
Carbamazepine	0.028	0.036	<0.004	<0.005
Trimethoprim	0.030	0.016	<0.005	<0.004
Gemfibrozil	0.033	0.034	N/A	N/A
Atenolol	0.038	0.074	<0.004	<0.007
Sulfamethoxazole	0.039	0.047	N/A	N/A
Naproxen	0.055	0.060	N/A	N/A
Phenytoin	0.110	0.112	0.055	0.018
Primidone	0.139	0.145	0.055	0.016
DEET	0.168	0.155	N/A	N/A
Atrazine	N/A	N/A	0.073	0.141
Meprobamate	0.361	0.245	0.142	0.043
Ibuprofen	0.393	0.269	N/A	N/A
TCPP	N/A	N/A	0.226	0.237
TCEP	1.169	1.371	0.461	0.419
NDMA	N/A	N/A	2.608	0.603

Note: N/A = not available.

Despite the additional “energy” cost of the hydrogen peroxide, the AOP (i.e., ozone/peroxide) was more efficient than ozone alone for CRW treatment, as indicated by lower TOrC EEO values. In contrast, the addition of hydrogen peroxide did not enhance contaminant removal in the wastewater samples, and in several cases the EEO values were higher because of the additional peroxide cost and the loss of efficiency in the reaction. This finding might occur because in wastewater ozone reacts directly with EfOM and other DOM to produce hydroxyl radicals, thereby creating a pseudo-AOP (Buffle et al., 2006; Nöthe et al., 2009; S. Lee et al., 2010; Pocostales et al., 2010). When compared to results from previous studies utilizing UV/peroxide or nonthermal plasma, the ozone and ozone/peroxide EEO values obtained for CRW and wastewater are significantly lower, emphasizing the cost-effectiveness of ozone-based treatment for TOrC mitigation (Benotti et al., 2009a; Gerrity et al., 2010; Katsoyiannis et al., 2011).

Table 7.18 provides a summary of the removal of trace contaminants at various UV fluence and UV/peroxide doses and the calculated EEO removal (kWh/m³-log) values for wastewater (WRF 2). The EEO values were determined on the basis of an equivalent transformation of atrazine between the bench-scale and pilot-scale reactors. The UV fluence, as determined by the atrazine-based actinometry, allowed the project team to correlate the pilot-scale feed water flow with the UV fluence. The EEO values presented in Table 7.18 are based on TOrC removal at specific UV fluence and hydrogen peroxide doses obtained during bench-scale UV reactor tests. However, the calculated electrical energy per volume of treated wastewater is based on the pilot-scale reactor configuration, total lamp power consumption, and specific flow rates to obtain targeted UV fluence conditions. Thus these EEO values were not directly determined in a pilot-scale reactor but do provide reasonable estimates of these values that are consistent with other studies (Kruithof et al., 2007; Benotti et al., 2009a; Gerrity et al., 2010).

Table 7.18. Electrical Energy per Order (EEO) of TOrC Removal by UV and UV/Peroxide in UF Filtrate

Contaminant	Results (kWh/m ³ -log) for:		
	EEO (UV, no H ₂ O ₂)	EEO (UV+ 5-mg/L H ₂ O ₂)	EEO (UV + 10-mg/L H ₂ O ₂)
Sulfamethoxazole	0.40	0.38	0.35
Carbamazepine	2.9	0.65	0.51
Dilantin	0.71	0.68	0.54
Trimethoprim	5.2	0.93	0.75
Primidone	4.9	1.2	0.75
Atenolol	2.8	1.2	0.67
Gemfibrozil	4.0	1.2	1.1
DEET	15	1.4	0.96
Meprobamate	24	2.6	1.5
Triclosan	0.99	N/A	N/A
NDMA	0.27	N/A	N/A
Atrazine	1.5	N/A	N/A

In general, UV/peroxide was more effective at TOrC removal than was UV, except for compounds such as NDMA and sulfamethoxazole that are directly photolyzed by UV. In comparison to the ozone and ozone/peroxide EEO values presented in Table 7.17, the UV/peroxide EEO values are considerably higher, indicating that ozone and ozone/peroxide provide a lower-energy treatment option for chemical oxidation of the TOrCs in this study with the exception of NDMA. Compounds such as meprobamate that are resistant to UV but moderately amenable to chemical oxidation by hydroxyl radicals would require unrealistic amounts of energy in a UV reactor to produce sufficient steady-state hydroxyl radical concentration.

7.5 Concluding Remarks

The results presented here indicate the potential benefit of ozone and ozone/peroxide for TOrC removal in water treatment and in wastewater treatment and as part of an advanced IPR treatment train. Consistent with the literature, the data indicate that the addition of hydrogen peroxide does not provide significant benefits for wastewater treatment, but the greater $\bullet\text{OH}$ exposure in surface water treatment was observed to be beneficial for the oxidation of the recalcitrant compounds, such as TCEP and DEET. Upon chloramination, NDMA FP was significantly reduced by ozone and ozone/peroxide pretreatment. Despite this reduction in NDMA FP and the NDMA destruction benefits for surface water treatment, the direct formation of NDMA in wastewater applications may require further mitigation measures. Therefore, the oxidation of TOrCs and potential microbial inactivation must be balanced with the formation of disinfection by-products, including bromate. For the waters tested in this study, an $\text{O}_3\text{:DOC}$ ratio of 0.50 proved to be the optimal dosing condition to balancing TOrC oxidation, direct NDMA formation, and bromate formation. Furthermore, this study demonstrated the potential use of differential UV_{254} or fluorescence at 254 nm as a surrogate for TOrC oxidation.

Alternately, the UV/peroxide strategy was effective to reduce both NDMA and NDMA-FP; however, in general it requires higher electrical energy input than does ozone to achieve similar TOrC (other than nitrosamines or compounds that undergo direct photolysis) removals. Thus, it is less feasible to use UV/peroxide ahead of RO to remove TOrC than to use ozone. The UV transmission of the wastewater is considerably higher than that of RO permeate, which is one of the main reasons for the higher energy costs needed to achieve the same level of TOrC removal that one relatively easily achieves with ozone, an observation that is consistent with other studies.

Chapter 8

Cost Comparison of Oxidative Pretreatment Strategies

8.1 Introduction

As mentioned in the previous chapters, the main hypothesis driving this study was that the application of oxidative processes upstream of RO membranes during treatment of wastewater for reuse applications could provide a benefit in minimizing fouling (specifically, *irreversible* fouling) associated with EfOM. The development of this hypothesis was driven in part by a conceptual reconfiguration of existing processes in California, where wastewater is pretreated by MF membranes, followed by addition of antiscalant(s), acids or bases for pH control, and chloramines for biofouling control, and then is treated by RO membranes and then with UV/peroxide for oxidation or photolysis of trace chemical contaminants, primarily 1,4-dioxane and NDMA, in the product water. Thus, the treatment process of MF-RO-UV/AOP was rearranged to become MF-UV/AOP-RO in order to ask three questions: (1) Can this reconfiguration still provide the advanced oxidation needed to remove TOrCs? (2) Can this reconfiguration provide a benefit by controlling fouling associated with EfOM, thereby potentially minimizing membrane replacement costs and CIP events? and (3) Can this rearrangement provide a meaningful reduction in the amount of energy required to drive water across the RO membranes by minimizing EfOM fouling of the RO membranes?

Whereas the majority of the previous chapters have addressed these questions through the demonstrated results from this study, this chapter is devoted to investigating the power consumption and cost from a conceptual standpoint. The flat sheet membrane test results clearly showed promise for both ozone use and UV/peroxide use as strategies to control flux decline in RO membranes. However, the pilot results were inconclusive on the applicability of these strategies in the waters tested and did not provide meaningful opportunities to evaluate the frequency of CIP events or long-term membrane life. Therefore, the focus of this chapter is on projecting costs and energy through several treatment scenarios in order to provide context for when and where oxidation pretreatment may be a viable option for a utility considering RO membranes for water reuse. Much of the information developed in this chapter is also used to support recommendations for future research needs.

8.2 Basis for Energy Calculations

8.2.1 RO Membrane Pressure and Pumping Power

All predictions and membrane design parameters were based on a typical full-scale membrane treatment plant with a 4:2:1 array with seven elements per vessel, operating at a total recovery of 85%, an average flux of 12.1 gfd, and a filtrate flow of 35 gpm (approximately 70,000 m³/year). Initially, Hydranautics' IMS Design software (IMS Design 2010, IMSdb3, v. 28) was used to calculate the feed pressure for membranes varying from 0 to 10 years of use with annual flux declines of 15%, 10%, and 7.5% (the default flux decline parameter for wastewater/reuse applications is 15% annual flux decline). The RO feed water quality was based on the WRF 2 post-UF characterization provided in Chapter 6 and was assumed to be at 25 °C. The starting feed pressure was later verified by using the

pilot data from both WRF 1 and WRF 2, confirming that initial feed pressure was in the range of 110 to 130 psi. Figure 8.1 shows the predicted change in feed pressure over time with the various flux decline scenarios, assuming no CIP events were to occur. As expected, the shape of each curve is similar to those observed in the short-term flat sheet tests presented in Chapter 4 (e.g., the value for ozone-treated wastewater is similar to the 7.5% flux decline curve, whereas the value for raw water is similar to the 15% flux decline curve, though the time scale is in years, not hours), though they clearly do not account for typical CIP events that would prevent such a precipitous increase in flux. Thus, a more realistic picture of the fouling curve is presented in Figure 8.2, where each CIP event is assumed to restore 85% of the original operating flux.

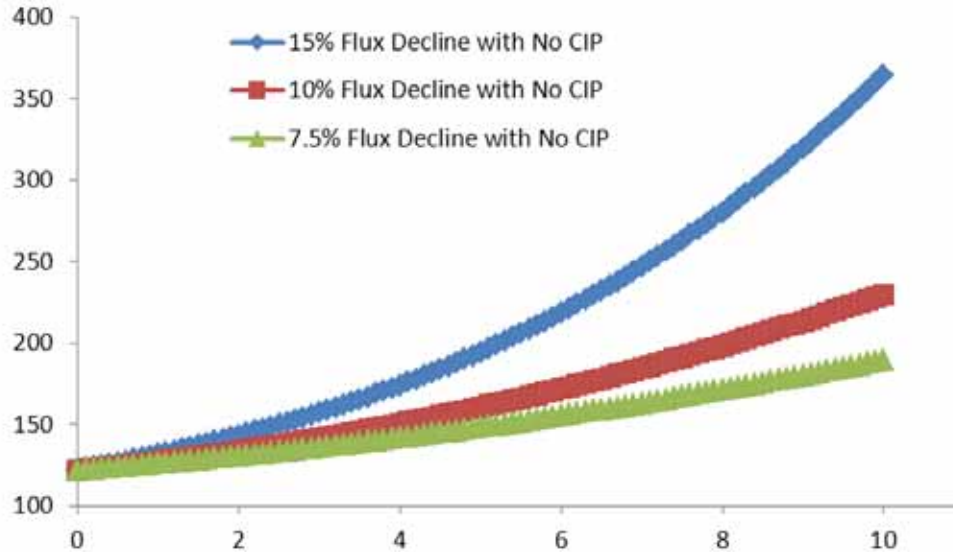


Figure 8.1. Changes in RO system operating pressure over time with different flux decline scenarios using WRF 2 post-UF water.

In conjunction with the feed pressure projections presented in Figure 8.1 and Figure 8.2, the following equations were used to convert feed pressure into power and cost of operation. The power required to maintain flux was calculated from pressure as follows:

$$Power (kWh) = \frac{Q * \rho * g * h}{3.6 \times 10^6} \quad (8.1)$$

where Q = flow (m³/h)

ρ = density of fluid (assumed 1000 kg/m³)

g = force of gravity (9.8 m/s²)

h = differential head (m)

$$Head = h = \frac{p}{62.4 \text{ lb/ft}^2} \quad (8.2)$$

where p = pressure (psi * 144 = lb/ft²)

and h (m) = h (ft) * 0.3048 m/ft

$$(8.3)$$

$$(8.4)$$

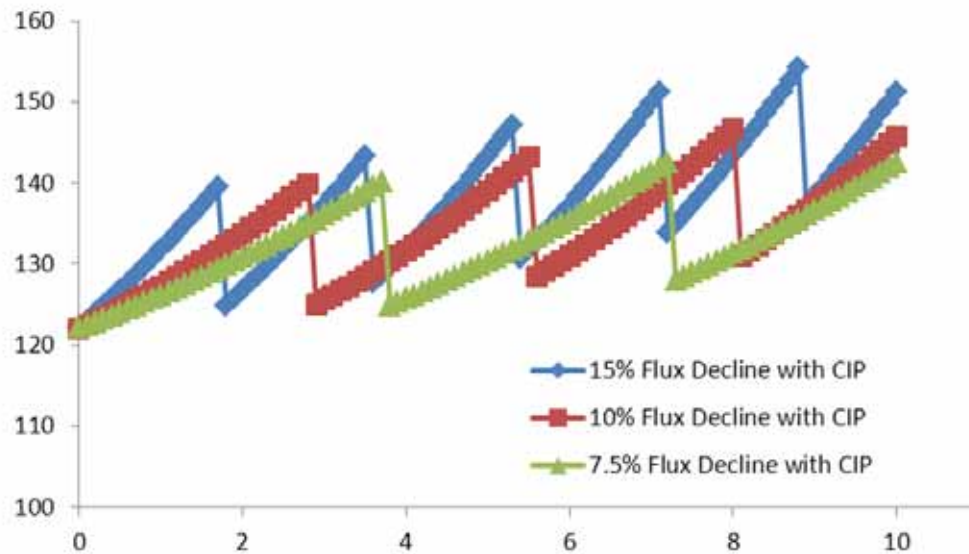


Figure 8.2. Changes in RO system operating pressure over time with different flux decline scenarios and CIP events, assuming 85% restoration of original flux using WRF 2 post-UF water.

Pump efficiency was not considered in these calculations in order to provide a more general, conceptual overview of the power comparisons. On the basis of Equations 8.1 through 8.4, the relationship between the change in feed pressure and amount of power required to treat 1 cu. m of water is illustrated in Figure 8. This relationship and potential flux-decline scenarios shown in Figure 8.1 provide the base power use for the “control” scenarios. It is important, however, that the power calculations (and later cost calculations) are based solely on feed pressure and do not incorporate various pretreatment filtration steps or the power associated with standard chemical feeds such as antiscalants, acids/bases for pH control, chloramines, etc.

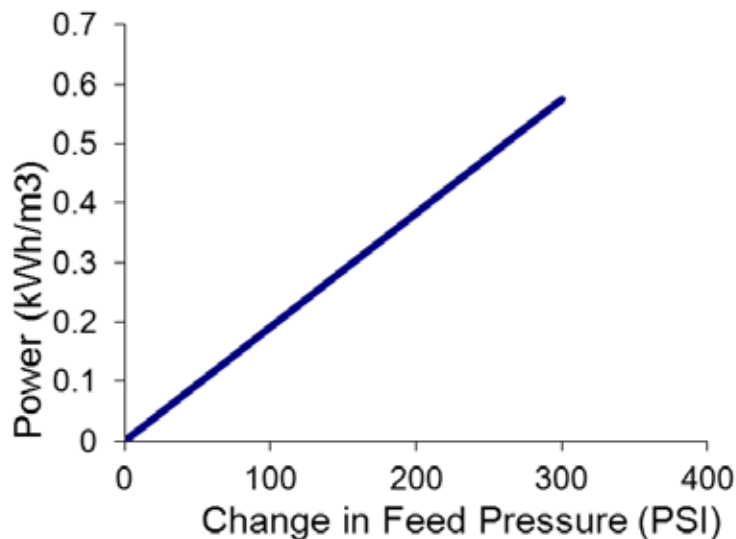


Figure 8.3. Relationship between feed pressure and power to drive water across the RO membranes, scaled to low-salt water, reuse application ranges.

8.2.2 UV and UV/Peroxide

As one would expect in a wastewater/water reuse application, there is considerable energy cost associated with providing the same UV fluence and advanced oxidation chemistry in a lower-UVT water with higher hydroxyl radical scavenging capacity (e.g., RO feed vs RO permeate) using the same reactor design for both processes. To demonstrate this fact, a series of relative energy ratios were developed for a given set of UV reactors with path lengths ranging from 5 cm to 25 cm and water quality parameters from the MF-UV/peroxide-RO pilot at WRF 2, listed in Table 8.1.

Table 8.1. Water Quality Parameters for UV Power Calculations

Parameter	Values for:	
	RO Feed Water Quality	RO Permeate Water Quality
UVT ^a	75% to 85%	96.5%
TOC	5.7 mg/L	0.2 mg/L
Alkalinity	130 mg/L as CaCO ₃	7 mg/L as CaCO ₃
pH	7.3	7.3
Monochloramine	0 mg/L	1.5 mg/L

^aUVT is for the demonstration calculations only and not intended to suggest an expected range.

In order to calculate the ratio of power required for an 85% UVT feed water versus a 96.5% UVT permeate with variable background scavenging capacity, the model demonstrated by Rosenfeldt et al. (2004, 2005, 2007) was used. The entire model is fundamentally based upon the steady-state hydroxyl radical assumption as shown in Equation 8.5

$$[\cdot OH]_{ss} = \frac{I_o(1-e^{-2.303 \cdot a \cdot b})\epsilon_{H_2O_2}[H_2O_2]\Phi_{H_2O_2}}{U_{254} \cdot 2.303 \cdot a \cdot b \sum k_{s,OH}S} \quad (8.5)$$

Where, I_o = incident (lamp) intensity at the surface of the quartz sleeve

a = water absorbance (cm^{-1})

b = reactor path length (cm)

$\epsilon_{H_2O_2}$ = molar extinction coefficient of hydrogen peroxide ($\text{M}^{-1} \text{cm}^{-1}$)

$\Phi_{H_2O_2}$ = quantum yield of hydrogen peroxide at 254 nm (mol Es^{-1})

$\sum k_{s,OH}S$ = sum of scavenging (s^{-1}) = $(k_{OH,TOC}(TOC) + k_{OH,HCO_3^-}[HCO_3^-] + k_{OH,CO_3^{2-}}[CO_3^{2-}] + \dots + k_{OH,H_2O_2}[H_2O_2])$

where k is the second order OH radical rate constants for each scavenger

$$k_{OH,TOC} = 2.5 \times 10^4 \text{ L mg}^{-1} \text{ s}^{-1}$$

$$k_{OH,HCO_3^-} = \text{M}^{-1} \text{ s}^{-1}$$

$$k_{OH,CO_3^{2-}} = \text{M}^{-1} \text{ s}^{-1}$$

$$k_{OH,H_2O_2} = 2.7 \times 10^7 \text{ M}^{-1} \text{ s}^{-1}$$

Because the objective is to search for the ratios of power, it makes sense to rearrange Equation 8.5 in terms of the input power-related term, I_o :

$$I_o = \frac{U_{254} \cdot 2.303 \cdot a \cdot b [\cdot OH]_{ss} \sum k_{s,OH}S}{(1-e^{-2.303 \cdot a \cdot b})\epsilon_{H_2O_2}[H_2O_2]\Phi_{H_2O_2}} \quad (8.6)$$

To determine the ratio of power between two situations (1 and 2), compare the ratios of I_o for the two situations ($I_{o,1}/I_{o,2}$):

$$\frac{I_{0,1}}{I_{0,2}} = \frac{\frac{U_{254} \cdot 2.303 \cdot a_1 \cdot b_1 [\cdot OH]_{ss,1} (\sum k_{s,OH} S)_1}{(1 - e^{-2.303 \cdot a_1 \cdot b_1}) \epsilon_{H_2O_2} [H_2O_2]_1 \Phi_{H_2O_2}}}{\frac{U_{254} \cdot 2.303 \cdot a_2 \cdot b_2 [\cdot OH]_{ss,2} (\sum k_{s,OH} S)_2}{(1 - e^{-2.303 \cdot a_2 \cdot b_2}) \epsilon_{H_2O_2} [H_2O_2]_2 \Phi_{H_2O_2}}} \quad (8.7)$$

The major assumption in this model is that the performance criterion used to compare the two situations is that an equivalent amount of oxidation occurs. To account for this theory, one must create an equivalent $[\cdot OH]_{ss}$ for each situation, such that $[\cdot OH]_{ss,1} = [\cdot OH]_{ss,2}$. Upon incorporation of this assumption and simplification of Equation 7.8, the following occurs:

$$\frac{I_{0,1}}{I_{0,2}} = \frac{\frac{a_1 \cdot b_1 (\sum k_{s,OH} S)_1}{(1 - e^{-2.303 \cdot a_1 \cdot b_1}) [H_2O_2]_1}}{\frac{a_2 \cdot b_2 (\sum k_{s,OH} S)_2}{(1 - e^{-2.303 \cdot a_2 \cdot b_2}) [H_2O_2]_2}} = \frac{a_1 \cdot b_1 (\sum k_{s,OH} S)_1 (1 - e^{-2.303 \cdot a_2 \cdot b_2}) [H_2O_2]_2}{a_2 \cdot b_2 (\sum k_{s,OH} S)_2 (1 - e^{-2.303 \cdot a_1 \cdot b_1}) [H_2O_2]_1} \quad (8.8)$$

With these equations, a spreadsheet was set up to calculate the ratio of power requirements for several scenarios, with major inputs being UVT, path length, H_2O_2 concentration, TOC, alkalinity, and chloramines. However, the worst-understood parameter of the inputs is the path length, because there is a limited understanding of the UV reflectance of the wall of the UV reactor. Thus, for a short-path-length scenario such as 5 cm, the power requirements actually favor the RO feed application when high peroxide doses are required post-RO because of the near-complete absorbance of the UV in the feed water versus the “loss” of UV to the reactor wall in the RO permeate. However, the reality of UV reactor design likely will be closer to the 25-cm path-length scenario because of some expected reflection of UV from the reactor wall. Therefore, for the calculations performed here, several path lengths were included to demonstrate the relative power ratios at each case and to show how chemical dosing, scavenging, and reactor design may all impact the final power use.

Table 8.2 shows the inputs used for each scenario, whereas Table 8.3 shows the ratio of calculated UV power needed, for each water, to produce the equivalent hydroxyl radical-based advanced oxidation for feed to the UV power needed to produce that property for permeate. Scenario 1 is the baseline comparison between the two waters, assuming a 2-mg/L peroxide dose for both cases. Scenario 2 ignores the hydroxyl radical scavenging between the two waters; thus, the TOC, alkalinity, pH, and chloramine concentration were effectively zero. Scenario 3 returns to the baseline conditions but incorporates an adjusted peroxide dose of 5 mg/L in the RO feed water. Scenario 4 then uses an adjusted peroxide concentration of 10 mg/L in the permeate and only 2 mg/L in the feed.

On the basis of these calculations, the majority of the scenarios presented would require more energy to apply UV/peroxide in the RO feed than in the RO permeate (e.g., the ratio is >1.0). Further, because of the greater volume of water in the RO feed than in the RO permeate (due to limitations in water recovery), the UV/peroxide system in the RO feed would require a larger system capacity (say, 10 mgd of RO feed water versus 8.5 mgd of permeate, assuming 85% recovery) and therefore inherently greater capital and operational costs.

Table 8.2. Description of Baseline and Adjusted Comparison Scenarios for UV Power Calculations

		UVT	H ₂ O ₂	TOC	Alk- alinity	pH	Chlor- amine (ClNH ₂)
Scenario	Composition	(%)	(mg/L)	(mg/L)	(mg/L as CaCO ₃)		(mg/L)
Scenario 1 (Baseline)	RO permeate	96.5	2	0.2	7	7.3	1.5
	RO feed	75–85	2	5.7	130	7.3	0
Scenario 2	RO permeate	96.5	2	0	0	7.3	0
	RO feed	75–85	2	0	0	7.3	0
Scenario 3	RO permeate	96.5	2	0.2	7	7.3	1.5
	RO feed	75–85	5	5.7	130	7.3	0
Scenario 4	RO permeate	96.5	10	0.2	7	7.3	1.5
	RO feed	75–85	2	5.7	130	7.3	0

Note: Gray areas represent changes in dose conditions between scenarios.

Table 8.3. Calculated Ratio of UV-Only Power Requirements for Test Case Scenarios

Scenario	Pre-RO UVT	Path Length (cm)				
		5	10	15	20	25
Scenario 1	75%	3.1	4.6	6.0	7.3	8.3
	80%	2.7	3.7	4.8	5.7	6.5
	85%	2.4	3.0	3.7	4.3	4.8
Scenario 2	75%	1.7	2.6	3.4	4.1	4.7
	80%	1.5	2.1	2.7	3.2	3.7
	85%	1.3	1.7	2.1	2.4	2.7
Scenario 3	75%	1.3	1.9	2.5	3.0	3.4
	80%	1.1	1.5	2.0	2.4	2.7
	85%	1.0	1.3	1.5	1.8	2.0
Scenario 4	75%	0.7	1.0	1.3	1.6	1.8
	80%	0.6	0.8	1.0	1.2	1.4
	85%	0.5	0.7	0.8	0.9	1.1

The data presented in Chapters 3 and 6 showed that UV alone, even at relatively high UV fluence rates of about 4000 mJ/cm², had very little impact on the EfOM and membrane fouling rates. When peroxide was added, the resulting AOP was able to impact EfOM and even showed promise in the initial flat sheet tests at high UV doses. However, no significant fouling reduction benefit was observed in the water tested for UV/peroxide at a more

reasonable dose of 1000 mJ/cm² over the control train, though oxidation and photolysis of the TOxCs and NDMA were significant. Further, the data obtained from this study were not able to provide any insight into potential changes in biofouling or long-term maintenance costs associated with membrane cleaning and replacement. On the basis of these observations, no further capital or O&M costs were developed for the UV/peroxide pretreatment scenarios.

8.2.3 Ozone

The calculation of energy associated with ozone production required a balance of assumptions, inputs, and complexity in order to keep the comparison at a conceptual level. The energy use associated with ozone production was based on a value of 0.01232 kWh/g of O₃, as provided by Applied Process Technology for its HiPOx[®] system. Although this number falls within the range of values reported by Chang et al. (2008), it does not include potential power or expense associated with delivery or production of oxygen (e.g., liquid oxygen or vacuum/pressure swing adsorption), either of which would increase the unit energy cost and should be considered on a system-specific basis. Further, the ozone–energy value assumes a linear relationship between the volume of ozone produced and energy requirements, which may be an oversimplification. Previous work indicates that there is a potential energy savings with greater ozone production capacity (Chang et al., 2008). Finally, the ozone energy calculations for this study were based on absolute ozone doses of 1.5, 3 and 6 mg/L, the calculations assumed 100% mass transfer efficiency, and the calculations were not adjusted for higher-DOC waters that may require higher ozone doses to achieve ozone:DOC ratios similar to those reported here.

Thus, the power associated with ozone production was based on a simple calculation:

$$\text{Production Power per Unit Water} = \text{Ozone Dose (g/m}^3\text{)} \times 0.01232 \text{ kWh/g} \quad (8.9)$$

Given the benefit observed from ozone alone in the flat sheet studies, peroxide was also not considered in these calculations though that calculation could be performed by converting peroxide costs to equivalent energy units and incorporating those values into the calculation (Rosenfeldt et al., 2006; Benotti et al., 2009a).

8.3 Combined Energy Projections

Given the apparent energy costs and lack of observed fouling benefit for the UV/peroxide preoxidation process, the energy projections for this section are limited to ozone alone. To compare energy costs, a series of scenarios and associated assumptions were considered. The assumptions and simplifications that were incorporated into the calculations include the following:

- Net energy use was related to the feed pressure + ozone generation.
- Chemical feed (chloramines, antiscalant, and pH control) was identical between treatment trains.
- The permeate flux across the membrane would decline at a set rate (7.5%, 10%, or 15%) until the feed pressure had increased by more than 15%.
- At each 15% flux decline threshold, a CIP would be performed and 85% of the difference in flux would be recovered.
- The initial feed pressure was identical between trains, except where noted.

- The cost of electricity was inflation adjusted to 9.88¢/kWh for 2011, on the basis of the average retail price for all customer classes in 2010 (9.83¢/kWh) according to the U.S. Energy Information Administration (2010) and ENR.com (2011).
- Energy associated with CIP was not considered.
- Cost associated with CIP chemicals was based on previously published data for ESPA-2 membranes (Bellona et al., 2012) and was calculated to be \$360 per CIP event for each 4:2:1 array with seven elements per vessel at 35 gpm (7.95 m³/h) configuration used here.

For each scenario, the applied ozone dose was set at 1.5, 3, or 6 mg/L and was added to the energy required to drive the case study water across the RO membranes at the given pressure based on the flux decline model. Thirteen scenarios were used in the cost curve calculations and are summarized in the matrix shown in Table 8.4.

Table 8.4. Parameters Used for Cost Curve Development

Control Train Flux Decline	O ₃ Train Flux Decline	Initial % Difference in Feed Pressure	O ₃ Dose-Label
15%	10%		1.5-A, 3-A, 6-A
10%	7.5%		1.5-B, 3-B, 6-B
10%	10%	O ₃ 20% lower than control	1.5-C, 3-C, 6-C
10%	10%	O ₃ 10% lower than control	1.5-D, 3-D, 6-D
15%	7.5%		6-E (only for 6 mg/L)

For scenario combinations A, B, and E, the different rates of flux decline resulted in different required cleaning frequencies; thus, CIP impacted the overall slope of the cost curve. For scenario combinations C and D, the rate of flux decline was the same for both the control and the ozone pretreatment processes, thereby discounting any differences in CIP frequency and focusing on the change in energy costs associated with potential benefits in feed pressure. The 10% and 20% values for feed pressure offsets are based on hypothetical scenarios for comparison purposes, though the most likely offset in pressure is in the range of 6% to 12% for the waters tested in this study (see Chapter 5).

Figures 8.4 and 8.5 show the calculated pumping and ozone generation power and treatment costs associated with the RO and the O₃RO treatment trains for a 3-mg/L ozone dose. The addition of ozone in front of the membranes clearly has an impact on the overall power consumption of the system, though in the case where the use of ozone may provide an offset in pressure (limiting initial flux decline), the power usage is similar (3-D) or even favorable (3-C) toward the O₃-RO application at a 3-mg/L dose. A comparison of total costs (including CIP chemicals but excluding membrane replacement) reveals similar trends.

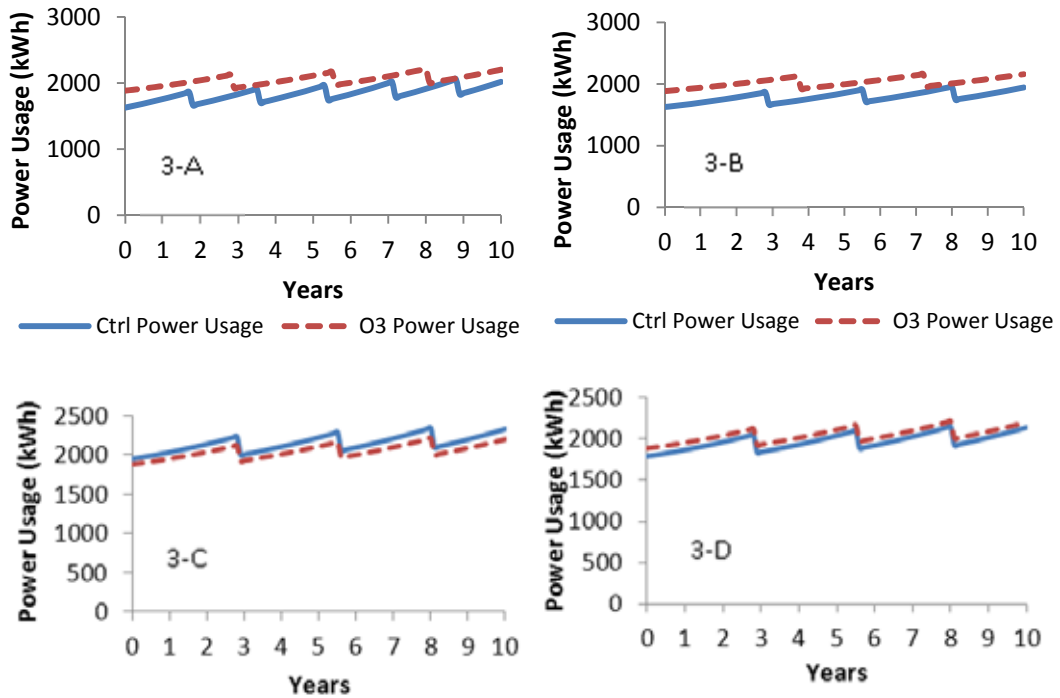


Figure 8.4. Power usage for 3-mg/L ozone pretreatment versus control with no ozone for Scenarios A, B, C, and D as described in Table 8.4.

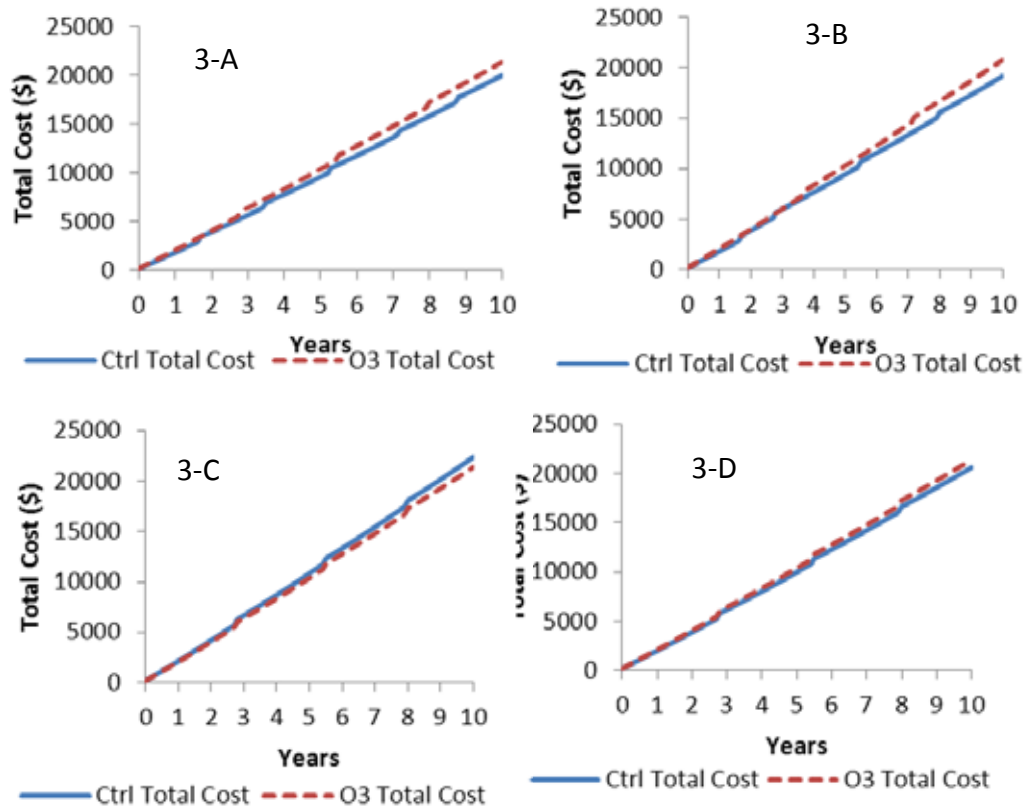


Figure 8.5. Ozone generation, pumping, and CIP chemical costs for a 3-mg/L O₃-RO system versus a control RO system.

Similar curves were developed for the 6- and 1.5-mg/L ozone doses. In the case of the 6-mg/L ozone preoxidation curves, the ozone resulted in higher operating costs for all scenarios tested, with 6-C providing the closest potential comparison (only 7% difference in operating costs at 5 years). The 1.5-mg/L ozone preoxidation strategy does appear to offer potential cost savings, however (Figure 8.6), even when there is only a 10% difference in operating pressure. If the long-term use of low-dose ozone can decrease membrane replacement frequency, have no negative impact on biofouling, and provide additional benefits of reducing the concentration of TOrCs in the reject water, then it may be a possible solution or alternative to consider for a given situation.

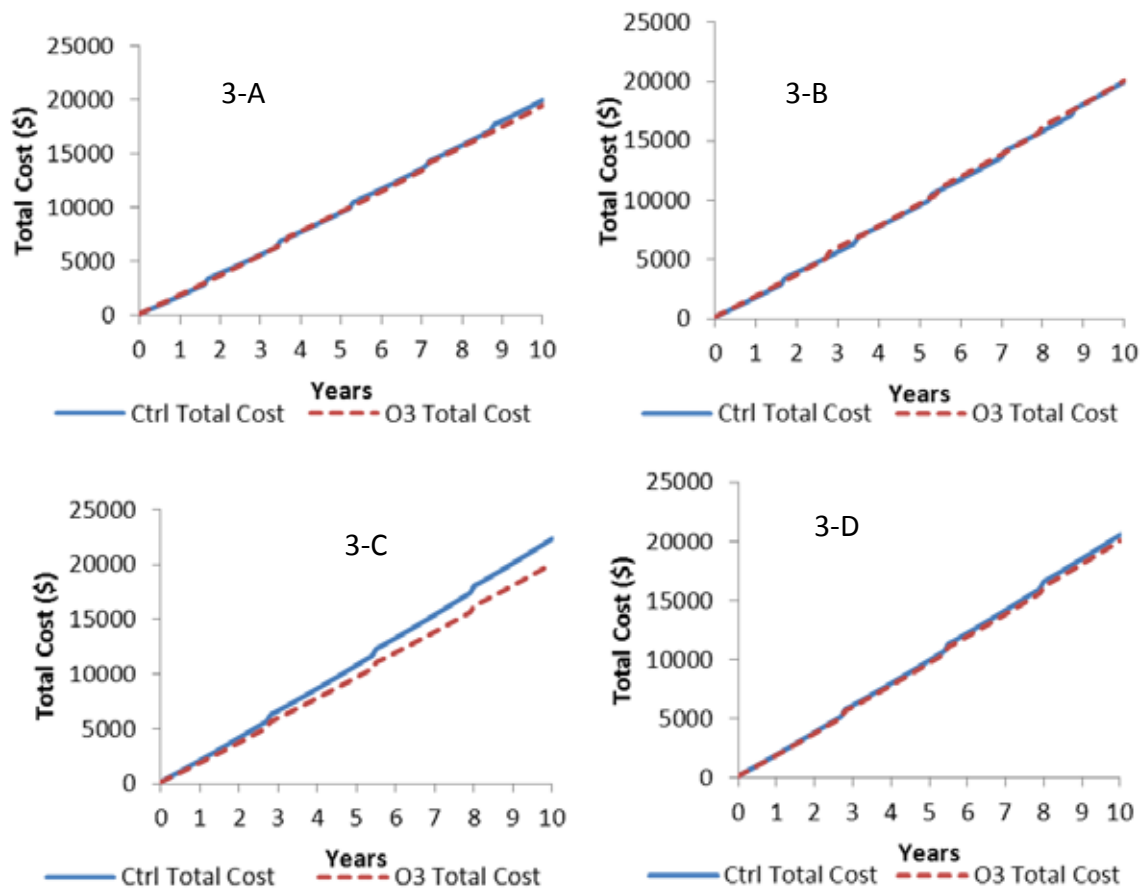


Figure 8.6. Ozone generation, pumping, and CIP chemical costs for a 1.5-mg/L O₃-RO system versus a control RO system.

8.4 Comparison of Costs and Summary

Additional long-term tests using other waters and with other membranes may provide insight into applications where ozone, even at a higher dose, may provide cost-effectiveness for the overall design. On the basis of Class 4 capital and O&M cost estimates developed for WRF-08-05, a direct comparison of an MF-O₃-RO system with an MF-RO-UV/AOP system can be performed. Table 8.5 summarizes the cost curves developed for that project (based on a 3-mg/L ozone dose and a UV/AOP system designed for 1.2-log NDMA removal and 0.5-log removal of 1,4-dioxane with 2.5- to 3.5-mg/L peroxide) whereas Tables 8.6 and 8.7 provide the normalized capital and O&M costs on a millions-of-dollars-per-mgd capacity basis.

Table 8.5. Summary of Capital and O&M Costs from WateReuse-08-05

Process	Capital Cost \$ million/mgd	O&M Cost \$ million/mgd
Ozone	$0.66 \times (\text{plant capacity, in mgd})^{-0.47}$	$0.0068 \times (\text{plant capacity, in mgd})^{-0.051}$
UV/peroxide	$0.25 \times (\text{plant capacity, in mgd})^{-0.056}$	$0.038 \times (\text{plant capacity, in mgd})^{-0.052}$
MF or UF	$1.89 \times (\text{plant capacity, in mgd})^{-0.22}$	$0.30 \times (\text{plant capacity, in mgd})^{-0.22}$
RO or NF	$3.79 \times (\text{plant capacity, in mgd})^{-0.22}$	$0.44 \times (\text{plant capacity, in mgd})^{-0.13}$

Table 8.6. Flow-Normalized Capital Costs for Combined Process Trains

Capacity (mgd)	Capital Costs (\$ million/mgd) for Process Trains		
	MF-RO	MF-RO-UV/AOP	MF-O ₃ -RO
1	\$5.7	\$5.9	\$6.3
5	\$4.0	\$4.2	\$4.3
10	\$3.4	\$3.6	\$3.6
25	\$2.8	\$3.0	\$2.9
50	\$2.4	\$2.6	\$2.5
80	\$2.2	\$2.4	\$2.3

Table 8.7. Flow-Normalized Annual O&M Costs for Combined Process Trains

Capacity (mgd)	O&M Costs (\$ million/mgd) for Process Trains		
	MF-RO	MF-RO-UV/AOP	MF-O ₃ -RO
1	\$0.54	\$0.58	\$0.55
5	\$0.51	\$0.55	\$0.52
10	\$0.48	\$0.51	\$0.48
25	\$0.42	\$0.46	\$0.43
50	\$0.38	\$0.41	\$0.39
80	\$0.36	\$0.39	\$0.36

From a cost-per-gallon basis, both MF-O₃-RO and MF-RO-UV/AOP systems are cost competitive at more than 10 mgd. If, however, UV/AOP could be eliminated as a final treatment step by replacing it with an ozone preoxidation step, then the ozone pretreatment would provide lower overall O&M costs. Even when one compares MF-RO with MF-O₃-RO, the potential exists for improvements in membrane fouling and overall costs for the low-dose ozone scenario. Thus, further site-specific and membrane-specific investigations may be necessary to determine the best applications of an ozone pretreatment system.

Chapter 9

Summary and Conclusions

9.1 Overview and Restatement of Project Objectives

The main hypothesis driving this multiyear study was that the application of oxidative processes upstream of RO membranes during treatment of wastewater for reuse applications could provide a benefit in minimizing fouling (specifically, *irreversible* fouling) associated with EfOM. To evaluate this hypothesis a series of bench-scale and pilot-scale experiments were conducted during a 3-year period on surface water and wastewater effluents from two separate water reclamation facilities. Various oxidation processes including those that used UV, UV/peroxide, ozone, and ozone/peroxide were applied to the waters and were evaluated for impacts on DOM, TOrCs, and membrane fouling at different doses and water combinations. Thus, three major questions were asked through this study: (1) Can a preoxidation strategy still provide the advanced oxidation needed to remove TOrCs? (2) Can preoxidation provide a benefit by controlling fouling associated with EfOM, thereby potentially minimizing membrane replacement costs and CIP events? and (3) Can preoxidation provide a meaningful reduction in the amount of energy required to drive water across the RO membranes by minimizing EfOM fouling of the RO membranes? Specifically, on the basis of a literature review and working knowledge among the project team and TAC, the following hypotheses were evaluated:

1. Oxidation of water and wastewater by ozone, ozone/peroxide, and UV/peroxide will produce quantifiable changes in the polarity, reactivity, and optical properties of DOM (present as NOM in surface waters and as EfOM in wastewater effluents).
2. UV alone will have little appreciable impact on NOM and EfOM.
3. The changes in EfOM and NOM resulting from oxidation will change the rate and extent of organic (irreversible) fouling observed in RO membrane applications relative to waters that have not been oxidized
4. Application of the oxidants upstream of RO membranes will not adversely impact the performance or integrity of the membranes.
5. By moving the oxidation step process typically reserved for RO permeate treatment (e.g., UV/peroxide) to the front of the RO membranes, a utility can achieve better membrane performance with less fouling, resulting in a net energy and operational cost benefit.
6. Oxidation processes applied upstream of RO membranes will produce a lower concentration of TOrCs in the RO reject water (brine) than in a comparable system without oxidation and will lower the concentration of TOrCs in the RO permeate to below detection or levels comparable with a typical RO membrane system followed by UV/peroxide treatment.

The following sections of this chapter provide a recap of the major findings from each of the major phases of the project and provide suggestions for further evaluation that may be needed to determine where and when such a preoxidation strategy may be necessary. A list of specific answers to the hypotheses is also included at the end of this chapter.

9.2 Summary of Results from This Study

9.2.1 Impact of Oxidation on Organic Matter

All forms of preoxidation (or photolysis in the case of UV alone) were demonstrated to provide quantifiable changes in the DOM present in solution provided enough energy was applied. In the case of UV alone, very little impact was observed on the organic matter, even at the highest UV fluence of approximately 5000 mJ/cm². When peroxide was added, the UV/peroxide combination was able to provide much more substantial impacts on the DOM than did UV alone because of the production of hydroxyl radicals in the AOP. In the case of ozone, both ozone and ozone/peroxide were able to impact DOM, even at applied doses as low as 1.5 mg/L. In CRW, the addition of peroxide was required to generate enough hydroxyl radicals to create an AOP. In the case of the wastewater matrices (MBR filtrate and MF filtrate), the ozone reacted with the EfOM to generate hydroxyl radicals, thereby creating an AOP without the addition of peroxide.

In all oxidation tests, changes in UVA, fluorescence, polarity, and molecular weight distribution were observed. In general, oxidation impacted the hydrophobic, aromatic organic matter components, fundamentally altering their chemical and optical properties. On the one hand, this was exactly the change that was hypothesized and widely expected. On the other hand, the changes in optical properties made the use of optical detection methods (e.g., those used in SEC-UV-fluorescence and PRAM) less quantitative because of the inability to track the transformation products. Further, whereas the data pointed toward the creation of lower-molecular-weight, more-polar organic matter, this could not be fully verified with the techniques employed in this study. Nevertheless, the data provided the information needed to support the observations and conclusions from the membrane fouling tests.

9.2.2 Bench-Scale Membrane Fouling Results

Results from the flat sheet testing indicated the potential benefit of ozone and UV/peroxide as a preoxidation step for the waters tested in this study using the flat sheet membrane setup. Both ozone- and ozone/peroxide-treated waters, even at the lowest ozone dose of 1.5 mg/L, fouled the membranes less (as indicated by a more stable flux) than did the MBR filtrate and surface control waters. Both the treated (preoxidized) and control waters maintained consistent levels of salt rejection throughout the tests, indicating that there was no damage to the membrane integrity from the preoxidation process. Whereas the results indicated that peroxide was not a beneficial addition at low ozone doses for the filtrates tested in this study, it is still possible that peroxide addition at higher ozone doses or in waters with less DOM could be required. Oxidation by a relatively high UV dose of approximately 5500 mJ/cm², without the addition of hydrogen peroxide, did not provide any benefit in reducing fouling of RO membrane. With addition of peroxide the UV treatments showed significant impact on EfOM, reflected by changes in fluorescence and by reduction of RO membrane fouling. Similar reductions in fouling were observed when UV doses of approximately 1900 and 2500 mJ/cm² were used. However, further tests with UF filtrate and more realistic UV fluence doses of 1000 mJ/cm² and 4.0-mg/L H₂O₂ did not prove to be effective in reducing organic fouling. Ineffectiveness of this pretreatment condition on reduction of the fouling rate was correlated to the relatively low impact on EfOM as measured by changes in UV₂₅₄ and fluorescence at 254 nm, reported in Chapter 3.

9.2.3 Pilot-Scale Fouling Results: MBR-O₃-RO

Although not as significant a result as the bench-scale tests, the pilot-scale results observed at the WRF 1 facility indicated a modest improvement in the performance of RO membranes with the use of ozone as a pretreatment step, though it is not clear whether this finding was related directly to organic fouling. The membrane autopsy results provided excellent information regarding the character of the foulants on the membrane surfaces, but the results failed to demonstrate definitively a difference in the presence of organic foulants. The lack of clarity regarding the potential benefit of ozone as a pretreatment step may have been due to the already effective pretreatment achieved by the biological processes and excellent filtration inherent in the MBR. It was observed that the initial flux decline that occurs within 100 to 150 h of commencement of operation was typically 5 to 10% less for the MBR-O₃-RO train than for the MBR-RO control. This difference was stable throughout most of the test period. At 14 gfd this difference was monitored out to 2500 h. At 17 gfd this difference seemed to vary, though it was observed until other mechanical and equipment problems were simultaneously encountered, thereby confusing the results. At 19 gfd both trains showed loss during the 420 h of run time, though the MBR-RO control train showed a cumulative loss in TCSF of 12%, whereas the MBR-O₃-RO lost only 6%. Thus, on the basis of the results of the operating parameters and permeability retests, a lower rate of flux was repeatedly observed in the preoxidation process train than in the control process train, indicating that the ozone pretreatment does have some beneficial impact on fouling and/or membrane performance.

9.2.4 Pilot-Scale Fouling Results: UF-UV/H₂O₂-RO

The pilot data from WRF 2 indicated that UV/H₂O₂ treatment offered some benefit to preserving the initial flux, similar to what was observed in the ozone preoxidation experiments. However, this effect was lost after continuous operation. Despite efforts to minimize scaling (e.g., pH adjustment of the feed to 6.5 and addition of antiscalant agent), the heaviest iron scaling was found on the lead element of the UF-UV/H₂O₂-RO train, as shown by ESEM/EDS analysis, characterization of the foulant layer, and an associated steady decline in the TCSF with a steady increase of dP. Overall, the results from this pilot-scale study showed that heavy iron-based deposits may have exacerbated organic fouling and biofouling occurring on the lead element of the UF-UV/H₂O₂-RO train, thus negating any benefit from oxidative pretreatment. This finding was significant, as it showed that, despite potential benefits that can be realized from preoxidation for organic fouling control, preoxidation with UV/H₂O₂ may actually increase scaling potential, leading to higher dP increases and more heterogeneous fouling where coagulant use is required for the UF or MF membrane operation.

9.2.5 Impact of Preoxidation on Trace Organic Contaminants

The results from this project indicated the potential benefit of ozone and ozone/peroxide for TOrC removal in water treatment and in wastewater treatment and as part of an advanced water reuse treatment train. Consistent with the literature, the data indicate that the addition of hydrogen peroxide does not provide significant benefits for TOrC removal in wastewater matrices, but the greater •OH exposure in surface water treatment was observed to be beneficial for the oxidation of the recalcitrant compounds, such as TCEP and DEET. Upon chloramination, NDMA formation potential was significantly reduced by ozone and ozone/peroxide pretreatment. However, the direct formation of NDMA by ozonation of secondary or tertiary wastewater may require further mitigation measures. Therefore, the oxidation of TOrCs and potential microbial inactivation must be balanced with the formation of disinfection by-products, including bromate. For the waters tested in this study, an

O₃:DOC ratio of 0.50 proved to be the optimal dosing condition to balancing TOrC oxidation, direct NDMA formation, and bromate formation. Furthermore, this study demonstrated the potential use of differential UV₂₅₄ or fluorescence at 254 nm as a surrogate for TOrC oxidation.

With regard to UV/AOP, the strategy was effective in reducing both NDMA and NDMA-FP; however, in general it requires higher electrical energy input than does ozone to achieve similar TOrC removals (other than nitrosamines or compounds that undergo direct photolysis). Thus, though effective, it is less feasible to use UV/peroxide ahead of the RO process to remove TOrC than to use ozone. The UVT of the wastewater is considerably lower than that of RO permeate, which is one of the main reasons that UV/AOP requires more energy than does ozone to achieve the same level of TOrC removal, an observation that is consistent with other studies. If the UVT could be improved, then UV/AOP could potentially be a viable option for TOrC removal.

9.2.6 Cost Considerations for Preoxidation Strategies

From a capital cost basis, both MF-O₃-RO and the typical MF-RO-UV/AOP systems are cost competitive above 10 mgd. If, however, UV/AOP could be replaced as a final treatment step by an ozone preoxidation step, then the ozone pretreatment would provide lower overall O&M costs. Even when one compares MF-RO with MF-O₃-RO, the potential exists for improvements in membrane fouling and overall costs for the low-dose ozone scenario. Thus, further site-specific and membrane-specific investigations may be necessary to determine the best applications of an ozone pretreatment system.

9.3 Conclusions and Recommendations

The results from this study provide compelling information regarding the benefits of ozone applied upstream of RO membranes for decreasing the aromatic, hydrophobic nature of EfOM and for oxidation of TOrCs, which minimizes their presence in the RO permeate and in the brine stream. The evidence regarding benefits in controlling membrane fouling was clearly observed in both the flat sheet and pilot-scale tests, though the difference in long-term operation, cleaning frequency, and biofouling potential could not be extrapolated from the flat sheet and pilot-scale results. It was also not possible to assess from the data if the use of ozone as a pretreatment would impact membrane life and/or recovery after cleaning. From a cost basis, there may be cases where ozone applied upstream of membranes could provide a benefit, though certainly that idea would need to be evaluated over a longer period for a given test water. Using the lowest dose of ozone possible to achieve the desired benefit would have long-term implications for overall O&M costs. Therefore, the hypotheses proposed at the beginning of the project can be answered as follows:

1. *Oxidation of water and wastewater by ozone, ozone/peroxide, and UV/peroxide will produce quantifiable changes in the polarity, reactivity, and optical properties of DOM present as NOM in surface waters and as EfOM in wastewater effluents.*

This hypothesis was strongly supported through the data collected throughout the project. Specific quantification of the impacts can be found in Chapter 3.

2. *UV alone will have little appreciable impact on NOM and EfOM.*

This hypothesis was also supported by the observations presented in Chapter 3 on the basis of EfOM in the UF and tertiary effluents from WRF 2. Although there was an observable impact on the properties of EfOM, the required UV fluence to provide an impact was well above typical AOP doses of about 400 mJ/cm².

3. *The changes in EfOM and NOM resulting from oxidation will change the rate and extent of organic (irreversible) fouling observed in RO membrane applications relative to waters that have not been oxidized.*

This hypothesis was supported by the observations presented in chapters 4 (flat sheet membrane tests), 5 (MBR-O₃-RO pilot), and 6 (UF-O₃-RO pilot), though there was only indirect evidence that the improvement in controlling flux decline was related to changes in EfOM. Although promising in concept and even in practice for in the experiments performed for this study, there was insufficient evidence to determine whether the ozone preoxidation step would provide long-term cost savings and operational benefits.

4. *Application of the oxidants upstream of RO membranes will not adversely impact the performance or integrity of the membranes.*

There were no observed adverse impacts to membrane integrity for any of the ozone preoxidation experiments. This finding occurred largely because ozone was rapidly consumed in the MBR and/or UF filtrate and because therefore no residual ever made it to the membrane. Any future studies investigating the use of ozone as a preoxidant should consider the size of the ozone contactor to ensure that sufficient reaction time is allowed to avoid carryover of any dissolved ozone residual to the membrane surfaces.

The UV/peroxide preoxidation strategy appeared to have some adverse impact on the membrane surface that may have had to do with the presence of colloidal iron precipitate/scale on the membrane surface. Whereas the autopsy and wet tests did not indicate any leakage, the salt transport across the membrane was high enough to create some degree of doubt about the long-term viability of the process when ferric chloride is used as a coagulant.

5. *By moving the oxidation step process typically reserved for RO permeate treatment (e.g., UV/peroxide) to the front of the RO membranes, a utility can achieve better membrane performance with less fouling, resulting in a net energy and operational cost benefit.*

From a capital expense perspective, systems treating over 10 mgd of reuse water can achieve comparable or even favorable costs by installing ozone in front of the RO membranes instead of installing UV/peroxide as a post-membrane treatment step. In some cases, and at low doses, ozone as a preoxidation strategy may provide a net energy and cost savings. However, this move should be thoroughly evaluated for each location with a unique water quality–membrane pairing and over a longer duration to determine impacts on membrane life and cleaning frequency. Further, if NDMA is a deciding factor on whether to place UV use as a post-RO treatment step, then ozone may not be a viable strategy. This interplay of NDMA formation, RO performance, energy, and costs needs to be further evaluated before a solid recommendation can be made regarding the applicability of the process.

6. *Oxidation processes applied upstream of RO membranes will produce a lower concentration of TOrCs in the RO reject water (brine) than in a comparable system without oxidation and will lower the concentration of TOrCs in the RO permeate to below detection or levels comparable with a typical RO membrane system followed by UV/peroxide treatment.*

This hypothesis was strongly supported through the bench-scale and pilot-scale experiments, with the TOrC data presented in Chapter 7. A preoxidation strategy with ozone lowered the concentration of all contaminants in both the reject and the permeate, with the exception of NDMA as previously noted.

As a closing thought, one of the observations made during the review of data from this study is that the membranes chosen for the work, the Hydranautics ESPA-2 membranes, are proven high-performance, low-fouling membranes for water reuse applications. It was also observed that the highly effective pretreatment achieved by the biological processes and excellent filtration inherent in the MBR provided a low-fouling water that did not necessarily require additional pretreatment. Therefore, in cases where other membranes are used or where organic fouling is observed to be a problem with the particular water–membrane pairing, then ozone should be evaluated as a possible pretreatment option. This choice may be particularly useful for facilities that either have only primary or nonnitrified secondary effluent (though the impact on EfOM from nonnitrified waters needs to be evaluated) or receive their feed water from a separate wastewater treatment facility. It is recommended that future work focus on evaluating oxidative pretreatment on waters with minimal biological treatment, such as partial nitrification or BOD removal only. Additional work should focus on determining strategies for minimizing the formation of NDMA by ozone during preoxidation and/or chloramines used as a biocide in the RO membranes.

References

- Aerni, H.-R.; Kobler, B.; Rutishauser, B.; Wettstein, F.; Fischer, R.; Giger, W.; Hungerbuhler, A.; Marazuela, M. D.; Peter, A.; Schonenberger, R.; Vogeli, A. C.; Suter, M.; Eggen, R. Combined biological and chemical assessment of estrogenic activities in wastewater treatment plant effluents. *Anal. Bioanal. Chem.* **2004**, *378*, 688–696.
- Ahel, M.; Mohlnar, E.; Ibric, S.; Giger, W. Estrogenic metabolites of alkylphenol polyethoxylates in secondary sewage effluents and rivers. *Water Sci. Technol.* **2000**, *42*, 15–22.
- Al-Amoudi, A. S. Factors affecting natural organic matter (NOM) and scaling fouling in NF membranes: a review. *Desalination* **2010**, *259*, 1–10.
- Al-Rifai, J. H.; Gabelish, C. L.; Schafer, A. I. Occurrence of pharmaceutically active and non-steroidal estrogenic compounds in three different wastewater recycling schemes in Australia. *Chemosphere* **2007**, *69*, 803–815.
- Andrzejewski, P.; Kasprzyk-Hordern, B.; Nawrocki, J. *N*-Nitrosodimethylamine (NDMA) formation during ozonation of dimethylamine-containing waters. *Water Res.* **2008**, *42*, 863–870.
- Archer, A. D.; Singer, P. C. Effect of SUVA and enhanced coagulation on removal of TOX precursors. *J.—Am. Water Works Assoc.* **2006a**, *98*, 97–107.
- Archer, A. D.; Singer, P. C. An evaluation of the relationship between SUVA and NOM coagulation using the ICR database. *J.—Am. Water Works Assoc.* **2006b**, *98*, 110–123.
- Bellona, C.; Drewes, J. E. The role of membrane surface charge and solute physico-chemical properties in the rejection of organic acids by NF membranes. *J. Membr. Sci.* **2005**, *249*, 227–234.
- Bellona, C.; Heil, D.; Yu, C.; Fu, P.; Drewes, J. The pros and cons of using nanofiltration in lieu of reverse osmosis for indirect potable reuse applications. *Sep. Purif. Technol.* **2005**, *85*, 69–76.
- Benitez, F. J.; Acero, J.; Leal, A.; Real, F. Ozone and membrane filtration based strategies for the treatment of cork processing wastewaters. *J. Hazard. Mater.* **2008**, *152*, 373–380.
- Benotti, M. J.; Stanford, B.; Wert, E.; Synder, S. Evaluation of a photocatalytic reactor membrane pilot system for the removal of pharmaceuticals and endocrine disrupting compounds from water. *Water Res.* **2009a**, *43*, 1513–1522.
- Benotti, M. J.; Trenholm, R.; Vanderford, B.; Holady, J.; Stanford, B.; Snyder, S. Pharmaceuticals and endocrine disrupting compounds in U.S. drinking water. *Environ. Sci. Technol.* **2009b**, *43*, 597–603.
- Bereschenko, L. A.; Prummel, H.; Euverink, G. J.; Stams, A. J.; vanLoosdrecht, M. C. Effect of conventional chemical treatment on the microbial population in a biofouling layer of reverse osmosis systems. *Water Res.* **2011**, *45*, 405–416.

- Bolton, J. R.; Stefan, M. I. Fundamental photochemical approach to the concepts of fluence (UV dose) and electrical energy efficiency in photochemical degradation reactions. *Res. Chem. Intermed.* **2002**, *28*, 857–870.
- Brant, J. A.; Childress, A. E. Assessing short-range membrane–colloid interactions using surface energetics. *J. Membr. Sci.* **2002**, *203*, 257–273.
- Brian, J. V.; Harris, C.; Scholze, M.; Kortenkamp, A.; Booy, P.; Lamoree, M.; Pojana, G.; Jonkers, N.; Marcomini, A.; Sumpter, J. Evidence of estrogenic mixture effects on the reproductive performance of fish. *Environ. Sci. Technol.* **2007**, *41*, 337–344.
- Brion, F.; Tyler, C. R.; Palazzi, X.; Laillet, B.; Porcher, J. M.; Garric, J.; Flammarion P. Impacts of 17[beta]-estradiol, including environmentally relevant concentrations, on reproduction after exposure during embryo-larval-, juvenile- and adult-life stages in zebrafish (*Danio Rerio*). *Aquat. Toxicol.* **2004**, *68*, 193–217.
- Buffle, M.-O.; Schmacher, J.; Salhi, E.; Jekel, M.; von Gunten, U. Measurement of the initial phase of ozone decomposition in water and wastewater by means of a continuous quench-flow system: application to disinfection and pharmaceutical oxidation. *Water Res.* **2006**, *40*, 1884–1894.
- Canonica, S.; Meunier, L.; von Gunten, U. Phototransformation of selected pharmaceuticals during UV treatment of drinking water. *Water Res.* **2008**, *42*, 121–128.
- Chang, Y.; Reardon, D.J.; Kwan, P.; Boyd, G.; Brant, J. *Evaluation of Dynamic Energy Consumption of Advanced Water and Wastewater Treatment Technologies*; AWWARF Project No. 3056; Awwa Research Foundation: Denver, CO, 2008.
- Chen, W.; Westerhoff, P.; Leenheer, J. A.; Booksh, K. Fluorescence excitation–emission matrix regional integration to quantify spectra for dissolved organic matter. *Environ. Sci. Technol.* **2003**, *37*, 5701–5710.
- Cheryan, M. *Ultrafiltration and Microfiltration Handbook*, 2nd ed. CRC Press: Boca Raton, FL, 1998.
- Cho, J. W.; Amy, G.; Pellegrino, J.; Yoon Y. M. Characterization of clean and natural organic matter (NOM) fouled NF and UF membranes, and foulants characterization. *Desalination* **1998**, *118*, 101–108.
- Cirja, M.; Zuehlke, S.; Ivashechkin, P.; Hollender, J.; Schaffer, A.; Corvini, P. F. X. Behavior of two differently radiolabelled 17[alpha]-ethinylestradiols continuously applied to a laboratory-scale membrane bioreactor with adapted industrial activated sludge. *Water Res.* **2007**, *41*, 4403–4412.
- Dialynas, E.; Diamadopoulos, E. Integration of a membrane bioreactor coupled with reverse osmosis for advanced treatment of municipal wastewater. *Desalination* **2009**, *238*, 302–311.
- Drewes, J. E.; Bellona, C.; Oedekoven, M.; Xu, P.; Kim, T. U.; Amy, G. Rejection of wastewater-derived micropollutants in high-pressure membrane applications leading to indirect potable reuse. *Environ. Prog.* **2005**, *24*, 400–409.
- Drewes, J. E.; Sedlak, D.; Snyder, S. A.; Dickenson, E. *Development of Indicators and Surrogates for Chemical Contaminant Removal during Wastewater Treatment and Reclamation*; WRF-03-014; WateReuse Foundation: Alexandria, VA, 2007.
- ENR.com. Engineering News-Record. Current Costs.
http://enr.construction.com/economics/current_costs/ (accessed December 12, 2011).

- Escobar, I. C.; Randall, A. A. Assimilable organic carbon (AOC) and biodegradable dissolved organic carbon (BDOC): complementary measurements. *Water Res.* **2001**, *35*, 4444–4454.
- Escobar, I. C.; Randall, A. A.; Taylor, J. S. Bacterial growth in distribution systems: effect of assimilable organic carbon and biodegradable dissolved organic carbon. *Environ. Sci. Technol.* **2001**, *35*, 3442–3447.
- Flemming, H.-C. Biofouling in water systems—cases, causes and countermeasures. *Appl. Microbiol. Biotechnol.* **2002**, *59*, 629–640.
- Gerrity, D.; Stanford, B. D.; Trenholm, R. A.; Snyder, S. A. An evaluation of a pilot-scale nonthermal plasma advanced oxidation process for trace organic compound degradation. *Water Res.* **2010**, *44*, 493–504.
- Gerrity, D.; Gamage, S.; Holady, J. C.; Mawhinney, D. B.; Quinones, O.; Trenholm, R. A.; Snyder, S. A. Pilot-scale evaluation of ozone and biological activated carbon for trace organic contaminant mitigation and disinfection. *Water Res.* **2011**, *45*, 2155–2165.
- Gibson, R.; Smith, M. D.; Spary, C. J.; Tyler, C. R.; Hill, E. M. Mixtures of estrogenic contaminants in bile of fish exposed to wastewater treatment works effluents. *Environ. Sci. Technol.* **2005**, *39*, 2461–2471.
- Gong, J.; Liu, Y.; Sun, X. O₃ and UV/O₃ oxidation of organic constituents of biotreated municipal wastewater. *Water Res.* **2008**, *42*, 1238–1244.
- Goosen, M. F. A.; Sablani, S. S.; Ai-Hinai, H.; Ai-Obeidani, S.; Al-Belushi, R.; Jackson, D. Fouling of reverse osmosis and ultrafiltration membranes: a critical review. *Sep. Sci. Technol.* **2005**, *39*, 2261–2297.
- Gray, S. R.; Ritchie, C. B.; Tran, T.; Bolto, B. A. Effect of NOM characteristics and membrane type on microfiltration performance. *Water Res.* **2007**, *41*, 3833–3841.
- Gyparakis, S.; Diamadopoulos, E. Formation and reverse osmosis removal of bromate ions during ozonation of groundwater in coastal areas. *Sep. Sci. Technol.* **2007**, *42*, 1465–1476.
- Haberkamp, J.; Ruhl, A. S.; Ernst, M.; Jekel, M. Impact of coagulation and adsorption on DOC fractions of secondary effluent and resulting fouling behaviour in ultrafiltration. *Water Res.* **2007**, *41*, 3794–3802.
- Her, N.; Amy, G.; Plottu-Pecheux, A.; Yoon, Y. Identification of nanofiltration membrane foulants. *Water Res.* **2007**, *41*, 3936–3947.
- Holady, J. C.; Trenholm, R. A.; Snyder, S. A. Analysis of NDMA and other nitrosamines in water using automated solid phase extraction and gas chromatography–tandem mass spectrometry. *Am. Lab.* **2012**, *44*, 25–30.
- Holbrook, R. D.; Higgins, M. J.; Murthy, S. N.; Fonseca, A. D.; Fleishcher, E. J.; Daigger, G. T.; Grizzard, T. J.; Love, N. G.; Novak, J. T. Effect of alum addition on the performance of submerged membranes for wastewater treatment. *Water Environ. Res.* **2004**, *76*, 2699–2702.
- Hollender, J.; Zimmerman, S. G.; Koepke, S.; Krauss, M.; McArdell, C. S.; Ort, C.; Singer, H.; Von Gunten, U.; Siegrist, H. Elimination of organic micropollutants in a municipal wastewater treatment plant upgraded with a full-scale post-ozonation followed by sand filtration. *Environ. Sci. Technol.* **2009**, *43*, 7862–7869.

- Hu, J. Y.; Chen, X.; Tao, G.; Kekred, K. Fate of endocrine disrupting compounds in membrane bioreactor systems. *Environ. Sci. Technol.* **2007**, *41*, 4097–4102.
- Huang, H.; Lee, N.; Young, T.; Gary, A.; Lozier, J. C.; Jacangelo, J. G. Natural organic matter fouling of low-pressure, hollow-fiber membranes: effects of NOM source and hydrodynamic conditions. *Water Res.* **2007**, *41*, 3823–3832.
- Huang, X.; Leal, M.; Li, Q. Degradation of natural organic matter by TiO₂ photocatalytic oxidation and its effect on fouling of low-pressure membranes. *Water Res.* **2008**, *42*, 1142–1150.
- Humbert, H.; Gallard, H.; Jacquemet, V.; Croue, J. P. Combination of coagulation and ion exchange for the reduction of UF fouling properties of a high DOC content surface water. *Water Res.* **2007**, *41*, 3803–3811.
- Jo, J.-S. Recycle of Filter Backwash Water in Aop-MF System for Drinking Water Treatment. Master's Thesis, University of Seoul, South Korea, 2007..
- Jung, C.-W.; Son, H.-J.; Kang, L.-S. Effects of membrane material and pretreatment coagulation on membrane fouling: Fouling mechanism and NOM removal. *Desalination* **2006**, *197*, 154–164.
- Kang, S. F.; Yen, H. Y.; Yang, M. H. Treatment of textile effluents by H₂O₂/UV oxidation combined with RO separation for reuse. *J. Environ. Health, Part A* **2003**, *38*, 1327–1339.
- Katsoyiannis, I. A.; Canonica, S.; von Gunten, U. Efficiency and energy requirements for the transformation of organic micropollutants by ozone, O₃/H₂O₂ and UV/H₂O₂. *Water Res.* **2011**, *45*, 3811–3822.
- Khan, E.; Sy-Savane, O.; Jittawattananarat, R. Application of commercial biochemical oxygen demand inocula for biodegradable dissolved organic carbon determination. *Water Res.* **2005**, *39*, 4824–4834.
- Kim, D.; Jung, S.; Sohn, J.; Kim, H.; Lee, S. Biocide application for controlling biofouling of SWRO membranes—an overview. *Desalination* **2009**, *238*, 43–52.
- Kimura, K.; Hane, Y.; Watanabe, Y.; Amy, G.; Ohkuma, N. Irreversible membrane fouling during ultrafiltration of surface water. *Water Res.* **2004**, *38*, 3431–3441.
- Kruithof, J. C.; Kamp, P. C.; Martijn, B. J. UV/H₂O₂ treatment: a practical solution for organic contaminant control and primary disinfection. *Ozone: Sci. Eng.* **2007**, *29*, 273–280.
- Kumar, K.; Margerum, D. W. Kinetics and mechanism of general-acid-assisted oxidation of bromide by hypochlorite and hypochlorous acid. *Inorg. Chem.* **1987**, *26*, 2706–2711.
- Kwon, B.; Lee, S.; Cho, J.; Ahn, H.; Lee, D.; Shin, H. S. Biodegradability, DBP formation, and membrane fouling potential of natural organic matter: characterization and controllability. *Environ. Sci. Technol.* **2005**, *39*, 732–739.
- Labadie, P.; Budzinski, H. Alteration of steroid hormone profile in juvenile turbot (*Psetta maxima*) as a consequence of short-term exposure to 17[alpha]-ethynylestradiol. *Chemosphere* **2006**, *64*, 1274–1286.
- Lee, C.; Schmidt, C.; Yoon, J.; von Gunten, U. Oxidation of N-nitrosodimethylamine (NDMA) precursors with ozone and chlorine dioxide: Kinetics and effect on NDMA formation potential. *Environ. Sci. Technol.* **2007a**, *41*, 2056–2063.

- Lee, C.; Yoon, J.; Von Gunten, U. Oxidative degradation of *N*-nitrosodimethylamine by conventional ozonation and the advanced oxidation process ozone/hydrogen peroxide. *Water Res.* **2007b**, *41*, 581–590.
- Lee, J.; Lee, B. C.; Ra, J. S.; Cho, J.; Kim, I. S.; Chang, N. I.; Kim, H. K.; Kim, S. D. Comparison of the removal efficiency of endocrine disrupting compounds in pilot scale sewage treatment processes. *Chemosphere* **2008**, *71*, 1582–1592.
- Lee, S.; Lee, C.-H. Effect of membrane properties and pretreatment on flux and NOM rejection in surface water nanofiltration. *Sep. Purif. Technol.* **2005**, *56*, 1–8.
- Lee, S.; Cho, J.; Elimelech, M. Combined influence of natural organic matter (NOM) and colloidal particles on nanofiltration membrane fouling. *J. Membr. Sci.* **2005**, *262*, 27–41.
- Lee, S.; Boo, C.; Elimelech, M.; Hong, S. Comparison of fouling behavior in forward osmosis (FO) and reverse osmosis (RO). *J. Membr. Sci.* **2010**, *365*, 34–39.
- Lee, W.; Westerhoff, P.; Croue, J. P. Dissolved organic nitrogen as a precursor for chloroform, dichloroacetonitrile, *N*-nitrosodimethylamine, and trichloronitromethane. *Environ. Sci. Technol.* **2007**, *41*, 5485–5490.
- Lee, Y.; Escher, B. I.; von Gunten, U. Efficient removal of estrogenic activity during oxidative treatment of waters containing steroid estrogens. *Environ. Sci. Technol.* **2008**, *42*, 6333–6339.
- Leiknes, T.; Lazarova, M.; Odegaard, H. Development of a hybrid ozonation biofilm-membrane filtration process for the production of drinking water. *Water Sci. Technol.* **2005**, *51*, 241–248.
- Li, C.; Li, X. Z.; Graham, N.; Gao, N. Y. The aqueous degradation of bisphenol A and steroid estrogens by ferrate. *Water Res.* **2008**, *42*, 109–120.
- Lim, M.; Kim, M. J. Removal of natural organic matter from river water using potassium ferrate(VI). *Water Air Soil Pollut.* **2009**, *200*, 181–189.
- MacDonald, B. C.; Lvin, S. J.; Patterson, H. Correction of fluorescence inner filter effects and the partitioning of pyrene to dissolved organic carbon. *Anal. Chim. Acta* **1997**, *338*, 155–162.
- Matin, A.; Khan, Z.; Zaidi, S. M. J.; Boyce, M. C. Biofouling in reverse osmosis membranes for seawater desalination: Phenomena and prevention. *Desalination* **2011**, *281*, 1–16.
- McKnight, D.M.; Boyer, E. W.; Westerhoff, P. K.; Doran, P. T.; Kulbe, T.; Anderson, D. T.. Spectrofluorometric characterization of dissolved organic matter for indication of precursor organic material and aromaticity. *Limnol. Oceanogr.* **2001**, *46*, 38–48.
- Metz, D. H.; Reynolds, K.; Meyer, M.; Dionysiou, D. D. The effect of UV/H₂O₂ treatment on biofilm formation potential. *Water Res.* **2011**, *45*, 497–508.
- Mitch, W. A.; Sedlak, D. L. Characterization and fate of *N*-nitrosodimethylamine precursors in municipal wastewater treatment plants. *Environ. Sci. Technol.* **2004**, *38*, 1445–1454.
- Mohamed, A. M. O.; Maraqa, M.; Al Handhaly, J. Impact of land disposal of reject brine from desalination plants on soil and groundwater. *Desalination* **2005**, *182*, 411–433.
- Mulder, M. *Basic Principles of Membrane Technology*, 2nd ed.; Kluwer Academic Publishers: Dordrecht, The Netherlands, 1997.

- Mulder, M. H. V.; van Voorthuizen, E. M.; Peeters, J. M. M. Membrane characterization. In *Nanofiltration: Principles and Applications*, Schäfer, A. I., Fane, A. G., Waite, T. D., Eds.; Elsevier Advanced Technology: Oxford, England, 2005; pp 89–117.
- Nawrocki, J.; Andrzejewski, P. Nitrosamines and water. *J. Hazard. Mater.* **2011**, *189*, 1–18.
- Ning, R. Y.; Troyer, T. L. Colloidal fouling of RO membranes following MF/UF in the reclamation of municipal wastewater. *Desalination* **2007**, *208*, 232–237.
- Nishijima, F. W.; Mukaidani, T.; Okada, M. DOC removal by multi-stage ozonation-biological treatment. *Water Res.* **2003**, *37*, 150–154.
- Nöthe, T.; Fahlenkamp, H.; von Sonntag, C. Ozonation of wastewater: rate of ozone consumption and hydroxyl radical yield. *Environ. Sci. Technol.* **2009**, *43*, 5990–5995.
- Oh, B. S.; Jang, H. Y.; Cho, J.; Lee, S.; Lee, L. E.; Kim, I. S.; Hwang, T. M.; Kang, J. W. Effect of ozone on microfiltration as a pretreatment of seawater reverse osmosis. *Desalination* **2009**, *238*, 90–97.
- Orlandini, E.; Kruitholf, J. C.; Vanderhoek, J. P.; Siebel, M. A.; Schippers, J. C. Impact of ozonation on disinfection and formation of biodegradable organic matter and bromate. *J. Water Supply Res. Technol.—Aqua* **1997**, *46*, 20–30.
- Park, C.; Kim, H.; Hong, S.; Choi, S. I. Variation and prediction of membrane fouling index under various feed water characteristics. *J. Membr. Sci.* **2006**, *284*, 248–254.
- Pehlivanoglu-Mantas, E.; Hawley, E. L.; Deeb, R. A.; Sedlak, D. L. Formation of nitrosodimethylamine (NDMA) during chlorine disinfection of wastewater effluents prior to use in irrigation systems. *Water Res.* **2006**, *40*, 341–347.
- Pisarenko, A.N.; Yan, D.; Snyder, S.; Stanford, B. D. Comparing oxidative organic fouling control in RO membrane applications. *IDA J.: Desalin. Water Reuse* **2011**, *3*, 45–49.
- Pisarenko, A.N.; Stanford, B. D.; Yan, D. X.; Gerrity, D.; Snyder, S. A. Effects of ozone and ozone/peroxide on trace organic contaminants and NDMA in drinking water and water reuse applications. *Water Res.* **2012**, *46*, 316–326.
- Plumlee, M. H.; Lopez-Mesas, M.; Heidlberger, A.; Ishida, K. P.; Reinhard, M. *N*-Nitrosodimethylamine (NDMA) removal by reverse osmosis and UV treatment and analysis via LC-MS/MS. *Water Res.* **2008**, *42*, 347–355.
- Pocostales, J. P.; Sein, M. M.; Knolle, W.; von Sonntag, C.; Schmidt, T. C. Degradation of ozone-refractory organic phosphates in wastewater by ozone and ozone/hydrogen peroxide (peroxone): the role of ozone consumption by dissolved organic matter. *Environ. Sci. Technol.* **2010**, *44*, 8248–8253.
- Radjenović, J.; Petrović, M.; Barceló, D. Fate and distribution of pharmaceuticals in wastewater and sewage sludge of the conventional activated sludge (CAS) and advanced membrane bioreactor (MBR) treatment. *Water Res.* **2009**, *43*, 831–841.
- Ramseier, M. K.; Peter, A.; Traber, J.; von Gunten, U. Formation of assimilable organic carbon during oxidation of natural waters with ozone, chlorine dioxide, chlorine, permanganate, and ferrate. *Water Res.* **2011**, *45*, 2002–2010.
- Rosario-Ortiz, F. L.; Snyder, S. A.; Suffet, I. H. Characterization of the polarity of natural organic matter under ambient conditions by the polarity rapid assessment method (PRAM). *Environ. Sci. Technol.* **2007a**, *41*, 4895–4900.

- Rosario-Ortiz, F. L.; Snyder, S. A.; Suffet, I. H. Characterization of dissolved organic matter in drinking water sources impacted by multiple tributaries. *Water Res.* **2007b**, *41*, 4115–4128.
- Rosario-Ortiz, F. L.; Wert, E. C.; Snyder, S. A. Evaluation of UV/H₂O₂ treatment for the oxidation of pharmaceuticals in wastewater. *Water Res.* **2010**, *44*, 1440–1448.
- Rosenfeldt, E. J.; Linden, K. G. Degradation of endocrine disrupting chemicals bisphenol A, ethinyl estradiol, and estradiol during UV photolysis and advanced oxidation processes. *Environ. Sci. Technol.* **2004**, *38*, 5476–5483.
- Rosenfeldt, E. J.; Linden, K. G. The ROH₂UV concept to characterize and the model UV/H₂O₂ process in natural waters. *Environ. Sci. Technol.* **2007**, *41*, 2548–2553.
- Rosenfeldt, E. J.; Linden, K. G.; Melcher, B. UV and UV/H₂O₂ treatment of methylisoborneol (Mib) and geosmin in water. *J. Water Supply Res. Technol.—Aqua* **2005**, *54*, 423–434.
- Rosenfeldt, E. J.; Linde, K. G.; Canonica, S.; von Gunten, U. Comparison of the efficiency of •OH radical formation during ozonation and the advanced oxidation processes O₃/H₂O₂ and UV/H₂O₂. *Water Res.* **2006**, *40*, 3695–3704.
- Salinas-Rodriguez, S. G.; Al-Rabaani, B.; Kennedy, M. D.; Amy, G. L.; Schippers, J. C. MFI-UF constant pressure at high ionic strength conditions. *Desalin. Water Treat.* **2009**, *10*, 64–72.
- Schechter, D. S.; Singer, P. C. Formation of aldehydes during ozonation. *Ozone: Sci. Eng.* **1995**, *17*, 53–69.
- Schmidt, C. K.; Brauch, H. J. N,N-Dimethylsulfamide as precursor for N-nitrosodimethylamine (NDMA) formation upon ozonation and its fate during drinking water treatment. *Environ. Sci. Technol.* **2008**, *42*, 6340–6346.
- Seidel, A.; Elimelech, M. Coupling between chemical and physical interactions in natural organic matter (NOM) fouling of nanofiltration membranes: implications for fouling control. *J. Membr. Sci.* **2002**, *203*, 245–255.
- Shon, H. K.; Vigneswaran, S.; Kim, I. S.; Cho, J.; Ngo, N. H. Fouling of ultrafiltration membrane by effluent organic matter: a detailed characterization using different organic fractions in wastewater. *J. Membr. Sci.* **2006**, *278*, 232–238.
- Snyder, S.; Tenholm, R. A.; Snyder, E. M.; Bruce, G. M.; Pleus, R. C.; Hemming, J. *Toxicological Relevance of EDCs and Pharmaceuticals in Drinking Water*; AWWARF Project No. 3085; AWWA Research Foundation: Denver, CO, 2008.
- Snyder, S. A.; Keith, T. L.; Verbrugge, D. A.; Snyder, E. M.; Gross, T. S.; Kannan, K.; Giesy, J. P. Analytical methods for detection of selected estrogenic compounds in aqueous mixtures. *Environ. Sci. Technol.* **1999**, *33*, 2814–2820.
- Snyder, S. A.; Villeneuve, D. L.; Snyder, E. M.; Giesy, J. P. Identification and quantification of estrogen receptor agonists in wastewater effluents. *Environ. Sci. Technol.* **2001**, *35*, 3620–3625.
- Snyder, S. A.; Adham, S.; Redding, A. M.; Cannon, F. S.; DeCarolis, J.; Oppenheimer, J.; Wert, E. C.; Yoon, Y. Role of membranes and activated carbon in the removal of endocrine disruptors and pharmaceuticals. *Desalination* **2006**, *202*, 156–181.

- Snyder, S. A.; Wert, E. C.; Lei, H.; Westerhoff, P.; Yoon, Y. *Removal of EDCs and Pharmaceuticals in Drinking and Reuse Treatment Processes*; AWWA Research Foundation: Denver, CO, 2007.
- Snyder, S. A.; Stanford, B. D.; Bruce, G. M.; Pleus, R. C.; Drewes, J. C. *Identifying Hormonally Active Compounds, Pharmaceuticals, and Personal Care Product Ingredients of Potential Health Concern from Potential Presence in Water Intended for Indirect Potable Reuse*; WaterReuse Research Foundation: Alexandria, VA, 2010.
- Spring, A. J.; Bagley, D. M.; Andrews, R. C.; Lemanik, S.; Yang, P. Removal of endocrine disrupting compounds using a membrane bioreactor and disinfection. *J. Environ. Eng. Sci.* **2007**, *6*, 131–137.
- Staehelin, J.; Hoigné, J. Decomposition of ozone in water: rate of initiation by hydroxide ions and hydrogen peroxide. *Environ. Sci. Technol.* **1982**, *16*, 676–681.
- Standard Methods for the Examination of Water and Wastewater*; 20th ed. Clesceri, L. S., Greenberg, A. E., Eaton, A. D., Eds.; American Public Health Association: Washington, DC, 1998.
- Stanford, B. D.; Snyder, S. A.; Trnholm, R. A.; Holady, J. C.; Vanderford, B. J. Estrogenic activity of US drinking waters: A relative exposure comparison. *J.—Am. Water Works Assoc.* **2010**, *102*, 55–65.
- Stanford, B. D.; Pisarenko, A. N.; Holbrook, R. D.; Snyder, S. A. Preozonation effects on the reduction of reverse osmosis membrane fouling in water reuse. *Ozone: Sci. Eng.* **2011**, *33*, 379–388.
- Steinle-Darling, E.; Zedda, M.; Plumlee, M. H.; Ridgeway, H. F.; Reinhard, M. Evaluating the impacts of membrane type, coating, fouling, chemical properties and water chemistry on reverse osmosis rejection of seven nitrosoalkylamines, including NDMA. *Water Res.* **2007**, *41*, 3959–3967.
- Tam, L. S.; Tang, T. W.; Lau, G. N.; Sharma, K. R.; Chen, G. H. A pilot study for wastewater reclamation and reuse with MBR-RO and MF/RO systems. *Desalination* **2007**, *202*, 106–113.
- Tang, C. Y.; Chong, T. H.; Fane, A. G. Colloidal interactions and fouling of NF and RO membranes: a review. *Adv. Colloid Interface Sci.* **2011**, *164*, 126–143.
- Ternes, T. A.; Meisenheimer, M.; McDowell, D.; Sacher, F.; Brauch, H. J.; Gulde, B. H.; Preuss, G.; Wilme, U.; Seibert, N. Z. Removal of pharmaceuticals during drinking water treatment. *Environ. Sci. Technol.* **2002**, *36*, 3855–3863.
- Tomiyasu, H.; Fukutomi, H.; Gordon, G. Kinetics and mechanism of ozone decomposition in basic aqueous solution. *Inorg. Chem.* **1985**, *24*, 2962–2966.
- Trenholm, R. A.; Vanderford, B. J.; Snyder, S. A. On-line solid phase extraction LC-MS/MS analysis of pharmaceutical indicators in water: A green alternative to conventional methods. *Talanta* **2009**, *79*, 1425–1432.
- U.S. Energy Information Administration. Electric Power Annual 2010. <http://www.eia.gov/electricity/annual/archive/03482010.pdf> (accessed December 12, 2011).
- U.S. Department of Agriculture. Economic Research Service: Irrigation & Water Use. <http://www.ers.usda.gov/topics/farm-practices-management/irrigation-water-use.aspx> (accessed December, 2011).

- Van Geluwe, S.; Braeken, L.; Van der Bruggen, B. Ozone oxidation for the alleviation of membrane fouling by natural organic matter: A review. *Water Res.* **2011**, *45*, 3551–3570.
- von Gunten, U.; Salhi, E.; Schmidt, C. K.; Arnold, W. A. Kinetics and mechanisms of N-nitrosodimethylamine formation upon ozonation of N,N-dimethylsulfamide-containing waters: Bromide catalysis. *Environ. Sci. Technol.* **2010**, *44*, 5762–5768.
- Voutsas, D.; Hartmann, P.; Schaffner, C.; Giger, W. Benzotriazoles, alkylphenols and bisphenol A in municipal wastewaters and in the Glatt River, Switzerland. *Environ. Sci. Pollut. Res. Int.* **2006**, *13*, 333–341.
- Vrouwenvelder, J. S.; Bakker, S. M.; Wessels, L. P.; van Paassen, J. A. M. The membrane fouling simulator as a new tool for biofouling control of spiral-wound membranes. *Desalination* **2007**, *204*, 170–174.
- Vrouwenvelder, J. S.; von der Schulenburg, D. A. G.; Kruithof, J. C.; Johns, M. L.; van Loosdrecht, M. C. M. Biofouling of spiral-wound nanofiltration and reverse osmosis membranes: A feed spacer problem. *Water Res.* **2009**, *43*, 583–594.
- Vrouwenvelder, J. S.; Van Loosdrecht, M. C. M.; Kruithof, J. C. A novel scenario for biofouling control of spiral wound membrane systems. *Water Res.* **2011**, *45*, 3890–3898.
- Wang, X.; Wang, L.; Liu, Y.; Duan, W. S. Ozonation pretreatment for ultrafiltration of the secondary effluent. *J. Membr. Sci.* **2007**, *287*, 187–191.
- Wert, E. C.; Rosario-Ortiz, F. L.; Drury, D. D.; Snyder, S. A. Formation of oxidation byproducts from ozonation of wastewater. *Water Res.* **2007**, *41*, 1481–1490.
- Wert, E. C.; Rosario-Ortiz, F. L.; Snyder, S. A. Effect of ozone exposure on the oxidation of trace organic contaminants in wastewater. *Water Res.* **2009**, *43*, 1005–1014.
- Westerhoff, P.; Yoon, Y.; Snyder, S.; Wert, E. Fate of endocrine-disruptor, pharmaceutical, and personal care product chemicals during simulated drinking water treatment processes. *Environ. Sci. Technol.* **2005**, *39*, 6649–6663.
- WHO. *Pharmaceuticals in Drinking Water*; World Health Organization: Geneva, Switzerland, 2011.
- Williams, M. D.; Pirbazari, M. Membrane bioreactor process for removing biodegradable organic matter from water. *Water Res.* **2007**, *41*, 3880–3893.
- Xu, P.; Drewes, J. E.; Kim, T. U.; Bellona, C.; Amy, G. Effect of membrane fouling on transport of organic contaminants in NF/RO membrane applications. *J. Membr. Sci.* **2006**, *279*, 165–175.
- Xu, P.; Bellona, C.; Drewes, J. E. Fouling of nanofiltration and reverse osmosis membranes during municipal wastewater reclamation: Membrane autopsy results from pilot-scale investigations. *J. Membr. Sci.* **2010**, *353*, 111–121.
- Yamamura, H.; Chae, S.; Kimura, K.; Watanabe, Y. Transition in fouling mechanism in microfiltration of a surface water. *Water Res.* **2007a**, *41*, 3812–3822.
- Yamamura, H.; Kimura, K.; Watanabe, Y. Mechanism involved in the evolution of physically irreversible fouling in microfiltration and ultrafiltration membranes used for drinking water treatment. *Environ. Sci. Technol.* **2007b**, *41*, 6789–6794.

- Yamamura, H.; Kimura, K.; Okajima, T.; Tokumoto, H.; Watanabe, Y. Affinity of functional groups for membrane surfaces: Implications for physically irreversible fouling. *Environ. Sci. Technol.* **2008**, *42*, 5310–5315.
- Yasar, A.; Ahmad, N.; Latif, H.; Khan, A. A. A. Pathogen re-growth in UASB effluent disinfected by UV, O₃, H₂O₂, and advanced oxidation processes. *Ozone: Sci. Eng.* **2007**, *29*, 485–492.
- Yavich, A. A.; Lee, K. H.; Chen, K. C.; Pape, L.; Masten, S. J. Evaluation of biodegradability of NOM after ozonation. *Water Res.* **2004**, *38*, 2839–2846.
- Yoon, Y.; Amy, G.; Cho, J. W.; Her, N. Effects of retained natural organic matter (NOM) on NOM rejection and membrane flux decline with nanofiltration and ultrafiltration. *Desalination* **2005**, *173*, 209–221.
- Yoon, Y.; Westerhoff, P.; Snyder, S. A.; Wert, E. C. Nanofiltration and ultrafiltration of endocrine disrupting compounds, pharmaceuticals and personal care products. *J. Membr. Sci.* **2006**, *270*, 88–100.
- Zeman, L. J.; Zydney, A. L. *Microfiltration and Ultrafiltration: Principles and Applications*; Marcel-Dekker: New York, NY, 1996.
- Zhao, Y.-Y.; Boyd, J. M.; Woodbeck, M.; Andrews, R. C.; Quin, F.; Hrudey, S. E.; Li, X. F. Formation of N-nitrosamines from eleven disinfection treatments of seven different surface waters. *Environ. Sci. Technol.* **2008**, *42*, 4857–4862.
- Zhao, Y.; Song, L.; Ong, S. L. Fouling behavior and foulant characteristics of reverse osmosis membranes for treated secondary effluent reclamation. *J. Membr. Sci.* **2010a**, *349*, 65–74.
- Zhao, Y.; Song, L.; Ong, S. L. Fouling of RO membranes by effluent organic matter (EfOM): Relating major components of EfOM to their characteristic fouling behaviors. *J. Membr. Sci.* **2010b**, *349*, 75–82.
- Zimmermann, S. G.; Wittenwiler, M.; Hollender, J.; Krauss, M.; Ort, C.; Siegrist, H.; con Guten, U. Kinetic assessment and modeling of an ozonation step for full-scale municipal wastewater treatment: Micropollutant oxidation, by-product formation and disinfection. *Water Res.* **2011**, *45*, 605–617.

Appendix A

RO Data Log Tables

A-1	Metals: 05-10/2010 MBR-Train 1-Concentrate ^a
A-2	Metals: 02-12/2011 MBR-Train 1-Concentrate
A-3	Metals: 05-10/2010 MBR-Train 1-Feed
A-4	Metals: 02-09/2011 MBR-Train 1-Feed
A-5	Metals: 05-10/2010 MBR-Train 1-Permeate
A-6	Metals: 02-09/2011 MBR-Train 1-Permeate
A-7	Metals: 05-10/2010 MBR-Train 2-Concentrate
A-8	Metals: 02-12/2011 MBR-Train 2-Concentrate
A-9	Metals: 05-10/2010 MBR-Train 2-Feed
A-10	Metals: 02-09/2011 MBR-Train 2-Feed
A-11	Metals: 05-10/2010 MBR-Train 2-Permeate
A-12	Metals: 02-09/2011 MBR-Train 2-Permeate
A-13	Metals: 05/10-03/11 UF-Train 1-Concentrate
A-14	Metals: 08-12/2011 UF-Train 1-Concentrate
A-15	Metals: 05/10-03/11 UF-Train 1-Feed
A-16	Metals: 08-12/2011 UF-Train 1-Feed
A-17	Metals: 05/10-03/11 UF-Train 1-Permeate
A-18	Metals: 08-12/2011 UF-Train 1-Permeate
A-19	Metals: 05/10-03/11 UF-Train 2-Concentrate
A-20	Metals: 08-12/2011 UF-Train 2-Concentrate
A-21	Metals: 05/10-03/11 UF-Train 2-Feed
A-22	Metals: 08-12/2011 UF-Train 2-Feed
A-23	Metals: 05/10-03/11 UF-Train 2-Permeate
A-24	Metals: 08-12/2011 UF-Train 2-Permeate
A-25	Anions: MBR-Train 1-Concentrate
A-26	Anions: MBR-Train 1-Feed
A-27	Anions: MBR-Train 1-Permeate
A-28	Anions: MBR-Train 2-Concentrate
A-29	Anions: MBR-Train 2-Feed
A-30	Anions: MBR-Train 2-Permeate
A-31	Anions: UF-Train 1-Concentrate
A-32	Anions: UF-Train 1-Feed
A-33	Anions: UF-Train 1-Permeate
A-34	Anions: UF-Train 2-Concentrate
A-35	Anions: UF-Train 2-Feed
A-36	Anions: UF-Train 2-Permeate
A-37	SDI ₁₅ Values for the Feed of the MBR/Ozone/RO Trains
A-38	SDI ₁₅ Values for the Feed of the UF/Ozone/RO Trains
A-39	SDI ₁₅ Values for the Feed of the UF/UV/H ₂ O ₂ /RO Trains

^aNote: Train 1 = with oxidation (e.g., ozone or UV/H₂O₂); Train 2 = control.

Table A.1. Metals: 05-10/2010 MBR-Train 1-Concentrate

Element	Unit									
		5/3/10	5/24/10	6/7/10	7/12/10	7/26/10	8/16/10	8/23/10	9/27/10	10/4/10
Be	µg/L	<2.0	NA	<2.00	N/A	N/A	<2.00	<2.00	<2.00	<2
B	µg/L	540	368	960	N/A	N/A	430	420	391	496
Na	mg/L	374	456	304	N/A	N/A	314	329	302	374
Mg	mg/L	68.4	74.6	60	N/A	N/A	69.7	65.6	63.9	60.2
Al	mg/L	<0.10	<0.10	<0.10	N/A	N/A	<0.10	<0.10	<0.10	<0.1
K	mg/L	46.2	44.4	40.4	N/A	N/A	36	41.8	30.8	32.4
Ca	mg/L	173	189	139	N/A	N/A	162	154	150	163
Ti	µg/L	<2.0	2.2	<2.00	N/A	N/A	<2.00	<2.00	<2.00	<2
V	µg/L	2.4	<2.00	<2.00	N/A	N/A	<2.00	2.7	<2.00	<2
Cr	µg/L	<2.0	<2.00	28.4	N/A	N/A	<2.00	<2.00	<2.00	<2
Mn	µg/L	15.4	59.9	67	N/A	N/A	70	43.7	58.4	54.6
Fe	mg/L	0.1	0.1	0.23	N/A	N/A	<0.10	0.1	<0.10	<0.1
Co	µg/L	<2.0	<2.00	<2.00	N/A	N/A	<2.00	<2.00	<2.00	<2
Ni	µg/L	6.4	2.9	18.2	N/A	N/A	6.7	7.1	5	4.6
Cu	µg/L	5.8	<2.00	<2.00	N/A	N/A	<2.00	6.2	<2.00	<2
Zn	µg/L	125	70.6	72	N/A	N/A	61.1	74.8	71.5	53.2
As	µg/L	4.2	<2.00	<2.00	N/A	N/A	<2.00	5.7	<2.00	<2
Se	µg/L	<2.0	<2.00	2	N/A	N/A	2	<2.00	<2.00	<2
Sr	µg/L	2290	2890	1870	N/A	N/A	2200	1980	2010	2210
Mo	µg/L	23	15.3	15.7	N/A	N/A	16.2	20.5	10.8	12.6
Ag	µg/L	<2.0	<2.00	<2.00	N/A	N/A	<2.00	<2.00	<2.00	<2
Cd	µg/L	<2.0	<2.00	<2.00	N/A	N/A	<2.00	<2.00	<2.00	<2
Sn	µg/L	<2.0	<2.00	<2.00	N/A	N/A	<2.00	<2.00	<2.00	<2
Sb	µg/L	2	<2.00	<2.00	N/A	N/A	<2.00	<2.00	<2.00	<2
Ba	µg/L	90.8	161	139	N/A	N/A	150	96.9	129	129
Tl	µg/L	<2.0	<2.00	<2.00	N/A	N/A	<2.00	<2.00	<2.00	<2
Pb	µg/L	<2.0	<2.00	<2.00	N/A	N/A	<2.00	<2.00	<2.00	<2
Si	µg/L	13,020	10,740	12,060	N/A	N/A	11,157	10,810	10,990	9501
SiO ₂ (calc)	mg/L	27.85	22.98	25.80	N/A	N/A	23.87	23.13	23.51	20.33

Note: Gray cells indicate results below detection limit.

Table A.2. Metals: 02-12/2011 MBR-Train 1-Concentrate

Element	Unit												
		2/28/11	3/7/11	3/21/11	4/25/11	5/2/11	5/23/11	6/6/11	6/20/11	8/15/11	9/6/11	12/12/11	12/27/11
Be	µg/L	<2	<2	<2	<2.00	<2	<2	<2	<2	<2	<2	<2.0	<2.0
B	µg/L	362	408	601	576	446	412	394	372	282	286	488	387
Na	mg/L	348	315	362	380	376	356	344	306	267	222	381	350
Mg	mg/L	60.2	59.5	60.5	61.9	59.5	60.8	65.7	61.7	71	60	66.9	62.3
Al	mg/L	<0.1	<0.1	<0.1	<0.10	0.19	1.5	0.17	0.12	0.12	0.78	<0.1	0.51
K	mg/L	34.3	31.8	34.3	36.9	32.1	34.5	40.4	32.3	31.3	28.4	44	35.2
Ca	mg/L	130	128	143	162	146	159	156	141	150	132	163	158
Ti	µg/L	2.1	2.1	<2	<2.00	<2	<2	<2	<2	<2	<2	<2.0	2
V	µg/L	<2	<2	<2	<2.00	<2	<2	<2	<2	<2	<2	<2.0	<2.0
Cr	µg/L	<2	<2	<2	<2.00	2.4	<2	<2	<2	<2	<2	<2.0	11.5
Mn	µg/L	61.9	56.5	44.4	61.2	41.7	52	71.9	67.4	58	63.8	84.7	86.1
Fe	mg/L	<0.1	0.1	<0.1	0.11	0.1	0.1	0.13	<0.1	0.1	0.12	0.1	0.16
Co	µg/L	<2	<2	<2	<2.00	<2	<2	<2	<2	<2	<2	<1.0	<1.0
Ni	µg/L	5	6.1	3.8	3.7	5.5	4.1	6.3	3	3.7	2.2	2.5	2.6
Cu	µg/L	11.8	4.5	3	<2.00	3.2	10.4	4.5	3.5	2.1	3.9	7.1	3.4
Zn	µg/L	84.7	80.8	73.4	46	52.4	81.2	53.3	37.2	32.2	31.3	73.2	57.2
As	µg/L	<2	<2	<2	<2.00	<2	<2	2	<2	2.2	2	1.9	1.1
Se	µg/L	<2	<2	<2	<2.00	2.1	<2	<2	<2	<2	<2	1.1	<1.0
Sr	µg/L	1880	1890	2000	2330	2230	2260	1930	1920	1960	1670	2020	2010
Mo	µg/L	14.1	12.6	12.9	12.5	11.9	15	17.5	11.6	13.4	9.5	11.8	8.8
Ag	µg/L	<2	<2	<2	<2.00	<2	<2	<2	<2	<2	<2	<0.5	<0.5
Cd	µg/L	<2	<2	<2	<2.00	<2	<2	<2	<2	<2	<2	<1.0	<1.0
Sn	µg/L	11.2	<2	<2	<2.00	<2	13.3	3.3	6.1	3.1	5.3	2.4	3.6
Sb	µg/L	<2	<2	<2	<2.00	<2	<2	<2	<2	<2	<2	<1.0	<1.0
Ba	µg/L	122	127	97.9	107	98.5	107	73.3	111	86.3	61.4	74.2	89.5
Tl	µg/L	<2	<2	<2	<2.00	<2	<2	<2	<2	<2	<2	<1.0	<1.0
Pb	µg/L	18.7	<2	<2	<2.00	<2	<2	<2	<2	<2	<2	<1.0	<1.0
Si	µg/L	6760	6828	9152	9045	9080	8930	10,560	10,200	13,000	12,000	10,200	9980
SiO2 (calc)	mg/L	14.46	14.61	19.58	19.35	19.43	19.10	22.59	21.82	27.81	25.67	21.82	21.35

Note: Gray cells indicate results below detection limit.

Table A.3. Metals: 05-10/2010 MBR-Train 1-Feed

Element	Unit									
		5/3/10	5/24/10	6/7/10	7/12/10	7/26/10	8/16/10	8/23/10	9/27/10	10/4/10
Be	µg/L	<2.0	NA	<2.00	<2.00	<2.00	<2.00	<2.00	<2.00	<2
B	µg/L	306	222	652	273	258	276	328	243	301
Na	mg/L	185	227	160	179	164	156	161	151	183
Mg	mg/L	29.2	37.9	33.2	36.3	33.8	34	31.9	31	29.4
Al	mg/L	<0.10	<0.10	<0.10	<0.10	<0.10	<0.10	<0.10	<0.10	<0.1
K	mg/L	21.1	21.3	22.7	19.1	17.4	17.8	20.1	15	15.9
Ca	mg/L	78.2	90.7	70.4	86.4	76	80.9	74.6	72.4	78.2
Ti	µg/L	<2.0	<2.00	<2.00	<2.00	<2.00	<2.00	<2.00	<2.00	<2
V	µg/L	<2.0	<2.00	<2.00	<2.00	<2.00	<2.00	<2.00	<2.00	<2
Cr	µg/L	<2.0	16	5.6	<2.00	<2.00	<2.00	<2.00	<2.00	<2
Mn	µg/L	6.6	31	32	38	34.4	33.7	20.9	28.9	25.4
Fe	mg/L	<0.10	0.11	<0.10	0.12	<0.10	<0.10	<0.10	<0.10	<0.1
Co	µg/L	<2.0	<2.00	<2.00	<2.00	<2.00	<2.00	<2.00	<2.00	<2
Ni	µg/L	2.8	10.7	5.5	2.4	<2.00	2.5	3.2	2.6	2.5
Cu	µg/L	2.9	<2.00	<2.00	<2.00	<2.00	<2.00	2.2	<2.00	<2
Zn	µg/L	61.8	36.1	37	24	26.8	30.4	35.6	31.5	27.7
As	µg/L	<2.0	<2.00	<2.00	<2.00	<2.00	<2.00	2.8	<2.00	<2
Se	µg/L	<2.0	<2.00	<2.00	<2.00	<2.00	<2.00	<2.00	<2.00	<2
Sr	µg/L	1040	1370	1000	1110	996	1090	988	912	956
Mo	µg/L	11.1	8.7	6	9.6	7.8	7.6	9.8	5.2	6
Ag	µg/L	<2.0	<2.00	<2.00	<2.00	<2.00	<2.00	<2.00	<2.00	<2
Cd	µg/L	<2.0	<2.00	<2.00	<2.00	<2.00	<2.00	<2.00	<2.00	<2
Sn	µg/L	<2.0	<2.00	<2.00	<2.00	<2.00	<2.00	<2.00	<2.00	<2
Sb	µg/L	<2.0	<2.00	<2.00	<2.00	<2.00	<2.00	<2.00	<2.00	<2
Ba	µg/L	42.4	94.4	69.2	101	75.6	71.8	46.5	61.8	58.6
Tl	µg/L	<2.0	<2.00	<2.00	<2.00	<2.00	<2.00	<2.00	<2.00	<2
Pb	µg/L	<2.0	<2.00	<2.00	<2.00	<2.00	<2.00	<2.00	<2.00	<2
Si	µg/L	5845	4800	6039	5927	NA	4695	5214	5218	4496
SiO ₂ (calc)	mg/L	12.50	10.27	12.92	12.68	NA	10.04	11.15	11.16	9.62

Note: Gray cells indicate results below detection limit.

Table A.4. Metals: 02-09/2011 MBR-Train 1-Feed

Element	Unit												
		2/28/11	3/7/11	3/21/11	4/25/11	5/2/11	5/23/11	6/6/11	6/20/11	8/15/11	9/6/11	12/12/11	12/27/11
Be	µg/L	<2	<2	<2	<2.00	<2	<2	<2	<2	<2	<2	<2.0	<2.0
B	µg/L	215	245	408	349	298	292	272	267	228	191	303	255
Na	mg/L	175	164	188	190	198	186	180	161	137	130	191	189
Mg	mg/L	30.2	30.5	31.9	32.4	32.1	32.4	34.6	33	32.7	35	28.9	31.2
Al	mg/L	<0.1	<0.1	<0.1	<0.10	<0.1	<0.1	<0.1	<0.1	<0.1	<0.1	<0.1	<0.1
K	mg/L	17.2	16.4	17.8	19.3	17.3	17.6	20.9	16.8	15.8	17.8	19.1	18.8
Ca	mg/L	65	65.9	75.7	78.4	75.2	80.8	78.5	73.2	61.7	63.9	77.4	85.1
Ti	µg/L	<2	<2	<2	<2.00	<2	<2	<2	<2	<2	<2	<2.0	<2.0
V	µg/L	<2	<2	<2	<2.00	<2	<2	<2	<2	<2	<2	<2.0	<2.0
Cr	µg/L	<2	<2	<2	<2.00	2.3	<2	<2	<2	<2	<2	<2.0	<2.0
Mn	µg/L	32.8	28.1	23	26.3	22.1	26.5	39.2	36.8	28.7	31.8	41.2	43.7
Fe	mg/L	<0.1	<0.1	<0.1	<0.10	<0.1	<0.1	<0.1	<0.1	<0.1	<0.1	<0.1	<0.1
Co	µg/L	<2	<2	<2	<2.00	<2	<2	<2	<2	<2	<2	<1.0	<1.0
Ni	µg/L	2	2	2	2.1	3.7	2.2	3.2	<2	2.3	<2	1.4	1.1
Cu	µg/L	6.2	2.3	<2	<2.00	<2	<2	<2	<2	<2	<2	2.1	<1.0
Zn	µg/L	46.8	42.3	44	29.5	30	31	27.7	20	16.8	15.1	66.1	34.7
As	µg/L	<2	<2	<2	<2.00	<2	<2	<2	<2	<2	<2	<1.0	<1.0
Se	µg/L	<2	<2	<2	<2.00	<2	<2	<2	<2	<2	<2	<1.0	<1.0
Sr	µg/L	949	944	1040	1110	1050	1130	1010	962	940	886	981	1090
Mo	µg/L	7.4	6.5	6.8	6.2	6.4	7.9	8.8	6.1	6.6	5	5.7	4.5
Ag	µg/L	<2	<2	<2	<2.00	<2	<2	<2	<2	<2	<2	<0.5	<0.5
Cd	µg/L	<2	<2	<2	<2.00	<2	<2	<2	<2	<2	<2	<1.0	<1.0
Sn	µg/L	<2	<2	<2	<2.00	<2	<2	<2	<2	<2	<2	<1.0	<1.0
Sb	µg/L	<2	<2	<2	<2.00	<2	<2	<2	<2	<2	<2	<1.0	<1.0
Ba	µg/L	62.8	63.8	50.5	51.2	52	55.4	38.6	58	43.6	32.1	36.1	47.7
Tl	µg/L	<2	<2	<2	<2.00	<2	<2	<2	<2	<2	<2	<1.0	<1.0
Pb	µg/L	<2	<2	<2	<2.00	<2	<2	<2	<2	<2	<2	<1.0	<1.0
Si	µg/L	3362	3405	4648	4588	4742	4740	5530	5480	5920	6260	4900	5000
SiO ₂ (calc)	mg/L	7.19	7.28	9.94	9.82	10.14	10.14	11.83	11.72	12.66	13.39	10.48	10.70

Note: Gray cells indicate results below detection limit.

Table A.5. Metals: 05-10/2010 MBR-Train 1-Permeate

Element	Unit									
		5/3/10	5/24/10	6/7/10	7/12/10	7/26/10	8/16/10	8/23/10	9/27/10	10/4/10
Be	µg/L	<2.0	NA	N/A	<2.00	<2.00	<2.00	<2.00	<2.00	<2
B	µg/L	NA	124	N/A	163	135	146	137	130	160
Na	mg/L	1.9	2.7	N/A	3.8	3.4	2.6	3	2.5	2.4
Mg	mg/L	<0.10	<0.10	N/A	0.12	<0.10	<0.10	<0.10	<0.10	<0.1
Al	mg/L	<0.10	<0.10	N/A	<0.10	<0.10	<0.10	<0.10	<0.10	<0.1
K	mg/L	0.19	0.2	N/A	0.37	0.3	0.22	0.31	0.2	0.16
Ca	mg/L	<0.10	0.12	N/A	0.26	<0.10	<0.10	<0.10	<0.10	<0.1
Ti	µg/L	<2.0	<2.00	N/A	<2.00	<2.00	<2.00	<2.00	<2.00	<2
V	µg/L	<2.0	<2.00	N/A	<2.00	<2.00	<2.00	<2.00	<2.00	<2
Cr	µg/L	2	<2.00	N/A	<2.00	<2.00	<2.00	<2.00	<2.00	<2
Mn	µg/L	<2.0	<2.00	N/A	<2.00	<2.00	<2.00	<2.00	<2.00	<2
Fe	mg/L	<0.10	<0.10	N/A	<0.10	<0.10	<0.10	<0.10	<0.10	<0.1
Co	µg/L	<2.0	<2.00	N/A	<2.00	<2.00	<2.00	<2.00	<2.00	<2
Ni	µg/L	<2.0	<2.00	N/A	<2.00	<2.00	<2.00	<2.00	<2.00	<2
Cu	µg/L	<2.0	<2.00	N/A	<2.00	<2.00	<2.00	<2.00	<2.00	<2
Zn	µg/L	<2.0	<2.00	N/A	<2.00	<2.00	<2.00	3.3	<2.00	<2
As	µg/L	<2.0	<2.00	N/A	<2.00	<2.00	<2.00	<2.00	<2.00	<2
Se	µg/L	<2.0	<2.00	N/A	<2.00	<2.00	<2.00	<2.00	<2.00	<2
Sr	µg/L	<2.0	<2.00	N/A	<2.00	<2.00	<2.00	<2.00	<2.00	<2
Mo	µg/L	<2.0	<2.00	N/A	<2.00	<2.00	<2.00	<2.00	<2.00	<2
Ag	µg/L	<2.0	<2.00	N/A	<2.00	<2.00	<2.00	<2.00	<2.00	<2
Cd	µg/L	<2.0	<2.00	N/A	<2.00	<2.00	<2.00	<2.00	<2.00	<2
Sn	µg/L	<2.0	<2.00	N/A	<2.00	<2.00	<2.00	<2.00	<2.00	<2
Sb	µg/L	<2.0	<2.00	N/A	<2.00	<2.00	<2.00	<2.00	<2.00	<2
Ba	µg/L	<2.0	<2.00	N/A	<2.00	<2.00	<2.00	<2.00	<2.00	<2
Tl	µg/L	<2.0	<2.00	N/A	<2.00	<2.00	<2.00	<2.00	<2.00	<2
Pb	µg/L	<2.0	<2.00	N/A	<2.00	<2.00	<2.00	<2.00	<2.00	<2
Si	µg/L	20.15	20.2	N/A	47.13	NA	35.26	38.81	33.27	30.6
SiO ₂ (calc)	mg/L	0.043	0.043	N/A	0.101	NA	0.075	0.083	0.071	0.065

Note: Gray cells indicate results below detection limit.

Table A.6. Metals: 02-09/2011 MBR-Train 1- Permeate

Element	Unit	Values for Date:											
		2/28/11	3/7/11	3/21/11	4/25/11	5/2/11	5/23/11	6/6/11	6/20/11	8/15/11	9/6/11	12/12/11	12/27/11
Be	µg/L	<2	<2	<2	<2.00	<2	<2	<2	<2	<2	<2	<2.0	<2.0
B	µg/L	121	141	209	160	151	165	143	159	148	158	115	112
Na	mg/L	2.4	2.2	1.8	2.6	2.7	3.3	3.4	2.9	3.4	2.9	2.2	2.2
Mg	mg/L	<0.1	<0.1	<0.1	<0.10	<0.1	<0.1	<0.1	<0.1	<0.1	<0.1	<0.5	<0.5
Al	mg/L	<0.1	<0.1	<0.1	<0.10	<0.1	<0.1	<0.1	<0.1	<0.1	<0.1	<0.1	<0.1
K	mg/L	0.14	0.14	<0.1	0.18	0.17	0.25	0.17	0.1	0.27	0.21	<0.5	<0.5
Ca	mg/L	<0.1	<0.1	<0.1	<0.10	<0.1	<0.1	<0.1	<0.1	<0.1	<0.1	<0.5	<0.5
Ti	µg/L	<2	<2	<2	<2.00	<2	<2	<2	<2	<2	<2	<2.0	<2.0
V	µg/L	<2	<2	<2	<2.00	<2	<2	<2	<2	<2	<2	<2.0	<2.0
Cr	µg/L	<2	<2	<2	<2.00	2.3	<2	<2	<2	<2	<2	<2.0	<2.0
Mn	µg/L	<2	<2	<2	<2.00	<2	<2	<2	<2	<2	<2	<2.0	<2.0
Fe	mg/L	<0.1	<0.1	<0.1	<0.10	<0.1	<0.1	<0.1	<0.1	<0.1	<0.1	0.19	<0.1
Co	µg/L	<2	<2	<2	<2.00	<2	<2	<2	<2	<2	<2	<1.0	<1.0
Ni	µg/L	<2	<2	<2	<2.00	<2	<2	<2	<2	<2	<2	<1.0	<1.0
Cu	µg/L	<2	<2	<2	<2.00	<2	<2	<2	<2	<2	<2	2.8	<1.0
Zn	µg/L	<2	<2	<2	<2.00	<2	<2	<2	<2	<2	<2	5.3	3.8
As	µg/L	<2	<2	<2	<2.00	<2	<2	<2	<2	<2	<2	<1.0	<1.0
Se	µg/L	<2	<2	<2	<2.00	<2	<2	<2	<2	<2	<2	<1.0	<1.0
Sr	µg/L	<2	<2	<2	<2.00	<2	<2	<2	<2	<2	<2	<5.0	<5.0
Mo	µg/L	<2	<2	<2	<2.00	<2	<2	<2	<2	<2	<2	<1.0	<1.0
Ag	µg/L	<2	<2	<2	<2.00	<2	<2	<2	<2	<2	<2	<0.5	<0.5
Cd	µg/L	<2	<2	<2	<2.00	<2	<2	<2	<2	<2	<2	<1.0	<1.0
Sn	µg/L	<2	<2	<2	<2.00	<2	<2	<2	<2	<2	<2	<1.0	<1.0
Sb	µg/L	<2	<2	<2	<2.00	<2	<2	<2	<2	<2	<2	<1.0	<1.0
Ba	µg/L	<2	<2	<2	<2.00	<2	<2	<2	<2	<2	<2	<1.0	<1.0
Tl	µg/L	<2	<2	<2	<2.00	<2	<2	<2	<2	<2	<2	<1.0	<1.0
Pb	µg/L	<2	<2	<2	<2.00	<2	<2	<2	<2	<2	<2	<1.0	<1.0
Si	µg/L	26.6	18.7	40.8	24.65	26.6	39.3	41.04	70.6	105	112	35	41.5
SiO ₂ (calc)	mg/L	0.057	0.040	0.087	0.053	0.057	0.084	0.088	0.151	0.225	0.240	0.0749	0.0888

Note: Gray cells indicate results below detection limit.

Table A.7. Metals: 05-10/2010 MBR-Train 2-Concentrate

Element	Unit	Values for Date:								
		5/3/10	5/24/10	6/7/10	7/12/10	7/26/10	8/16/10	8/23/10	9/27/10	10/4/10
Be	µg/L	<2.0	NA	<2.00	N/A	N/A	<2.00	<2.00	<2.00	<2
B	µg/L	520	375	1040	N/A	N/A	416	435	415	496
Na	mg/L	423	462	325	N/A	N/A	313	336	320	374
Mg	mg/L	68	77	65.4	N/A	N/A	66.7	67.2	66.6	60.2
Al	mg/L	<0.10	<0.10	<0.10	N/A	N/A	<0.10	<0.10	<0.10	<0.1
K	mg/L	44.6	46	43.2	N/A	N/A	34.6	41	32.1	32.4
Ca	mg/L	170	194	150	N/A	N/A	162	160	156	163
Ti	µg/L	<2.0	2.1	<2.00	N/A	N/A	<2.00	<2.00	<2.00	<2
V	µg/L	2.4	<2.00	<2.00	N/A	N/A	<2.00	2.6	<2.00	<2
Cr	µg/L	<2.0	<2.00	7.2	N/A	N/A	<2.00	<2.00	<2.00	<2
Mn	µg/L	18.4	61	68.8	N/A	N/A	69.6	47.5	62.4	54.6
Fe	mg/L	0.1	0.1	0.14	N/A	N/A	<0.10	0.1	<0.10	<0.1
Co	µg/L	<2.0	<2.00	<2.00	N/A	N/A	<2.00	<2.00	<2.00	<2
Ni	µg/L	6.3	3.2	8.5	N/A	N/A	4.8	6.8	5.2	4.6
Cu	µg/L	5.2	<2.00	<2.00	N/A	N/A	<2.00	2.4	<2.00	<2
Zn	µg/L	122	70.1	75.4	N/A	N/A	57.9	69.3	62.5	53.2
As	µg/L	4.2	<2.00	<2.00	N/A	N/A	<2.00	5.2	<2.00	<2
Se	µg/L	<2.0	<2.00	2	N/A	N/A	<2.00	<2.00	<2.00	<2
Sr	µg/L	2240	2830	2050	N/A	N/A	2060	2040	2060	2210
Mo	µg/L	22.5	15.5	13.3	N/A	N/A	15.6	20.5	11.1	12.6
Ag	µg/L	<2.0	<2.00	<2.00	N/A	N/A	<2.00	<2.00	<2.00	<2
Cd	µg/L	<2.0	<2.00	<2.00	N/A	N/A	<2.00	<2.00	<2.00	<2
Sn	µg/L	<2.0	<2.00	<2.00	N/A	N/A	<2.00	<2.00	<2.00	<2
Sb	µg/L	2	<2.00	<2.00	N/A	N/A	<2.00	<2.00	<2.00	<2
Ba	µg/L	93.5	164	151	N/A	N/A	150	103	133	129
Tl	µg/L	<2.0	<2.00	<2.00	N/A	N/A	<2.00	<2.00	<2.00	<2
Pb	µg/L	<2.0	<2.00	<2.00	N/A	N/A	<2.00	<2.00	<2.00	<2
Si	µg/L	11,770	10530	12760	N/A	N/A	10382	11160	11650	9501
SiO ₂ (calc)	mg/L	25.18	22.53	27.30	N/A	N/A	22.21	23.87	24.92	20.33

Note: Gray cells indicate results below detection limit.

Table A.8. Metals: 02-09/2011 MBR-Train 2-Concentrate

Element	Unit	Values for Date:											
		2/28/11	3/7/11	3/21/11	4/25/11	5/2/11	5/23/11	6/6/11	6/20/11	8/15/11	9/6/11	12/12/11	12/27/11
Be	µg/L	<2	<2	<2	<2.00	<2	<2	<2	<2	<2	<2	<2.0	<2.0
B	µg/L	372	429	626	576	490	461	390	380	354	343	499	385
Na	mg/L	343	327	375	380	428	377	348	309	289	272	375	357
Mg	mg/L	60.2	61.2	60.6	61.9	66.8	64.9	68.3	60.7	74.5	68.1	65.7	63.3
Al	mg/L	<0.1	<0.1	<0.1	<0.10	<0.1	<0.1	<0.1	<0.1	<0.1	<0.1	0.11	<0.1
K	mg/L	34.2	32.8	34.8	36.9	35.4	36.2	41.3	31.5	32.7	28.5	38.4	34.6
Ca	mg/L	130	132	148	162	165	168	160	143	152	132	161	160
Ti	µg/L	2	2.1	<2	<2.00	<2	<2	<2	<2	<2	<2	<2.0	2
V	µg/L	<2	<2	<2	<2.00	<2	<2	<2	<2	<2	<2	<2.0	<2.0
Cr	µg/L	<2	<2	<2	<2.00	2.6	<2	<2	<2	<2	<2	<2.0	<2.0
Mn	µg/L	66.2	55.4	45.1	61.2	47.6	52.2	80.3	71.1	62.7	61	96.5	86.5
Fe	mg/L	<0.1	0.1	<0.1	0.11	0.11	0.1	0.14	<0.1	0.11	0.11	0.11	0.12
Co	µg/L	<2	<2	<2	<2.00	<2	<2	<2	<2	<2	<2	<1.0	<1.0
Ni	µg/L	4.8	3.7	3.7	3.7	6	4.3	6.1	3	4.3	<2	2.6	2.7
Cu	µg/L	24	4.2	3.8	<2.00	2.9	2.5	2.6	<2	<2	<2	5.9	<1.0
Zn	µg/L	140	94.3	74.9	46	55.4	60.1	55.9	36.7	35.9	28.4	78.3	58.1
As	µg/L	<2	<2	<2	<2.00	<2	<2	2	<2	2.4	2	1.8	1
Se	µg/L	<2	<2	<2	<2.00	2.4	2	<2	<2	<2	<2	1.2	<1.0
Sr	µg/L	1880	1960	2090	2330	2460	2360	1980	1870	1970	1790	2000	2040
Mo	µg/L	14.4	12.5	13	12.5	13.2	15.9	17.8	11.5	13.6	10.7	11.6	8.8
Ag	µg/L	<2	<2	<2	<2.00	<2	<2	<2	<2	<2	<2	<0.5	<0.5
Cd	µg/L	<2	<2	<2	<2.00	<2	<2	<2	<2	<2	<2	<1.0	<1.0
Sn	µg/L	4	<2	<2	<2.00	<2	<2	2.7	2.4	3.1	<2	2.9	<1.0
Sb	µg/L	<2	<2	<2	<2.00	<2	<2	<2	<2	<2	<2	<1.0	<1.0
Ba	µg/L	124	128	98.9	107	113	112	75.9	111	89.8	71.2	75	92.7
Tl	µg/L	<2	<2	<2	<2.00	<2	<2	<2	<2	<2	<2	<1.0	<1.0
Pb	µg/L	5.6	<2	<2	<2.00	<2	<2	<2	<2	<2	<2	1.2	<1.0
Si	µg/L	6704	7196	9426	9045	9790	9430	10910	10500	11600	12400	10200	9450
SiO ₂ (calc)	mg/L	14.34	15.39	20.17	19.35	20.94	20.17	23.34	22.46	24.82	26.53	21.82	20.22

Note: Gray cells indicate results below detection limit.

Table A.9. Metals: 05-10/2010 MBR-Train 2-Feed

Element	Unit	Values for Date:								
		5/3/10	5/24/20	6/7/10	7/12/10	7/26/10	8/16/10	8/23/10	9/27/10	10/4/10
Be	µg/L	<2.0	NA	<2.00	<2.00	<2.00	<2.00	<2.00	<2.00	<2
B	µg/L	310	231	688	281	259	259	298	235	306
Na	mg/L	184	236	163	180	157	155	164	153	189
Mg	mg/L	29	38.6	33.4	36.5	32.8	32.9	32.8	30.9	29.8
Al	mg/L	<0.10	<0.10	<0.10	<0.10	<0.10	<0.10	<0.10	<0.10	<0.1
K	mg/L	20.5	22.3	22.9	19.2	16.8	17.3	19.9	15.1	16.2
Ca	mg/L	78.4	94.8	70.8	86.6	74.4	79.6	76.8	72.9	81.1
Ti	µg/L	<2.0	<2.00	<2.00	<2.00	<2.00	<2.00	<2.00	<2.00	<2
V	µg/L	<2.0	<2.00	<2.00	<2.00	<2.00	<2.00	<2.00	<2.00	<2
Cr	µg/L	<2.0	<2.00	9.2	<2.00	<2.00	<2.00	<2.00	<2.00	<2
Mn	µg/L	9	29.5	33.6	43.1	35.3	33.6	23.6	29.5	27.5
Fe	mg/L	<0.10	<0.10	<0.10	0.16	<0.10	<0.10	<0.10	<0.10	<0.1
Co	µg/L	<2.0	<2.00	<2.00	<2.00	<2.00	<2.00	<2.00	<2.00	<2
Ni	µg/L	2.8	<2.00	7.7	2.6	<2.00	2.4	3.6	2.5	2.4
Cu	µg/L	2.7	<2.00	<2.00	<2.00	<2.00	<2.00	<2.00	<2.00	<2
Zn	µg/L	61.8	37.6	41.6	26.2	24.3	31.4	39.4	34	28.1
As	µg/L	2	<2.00	<2.00	<2.00	<2.00	<2.00	2.6	<2.00	<2
Se	µg/L	<2.0	<2.00	<2.00	<2.00	<2.00	<2.00	<2.00	<2.00	<2
Sr	µg/L	1060	1420	983	1150	994	1060	914	895	985
Mo	µg/L	10.8	7.3	6.5	9.6	7.6	7.7	9.8	5.8	6.1
Ag	µg/L	<2.0	<2.00	<2.00	<2.00	<2.00	<2.00	<2.00	<2.00	<2
Cd	µg/L	<2.0	<2.00	<2.00	<2.00	<2.00	<2.00	<2.00	<2.00	<2
Sn	µg/L	<2.0	<2.00	<2.00	<2.00	<2.00	<2.00	<2.00	<2.00	<2
Sb	µg/L	<2.0	<2.00	<2.00	<2.00	<2.00	<2.00	<2.00	<2.00	<2
Ba	µg/L	45.7	98.5	71.2	105	73.1	73.7	49.4	67.7	62
Tl	µg/L	<2.0	<2.00	<2.00	<2.00	<2.00	<2.00	<2.00	<2.00	<2
Pb	µg/L	<2.0	<2.00	<2.00	<2.00	<2.00	<2.00	<2.00	<2.00	<2
Si	µg/L	6066	5023	6047	5875	NA	4721	5235	5288	4446
SiO ₂ (calc)	mg/L	12.98	10.75	12.94	12.57	NA	10.10	11.20	11.31	9.51

Note: Gray cells indicate results below detection limit.

Table A.10. Metals: 02-09/2011 MBR-Train 2-Feed

Element	Unit												
		2/28/11	3/7/11	3/21/11	4/25/11	5/2/11	5/23/11	6/6/11	6/20/11	8/15/11	9/6/11	12/12/11	12/27/11
Be	µg/L	<2	<2	<2	<2.00	<2	<2	<2	<2	<2	<2	<2.0	<2.0
B	µg/L	215	233	413	350	306	307	268	273	244	199	315	252
Na	mg/L	177	162	195	189	200	185	179	160	151	135	190	191
Mg	mg/L	30.7	30.4	32.7	31.9	32.6	32.5	34.8	33.4	34.4	31.3	30.4	31.4
Al	mg/L	<0.1	<0.1	<0.1	<0.10	<0.1	<0.1	<0.1	<0.1	<0.1	<0.1	<0.1	<0.1
K	mg/L	17.6	16.2	18.5	19.6	17.2	17.8	21	17.2	17.2	15.3	19.9	18.5
Ca	mg/L	66.3	65.6	77.6	78.8	76.8	81.6	78.7	73	78.7	62.8	81.8	84.7
Ti	µg/L	<2	<2	<2	<2.00	<2	<2	<2	<2	<2	<2	<2.0	<2.0
V	µg/L	<2	<2	<2	<2.00	<2	<2	<2	<2	<2	<2	<2.0	<2.0
Cr	µg/L	<2	<2	<2	<2.00	2.5	<2	<2	<2	<2	<2	<2.0	<2.0
Mn	µg/L	34.3	26.7	23.6	26.7	22.6	25.8	40.8	37.9	26.5	32	48.9	46.6
Fe	mg/L	<0.1	<0.1	<0.1	<0.10	<0.1	<0.1	<0.1	<0.1	<0.1	<0.1	<0.1	0.14
Co	µg/L	<2	<2	<2	<2.00	<2	<2	<2	<2	<2	<2	<1.0	<1.0
Ni	µg/L	2.1	<2	2	2	3.8	2.4	3.2	<2	2	<2	1.1	2
Cu	µg/L	8.5	2.2	<2	<2.00	<2	<2	<2	<2	<2	<2	3.6	1.6
Zn	µg/L	57.6	49.6	44.7	29.2	33.2	36.2	29.1	21.8	17.4	14.9	52.3	37.8
As	µg/L	<2	<2	<2	<2.00	<2	<2	<2	<2	<2	<2	<1.0	<1.0
Se	µg/L	<2	<2	<2	<2.00	<2	<2	<2	<2	<2	<2	<1.0	<1.0
Sr	µg/L	963	934	1050	1090	1150	1150	1010	985	988	857	1030	1100
Mo	µg/L	7.5	6.3	6.7	6.3	6.4	7.8	9	5.9	6.8	5	5.9	5
Ag	µg/L	<2	<2	<2	<2.00	<2	<2	<2	<2	<2	<2	<0.5	<0.5
Cd	µg/L	<2	<2	<2	<2.00	<2	<2	<2	<2	<2	<2	<1.0	<1.0
Sn	µg/L	<2	<2	<2	<2.00	<2	<2	<2	<2	<2	<2	<1.0	<1.0
Sb	µg/L	<2	<2	<2	<2.00	<2	<2	<2	<2	<2	<2	<1.0	<1.0
Ba	µg/L	64.1	63.6	51.7	52.3	53.9	54.7	38.5	57.6	44.8	33	38	48.7
Tl	µg/L	<2	<2	<2	<2.00	<2	<2	<2	<2	<2	<2	<1.0	<1.0

Pb	µg/L	<2	<2	<2	<2.00	<2	<2	<2	<2	<2	<2	<1.0	<1.0
Si	µg/L	3408	3274	4732	4700	4804	4870	5540	5500	6360	6160	5160	5000
SiO ₂ (calc)	mg/L	7.29	7.00	10.12	10.05	10.28	10.42	11.85	11.77	13.61	13.18	11.04	10.70

Note: Gray cells indicate results below detection limit.

Table A.11. Metals: 05-10/2010 MBR-Train 2-Permeate

Element	Unit	Values for Date:								
		5/3/10	5/24/10	6/7/10	7/12/10	7/26/10	8/16/10	8/23/10	9/27/10	10/4/10
Be	µg/L	<2.0	NA	N/A	<2.00	<2.00	<2.00	<2.00	<2.00	<2
B	µg/L	2.3	126	N/A	136	165	125	116	104	125
Na	mg/L	0.11	2.6	N/A	3	3.4	2.5	2.6	2.2	2.3
Mg	mg/L	<0.10	<0.10	N/A	<0.10	<0.10	<0.10	<0.10	<0.10	<0.1
Al	mg/L	0.23	<0.10	N/A	<0.10	<0.10	<0.10	<0.10	<0.10	<0.1
K	mg/L	0.31	0.18	N/A	0.26	0.32	0.21	0.23	0.17	0.16
Ca	mg/L	<2.0	0.1	N/A	0.11	<0.10	<0.10	<0.10	<0.10	<0.1
Ti	µg/L	<2.0	<2.00	N/A	<2.00	<2.00	<2.00	<2.00	<2.00	<2
V	µg/L	<2.0	<2.00	N/A	<2.00	<2.00	<2.00	<2.00	<2.00	<2
Cr	µg/L	<2.0	<2.00	N/A	<2.00	<2.00	<2.00	<2.00	<2.00	<2
Mn	µg/L	<2.0	<2.00	N/A	<2.00	<2.00	<2.00	<2.00	<2.00	<2
Fe	mg/L	<0.10	<0.10	N/A	<0.10	<0.10	<0.10	<0.10	<0.10	<0.1
Co	µg/L	<2.0	<2.00	N/A	<2.00	<2.00	<2.00	<2.00	<2.00	<2
Ni	µg/L	<2.0	<2.00	N/A	<2.00	<2.00	<2.00	<2.00	<2.00	<2
Cu	µg/L	<2.0	<2.00	N/A	<2.00	<2.00	<2.00	7.1	<2.00	<2
Zn	µg/L	<2.0	<2.00	N/A	2.4	2.2	<2.00	3.1	<2.00	<2
As	µg/L	<2.0	<2.00	N/A	<2.00	<2.00	<2.00	<2.00	<2.00	<2
Se	µg/L	<2.0	<2.00	N/A	<2.00	<2.00	<2.00	<2.00	<2.00	<2
Sr	µg/L	<2.0	<2.00	N/A	<2.00	4.6	<2.00	<2.00	<2.00	<2
Mo	µg/L	<2.0	<2.00	N/A	<2.00	<2.00	<2.00	<2.00	<2.00	<2
Ag	µg/L	<2.0	<2.00	N/A	<2.00	<2.00	<2.00	<2.00	<2.00	<2
Cd	µg/L	<2.0	<2.00	N/A	<2.00	<2.00	<2.00	<2.00	<2.00	<2
Sn	µg/L	<2.0	<2.00	N/A	<2.00	<2.00	<2.00	<2.00	<2.00	<2
Sb	µg/L	<2.0	<2.00	N/A	<2.00	<2.00	<2.00	<2.00	<2.00	<2
Ba	µg/L	<2.0	<2.00	N/A	<2.00	<2.00	<2.00	<2.00	<2.00	<2
Tl	µg/L	<2.0	<2.00	N/A	<2.00	<2.00	<2.00	<2.00	<2.00	<2
Pb	µg/L	<2.0	<2.00	N/A	<2.00	<2.00	<2.00	<2.00	<2.00	<2
Si	µg/L	19.45	23.6	N/A	30.21	N/A	27.2	26.54	25.9	20.66
SiO ₂ (calc)	mg/L	0.042	0.050	N/A	0.065	N/A	0.058	0.057	0.055	0.044

Note: Gray cells indicate results below detection limit.

Table A.12. Metals: 02-12/2011 MBR-Train 2-Permeate

Element	Unit												
		2/2 8/1 1	3/7/ 11	3/21/ 11	4/25/ 11	5/2/ 11	5/23/ 11	6/6/ 11	6/20/ 11	8/15/ 11	9/6/ 11	12/12/ 11	12/27/ 11
Be	µg/L	<2	<2	<2	<2.00	<2	<2	<2	<2	<2	<2	<2.0	<2.0
B	µg/L	10 0	112	164	160	138	151	150	143	137	136	105	95.7
Na	mg/ L	2.4	2.1	1.6	2.6	2.5	2.5	3.9	4.1	3.7	3	2.3	2.2
Mg	mg/ L	<0. 1	<0.1	<0.1	<0.10	<0.1	<0.1	<0.1	<0.1	<0.1	<0.1	<0.5	<0.5
Al	mg/ L	<0. 1	<0.1	<0.1	<0.10	<0.1	<0.1	<0.1	<0.1	<0.1	<0.1	<0.1	<0.1
K	mg/ L	0.1 4	0.14	<0.1	0.18	0.15	0.18	0.36	0.35	0.35	0.28	<0.5	<0.5
Ca	mg/ L	0.1 1	0.1	<0.1	<0.10	<0.1	<0.1	<0.1	<0.1	<0.1	<0.1	<0.5	<0.5
Ti	µg/L	4	<2	<2	<2.00	<2	<2	<2	<2	<2	<2	<2.0	<2.0
V	µg/L	<2	<2	<2	<2.00	<2	<2	<2	<2	<2	<2	<2.0	<2.0
Cr	µg/L	<2	<2	<2	<2.00	2.7	<2	<2	<2	<2	<2	<2.0	<2.0
Mn	µg/L	<2	<2	<2	<2.00	<2	<2	<2	<2	<2	<2	<2.0	<2.0
Fe	mg/ L	<0. 1	<0.1	<0.1	<0.10	<0.1	<0.1	<0.1	<0.1	<0.1	<0.1	<0.1	<0.1
Co	µg/L	<2	<2	<2	<2.00	<2	<2	<2	<2	<2	<2	<1.0	<1.0
Ni	µg/L	<2	<2	<2	<2.00	2.2	<2	<2	<2	<2	<2	<1.0	<1.0
Cu	µg/L	<2	<2	<2	<2.00	<2	<2	<2	<2	<2	<2	<1.0	<1.0
Zn	µg/L	<2	<2	<2	<2.00	<2	<2	<2	<2	<2	<2	<2.0	<2.0
As	µg/L	<2	<2	<2	<2.00	<2	<2	<2	<2	<2	<2	<1.0	<1.0
Se	µg/L	<2	<2	<2	<2.00	<2	<2	<2	<2	<2	<2	<1.0	<1.0
Sr	µg/L	<2	<2	<2	<2.00	<2	<2	<2	<2	<2	<2	<5.0	<5.0
Mo	µg/L	<2	<2	<2	<2.00	<2	<2	<2	<2	<2	<2	<1.0	<1.0
Ag	µg/L	<2	<2	<2	<2.00	<2	<2	<2	<2	<2	<2	<0.5	<0.5
Cd	µg/L	<2	<2	<2	<2.00	<2	<2	<2	<2	<2	<2	<1.0	<1.0
Sn	µg/L	<2	<2	<2	<2.00	<2	<2	<2	<2	<2	<2	<1.0	<1.0
Sb	µg/L	<2	<2	<2	<2.00	<2	<2	<2	<2	<2	<2	<1.0	<1.0
Ba	µg/L	<2	<2	<2	<2.00	<2	<2	<2	<2	<2	<2	<1.0	<1.0
Tl	µg/L	<2	<2	<2	<2.00	<2	<2	<2	<2	<2	<2	<1.0	<1.0
Pb	µg/L	<2	<2	<2	<2.00	<2	<2	<2	<2	<2	<2	<1.0	<1.0
Si	µg/L	20. 8	16	24.7	24.65	18.4	28.1	45.5 3	39.3	75	59.8	24.1	24.2
SiO ₂ (calc)	mg/ L	0.0 44	0.03 4	0.053	0.053	0.03 9	0.06	0.09 7	0.084	0.160	0.12 8	0.052	0.052

Note: Gray cells indicate results below detection limit.

Table A.13. Metals: 05/10-03/11 UF-Train 1-Concentrate

Element	Unit	5/3/10	6/7/10	6/28/10	9/13/10	10/4/10	2/7/11	3/7/11
Be	µg/L	<2.0	<2.00	N/A	<2.00	<2	<2	<2
B	µg/L	618	484	N/A	517	492	594	412
Na	mg/L	453	420	N/A	383	402	432	365
Mg	mg/L	99.8	96.7	N/A	88.3	84.4	98.6	84.4
Al	mg/L	0.12	0.18	N/A	0.31	0.25	0.13	0.23
K	mg/L	42.1	47	N/A	38.7	38.2	42.2	42.5
Ca	mg/L	230	216	N/A	209	214	219	186
Ti	µg/L	2.2	2	N/A	<2.00	<2	<2	2.7
V	µg/L	<2.0	2.1	N/A	<2.00	<2	<2	<2
Cr	µg/L	6.4	14.5	N/A	<2.00	<2	<2	<2
Mn	µg/L	66.4	67.4	N/A	52.7	43.8	58.1	185
Fe	mg/L	0.13	0.13	N/A	<0.10	<0.1	<0.1	0.14
Co	µg/L	<2.0	<2.00	N/A	<2.00	<2	<2	<2
Ni	µg/L	6.9	12	N/A	3.2	2.6	3.8	4.1
Cu	µg/L	7.8	<2.00	N/A	<2.00	2	5	3.8
Zn	µg/L	60.8	44.6	N/A	58.8	54.1	63.3	127
As	µg/L	2.1	2.2	N/A	2.1	<2	2.0	2.1
Se	µg/L	4.2	2.9	N/A	3	2.5	3.5	3.9
Sr	µg/L	3480	3150	N/A	3100	3060	3380	2560
Mo	µg/L	25.8	34.9	N/A	27.3	24.3	18.6	20.5
Ag	µg/L	<2.0	<2.00	N/A	<2.00	<2	<2	<2
Cd	µg/L	<2.0	<2.00	N/A	<2.00	<2	<2	<2
Sn	µg/L	<2.0	<2.00	N/A	<2.00	<2	<2	<2
Sb	µg/L	<2.0	<2.00	N/A	<2.00	<2	<2	<2
Ba	µg/L	134	146	N/A	143	131	93.2	125
Tl	µg/L	<2.0	<2.00	N/A	<2.00	<2	<2	<2
Pb	µg/L	<2.0	<2.00	N/A	<2.00	<2	<2	<2
Si	µg/L	12,050	14,920	N/A	11,730	10,780	12,130	9572
SiO ₂	mg/L	25.78	31.92	N/A	25.09	23.06	25.95	20.48

Note: Gray cells indicate results below detection limit.

Table A.14. Metals: 08-12/2011 UF-Train 1-Concentrate

Element	Unit	:							
		8/8/11	9/6/11	9/19/11	10/11/11	10/17/11	11/14/11	12/12/11	12/27/11
Be	µg/L	<2	<2	N/A	<2	<2	N/A	<2.0	<2.0
B	µg/L	448	403	N/A	431	452	462	549	463
Na	mg/L	380	391	370	389	391	403	425	410
Mg	mg/L	93.3	92.1	90	90.5	90.6	86.8	99.6	91.8
Al	mg/L	<0.1	<0.1	N/A	<0.1	<0.1	<0.1	<0.1	<0.1
K	mg/L	39.3	36.8	40.2	39.2	39.2	38.9	39.9	41.1
Ca	mg/L	216	216	206	221	216	213	234	216
Ti	µg/L	2	2.1	N/A	<2	<2	2.9	<2.0	<2.0
V	µg/L	<2	<2	N/A	<2	<2	<2	<2.0	<2.0
Cr	µg/L	<2	<2	N/A	<2	<2	<2	<2.0	<2.0
Mn	µg/L	101	120	N/A	150	110	208	147	138
Fe	mg/L	<0.1	<0.1	N/A	0.13	<0.1	<0.1	<0.1	0.11
Co	µg/L	<2	<2	N/A	<2	<1	<1	<1.0	<1.0
Ni	µg/L	3.9	3.6	N/A	5.9	3.7	3.9	4.3	5.2
Cu	µg/L	2.2	2	N/A	2.5	2.9	1.7	3.3	3
Zn	µg/L	49.8	47.2	N/A	61.1	51.9	49.9	47.9	42.2
As	µg/L	2.5	<2	N/A	<2	1.2	1.1	1.1	1.2
Se	µg/L	3	3	N/A	3.1	2.8	3.1	3.2	3.4
Sr	µg/L	3040	3070	3000	2890	2860	2890	3280	2900
Mo	µg/L	27.2	23.9	N/A	24.1	23.5	15.9	18.9	12.4
Ag	µg/L	<2	<2	N/A	<2	<0.5	<0.5	<0.5	<0.5
Cd	µg/L	<2	<2	N/A	<2	<1	<1	<1.0	<1.0
Sn	µg/L	<2	<2	N/A	<2	<1	<1	<1.0	<1.0
Sb	µg/L	<2	<2	N/A	<2	<1	<1	<1.0	<1.0
Ba	µg/L	87	101	89.9	85	81.4	84.2	94.6	81.6
Tl	µg/L	<2	<2	N/A	<2	<1	<1	<1.0	<1.0
Pb	µg/L	<2	<2	N/A	<2	<1	<1	<1.0	<1.0
Si	µg/L	12,800	13,500	11,800	12,100	11,800	11,500	12,600	12,100
SiO ₂	mg/L	27.38	28.88	25.24	25.89	25.24	24.60	26.96	25.89

Note: Gray cells indicate results below detection limit.

Table A.15. Metals: 05/10-03/11 UF-Train 1-Feed

Element	Unit							
		5/3/10	6/7/10	6/28/10	9/13/10	10/4/10	2/7/11	3/7/11
Be	µg/L	<2.0	<2.00	<2.00	<2.00	<2	<2	<2
B	µg/L	374	344	390	390	376	398	282
Na	mg/L	188	190	200	180	190	194	154
Mg	mg/L	40.4	50	48.2	41.3	38.9	47	38
Al	mg/L	<0.10	<0.10	0.14	0.15	0.12	<0.1	<0.1
K	mg/L	18.1	32.2	20.4	18.4	17.9	19.5	17.4
Ca	mg/L	98.3	104	105	97.5	99.8	100	76.7
Ti	µg/L	<2.0	<2.00	<2.00	<2.00	<2	<2	<2
V	µg/L	<2.0	<2.00	<2.00	<2.00	<2	<2	<2
Cr	µg/L	4.4	10	<2.00	<2.00	<2	<2	<2
Mn	µg/L	30.2	30.8	27.3	25.1	20.2	29.7	24.4
Fe	mg/L	<0.10	<0.10	<0.10	<0.10	<0.1	<0.1	<0.1
Co	µg/L	<2.0	<2.00	<2.00	<2.00	<2	<2	<2
Ni	µg/L	3.8	7.7	<2.00	<2.00	<2	<2	<2
Cu	µg/L	2.2	<2.00	<2.00	<2.00	<2	3.7	<2
Zn	µg/L	27.7	21.5	23.2	30	26.2	30.5	30.8
As	µg/L	<2.0	<2.00	<2.00	<2.00	<2	<2	<2
Se	µg/L	<2.0	<2.00	<2.00	<2.00	<2	<2	<2
Sr	µg/L	1490	1510	1550	1460	1330	1580	1170
Mo	µg/L	12.0	15.6	15.7	12.6	11.1	8.4	9.6
Ag	µg/L	<2.0	<2.00	<2.00	<2.00	<2	<2	<2
Cd	µg/L	<2.0	<2.00	<2.00	<2.00	<2	<2	<2
Sn	µg/L	<2.0	<2.00	<2.00	<2.00	<2	<2	<2
Sb	µg/L	<2.0	<2.00	<2.00	<2.00	<2	<2	<2
Ba	µg/L	60.4	66.3	69.5	65.6	59	42.8	55
Tl	µg/L	<2.0	<2.00	<2.00	<2.00	<2	<2	<2
Pb	µg/L	<2.0	<2.00	<2.00	<2.00	<2	<2	<2
Si	µg/L	5319	NA	6725	6065	4829	5997	3976
SiO ₂	mg/L	11.38	NA	14.39	12.98	10.33	12.83	8.51

Note: Gray cells indicate results below detection limit.

Table A.16. Metals: 08-12/2011 UF-Train 1-Feed

Element	Unit								
		8/8/11	9/6/11	9/19/11	10/11/11	10/17/11	11/14/11	12/12/11	12/27/11
Be	µg/L	<2	<2	<2	<2	<2	<2	<2.0	<2.0
B	µg/L	330	351	160	349	338	357	405	339
Na	mg/L	156	172	178	167	188	190	204	199
Mg	mg/L	39.1	38.2	20.8	38.9	40	39	44.2	NA
Al	mg/L	<0.1	<0.1	<0.1	<0.1	<0.1	<0.1	<0.1	<0.1
K	mg/L	19	17.6	9.6	18.5	19	18.4	19.4	19.8
Ca	mg/L	86.7	94.3	48.6	92	100	98.3	110	102
Ti	µg/L	<2	<2	<2	<2	<2	<2	<2.0	<2.0
V	µg/L	<2	<2	<2	<2	<2	<2	<2.0	<2.0
Cr	µg/L	<2	<2	<2	<2	7.2	<2	<2.0	<2.0
Mn	µg/L	47.1	53.3	61.5	70.8	49.9	93.6	69.4	66.5
Fe	mg/L	0.35	0.13	<0.1	<0.1	<0.1	<0.1	<0.1	<0.1
Co	µg/L	<2	<2	<2	<2	<1	<1	<1.0	<1.0
Ni	µg/L	2.4	<2	3.0	2.8	4.2	1.7	1.8	2.5
Cu	µg/L	<2	<2	<2	<2	1.7	<1	1.7	1.6
Zn	µg/L	26.3	20.4	21.2	25.7	25	24	24	22.5
As	µg/L	<2	<2	<2	<2	<1	<1	<1.0	<1.0
Se	µg/L	<2	<2	<2	<2	1.4	1.4	1.6	1.5
Sr	µg/L	1330	1380	647	1400	1360	1330	1550	1420
Mo	µg/L	11.7	10.7	9	11.2	12.1	7.1	8.9	5.8
Ag	µg/L	<2	<2	<2	<2	<0.5	<0.5	<0.5	<0.5
Cd	µg/L	<2	<2	<2	<2	<1	<1	<1.0	<1.0
Sn	µg/L	<2	<2	<2	<2	<1	<1	<1.0	<1.0
Sb	µg/L	<2	<2	<2	<2	<1	<1	<1.0	<1.0
Ba	µg/L	38	44.4	39.6	39.1	38.4	38.7	45	38.7
Tl	µg/L	<2	<2	<2	<2	<1	<1	<1.0	<1.0
Pb	µg/L	<2	<2	<2	<2	<1	<1	<1.0	<1.0
Si	µg/L	6080	6120	5860	6570	5380	5060	5990	5740
SiO ₂	mg/L	13.01	13.09	12.54	14.06	11.51	10.83	12.81	12.28

Note: Gray cells indicate results below detection limit.

Table A.17. Metals: 05/10-03/11 UF-Train 1-Permeate

Element	Unit							
		5/3/10	6/7/10	6/28/10	9/13/10	10/4/10	2/7/11	3/7/11
Be	µg/L	<2.0	<2.00	<2.00	<2.00	<2	<2	<2
B	µg/L	243	486	248	255	267	259	253
Na	mg/L	NA	NA	5.5	5.9	5.8	4.6	6.8
Mg	mg/L	NA	NA	0.1	<0.10	<0.1	<0.1	<0.1
Al	mg/L	<0.10	<0.10	<0.10	<0.10	<0.1	<0.1	<0.1
K	mg/L	NA	NA	0.48	0.52	0.48	0.37	0.64
Ca	mg/L	NA	NA	0.22	<0.10	<0.1	0.54	<0.1
Ti	µg/L	<2.0	<2.00	<2.00	<2.00	<2	<2	<2
V	µg/L	<2.0	<2.00	<2.00	<2.00	<2	<2	<2
Cr	µg/L	3.0	5.4	<2.00	<2.00	<2	<2	<2
Mn	µg/L	<2.0	<2.00	<2.00	<2.00	<2	<2	<2
Fe	mg/L	<0.10	<0.10	<0.10	<0.10	<0.1	<0.1	<0.1
Co	µg/L	<2.0	<2.00	<2.00	<2.00	<2	<2	<2
Ni	µg/L	<2.0	3.3	<2.00	<2.00	<2	<2	<2
Cu	µg/L	<2.0	<2.00	<2.00	<2.00	<2	<2	<2
Zn	µg/L	<2.0	<2.00	<2.00	<2.00	<2	<2	<2
As	µg/L	<2.0	<2.00	<2.00	<2.00	<2	<2	<2
Se	µg/L	<2.0	<2.00	<2.00	<2.00	<2	<2	<2
Sr	µg/L	NA	NA	3.3	<2.00	<2	<2	<2
Mo	µg/L	<2.0	<2.00	<2.00	<2.00	<2	<2	<2
Ag	µg/L	<2.0	<2.00	<2.00	<2.00	<2	<2	<2
Cd	µg/L	<2.0	<2.00	<2.00	<2.00	<2	<2	<2
Sn	µg/L	<2.0	<2.00	<2.00	<2.00	<2	<2	<2
Sb	µg/L	<2.0	<2.00	<2.00	<2.00	<2	<2	<2
Ba	µg/L	<2.0	<2.00	<2.00	<2.00	<2	<2	<2
Tl	µg/L	<2.0	<2.00	<2.00	<2.00	<2	<2	<2
Pb	µg/L	<2.0	<2.00	<2.00	<2.00	<2	<2	<2
Si	µg/L	90.99	139.9	178.7	189.12	171.9	140	222
SiO ₂	mg/L	0.19	0.30	0.38	0.40	0.37	0.30	0.47

Note: Gray cells indicate results below detection limit.

Table A.18. Metals: 08-12/2011 UF-Train 1-Permeate

Element	Unit	:							
		8/8/11	9/6/11	9/19/11	10/11/11	10/17/11	11/14/11	12/12/11	12/27/11
Be	µg/L	<2	<2	<2	<2	<2	<2	<2.0	<2.0
B	µg/L	225	240	263	252	244	261	270	230
Na	mg/L	5.1	5.5	17.1	7.6	7	6.9	5.8	5.8
Mg	mg/L	<0.1	<0.1	0.13	<0.1	<0.5	<0.5	<0.5	<0.5
Al	mg/L	<0.1	<0.1	<0.1	<0.1	<0.1	<0.1	<0.1	<0.1
K	mg/L	0.49	0.51	1.9	0.73	0.67	0.58	0.55	0.55
Ca	mg/L	<0.1	<0.1	0.62	<0.1	<0.5	<0.5	<0.5	<0.5
Ti	µg/L	<2	<2	<2	<2	<2	<2	<2.0	<2.0
V	µg/L	<2	<2	<2	<2	<2	<2	<2.0	<2.0
Cr	µg/L	<2	<2	<2	<2	<2	<2	<2.0	<2.0
Mn	µg/L	<2	<2	<2	<2	<2	<2	<2.0	<2.0
Fe	mg/L	<0.1	<0.1	<0.1	<0.1	<0.1	<0.1	<0.1	<0.1
Co	µg/L	<2	<2	<2	<2	<1	<1	<1.0	<1.0
Ni	µg/L	<2	<2	<2	<2	<1	<1	<1.0	<1.0
Cu	µg/L	<2	<2	<2	<2	<1	<1	<1.0	<1.0
Zn	µg/L	<2	<2	<2	<2	<2	<2	<2.0	<2.0
As	µg/L	<2	<2	<2	<2	<1	<1	<1.0	<1.0
Se	µg/L	<2	<2	<2	<2	<1	<1	<1.0	<1.0
Sr	µg/L	<2	<2	8	<2	<5	<5	<5.0	<5.0
Mo	µg/L	<2	<2	<2	<2	<1	<1	<1.0	<1.0
Ag	µg/L	<2	<2	<2	<2	<0.5	<0.5	<0.5	<0.5
Cd	µg/L	<2	<2	<2	<2	<1	<1	<1.0	<1.0
Sn	µg/L	<2	<2	<2	<2	<1	<1	<1.0	<1.0
Sb	µg/L	<2	<2	<2	<2	<1	<1	<1.0	<1.0
Ba	µg/L	<2	<2	<2	<2	<1	<1	<1.0	<1.0
Tl	µg/L	<2	<2	<2	<2	<1	<1	<1.0	<1.0
Pb	µg/L	<2	<2	<2	<2	<1	<1	<1.0	<1.0
Si	µg/L	130	170	425	185	198	200	139	155
SiO ₂	mg/L	0.28	0.36	0.91	0.40	0.42	0.43	0.30	0.33

Note: Gray cells indicate results below detection limit.

Table A.19. Metals: 05/10-03/11 UF-Train 2-Concentrate

Element	Unit							
		5/3/10	6/7/10	6/28/10	9/13/10	10/4/10	2/7/11	3/7/11
Be	µg/L	<2.0	<2.00	N/A	<2.00	<2	<2	<2
B	µg/L	644	1160	N/A	497	496	634	435
Na	mg/L	448	382	N/A	402	411	431	341
Mg	mg/L	97.2	96	N/A	90	84.6	101	80.2
Al	mg/L	0.13	0.24	N/A	0.35	0.25	0.15	0.16
K	mg/L	40.9	52.2	N/A	39.4	36.9	42.4	39.3
Ca	mg/L	225	218	N/A	213	215	221	174
Ti	µg/L	2.1	2	N/A	<2.00	<2	<2	2.5
V	µg/L	2.0	<2.00	N/A	2.0	<2	<2	2
Cr	µg/L	3.7	5.8	N/A	<2.00	<2	<2	<2
Mn	µg/L	72.5	65.6	N/A	52.6	52.5	73.9	48.5
Fe	mg/L	0.12	0.16	N/A	<0.10	<0.1	0.1	0.12
Co	µg/L	<2.0	<2.00	N/A	<2.00	<2	<2	<2
Ni	µg/L	5.3	6.6	N/A	3.6	2.8	3.8	4
Cu	µg/L	6.2	<2.00	N/A	<2.00	<2	3.9	3.5
Zn	µg/L	49.1	44	N/A	59.8	52	58.8	68.5
As	µg/L	2.0	2.2	N/A	2.3	<2	2.1	2.3
Se	µg/L	3.9	3.3	N/A	3	2.7	3.6	3.2
Sr	µg/L	3380	3290	N/A	3120	3040	3720	2610
Mo	µg/L	25.9	34.7	N/A	28.5	23.4	19.1	20.4
Ag	µg/L	<2.0	<2.00	N/A	<2.00	<2	<2	<2
Cd	µg/L	<2.0	<2.00	N/A	<2.00	<2	<2	<2
Sn	µg/L	<2.0	<2.00	N/A	<2.00	<2	<2	<2
Sb	µg/L	<2.0	<2.00	N/A	<2.00	<2	<2	<2
Ba	µg/L	135	149	N/A	150	127	94.3	118
Tl	µg/L	<2.0	<2.00	N/A	<2.00	<2	<2	<2
Pb	µg/L	<2.0	<2.00	N/A	<2.00	<2	<2	<2
Si	µg/L	11,980	14,750	N/A	12,830	10,850	11,010	10,580
SiO ₂	mg/L	25.63	31.56	N/A	27.45	23.21	23.55	22.63

Note: Gray cells indicate results below detection limit.

Table A.20. Metals: 08-12/2011 UF-Train 2-Concentrate

Element	Unit								
		8/8/11	9/6/11	9/19/11	10/11/11	10/17/11	11/14/11	12/12/11	12/27/11
Be	µg/L	<2	<2	<2	<2	<2	<2	<2.0	<2.0
B	µg/L	483	445	343	438	435	475	539	458
Na	mg/L	378	359	388	374	390	381	421	400
Mg	mg/L	91.4	83.1	95	91.7	90.8	83.1	98.1	91
Al	mg/L	<0.1	<0.1	<0.1	<0.1	<0.1	<0.1	<0.1	<0.1
K	mg/L	39.3	35.8	39.4	41.6	42.2	38.5	39.9	41.4
Ca	mg/L	215	195	214	223	217	202	231	215
Ti	µg/L	2	2.2	2	2.4	<2	2.4	<2.0	<2.0
V	µg/L	<2	<2	<2	<2	<2	<2	<2.0	<2.0
Cr	µg/L	<2	<2	<2	3.7	<2	<2	<2.0	<2.0
Mn	µg/L	92.8	114	138	178	110	194	140	139
Fe	mg/L	<0.1	0.1	<0.1	0.12	0.1	0.11	0.16	0.17
Co	µg/L	<2	<2	<2	<2	<1	<1	<1.0	<1.0
Ni	µg/L	3.6	3.5	5.2	8.0	3.6	3.8	4.2	5.4
Cu	µg/L	<2	2	2.4	2.7	14.5	1.7	2.5	3.2
Zn	µg/L	48.4	40.4	45.9	53	52.8	51.3	47.6	43.3
As	µg/L	2.2	<2	<2	<2	1.2	1.1	1.1	1.3
Se	µg/L	3	2.6	2.9	3	2.6	3	3.2	3.3
Sr	µg/L	3060	2860	3250	3140	2840	2810	3260	2880
Mo	µg/L	25.6	23.4	21	20.6	23.7	15.7	18.7	12.4
Ag	µg/L	<2	<2	<2	<2	<0.5	<0.5	<0.5	<0.5
Cd	µg/L	<2	<2	<2	<2	<1	<1	<1.0	<1.0
Sn	µg/L	<2	<2	<2	<2	<1	<1	<1.0	<1.0
Sb	µg/L	<2	<2	<2	<2	<1	<1	<1.0	<1.0
Ba	µg/L	80.7	97.3	91.2	80.7	84.6	85.9	94.2	83
Tl	µg/L	<2	<2	<2	<2	<1	<1	<1.0	<1.0
Pb	µg/L	<2	<2	<2	<2	<1	<1	<1.0	<1.0
Si	µg/L	13,800	12,800	13,500	12,500	11,600	10,800	12,400	11,800
SiO ₂	mg/L	29.52	27.38	28.88	26.74	24.82	23.10	26.53	25.24

Note: Gray cells indicate results below detection limit.

Table A.21. Metals: 05/10-03/11 UF-Train 2-Feed

Element	Unit							
		5/3/10	6/7/10	6/28/10	9/13/10	10/4/10	2/7/11	3/7/11
Be	µg/L	<2.0	<2.00	<2.00	<2.00	<2	<2	<2
B	µg/L	387	764	394	385	349	414	278
Na	mg/L	186	178	195	185	180	197	151
Mg	mg/L	40.4	46.1	47.4	42	37.8	48.2	37.6
Al	mg/L	<0.10	0.1	0.16	0.16	0.11	<0.1	<0.1
K	mg/L	17.9	24.2	20	18.7	17	19.6	17.2
Ca	mg/L	97.6	95.8	102	98.2	95.5	102	75.6
Ti	µg/L	<2.0	<2.00	<2.00	<2.00	<2	<2	<2
V	µg/L	<2.0	<2.00	<2.00	<2.00	<2	<2	<2
Cr	µg/L	6.4	6.2	<2.00	<2.00	<2	<2	<2
Mn	µg/L	33.1	29.2	30.2	24.6	23.4	33.9	21
Fe	mg/L	<0.10	<0.10	<0.10	<0.10	<0.1	<0.1	<0.1
Co	µg/L	<2.0	<2.00	<2.00	<2.00	<2	<2	<2
Ni	µg/L	5.0	5.2	2	2.1	<2	<2	<2
Cu	µg/L	2.4	<2.00	<2.00	<2.00	<2	2.5	<2
Zn	µg/L	22.8	20.7	22.5	29.6	24.2	27.8	30.4
As	µg/L	<2.0	<2.00	<2.00	<2.00	<2	<2	<2
Se	µg/L	<2.0	<2.00	<2.00	<2.00	<2	<2	<2
Sr	µg/L	1510	1540	1520	1450	1220	1610	1160
Mo	µg/L	12.2	15.4	15.3	13.1	10.4	8.6	9.3
Ag	µg/L	<2.0	<2.00	<2.00	<2.00	<2	<2	<2
Cd	µg/L	<2.0	<2.00	<2.00	<2.00	<2	<2	<2
Sn	µg/L	<2.0	<2.00	<2.00	<2.00	<2	<2	<2
Sb	µg/L	<2.0	<2.00	<2.00	<2.00	<2	<2	<2
Ba	µg/L	59.4	65	68.5	66.3	56.3	43.2	53.7
Tl	µg/L	<2.0	<2.00	<2.00	<2.00	<2	<2	<2
Pb	µg/L	<2.0	<2.00	<2.00	<2.00	<2	<2	<2
Si	µg/L	5550	6426	6783	5566	4798	5881	3926
SiO ₂	mg/L	11.87	13.75	14.51	11.91	10.26	12.58	8.40

Note: Gray cells indicate results below detection limit.

Table A.22. Metals: 08-12/2011 UF-Train 2-Feed

Element	Unit								
		8/8/11	9/6/11	9/19/11	10/11/11	10/17/11	11/14/11	12/12/11	12/27/11
Be	µg/L	<2	<2	<2	<2	<2	<2	<2.0	<2.0
B	µg/L	331	348	310	362	329	370	396	339
Na	mg/L	172	211	176	183	179	189	204	200
Mg	mg/L	38.3	37.7	38.2	N/A	42.5	38.1	47.8	N/A
Al	mg/L	<0.1	<0.1	<0.1	<0.1	<0.1	<0.1	<0.1	0.21
K	mg/L	18.3	17	17.3	18.3	18.4	17.9	19.2	19.9
Ca	mg/L	94.6	80.2	N/A	106	99.3	97.2	108	108
Ti	µg/L	<2	<2	<2	<2	<2	<2	<2.0	<2.0
V	µg/L	<2	<2	<2	<2	<2	<2	<2.0	<2.0
Cr	µg/L	<2	<2	<2	<2	<2	<2	<2.0	<2.0
Mn	µg/L	45	53.5	69.2	76.1	49.3	88.3	66.6	7.8
Fe	mg/L	<0.1	<0.1	<0.1	<0.1	<0.1	<0.1	<0.1	<0.1
Co	µg/L	<2	<2	<2	<2	<1	<1	<1.0	<1.0
Ni	µg/L	2.4	<2	2.8	2.8	1.3	1.9	1.5	1.9
Cu	µg/L	<2	<2	<2	<2	1.4	<1	1.4	1.3
Zn	µg/L	23.2	19.9	23.8	23.3	25.4	24.2	23.7	26.9
As	µg/L	<2	<2	<2	<2	<1	<1	<1.0	<1.0
Se	µg/L	<2	<2	<2	<2	1.3	1.3	1.5	1.7
Sr	µg/L	1370	1380	7310	1430	1300	1320	1540	1510
Mo	µg/L	12.0	10.8	9.1	10.2	11.5	7.3	8.9	9.4
Ag	µg/L	<2	<2	<2	<2	<0.5	<0.5	<0.5	<0.5
Cd	µg/L	<2	<2	<2	<2	<1	<1	<1.0	<1.0
Sn	µg/L	<2	<2	<2	<2	<1	<1	<1.0	<1.0
Sb	µg/L	<2	<2	<2	<2	<1	<1	<1.0	<1.0
Ba	µg/L	36.8	45.1	40.2	39.9	41.2	39.2	44.7	46.8
Tl	µg/L	<2	<2	<2	<2	<1	<1	<1.0	<1.0
Pb	µg/L	<2	<2	<2	<2	<1	<1	<1.0	<1.0
Si	µg/L	6480	6080	5910	5820	5300	5240	5940	5760
SiO ₂	mg/L	13.86	13.01	12.64	12.45	11.34	11.21	12.71	12.32

Note: Gray cells indicate results below detection limit.

Table A.23. Metals: 05/10-03/11 UF-Train 2-Permeate

Element	Unit	:						
		5/3/10	6/7/10	6/28/10	9/13/10	10/4/10	2/7/11	3/7/11
Be	µg/L	<2.0	<2.00	<2.00	<2.00	<2	<2	<2
B	µg/L	179	429	228	264	277	245	269
Na	mg/L	3.4	NA	5.8	7	6.5	4.2	6.8
Mg	mg/L	<0.10	NA	0.22	<0.10	<0.1	<0.1	<0.1
Al	mg/L	<0.10	<0.10	<0.10	<0.10	<0.1	<0.1	<0.1
K	mg/L	0.31	NA	0.53	0.63	0.54	0.34	0.65
Ca	mg/L	0.15	NA	0.48	<0.10	<0.1	0.52	0.14
Ti	µg/L	<2.0	<2.00	<2.00	<2.00	<2	<2	<2
V	µg/L	<2.0	<2.00	<2.00	<2.00	<2	<2	<2
Cr	µg/L	6.2	4.9	<2.00	<2.00	<2	<2	<2
Mn	µg/L	<2.0	<2.00	<2.00	<2.00	<2	<2	<2
Fe	mg/L	<0.10	<0.10	<0.10	<0.10	<0.1	<0.1	<0.1
Co	µg/L	<2.0	<2.00	<2.00	<2.00	<2	<2	<2
Ni	µg/L	3.6	3	<2.00	<2.00	<2	<2	<2
Cu	µg/L	<2.0	<2.00	<2.00	<2.00	<2	<2	<2
Zn	µg/L	<2.0	<2.00	<2.00	<2.00	<2	3.5	<2
As	µg/L	<2.0	<2.00	<2.00	<2.00	<2	<2	<2
Se	µg/L	<2.0	<2.00	<2.00	<2.00	<2	<2	<2
Sr	µg/L	<2.0	NA	4.1	<2.00	<2	<2	2.3
Mo	µg/L	<2.0	<2.00	<2.00	<2.00	<2	<2	<2
Ag	µg/L	<2.0	<2.00	<2.00	<2.00	<2	<2	<2
Cd	µg/L	<2.0	<2.00	<2.00	<2.00	<2	<2	<2
Sn	µg/L	<2.0	<2.00	<2.00	<2.00	<2	<2	<2
Sb	µg/L	<2.0	<2.00	<2.00	<2.00	<2	<2	<2
Ba	µg/L	<2.0	<2.00	<2.00	<2.00	<2	<2	<2
Tl	µg/L	<2.0	<2.00	<2.00	<2.00	<2	<2	<2
Pb	µg/L	<2.0	<2.00	<2.00	<2.00	<2	<2	<2
Si	µg/L	55.46	108.6	203.1	285.08	240.2	137	223
SiO ₂	mg/L	0.12	0.23	0.43	0.61	0.51	0.29	0.48

Note: Gray cells indicate results below detection limit.

Table A.24. Metals: 08-12/2011 UF-Train 2-Permeate

Element	Unit								
		8/8/11	9/6/11	9/19/11	10/11/11	10/17/11	11/14/11	12/12/11	12/27/11
Be	µg/L	<2	<2	<2	<2	<2	<2	<2	<2
B	µg/L	182	236	246	254	244	261	261	234
Na	mg/L	3.2	5.1	6.1	7.2	7	6.9	10.4	6
Mg	mg/L	<0.1	<0.1	<0.1	<0.1	<0.5	<0.5	<0.5	<0.5
Al	mg/L	<0.1	<0.1	<0.1	<0.1	<0.1	<0.1	<0.1	<0.1
K	mg/L	0.31	0.49	0.59	0.71	0.67	0.58	0.55	0.56
Ca	mg/L	<0.1	<0.1	<0.1	0.13	<0.5	<0.5	<0.5	<0.5
Ti	µg/L	<2	<2	<2	<2	<2	<2	<2.0	<2.0
V	µg/L	<2	<2	<2	<2	<2	<2	<2.0	<2.0
Cr	µg/L	<2	<2	<2	<2	<2	<2	<2.0	<2.0
Mn	µg/L	<2	<2	<2	<2	<2	<2	<2.0	<2.0
Fe	mg/L	<0.1	<0.1	<0.1	<0.1	<0.1	<0.1	<0.1	<0.1
Co	µg/L	<2	<2	<2	<2	<1	<1	<1.0	<1.0
Ni	µg/L	<2	<2	<2	<2	<1	<1	<1.0	<1.0
Cu	µg/L	<2	<2	<2	<2	<1	<1	<1.0	<1.0
Zn	µg/L	<2	<2	<2	<2	<2	<2	<2.0	<2.0
As	µg/L	<2	<2	<2	<2	<1	<1	<1.0	<1.0
Se	µg/L	<2	<2	<2	<2	<1	<1	<1.0	<1.0
Sr	µg/L	<2	<2	<2	<2	<5	<5	<5.0	<5.0
Mo	µg/L	<2	<2	<2	<2	<1	<1	<1.0	<1.0
Ag	µg/L	<2	<2	<2	<2	<0.5	<0.5	<0.5	<0.5
Cd	µg/L	<2	<2	<2	<2	<1	<1	<1.0	<1.0
Sn	µg/L	<2	<2	<2	<2	<1	<1	<1.0	<1.0
Sb	µg/L	<2	<2	<2	<2	<1	<1	<1.0	<1.0
Ba	µg/L	<2	<2	<2	<2	<1	<1	<1.0	<1.0
Tl	µg/L	<2	<2	<2	<2	<1	<1	<1.0	<1.0
Pb	µg/L	<2	<2	<2	<2	<1	<1	<1.0	<1.0
Si	µg/L	57.3	171	273	255	198	200	184	155
SiO ₂	mg/L	0.12	0.37	0.58	0.55	0.42	0.43	0.39	0.33

Note: Gray cells indicate results below detection limit.

Table A.25. MBR-Train 1-Concentrate

Date	Alkalinity (mg/L as CaCO ₃)															
		TDS (mg/L)	TSS (mg/L)	OPO ₄ - P (mg/L)	TPO ₄ - P (mg/L)	NO ₂ - N (mg/L)	NO ₃ - N (mg/L)	Ammonia (mg/L)	TKN (mg/L)	Chlorid e (mg/L)	Fluorid e (mg/L)	Sulfat e (mg/L)	TN (mg/L)	TOC (mg/L)	UV ₂₅₄ (1/cm)	UV ₂₈₀ (1/cm)
5/3/10	189	2064	<3	3.10	4.01	<0.05	37.45	2.53	5.71	446	1.93	613	N/A	N/A	N/A	N/A
5/24/10	312	2438	<3	0.08	0.81	3.02	6.03	22.56	24.45	716	2.10	635	N/A	N/A	N/A	N/A
6/7/10	260	1690	<3	<0.05	0.40	1.46	9.52	3.32	5.82	391	1.69	496	N/A	N/A	N/A	N/A
7/12/10	N/A	N/A	N/A	N/A	N/A	N/A	N/A	N/A	N/A	N/A	N/A	N/A	N/A	N/A	N/A	N/A
7/26/10	N/A	N/A	N/A	N/A	N/A	N/A	N/A	N/A	N/A	N/A	N/A	N/A	N/A	N/A	N/A	N/A
8/16/10	296	1719	<3	0.11	0.36	0.83	10.62	12.45	13.67	375	1.93	516	13	23	0.196	0.136
8/23/10	167	1979	<3	4.10	4.40	0.06	27.64	2.86	4.80	454	2.03	544	16	N/A	0.233	0.162
9/27/10	259	1716	<3	<0.05	0.33	0.32	13.40	5.05	6.19	397	1.82	470	11	18	0.175	0.118
10/4/10	228	1944	<3	0.08	0.43	0.08	13.37	4.22	4.94	472	3.19	553	12	16	0.166	0.106
2/28/11	172	2140	<3	0.49	0.75	<N/A	17.94	4.88	6.3	575	2.04	601	24	14	0.201	0.137
3/7/11	173	2092	<3	0.15	0.43	<0.05	20.41	3.78	5	513	1.97	622	26	13	0.187	0.119
3/21/11	256	1826	<3	0.25	0.39	<0.05	15.86	2.50	3.84	416	2.01	530	20	12	0.175	0.106
4/25/11	183	1838	<3	0.09	0.35	<0.05	17.07	1.85	3.51	411	2.32	590	20	12	0.184	0.116
5/2/11	214	1914	<3	0.16	0.42	<0.05	14.85	2.19	4.03	480	2.44	590	18	12	0.175	0.107
5/23/11	163	1968	5	0.15	0.46	<0.05	14.11	28.81	30.13	543	2.19	625	38	11	0.212	0.146
6/6/11	93	1984	<3	0.18	0.47	<0.05	52.22	5.77	8.79	493	1.75	537	62	14	0.267	0.163
6/20/11	220	1626	<3	<0.05	0.33	<0.05	9.29	3.28	4.58	382	1.73	498	14	9.4	0.142	0.0825
8/15/11	215	1757	<3	0.78	1.25	<0.05	18.59	4.28	5.6	409	1.63	489	23	9.9	0.151	0.102
8/22/11	N/A	1588	<3	0.77	1.21	<0.05	33.17	3.88	6.05	365	1.34	460	37	11	0.19	0.13
9/6/11	265	1480	4	0.84	1.39	<0.05	20.94	4.08	5.02	325	1.33	352	26	8.7	0.113	0.0677
12/12/11	157	1860	<3	1.08	1.65	<0.05	22.06	8.65	10.52	437	1.6	585	29	12	0.158	0.0842
12/27/11	265	1862	<3	0.31	0.84	<0.05	7.54	21.26	21.71	456	1.47	566	30	11	0.141	0.0716

Note: Gray cells indicate results below detection limit.

Table A.26. MBR-Train 1-Feed

Date	Alkalinity (mg/L as CaCO ₃)	TDS (mg/ L)	TSS (mg/ L)	OPO ₄ - P (mg/L)	TPO ₄ - P (mg/L)	NO ₂ -N (mg/L)	NO ₃ -N (mg/L)	Ammonia (mg/L)	TK N (mg /L)	Chloride (mg/L)	Fluoride (mg/L)	Sulfate (mg/L)	TN (mg/ L)	TOC (mg/ L)	UV ₂₅₄ (1/cm)	UV ₂₈₀ (1/cm)
5/3/10	97	1004	<3	1.37	1.84	<0.05	17.57	1.39	2.97	213	0.95	290	19	8.3	0.132	0.080
5/24/10	153	1150	<3	<0.05	0.38	1.30	3.20	9.97	11.7 1	342	0.97	297	15.2	6.6	0.114	0.082
6/7/10	138	847	<3	<0.05	0.19	0.65	5.02	1.89	2.78	198	0.88	245	6.7	5.5	0.103	0.076
7/12/10	168	912	<3	0.14	0.29	0.06	0.42	10.85	10.7 1	231	0.9	262	11	5.5	0.108	0.0681
7/26/10	140	865	<3	<0.05	0.18	2.89	2.18	4.73	5.31	197	1.01	260	9.1	5.4	0.100	0.071
8/16/10	151	830	<3	0.06	0.19	0.33	5.41	6.27	7.74	181	0.95	245	12	5.8	0.099	0.067
8/23/10	87	947	<3	1.95	2.06	<0.05	13.74	1.52	2.91	220	1.02	257	7.7	N/A	0.117	0.080
9/27/10	132	813	<3	<0.05	0.17	0.11	6.57	2.77	3.51	191	0.89	227	9.2	5.4	0.0883	0.0573
10/4/10	116	934	<3	<0.05	0.21	<0.05	6.51	2.33	3.13	229	1.59	267	7.9	6	0.086	0.052
2/28/11	99	1080	<3	0.26	0.39	N/A	9.55	2.66	3.61	299	1.12	301	12	6.5	0.112	0.0681
3/7/11	94	1048	<3	0.08	0.22	<0.05	10.41	2.24	2.89	258	1.04	302	13	6.2	0.0984	0.059
3/21/11	134	956	<3	0.07	0.19	<0.05	8.38	1.60	2.92	215	1.07	270	10.0	6.0	0.0948	0.0534
4/25/11	100	945	<3	0.05	0.17	<0.05	9.05	1.24	1.94	215	1.23	300	10	5.8	0.0971	0.0584
5/2/11	108	990	<3	0.08	0.19	<0.05	7.69	1.40	2.48	243	1.27	296	8.5	5.6	0.0903	0.0525
5/23/11	94	1026	<3	0.08	0.22	<0.05	7.40	19.23	19.0 5	289	1.24	317	23.0	5.5	0.115	0.0761
6/6/11	52	1026	<3	0.1	0.24	<0.05	27.2	3.96	5.33	253	0.97	271	31.0	6.7	0.148	0.0829
6/20/11	123	850	<3	<0.05	0.17	<0.05	4.98	2.06	3.01	200	0.93	251	7	4.6	0.078	0.042
8/15/11	114	903	<3	0.39	0.65	<0.05	9.52	2.35	3.07	205	0.84	242	12	4.6	0.0993	0.0699
8/22/11	NR	869	<3	0.42	0.64	<0.05	18.67	2.26	3.2	197	0.78	247	21.0	6.4	0.114	0.0762
9/6/11	139	771	<3	0.41	0.63	<0.05	11.21	2.43	1.97	169	0.7	184	14.0	4.5	0.0618	0.0341
12/12/11	81	916	<3	0.53	0.75	<0.05	11.18	4.6	5.61	215	0.83	284	16.0	6.0	0.0988	0.045
12/27/11	138	952	<3	0.14	0.42	<0.05	3.96	10.61	12.1 7	232	0.78	283	15.0	5.3	0.0835	0.0363

Note: Gray cells indicate results below detection limit.

Table A.27. MBR-Train 1-Permeate

Date	Alkalinity (mg/L as CaCO ₃)															
		TDS (mg/L)	TSS (mg/L)	OPO ₄ -P (mg/L)	TPO ₄ -P (mg/L)	NO ₂ -N (mg/L)	NO ₃ -N (mg/L)	Ammonia (mg/L)	TKN (mg/L)	Chloride (mg/L)	Fluoride (mg/L)	Sulfate (mg/L)	TN (mg/L)	TOC (mg/L)	UV ₂₅₄ (1/cm)	UV ₂₈₀ (1/cm)
5/3/10	7	13	<3	<0.05	<0.05	<0.05	0.33	0.66	<1.00	<4	<0.05	<4	N/A	N/A	N/A	N/A
5/24/10	8	<10	<3	<0.05	<0.05	<0.05	0.10	0.57	<1.00	<4	<0.05	<4	N/A	N/A	N/A	N/A
6/7/10	N/A	N/A	N/A	N/A	N/A	N/A	N/A	N/A	N/A	N/A	N/A	N/A	N/A	N/A	N/A	N/A
7/12/10	10	<10	<3	<0.05	<0.05	<0.05	<0.05	0.85	<1.00	<4	<0.05	<4	N/A	N/A	N/A	N/A
7/26/10	9	11	<3	<0.05	<0.05	<0.05	0.22	0.43	<1.00	<4	<0.05	<4	<0.20	0.65	0.005	0.002
8/16/10	9	<10	<3	<0.05	<0.05	<0.05	0.14	0.41	<1.00	<4	<0.05	<4	<0.20	0.63	0.011	0.004
8/23/10	7	11	<3	<0.05	<0.05	<0.05	0.37	0.36	<1.00	<4	<0.05	<4	0.26	N/A	0.007	0.003
9/27/10	8	<10	<3	<0.05	<0.05	<N/A	0.16	0.57	<1.00	<0	<0.05	<N/A	<0.20	0.52	0.0107	0.0029
10/4/10	8	10	<3	<0.05	<0.05	<0.05	0.16	0.53	<1.00	<4	0.06	<4	<0.20	0.53	0.011	0.005
2/28/11	7	<10	<3	<0.05	<0.05	<N/A	0.17	0.47	<1.00	<N/A	<0.05	<N/A	0.53	<0.20	0.0093	0.0029
3/7/11	7	11	<3	<0.05	<0.05	<0.05	0.21	0.57	<1.00	<N/A	<0.05	<N/A	0.68	<0.20	0.0117	0.0042
3/21/11	6	<10	<3	<0.05	<0.05	<0.05	0.23	0.60	<1.00	<4	<0.05	<4	0.65	<0.20	0.0119	0.0042
4/25/11	8	10	<3	<0.05	<0.05	<0.05	0.22	0.49	<1.00	<4	<0.05	<4	0.56	<0.20	0.0089	0.0026
5/2/11	7	12	<3	<0.05	<0.05	<0.05	0.21	0.42	<1.00	<4	0.05	<4	0.57	<0.20	0.0107	0.0039
5/23/11	9	10	<3	<0.05	<0.05	<0.05	0.29	0.57	<1.00	<4	0.06	<4	0.83	<0.20	0.008	0.0029
6/6/11	8	13	<3	<0.05	<0.05	0.1	0.87	1.7	2.16	<4	0.08	<4	2.1	<0.20	0.0243	0.0113
6/20/11	8	10	<3	<0.05	<0.05	0.1	0.18	0.72	<1.00	<4	<0.05	<4	0.74	<0.20	0.0088	0.0046
8/15/11	8	15	<3	<0.05	<0.05	<0.05	0.43	0.49	<1.00	<4	<0.05	<4	0.8	<0.20	0.0445	0.0389
8/22/11	N/A	11	<3	<0.05	<0.05	<0.05	1.28	0.47	<1.00	<4	0.07	<4	1.7	0.2	0.0457	0.0384
9/6/11	7	<10	<3	<0.05	<0.05	<0.05	0.51	0.5	<1.00	<4	<0.05	<4	0.9	<0.20	0.0084	0.00253
12/12/11	7	<10	<3	<0.05	<0.05	0.08	0.25	1.27	1.31	<4	<0.05	<4	1	<0.20	0.0289	0.00623
12/27/11	7	14	<3	<0.05	<0.05	0.05	0.11	1.19	1.21	<4	<0.05	<4	0.9	<0.20	0.0326	0.0139

Note: Gray cells indicate results below detection limit.

Table A.28. MBR-Train 2-Concentrate

Date	Alkalinity (mg/L as CaCO ₃)	TDS (mg/L)	TSS (mg/L)	OPO ₄ -P (mg/L)	TPO ₄ -P (mg/L)	NO ₂ -N (mg/L)	NO ₃ -N (mg/L)	Ammonia (mg/L)	TKN (mg/L)	Chloride (mg/L)	Fluoride (mg/L)	Sulfate (mg/L)	TN (mg/L)	TOC (mg/L)	UV ₂₅₄ (1/cm)	UV ₂₈₀ (1/cm)
5/3/10	196	2136	<3	3.35	4.14	0.07	38.99	3.89	6.78	460	1.99	602	N/A	N/A	N/A	N/A
5/24/10	310	2448	<3	0.08	0.65	3.78	5.38	28.11	25.52	727	2.10	641	N/A	N/A	N/A	N/A
6/7/10	261	1776	<3	<0.05	0.41	2.12	9.6	8.28	10.27	427	1.79	532	N/A	N/A	N/A	N/A
7/12/10	N/A	N/A	N/A	N/A	N/A	N/A	N/A	N/A	N/A	N/A	N/A	N/A	N/A	N/A	N/A	N/A
7/26/10	N/A	N/A	N/A	N/A	N/A	N/A	N/A	N/A	N/A	N/A	N/A	N/A	N/A	N/A	N/A	N/A
8/16/10	286	1756	<3	0.10	0.37	1.51	10.11	12.46	12.85	392	1.89	528	23	12	0.217	0.157
8/23/10	171	2011	<3	3.62	4.07	0.89	26.66	3.35	5.20	473	2.08	553	N/A	16	0.277	0.204
9/27/10	245	1754	<3	<0.05	0.35	0.60	13.38	5.24	7.06	419	1.84	490	18	11	0.204	0.142
10/4/10	216	2002	<3	0.07	0.43	0.2	14.05	4.17	5.02	500	3.23	576	17	12	0.204	0.142
2/28/11	147	2210	<3	0.51	0.86	0.31	19.23	4.88	6.43	590	2.15	646	23	14	0.241	0.171
3/7/11	149	2112	<3	0.14	0.43	<0.05	20.97	3.5	5.15	531	2.05	653	26	13	0.223	0.153
3/21/11	259	1848	<3	0.23	0.36	<0.05	16.28	2.07	4.35	426	2.05	542	20	13	0.236	0.155
4/25/11	180	1928	<3	0.09	0.37	<0.05	17.95	2.91	4.42	444	2.45	636	21	12	0.233	0.16
5/2/11	179	2118	<3	0.15	0.39	<0.05	16.97	3.30	5.17	539	2.64	678	20	12	0.228	0.157
5/23/11	197	1998	<3	0.14	0.47	<0.05	13.68	4.30	5.29	491	2.33	625	17	12	0.224	0.154
6/6/11	103	2032	<3	0.18	0.55	<0.05	53.27	2.51	4.68	498	1.8	546	59	14	0.307	0.21
6/20/11	142	1620	<3	<0.05	0.27	<0.05	9.44	3.06	4.74	374	1.73	566	13	9.6	0.205	0.141
8/15/11	210	1840	<3	0.79	1.22	<0.05	19.52	4.1	5.45	429	1.7	511	23	9	0.243	0.18
8/22/11	N/A	1598	<3	0.73	1.19	<0.05	34.14	3.56	5.14	376	1.44	472	38	12	0.296	0.22
9/6/11	178	1596	<3	0.83	1.26	<0.05	22.93	3.84	5.26	347	1.4	469	29	10	0.198	0.14
12/12/11	120	1857	<3	1.07	1.64	<0.05	23.04	9.16	11.16	437	1.71	614	31	13	0.264	0.179
12/27/11	221	1864	<3	0.22	0.65	<0.05	7.25	19.29	20.7	457	1.45	596	30	11	0.233	0.157

Note: Gray cells indicate results below detection limit.

Table A.29. MBR-Train 2-Feed

Date	Alkalinity (mg/L as CaCO ₃)															
		TDS (mg/L)	TSS (mg/L)	OPO ₄ -P (mg/L)	TPO ₄ -P (mg/L)	NO ₂ -N (mg/L)	NO ₃ -N (mg/L)	Ammonia (mg/L)	TKN (mg/L)	Chloride (mg/L)	Fluoride (mg/L)	Sulfate (mg/L)	TN (mg/L)	TOC (mg/L)	UV ₂₅₄ (1/cm)	UV ₂₈₀ (1/cm)
5/3/10	99	1028	<3	1.63	2.01	<0.05	18.98	2.24	3.57	223	0.94	284	21	8.4	0.160	0.109
5/24/10	153	1153	<3	<0.05	0.30	1.66	2.89	12.03	12.53	347	0.97	298	15.5	6.5	0.126	0.09
6/7/10	133	863	<3	<0.05	0.19	0.95	4.76	1.89	2.56	199	0.88	250	6.6	5.6	0.114	0.087
7/12/10	177	905	<3	0.14	0.3	0.36	0.12	11.14	11.43	232	0.9	256	11	5.5	0.121	0.0856
7/26/10	137	877	<3	<0.05	0.18	3.19	1.7	4.54	5.43	198	1.01	264	9.5	5.4	0.106	0.077
8/16/10	144	849	<3	0.05	0.18	0.59	4.98	6.27	7.18	190	0.94	252	12	5.7	0.105	0.075
8/23/10	84	950	<3	1.78	1.90	0.28	13.24	1.75	2.83	226	1.01	260	N/A	7.4	0.133	0.098
9/27/10	127	830	<3	<0.05	0.17	0.09	6.59	2.83	3.49	195	0.89	233	8.7	5.4	0.104	0.0688
10/4/10	111	952	<3	<0.05	0.22	<0.05	6.82	2.35	3.18	239	1.6	271	8.3	6.1	0.106	0.072
2/28/11	83	1078	<3	0.28	0.42	0.07	10.15	2.67	3.5	297	1.12	315	12	6.7	0.12	0.0828
3/7/11	77	1066	<3	0.08	0.2	<0.05	10.62	1.98	2.81	264	1.05	318	13	5.9	0.112	0.0738
3/21/11	135	956	<3	0.07	0.20	<0.05	8.39	1.44	2.64	216	1.09	270	10	6	0.124	0.0759
4/25/11	98	957	<3	<0.05	0.16	<0.05	9.07	1.62	2.68	218	1.24	303	11	5.7	0.12	0.0792
5/2/11	93	1012	<3	0.07	0.19	<0.05	7.98	1.88	3.00	251	1.28	309	10	5.7	0.114	0.0751
5/23/11	109	991	<3	0.07	0.23	<0.05	6.42	2.32	2.86	240	1.24	306	7.9	5.5	0.114	0.0759
6/6/11	57	1024	<3	0.1	0.26	<0.05	27.09	1.99	3.53	250	0.98	267	30	6.7	0.164	0.107
6/20/11	87	856	<3	<0.05	0.14	<0.05	5.04	1.95	2.85	197	0.94	284	6.4	4.7	0.104	0.0682
8/15/11	110	932	<3	0.4	0.61	<0.05	9.72	2.31	3.23	210	0.87	245	12	4.7	0.143	0.106
8/22/11	NR	864	<3	0.41	0.58	<0.05	18.67	2.15	2.24	200	0.79	251	19	6.4	0.17	0.126
9/6/11	98	797	<3	0.41	0.61	<0.05	11.67	2.21	3.09	174	0.71	225	14	4.6	0.101	0.0693
12/12/11	66	931	<3	0.53	0.71	<0.05	11.76	4.91	6.01	218	0.85	301	16	6.1	0.138	0.0863
12/27/11	122	968	<3	0.12	0.33	<0.05	3.82	10.54	12.81	234	0.82	301	15	5.5	0.123	0.0765

Note: Gray cells indicate results below detection limit.

Table A.30. MBR-Train 2-Permeate

Date	Alkalinity (mg/L as CaCO ₃)	TDS (mg/ L)	TSS (mg/ L)	OPO ₄ -P (mg/L)	TPO ₄ -P (mg/L)	NO ₂ -N (mg/L)	NO ₃ -N (mg/L)	Ammonia (mg/L)	TKN (mg/L)	Chloride (mg/L)	Fluoride (mg/L)	Sulfate (mg/L)	TN (mg/L)	TOC (mg/L)	UV ₂₅₄ (1/cm)	UV ₂₈₀ (1/cm)
5/3/10	7	12	<3	<0.05	<0.05	<0.05	0.28	0.72	<1.00	<4	<0.05	<4	N/A	N/A	N/A	N/A
5/24/10	8	<10	<3	<0.05	<0.05	<0.05	0.09	0.60	<1.00	<4	<0.05	<4	N/A	N/A	N/A	N/A
6/7/10	N/A	N/A	N/A	N/A	N/A	N/A	N/A	N/A	N/A	N/A	N/A	N/A	N/A	N/A	N/A	N/A
7/12/10	9	<10	<3	<0.05	<0.05	<0.05	<0.05	0.61	<1.00	<4	<0.05	<4	N/A	N/A	N/A	N/A
7/26/10	9	<10	<3	<0.05	<0.05	<0.05	0.23	0.38	<1.00	<4	<0.05	<4	0.52	<0.20	0.002	0.002
8/16/10	10	<10	<3	<0.05	<0.05	<0.05	0.10	0.56	<1.00	<4	<0.05	<4	0.56	<0.20	0.010	0.004
8/23/10	7	11	<3	<0.05	<0.05	<0.05	0.28	0.33	<1.00	<4	<0.05	<4	N/A	<0.20	0.007	0.003
9/27/10	8	<10	<3	<0.05	<0.05	0.08	0.11	0.83	<1.00	<4	<0.05	<N/A	0.55	<0.20	0.0137	0.004
10/4/10	9	12	<3	<0.05	<0.05	0.05	0.11	0.69	<1.00	<4	<0.05	<4	0.56	<0.20	0.014	0.005
2/28/11	7	<10	<3	<0.05	<0.05	<N/A	0.15	0.33	<1.00	N/A	<0.05	<N/A	0.4	<0.20	0.0058	<0.002
3/7/11	7	<10	<3	<0.05	<0.05	<0.05	0.16	0.52	<1.00	N/A	<0.05	<N/A	0.57	<0.20	0.0097	0.0034
3/21/11	6	<10	<3	<0.05	<0.05	<0.05	0.16	0.81	1.11	<4	<0.05	<4	0.65	<0.20	0.0155	0.006
4/25/11	8	<10	<3	<0.05	<0.05	<0.05	0.19	0.53	<1.00	<4	<0.05	<4	0.52	<0.20	0.0115	0.004
5/2/11	8	12	<3	<0.05	<0.05	<0.05	0.16	0.49	1.36	<4	0.05	<4	0.51	<0.20	0.0106	0.0035
5/23/11	8	<10	<3	<0.05	<0.05	<0.05	0.18	0.46	<1.00	<4	<0.05	<4	0.5	<0.20	0.0066	0.0027
6/6/11	9	13	<3	<0.05	<0.05	<0.05	1.02	1.4	1.56	<4	0.07	<4	2	<0.20	0.0215	0.0096
6/20/11	11	16	<3	<0.05	<0.05	<0.05	0.15	0.7	<1.00	<4	0.1	<4	0.68	<0.20	0.0086	0.0048
8/15/11	9	10	<3	<0.05	<0.05	<0.05	0.33	0.75	1.04	<4	<0.05	<4	0.73	<0.20	0.0461	0.0398
8/22/11	N/A	10	<3	<0.05	<0.05	<0.05	0.94	0.39	<1.00	<4	0.07	<4	1.3	<0.20	0.0449	0.034
9/6/11	9	10	<3	<0.05	<0.05	<0.05	0.3	0.38	<1.00	<4	<0.05	<4	0.6	<0.20	0.00654	0.00219
12/12/11	8	<10	<3	<0.05	<0.05	0.07	0.18	1.01	1.11	<4	<0.05	<4	0.94	<0.20	0.0223	0.00424
12/27/11	8	13	<3	<0.05	<0.05	<0.05	0.07	0.99	<1.00	<4	<0.05	<4	0.71	<0.20	0.0188	0.00545

Note: Gray cells indicate results below detection limit.

Table A.31. UF-Train 1-Concentrate

Date	Alkalinity (mg/L as CaCO ₃)															
		TDS (mg/L)	TSS (mg/L)	OPO ₄ -P (mg/L)	TPO ₄ -P (mg/L)	NO ₂ -N (mg/L)	NO ₃ -N (mg/L)	Ammonia (mg/L)	TKN (mg/L)	Chloride (mg/L)	Fluoride (mg/L)	Sulfate (mg/L)	TN (mg/L)	TOC (mg/L)	UV ₂₅₄ (1/cm)	UV ₂₈₀ (1/cm)
5/3/10	251	2480	<3	<0.05	0.54	<0.05	29.01	3.79	5.45	491	1.39	844	N/A	N/A	N/A	N/A
6/7/10	272	2424	<3	<0.05	0.27	<0.05	30.13	2.67	4.62	481	1.63	786	N/A	N/A	N/A	N/A
6/28/10	N/A	N/A	N/A	N/A	N/A	N/A	N/A	N/A	N/A	N/A	N/A	N/A	N/A	N/A	N/A	N/A
9/13/10	301	2306	<3	<0.05	0.31	<0.05	25.09	2.60	4.58	467	1.56	733	N/A	N/A	N/A	N/A
10/4/10	281	2318	<3	0.07	0.33	<0.05	27.33	1.58	2.96	483	1.71	749	28	12	0.193	0.113
2/7/11	232	2520	<3	<0.05	0.27	<0.05	31.52	2.9	4.63	501	1.57	873	33	12	0.179	0.108
3/7/11	243	2448	<3	<0.05	0.22	<N/A	32.04	2.19	4.34	492	1.54	821	38	13	0.183	0.113
8/8/11	296	2303	<3	0.23	0.5	0.08	28.89	1.94	4.33	491	1.61	734	31	12	0.199	0.151
8/22/11	NR	2302	<3	<0.05	0.27	<0.05	27.04	2.16	3.82	537	1.55	726	29	9.3	0.187	0.148
9/6/11	282	2248	<3	<0.05	0.31	<0.05	25.06	1.77	3.69	459	1.66	693	28	13	0.186	0.137
9/19/11	279	2216	<3	<0.05	0.38	<0.05	23.91	1.49	3.15	467	1.58	695	27	<2	0.161	0.116
10/11/11	248	2318	<3	<0.05	0.33	<0.05	29.12	1.75	3.28	513	1.64	757	30	11	0.185	0.136
10/17/11	257	2320	<3	<0.05	0.39	<0.05	26.22	1.22	2.72	499	1.68	759	N/A	N/A	0.184	0.129
11/14/11	259	2310	<3	<0.05	0.44	<0.05	25.31	2.32	4.33	509	1.62	720	26	11	0.189	0.133
12/12/11	204	2456	<3	<0.05	0.38	<0.05	22.85	2.27	3.68	510	1.55	816	24	11	0.160	0.112
12/27/11	172	2404	<3	<0.05	0.36	<0.05	27.62	3.39	4.93	525	1.45	799	29	11	0.167	0.120

Note: Gray cells indicate results below detection limit.

Table A.32. UF-Train 1-Feed

Date	Alkalinity (mg/L as CaCO ₃)															
		TDS (mg/L)	TSS (mg/L)	OPO ₄ -P (mg/L)	TPO ₄ -P (mg/L)	NO ₂ -N (mg/L)	NO ₃ -N (mg/L)	Ammonia (mg/L)	TKN (mg/L)	Chloride (mg/L)	Fluoride (mg/L)	Sulfate (mg/L)	TN (mg/L)	TOC (mg/L)	UV ₂₅₄ (1/cm)	UV ₂₈₀ (1/cm)
5/3/10	117	1138	<3	<0.05	0.36	<0.05	13.5	2.19	3.1	224	0.63	374	15	5.7	0.0852	0.0479
6/7/10	126	1095	<3	<0.05	0.16	<0.05	14.06	1.73	2.53	226	0.75	353	6.3	5.6	0.0832	0.0606
6/28/10	127	1098	<3	<0.05	0.13	<0.05	13.38	1.54	2.48	222	0.79	349	15	5.6	0.0912	0.0574
9/13/10	143	1062	<3	<0.05	0.16	<0.05	12.09	1.51	3.26	214	0.72	331	N/A	N/A	N/A	N/A
10/4/10	130	1076	<3	<0.05	0.15	<0.05	13.04	1.38	2.44	220	0.77	335	13	6	0.104	0.0556
2/7/11	107	1150	<3	<0.05	0.12	<0.05	14.66	1.66	2.86	226	0.72	385	16	5.6	0.0149	0.0047
3/7/11	115	1122	<3	<0.05	0.13	<N/A	15.19	1.39	2.48	222	0.71	363	19	6.1	0.0941	0.0545
8/8/11	136	1041	<3	0.13	0.32	<0.05	13.55	1.11	2.22	221	0.75	325	15	5.8	0.093	0.067
8/22/11	NR	1070	<3	<0.05	0.16	<0.05	12.7	1.13	1.92	243	0.74	324	14	4.8	0.038	0.030
9/6/11	130	1026	<3	<0.05	0.17	<0.05	12.01	1.04	1.93	211	0.77	310	14	5.7	0.092	0.064
9/19/11	130	1009	<3	<0.05	0.16	<0.05	11.51	1	1.65	216	0.74	311	13	5.3	0.086	0.057
10/11/11	115	1056	<3	<0.05	0.17	<0.05	13.92	1.03	1.86	232	0.77	334	15	5.7	0.090	0.062
10/17/11	119	1052	<3	<0.05	0.17	<0.05	12.69	0.94	1.61	230	0.8	340	13	5.1	0.0935	0.0604
11/14/11	120	1055	<3	<0.05	0.17	<0.05	12.02	1.7	2.19	230	0.75	320	13	5.3	0.095	0.061
12/12/11	97	1123	<3	<0.05	0.17	<0.05	10.99	1.34	2.28	237	0.77	372	12	5	0.083	0.053
12/27/11	81	1106	<3	<0.05	0.15	<0.05	13.15	1.88	2.35	241	0.73	360	15	5.2	0.086	0.057

Note: Gray cells indicate results below detection limit.

Table A.33. UF-Train 1-Permeate

Date	Alkalinity (mg/L as CaCO ₃)															
		TDS (mg/L)	TSS (mg/L)	OPO ₄ -P (mg/L)	TPO ₄ -P (mg/L)	NO ₂ -N (mg/L)	NO ₃ -N (mg/L)	Ammonia (mg/L)	TKN (mg/L)	Chloride (mg/L)	Fluoride (mg/L)	Sulfate (mg/L)	TN (mg/L)	TOC (mg/L)	UV ₂₅₄ (1/cm)	UV ₂₈₀ (1/cm)
5/3/10	7	19	<3	<0.05	<0.05	<0.05	0.85	0.62	<1.00	<4	<0.05	<4	N/A	N/A	N/A	N/A
6/7/10	7	14	<3	<0.05	<0.05	<0.05	0.87	0.14	<1.00	<4	<0.05	<4	N/A	N/A	N/A	N/A
6/28/10	6	14	<3	<0.05	<0.05	<0.05	0.99	0.43	<1.00	<4	<0.05	<4	N/A	N/A	N/A	N/A
9/13/10	8	21	<3	<0.05	<0.05	<0.05	1.14	0.75	<1.00	5	<0.05	N/A	N/A	N/A	N/A	N/A
10/4/10	8	26	<3	<0.05	<0.05	0.06	1.20	1.29	1.71	6	<0.05	<4	1.7	<0.20	0.0258	0.0095
2/7/11	5	18	<3	<0.05	<0.05	<0.05	1.05	0.73	<1.00	<4	<0.05	<4	1.5	<0.20	0.093	0.0514
3/7/11	7	22	<3	<0.05	<0.05	N/A	1.62	0.77	<1.00	6	<0.05	N/A	2.3	0.21	0.0149	0.0055
8/8/11	7	17	<3	<0.05	<0.05	<0.05	1.07	0.34	<1.00	<4	<0.05	<4	1.5	<.2	0.006	<0.002
8/22/11	N/A	17	<3	<0.05	<0.05	<0.05	1.12	0.16	<1.00	4	<0.05	<4	1.4	<.2	0.105	0.083
9/6/11	8	16	<3	<0.05	<0.05	<0.05	1.03	0.64	<1.00	4	<0.05	<4	1.6	<.2	0.013	0.006
9/19/11	18	54	<3	<0.05	<0.05	<0.05	3.22	0.63	<1.00	13	0.09	<4	1.8	<.2	0.009	<0.002
10/11/11	8	20	<3	<0.05	<0.05	<0.05	1.58	0.42	<1.00	5	<0.05	<4	2.2	<0.20	0.011	0.005
10/17/11	8	23	<3	<0.05	<0.05	<0.05	1.37	0.51	1.48	5	<0.05	<4	1.8	<0.20	0.0149	0.0042 1
11/14/11	8	22	<3	<0.05	<0.05	<0.05	1.3	0.69	<1.00	5	<0.05	<4	2	<.2	0.017	0.004
12/12/11	8	22	<3	<0.05	<0.05	<0.05	0.86	0.66	<1.00	4	<0.05	<4	1.4	<.2	0.012	0.003
12/27/11	8	24	<3	<0.05	<0.05	<0.05	1.05	0.57	<1.00	4	<0.05	<4	1.7	<.2	0.013	0.006

Note: Gray cells indicate results below detection limit.

Table A.34. UF-Train 2-Concentrate

Date	Alkalinity (mg/L as CaCO ₃)															
		TDS (mg/L)	TSS (mg/L)	OPO ₄ -P (mg/L)	TPO ₄ -P (mg/L)	NO ₂ -N (mg/L)	NO ₃ -N (mg/L)	Ammonia (mg/L)	TKN (mg/L)	Chloride (mg/L)	Fluoride (mg/L)	Sulfate (mg/L)	TN (mg/L)	TOC (mg/L)	UV ₂₅₄ (1/cm)	UV ₂₈₀ (1/cm)
5/3/10	261	2524	<3	<0.05	<0.05	<0.05	28.76	3.25	4.64	490	1.49	849	N/A	N/A	N/A	N/A
6/7/10	290	2412	<3	<0.05	0.3	0.06	29.03	3.67	5.7	479	1.66	797	N/A	N/A	N/A	N/A
6/28/10	N/A	N/A	N/A	N/A	N/A	N/A	N/A	N/A	N/A	N/A	N/A	N/A	N/A	N/A	N/A	N/A
9/13/10	305	2324	<3	<0.05	0.37	<0.05	24.74	2.43	4.58	458	1.58	729	N/A	N/A	N/A	N/A
10/4/10	277	2326	<3	<0.05	0.35	<0.05	27.57	1.31	3.32	483	1.67	748	12	27	0.22	0.144
2/7/11	234	2496	<3	<0.05	0.33	<0.05	30.86	3.12	4.88	500	1.55	874	13	32	0.238	0.164
3/7/11	254	2424	<3	<0.05	0.28	<0.05	30.93	2.14	3.32	484	1.56	821	38	13	0.262	0.186
8/8/11	292	2270	<3	0.2	0.53	<0.05	29.37	1.99	3.77	484	1.6	722	31	12	0.241	0.172
8/22/11	NR	2332	<3	<0.05	0.37	<0.05	27.44	2.41	4.07	540	1.62	726	29	10	0.231	0.171
9/6/11	284	2256	<3	<0.05	0.4	<0.05	25.26	2.49	4.49	465	1.68	698	28	13	0.233	0.161
9/19/11	283	2262	<3	<0.05	0.47	<0.05	24.79	1.98	3.65	481	1.56	714	27	12	0.218	0.148
10/11/11	270	2314	<3	<0.05	0.46	0.14	27.24	2.89	4.28	505	1.68	769	N/A	N/A	N/A	N/A
10/17/11	256	2274	<3	<0.05	0.44	0.1	26.14	2.62	4.58	490	1.71	762	27	11	0.229	0.175
11/14/11	261	2318	<3	<0.05	0.46	<0.05	25.05	2.44	4.5	507	1.63	722	26	11	0.226	0.155
12/12/11	203	2450	<3	<0.05	0.44	<0.05	22.06	2.2	3.32	495	1.52	801	24	11	0.207	0.142
12/27/11	176	2410	<3	<0.05	0.41	<0.05	27.5	3.67	5.26	524	1.46	802	29	11	0.209	0.147

Note: Gray cells indicate results below detection limit.

Table A.35. UF-Train 2-Feed

Date	Alkalinity (mg/L as CaCO ₃)															
		TDS (mg/L)	TSS (mg/L)	OPO ₄ -P (mg/L)	TPO ₄ -P (mg/L)	NO ₂ -N (mg/L)	NO ₃ -N (mg/L)	Ammonia (mg/L)	TKN (mg/L)	Chloride (mg/L)	Fluoride (mg/L)	Sulfate (mg/L)	TN (mg/L)	TOC (mg/L)	UV ₂₅₄ (1/cm)	UV ₂₈₀ (1/cm)
5/3/10	120	1133	<3	<0.05	<0.05	<0.05	13.26	1.69	2.63	222	0.67	375	15	5.5	0.0979	0.0628
6/7/10	135	1088	<3	<0.05	0.18	<0.05	12.97	1.73	2.58	218	0.78	351	14	5.7	0.115	0.089
6/28/10	130	1098	<3	<0.05	<0.05	<0.05	13.24	<0.10	<1.00	218	0.79	348	14	5.5	0.0985	0.0684
9/13/10	143	1064	<3	<0.05	0.19	<0.05	12.06	1.38	3.06	210	0.72	327	N/A	N/A	N/A	N/A
10/4/10	131	1076	<3	<0.05	0.16	<0.05	13.33	1.15	1.94	221	0.76	335	14	5.9	0.111	0.0687
2/7/11	109	1148	<3	<0.05	0.14	<0.05	14.53	1.62	2.76	229	0.75	392	15	5.7	0.012	0.0039
3/7/11	119	1122	<3	<0.05	0.16	<N/A	14.51	1.28	1.76	219	0.74	362	18	6	0.126	0.0862
8/8/11	136	1032	<3	0.1	0.25	<0.05	13.54	1.12	2.11	221	0.76	327	14	6.1	0.114	0.078
8/22/11	NR	1066	<3	<0.05	0.18	<0.05	12.6	1.19	1.16	244	0.75	327	14	5	0.039	0.031
9/6/11	131	1027	<3	<0.05	0.19	<0.05	11.96	1.46	2.35	212	0.77	310	14	5.8	0.115	0.074
9/19/11	129	1017	<3	<0.05	0.22	<0.05	11.71	1.28	1.86	217	0.74	313	13	5.4	0.105	0.066
10/11/11	122	1022	<3	<0.05	0.19	0.07	12.65	1.24	2.07	222	0.78	329	N/A	N/A	N/A	N/A
10/17/11	119	1040	<3	<0.05	0.19	0.05	12.63	1.17	2	224	0.81	341	13	5.4	0.104	0.0798
11/14/11	121	1040	<3	<0.05	0.19	<0.05	11.87	1.42	2.54	229	0.76	320	13	5.4	0.111	0.072
12/12/11	96	1115	<3	<0.05	0.19	<0.05	10.85	1.36	2.31	234	0.78	374	12	5.2	0.101	0.065
12/27/11	83	1100	<3	<0.05	0.18	<0.05	12.99	1.83	2.69	238	0.73	359	14	5.4	0.106	0.073

Note: Gray cells indicate results below detection limit.

Table A.36. UF-Train 2-Permeate

Date	Alkalinity (mg/L as CaCO ₃)	TDS (mg/L)	TSS (mg/L)	OPO ₄ -P (mg/L)	TPO ₄ -P (mg/L)	NO ₂ -N (mg/L)	NO ₃ -N (mg/L)	Ammonia (mg/L)	TKN (mg/L)	Chloride (mg/L)	Fluoride (mg/L)	Sulfate (mg/L)	TN (mg/L)	TOC (mg/L)	UV ₂₅₄ (1/cm)	UV ₂₈₀ (1/cm)
5/3/10	8	13	<3	<0.05	<0.05	<0.05	0.49	0.52	<1.0	<4	<0.05	<4	N/A	N/A	N/A	N/A
6/7/10	7	10	<3	<0.05	<0.05	<0.05	0.62	0.16	<1.00	<4	<0.05	<4	N/A	N/A	N/A	N/A
9/13/10	8	24	<3	<0.05	<0.05	<0.05	1.37	0.69	<1.00	5	<0.05	<N/A	N/A	N/A	N/A	N/A
10/4/10	9	25	<3	<0.05	<0.05	<0.05	1.41	0.96	1.34	7	<0.05	<4	1.7	<0.2	0.017	0.0076
2/7/11	6	<10	<3	<0.05	<0.05	<0.05	0.91	0.64	<1.00	<4	<0.05	<4	1.2	<0.2	0.116	0.0754
3/7/11	7	28	<3	<0.05	<0.05	<N/A	1.51	0.68	<1.00	5	<0.05	<N/A	1.7	<0.2	0.0116	0.0041
8/8/11	7	11	<3	<0.05	<0.05	<0.05	0.47	0.35	<1.00	<4	<0.05	<4	0.74	<0.2	0.005	<0.002
8/22/11	N/A	<10	<3	<0.05	<0.05	<0.05	0.47	0.2	<1.00	<4	<0.05	<4	0.68	<0.2	0.126	0.093
9/6/11	7	20	<3	<0.05	<0.05	<0.05	0.97	0.7	<1.00	<4	<0.05	<4	1.4	<0.2	0.012	0.004
9/19/11	10	19	<3	<0.05	<0.05	<0.05	1.12	0.69	<1.00	5	<0.05	<4	1.7	<0.2	0.013	0.004
10/11/11	8	21	<3	<0.05	<0.05	<0.05	1.39	<0.10	<1.00	5	<0.05	<4	N/A	N/A	N/A	N/A
10/17/11	8	23	<3	<0.05	<0.05	<0.05	1.27	<0.10	<1.00	4	<0.05	<4	1.3	<0.2	<0.002	<0.002
11/14/11	7	15	<3	<0.05	<0.05	<0.05	1.25	0.6	<1.00	5	<0.05	<4	1.7	<0.2	0.014	0.004
12/12/11	8	22	<3	<0.05	<0.05	<0.05	0.84	0.58	<1.00	4	<0.05	<4	1.1	<0.2	0.010	0.002
12/27/11	8	25	<3	<0.05	<0.05	<0.05	1.04	0.6	<1.00	4	<0.05	<4	1.3	<0.2	0.013	0.008

Table A.37. SDI₁₅ Values for the Feed of the MBR/Ozone/RO Trains

Date	Flux (gfd)		
		MBR-O ₃ -RO	MBR-RO
4/21/2011	17	7.23	2.40
5/4/2011	17	3.85	0.00
5/18/2011	17	2.95	2.58
6/8/2011	17	5.35	3.33
6/15/2011	17	3.47	2.11
6/22/2011	17	5.41	2.76
6/30/2011	17	2.69	2.95
11/17/2011	19	5.06	5.78
12/20/2011	19	5.69	2.42
12/28/2011	19	4.03	4.55

Table A.38. SDI₁₅ Values for the Feed of the UF/Ozone/RO Trains

Date	Flux (gfd)		
		UF-O ₃ -RO	UF-RO
4/20/2010	14	4.32	2.69
4/27/2010	14	5.22	0.43
5/4/2010	14	4.05	1.42
6/1/2010	14	5.82	3.74
6/8/2010	14	6.23	<1
6/17/2010	14	6.09	<1
6/22/2010	14	9.06	<1
6/27/2010	14	6.01	2.54
02/23/2011	14	6.26	2.86

Table A.39. SDI₁₅ Values for the Feed of the UF/UV/H₂O₂/RO Trains

Date	Flux (gfd)		
		UF-UV/H ₂ O ₂ -RO	UF-RO
8/3/2011	14	>5	>5
9/8/2011	14	8.9	6.5
9/14/2011	14	5.6	3.2
9/21/2011	14	5.6	5.4
9/27/2011	14	3.3	2.8
10/5/2011	14	5.6	2.5
10/11/2011	14	5.6	2.8
10/19/2011	14	5.3	5.4
10/25/2011	14	5.8	4.5
11/8/2011	15.5	5.1	5.9
11/15/2011	15.5	3.6	4.4
12/13/2011	15.5	3.7	4.2
12/21/2011	15.5	4.2	5.5
1/3/2012	15.5	2.4	5.6

Appendix B

UV₂₅₄ and Fluorescence Log Figures

- B-1 UV₂₅₄ log for MBR filtrate and MBR-ozone effluent
- B-2 Fluorescence log for MBR filtrate and MBR-ozone effluent
- B-3 UV₂₅₄ log for MBR filtrate and MBR-ozone effluent
- B-4 Fluorescence log for MBR filtrate and MBR-ozone effluent

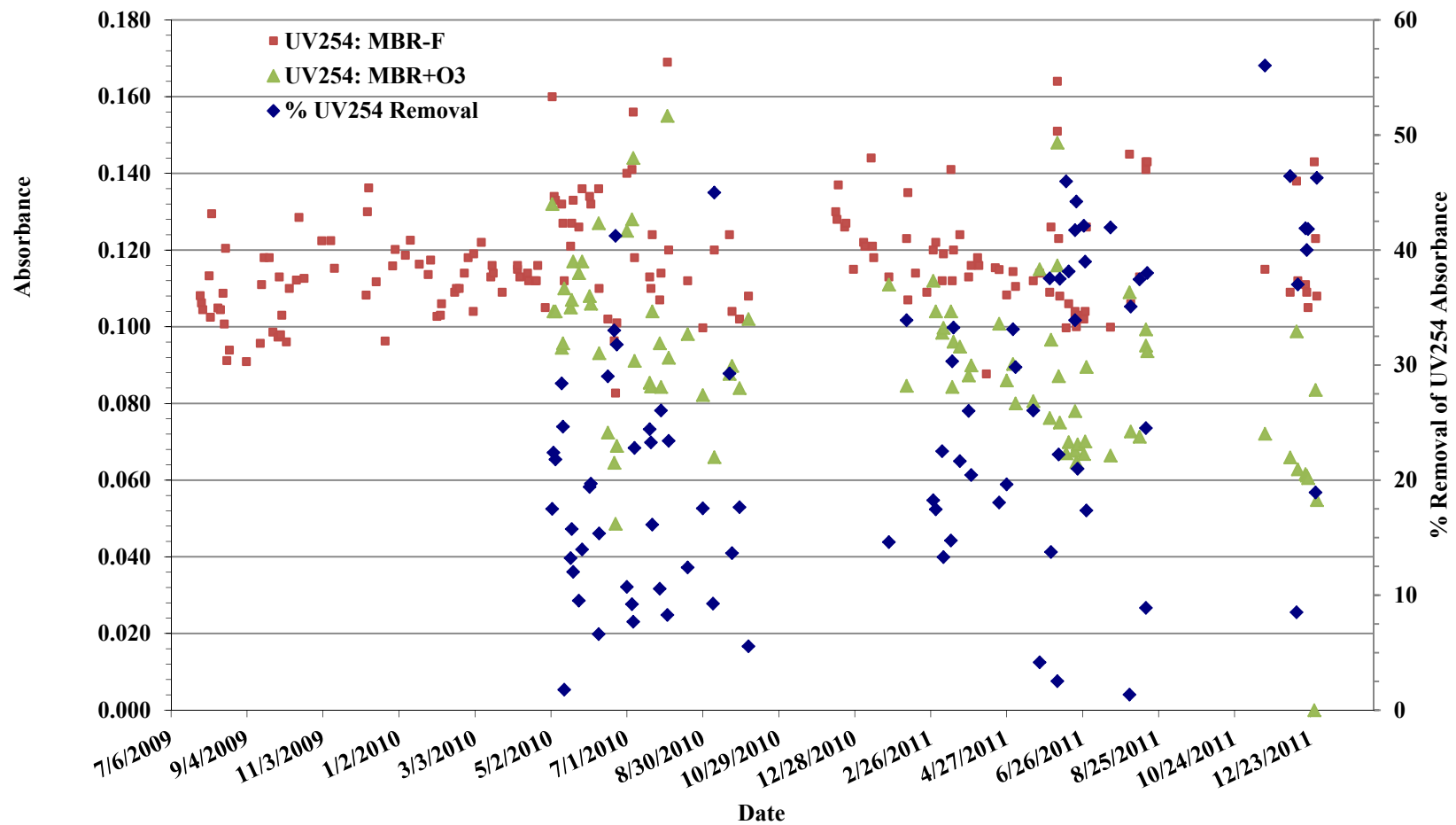


Figure B.1. UV₂₅₄ log for MBR filtrate and MBR-ozone effluent.

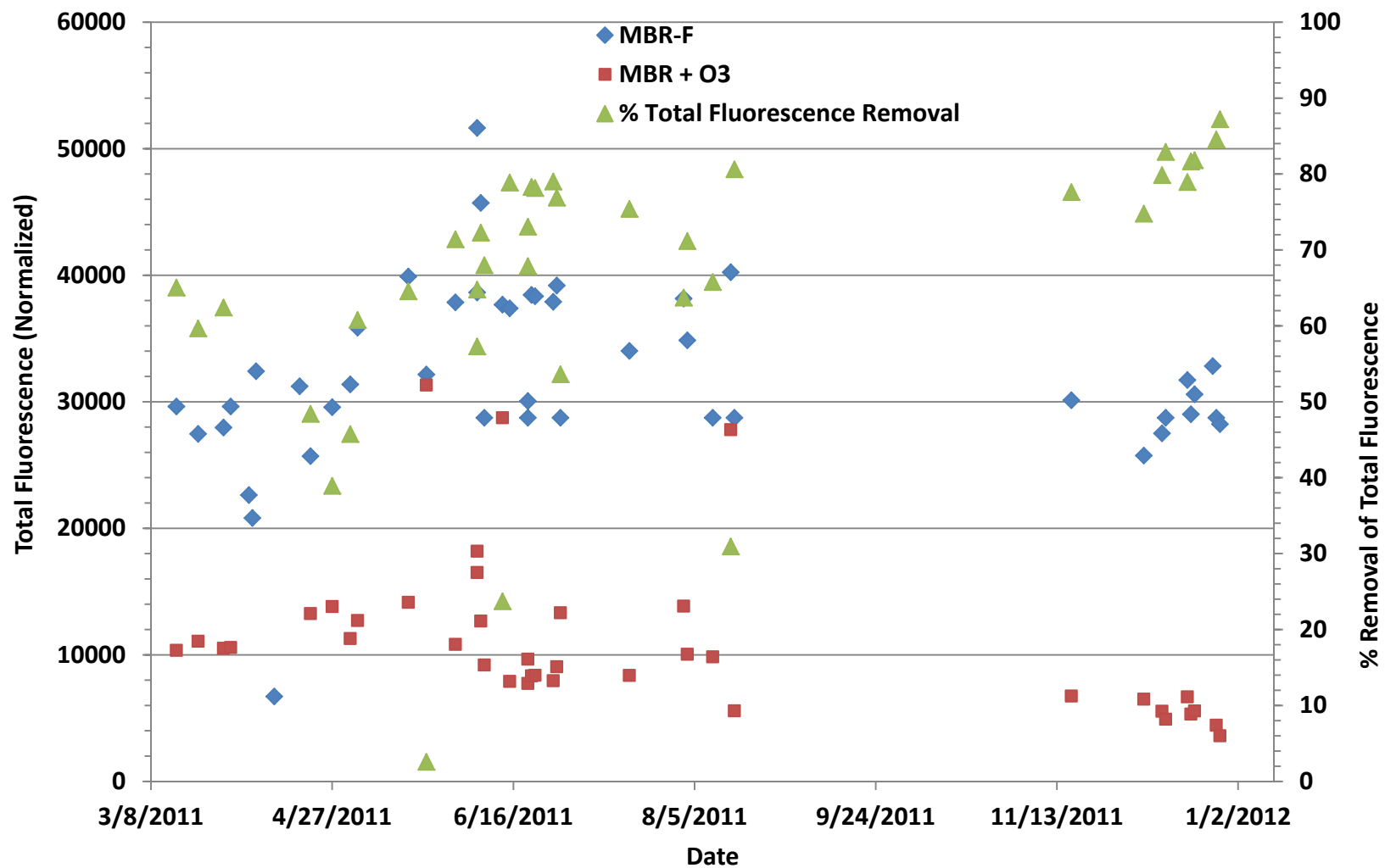


Figure B.2. Fluorescence log for MBR filtrate (MBR-F) and MBR-ozone effluent (MBR+O₃).

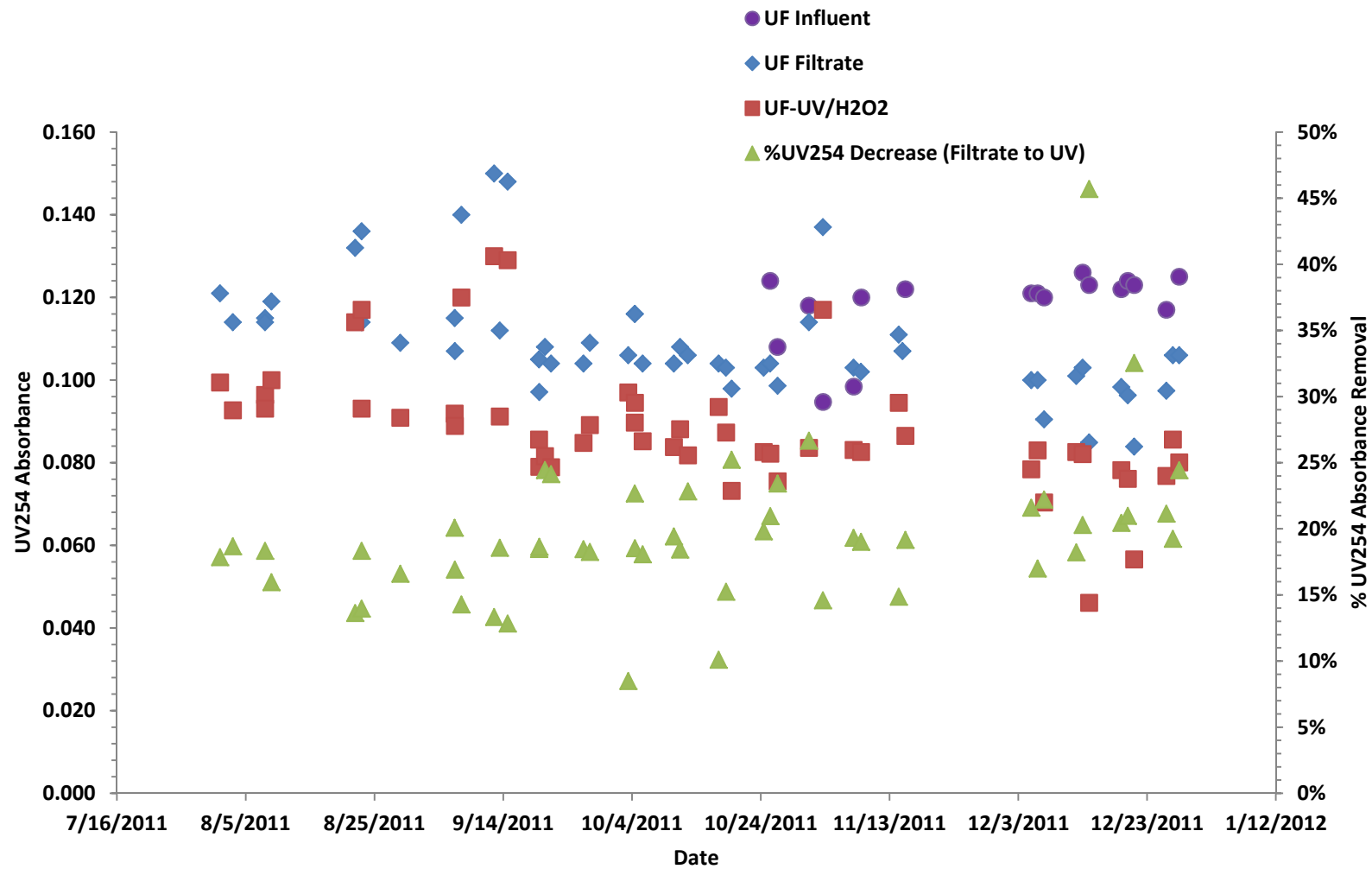


Figure B.3. UV₂₅₄ log for UF filtrate and UF-UV/H₂O₂ effluent.

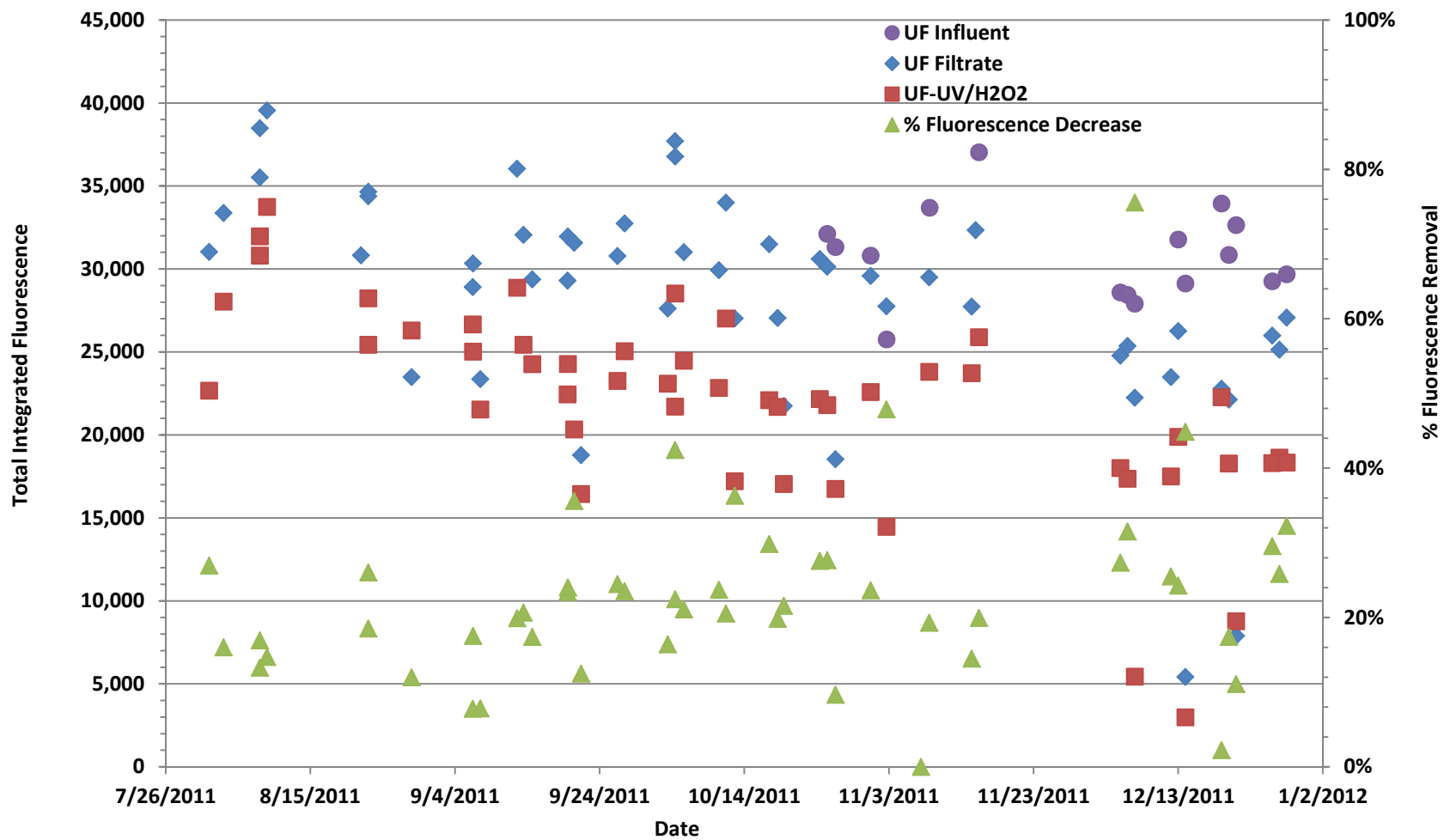


Figure B.4. Fluorescence log for UF filtrate and UF-UV/H₂O₂ effluent.

Appendix C

MBR Pilot Water Quality Log Tables

C-1	01-03/10 MBR Pilot Water Quality Log
C-2	04-06/10 MBR Pilot Water Quality Log
C-3	07-12/10 MBR Pilot Water Quality Log
C-4	01-04/11 MBR Pilot Water Quality Log
C-5	05-12/11 MBR Pilot Water Quality Log

Date	Table C.1. 01-03/10 MBR Pilot Water Quality Log																		
	MBR Influent							Aerobic Tank 1		Membrane Tank			MBR Filtrate						
	COD (mg/L)	BOD (mg/L)	o-P (mg/L)	TP (mg/L)	NH ₃ (mg/L N)	TK N (mg/L N)	MLS S (mg/L)	MLV SS (mg/L)	MLS S (mg/L)	MLVSS (mg/L)	TON * ^a (mg/L N)	COD (mg/L)	BOD (mg/L)	o-P (mg/L)	TP (mg/L)	NH ₄ (mg/L N)	TK N (mg/L N)	COD (mg/L)	BOD (mg/L)
1/4/10										12,200			21.0				0.51		5.2
1/7/10										11,200	8980	nd	8.5		0.04	0.07	<0.1		7.1
1/14/10	245	104			26.3	34.7	<0.2	6080	4940	9800	7840		15.8	<2			<0.1		8
1/18/10	183	81			27.7		<0.2	4720		8540			16.8	<2			0.16		8.3
1/21/10	161	76	1.6	2.26	24.9	30.5	<0.2	4440	3540	8480	6780	8.0	23.9	<3	0.06	0.07	<0.1		8.2
1/25/10	214	90			26.6			10,900		9340			34.3	<3			<0.1		
1/28/10	215	97			31.3	29.9	<0.2	4920	3960	10,400	8280		27.4	<2			<0.1		7.8
2/1/10	208				29		<0.2	7930		10,100			22						8.22
2/4/10	198	94			24.8		<0.2	2760	2260	10,000	8060	0.5	15	<2	0.09	0.11	<0.1		7.9
2/8/10	240				25.9		<0.2	7880		9680			13.9				<0.1		7.7
2/11/10	264						<0.2	6060	4880	9600	7700		34.9						4.8
2/15/10	228							2880		4060			17.4						
2/18/10	243		2.64	3.54	27.1			4480	3640	5160	4180		15.6		0.05	0.08	<0.1		
2/22/10	249	104			27.4		<0.2	4460		4200			18.5				<0.1		9.3
2/25/10	122	63			26.3		<0.2	3090	2520	6540	5270		10.3	<2			0.13		8.9
3/1/10	275				25.3		<0.2	8960		8560			16.4				0.3		
3/4/10	265	130	1.90	2.89	15.1		<0.2	7140	5840	8500	6900	3.6							
3/8/10	262						<0.2	4860		6640			10						9.2
3/11/10	214	88					<0.2	3040	2480	6760	5520		24.1	<4			<0.1		12.1

3/15/1 0	267	118			28.3			3740		5900			15.1	<2			0.15		10.2
3/18/1 0	249	118	1.76	2.63	26.6			4060	3340	5480	4440	8.5	24.6	<2	0.07	0.11	<0.1		8.5
3/22/1 0	316				28.2			5360		7240			44.4				0.41		6.6
3/25/1 0					24.5			5660	4620	7440	6000						0.22		
3/29/1 0	231	87			27.6			5480		7240			15.3	<2			0.2		7.3

Note: nd= non detect

^aTON* = Sum of nitrate and nitrite ions.

Table C.2. 04-06/10 MBR Pilot Water Quality Log

Date	MBR Influent						Aerobic Tank 1		Membrane Tank			MBR Filtrate						
	COD (mg/L)	BOD (mg/L)	o-P (mg/L)	TP (mg/L)	NH ₃ (mg/L N)	TKN (mg/L N)	MLSS (mg/L)	MLVSS (mg/L)	MLSS (mg/L)	MLVSS (mg/L)	TON ^{a,d} (mg/L N)	COD (mg/L)	BOD (mg/L)	o-P (mg/L)	TP (mg/L)	NH ₄ (mg/L N)	TKN (mg/L N)	COD (mg/L)
4/1/10	263	140	2.25	3.16	27	33	7160	5760	5260	4200	8.5	15	<2	0.11	0.14	<.1	1.1	
4/5/10	275	95			27.5		4180		6290			22	<2			0.2		
4/8/10	148	100			25.9	31.1	4840	4000	6900	5680		49.9	<2			0.11	1	8
4/12/10	251	107			26.5		4820		7080			14.1	<2			0.15		7.14
4/15/10	203	94	1.51	2.53	25.4	30.7	4360	3600	6100	4940	8	6.1	<2	0.04	0.07	<0.1	<1	9.1
4/19/10	281	133			24.5		3820		5480			21.1	<2			<0.1		
4/22/10	223	104			25.4	30.1	4160	3400	5840	4740		43.2	<2			<0.1	<1	
4/26/10	223	81			26.8		5200		7100									
4/29/10	217	101	4.45	6.48	27.2	28.4	5740	4700	7540	6160	11.1	14.5		0.12	0.14	<0.1	<1	14.1
5/3/10	248	88			26.6		6300		6320									
5/6/10	208	101			23.2	82.9	8320	6720	11,800	9480		42.8	<2			15.4	17.3	
5/10/10	279	114			25		9000		11,900			2.2	<2			17.3		<0.2
5/13/10	231	109	1.71	2.32	23.1		8800	7240	11,700	9540	<0.2	11.8	<2	0.11	0.15	21	24.1	<0.2
5/17/10	234	99			22.5		7860		11,700			15.9	>8			10.4		1.49
5/20/10	208	118			23.8	56.8	8340	6860	9720	7960		42.6	<2			9.5	11.5	2.2
5/24/10	226	110			24		6240		8260			21.3	<4			4.2		
5/27/10	254	123	1.85	2.59	23.6	31.2	6500	5360	8650	7120	<0.2	49.5	<2	0.05	0.08	8.9	9.6	2.5
5/31/10	253	127			25.3		6580		8800			16.4	<2			16.7		
6/3/10	281	90			26.4		7340	5940	7860	6290								
6/7/10		106			26		4560		5820			18.3	<2			0.3	1.2	6.5
6/10/10	205	106	1.45	2.07		32.4	3520	2820	4580	3620	<0.2	15.1	<2	0.04	0.07		<1	7.1
6/14/10	249	110					3640		4880			12.7	<2					5.5
6/17/10	202	99				31.9	3740	4120	5140	2990		8.6	<2					
6/21/10	239	100					3860		4940			11	<2					
6/24/10	200	110	1.5	2.14	25.4	31.5	3880	4340	5440	3100	5.1	19.8	<2	0.09	0.11	0.28	<1	6.5
6/28/10	217	85			27.5		3880		5440									

^aTON* = Sum of nitrate and nitrite ions.

Table C.3. 07/12/10 MBR Pilot Water Quality Log

Date	MBR Influent						Aerobic Tank 1		Membrane Tank				MBR Filtrate					
	COD (mg/L)	BOD (mg/L)	o-P (mg/L)	TP (mg/L)	NH ₃ (mg/L N)	TKN (mg/L N)	MLSS (mg/L)	MLVSS (mg/L)	MLSS (mg/L)	MLVSS (mg/L)	TON* ^a (mg/L N)	COD (mg/L)	BOD (mg/L)	o-P (mg/L)	TP (mg/L)	NH ₄ (mg/L N)	TKN (mg/L N)	TON* mg/(mg/L N)
7/1/10	195	96			25.6	30.2	1310	1080	1590	1330		53.3	<2			>10	16.6	0.34
7/5/10	224	97			28.5		3860		3940			21.8	<2			20.3		2.11
7/8/10	182	47	1.63	2.31	25.7	31.9	4590	3540	6080	4800	0.2	53.3	<2	0.1	0.14	15	16.6	0.34
7/12/10	208						4420		6440			21.8	<2			7.6		2.11
7/15/10	207	97			25.6	30.6	5580	4380	7690	5970		50.2	<2			0.93	1.8	2.84
7/19/10	204	92			23.6		5940		8080			14.3	<2			19.4		<0.2
7/22/10	271	100	3.05	4.17	22.63	31.1	6060	4820	8110	6370	<0.2	51.9	<2	0.03	0.05	15.4	16.8	<0.2
7/26/10	196				23.8		5120		7620			58.4				4.1		
7/29/10							5580	4500	7800	6290								
8/19/10							4520	3660	6700	5340								
8/23/10	474	144			32.3								<2					
8/26/10	230	123			28.4	32.4	3940	3180	5810	4690	6.9	22.6	<2			0.93	2.4	6.9
8/30/10	225	99			24.1		3880		3000			37	<2			2.54		5.6
9/2/10	198	97			23.6	30.8	3320	2760	4500	3660	0.23	13	<2			1.8	2.5	4.7
9/9/10	227	99	0.08	2.1	23.9	30.2	4400	5570	6900	3640		28.7	<2	0.08	0.09	8.46	8.7	4
9/13/10	205	86			23.2				9140			11.5						
9/16/10	369	164	0.04	5.5	24.5		2320	1860	2830	2330	9.79	17.7	<2	0.04	0.07	<0.1		12
9/20/10	209	101			23.6		6040		8180			4	<2			12.5		0.26
9/23/10	182	94			25		4560	3580	6580	5220		20.6	<2			6.9		
9/27/10	196				23.3		3920		6620			23				2.1		
9/30/10	170		0.02	1.94			3740	3040	5480	4420		47.4		0.02	0.04			
12/13/10	269	123			24.2		4140		6250			27	<2			17.5		
12/20/10	248	110			25.1		4080		6180			31	<2			8.5		
12/23/10	231		1.5	2.4			3880	3200	7160	6120		53		0.33	0.4			
12/30/10	122	111			28.3	35	4200	3480	6740	3480		<20	<3			2	4.1	9.3

^aTON* = Sum of nitrate and nitrite ions.

Table C.4. 01-4/11 MBR Pilot Water Quality Log

Date	MBR Influent						Aerobic Tank 1		Membrane Tank			MBR Filtrate						
	COD (mg/ L)	BOD (mg/ L)	o-P (mg/ L)	TP (mg/ L)	NH ₃ (mg/ L N)	TKN (mg/ L N)	MLS S (mg/ L)	MLVS S (mg/L)	MLS S (mg/ L)	MLVS S (mg/L)	TON * ^a (mg/ L N)	COD (mg/ L)	BOD (mg/ L)	o-P (mg/ L)	TP (mg/ L)	NH ₄ (mg/ L N)	TKN (mg/ L N)	TON* mg/(mg/ L N)
1/3/11	252	122			26.4				3980			<20	4			4.7		
1/6/11	206	96		5.5	24.4	33	2900	2400	4620	2400	7.4	39	<2		0.19	0.8	2.5	8.1
12/30/10	122	111			28.3	35	4200	3480	6740	3480		<20	<3			2	4.1	9.3
1/3/11	252	122			26.4				3980			<20	4			4.7		
1/6/11	206	96		5.5	24.4	33	2900	2400	4620	2400	7.4	39	<2		0.19	0.8	2.5	8.1
1/10/11	232				30.5		4200		4420									
1/13/11	211					36												8
2/24/11	254						5390	4430	8120	6580		19						
2/28/11					24.1		5120		7960			29				0.1		
3/7/11		118			25.1		4630		7460			<20	<2			<0.1		8.8
3/10/11		93			24.8		4660	3820	7370	6120		<20	<2			<0.1	3.3	8.9
3/17/11	282	124	1.25	2.16	24.1		4460	3700	7120	5840	2.1	32	<2	0.14	0.17	<0.1		8.7
3/21/11	216	102			23		4580		7060			21	<2			<0.1		
3/24/11	243	105			23		4700	38,800	7460	6080		20	<2			<0.1		8.8
3/28/11	251	113			22.2		4380		6800			22	<2			<0.1		
3/31/11	203	80	0.87	1.7	20.5		3660	3000	6080	4960	8	<20	<2	0.09	0.12	<0.1		9.2
4/7/11	212	96			23.6	33	4180	3400	5480	4520		23	<2			<0.1	1.1	9.6
4/11/11	244	104					4400		6680			22	<2			<0.1		
4/14/11	234	118	1.27	2.04	24.4	34	4630	3670	6360	5040	9.9	22	<2	0.72	0.75	<0.1	1.1	9.7
4/18/11	289	134			25.2		6000		7760			<20	<2			<0.1		
4/21/11	243	119			23.9	32	4980	4080	7490	3040		29	<2			<0.1	<1.0	9.5
4/25/11	287	146			26		5360		7300			20	<2			<0.1		
4/28/11	258	125			24.2	40	5760	4740	4300	3620	8.7	20				<0.1	<1.0	10.5

^aTON* = Sum of nitrate and nitrite ions.

Table C.5. 05-12/11 MBR Pilot Water Quality Log

Date	MBR Influent						Aerobic Tank 1		Membrane Tank			MBR Filtrate						
	COD (mg/ L)	BOD (mg/ L)	o-P (mg/ L)	TP (mg/ L)	NH ₃ (mg/ L N)	TKN (mg/ L N)	MLS S (mg/ L)	MLVS S (mg/L)	MLS S (mg/ L)	MLVS S (mg/L)	TON * ^a (mg/ L N)	COD (mg/ L)	BOD (mg/ L)	o-P (mg/ L)	TP (mg/ L)	NH ₄ (mg/ L N)	TKN (mg/ L N)	TON* mg/(mg/ L N)
5/2/11	256	99			23.8		5000		5720			21				<0.1		
5/9/11	310				21.7		5920		8340			20				<0.1		
5/12/11	204	97	1.02	1.73	27.5	34	5820	4720	8180	6640	5.9	<20	<2	0.07	0.09	<0.1	<1.0	7.8
5/16/11	259	109			24.3		7560		7560			<20	<2			<0.1		7.9
5/19/11		118			26.8	50	7640	4850	6000	6120		22	<2			<0.1	<1.0	6.2
5/23/11		115					7300		6420			22	<2					
5/26/11		95	1.46	2.32	24.5	27	6640	4420	5540	6090	4.9	<20	<2	0.21	0.23	<0.1	<1.0	5.9
5/30/11					27.5		6840		5460			<20				0.22		
6/2/11	130	60	0.54	1.45	16		6150	4800	7540	5820	3.6	21	<2	0.03	0.09	<0.1		5.7
6/9/11	267	107			21.9		5100	3920	6390	4900	3.64	25	<2			<0.1		5.4
6/13/11	240						6300		6900			20				<0.1		
6/16/11	591		3.34	6.25	22.6		6280	4960	7340	5780		20		0.09	0.11	<0.1		
7/28/11	236		0.56	2.54			2810	2270	3320	2680	7.8	20		0.54	1.62			9
8/4/11	204	89			21.4		3720	2920	4360	3390		<20	<2			<0.1		
8/11/11	209	98	1.65	2.36	23.4	29	5020	4060	6220	4960		<20	<2	0.56	0.58	<0.1	<1.0	10.8
8/18/11	229	95	1.43	2.06	23.8	33	4570	3630	5340	4240		23	<2	0.43	0.46	<0.1	<1.0	8.6
8/25/11	194	79	1.43	2.06	23.8	34	5240	4140	6260	4940	9.6	<20	<2	0.43	0.46	<0.1	<1.0	9.1
9/8/11	208	80	1.68	2.3	27	34	5580	4300	5600	4340		<20	<2	0.43	0.45	<0.1	<1.0	
9/15/11	196	85			26.7	36	3760	2940	3960	3080		<20	<2			<0.1	<1.0	

1																		
9/22/11	219	101	1.5	2.18	26.9	34.3	4040	3180	4880	3780	9.1	<20	<2	0.4	0.43	0.23	1.3	9.1
9/29/11	206	86			26.9	33.4	5600	4400	6540	5080	18.7	<20	<2			0.18	1.5	
10/6/11	198	91	1.52	2.26	24.9		5840	4520	6400	4940	18.3	<20	<2	0.18	0.2	<.1	<1.0	5
10/13/11	457	120			26.7		6060	4640	7940	6110	7.7	<20	3.5			1.07	1.07	
11/3/11	177		1.34	2.14			440	380	380	340		26		0.14	0.19			
11/10/11	161	60				37	1860	2320	3260	2600		20	2					
11/17/11	204	91	1.36	2.12	28.6	38.9	3360	2720	4120	3300	13.3	<20	<2	0.56	0.56	<.1	1.4	15.5
11/24/11	331	135			30.3	45.7	4000	3220	4600	3700			<2			0.14	1.8	12.2
12/8/11	211	83	1.36	2.1	26.4		5540	4480	7060	5660	10.4	36	<2	0.31	0.32	0.19	0.8	10.9
12/15/11	147	60	0.36	0.83	31.7		6860	5560	7960	6450		<20	<2	0.54	0.57			4.7
12/22/11	243	107					6450	5240	8400	6820		22	5					
12/29/11	261	118	1.55	2.42	34.3	34	6900	5640	8430	6860		<20	<2	0.2	0.21	9.5	>15	

"TON*" = Sum of nitrate and nitrite ions.

Appendix D

Tables and Figures of Supporting Information for the RO Element Microscopy and Associated Analyses

Table D.1 Inspection of Exterior of Membrane Elements

Table D.2 Inspection of Interior of Membrane Elements

Table D.3 Dye Testing using Rhodamine B Solution

Table D.4 MATLAB-Generated Images for F-EEM Analysis

[Table D.5 Inductively Coupled Analysis of Membrane Elements in mg of Membrane Surface/cm²](#)

Table D.6 ICP Results in mg of Membrane Surface/cm²

Figure D.1 SEM micrographs and EDS spectra of virgin membrane

Figure D.2 SEM micrographs and EDS spectra of MBR-RO lead element 10126184

Figure D.3 SEM micrographs and EDS spectra of MBR-RO tail element 10126171

Figure D.4 SEM micrographs and EDS spectra of MBR-O₃-RO lead element S9790307

Figure D.5 SEM micrographs and EDS spectra of MBR-O₃-RO tail element S9790327

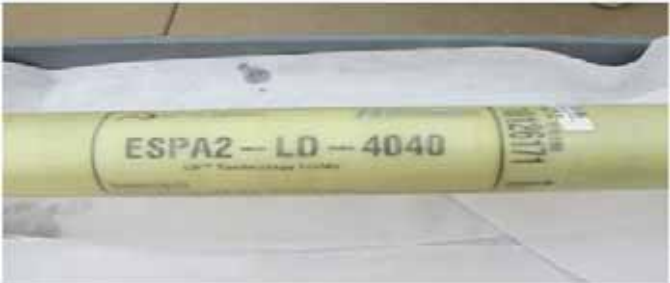


Figure D.6 SEM micrographs and EDS spectra of UF-RO lead element 6008014687

Figure D.7 SEM micrographs and EDS spectra of UF-RO tail element 600804562

Figure D.8 SEM micrographs and EDS spectra of UF-UV/H₂O₂-RO lead element 600804638

Figure D.9 SEM micrographs and EDS spectra of UF-UV/H₂O₂-RO tail element 600804106

Table D.1. Inspection of Exterior of Membrane Elements

Serial No. Pretreatment Lead or Tail	Comments	
10126184 MBR-RO lead element	Brine seal, hard shell (fiberglass outer wrap), ATDs, and glue lines of the element were all in good condition. No visible defects were observed. Both the feed end and brine end of the element were very clean. There were no deposits of scale or organic growth and no unusual features on the hard shell. Clear spacers were observed.	
10126171 MBR-RO tail element	Brine seal, hard shell (fiberglass outer wrap), ATDs, and glue lines of the element were all in good condition. No visible defects were observed. Both the feed end and brine end of the element were very clean. There were no deposits of scale or organic growth and no unusual features on the hard shell. Clear spacers were observed.	
S9790307 MBR-O ₃ -RO lead element	Brine seal, hard shell (fiberglass outer wrap), ATDs, and glue lines of the element were all in good condition. No visible defects were observed. Both the feed end and brine end of the element were very clean. There were no deposits of scale or organic growth and no unusual features on the hard shell. Clear spacers were observed.	
S9790237 MBR-O ₃ -RO tail element	Brine seal, hard shell (fiberglass outer wrap), ATDs, glue lines of the element were all in good condition. No visible defects were observed. Both the feed end and brine end of the element were very clean. There were no deposits of scale or organic growth and no unusual features on the hard shell. Clear spacers were observed.	



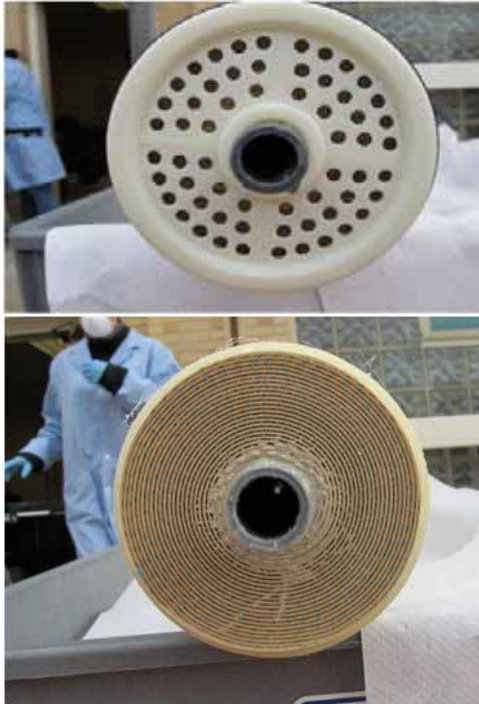



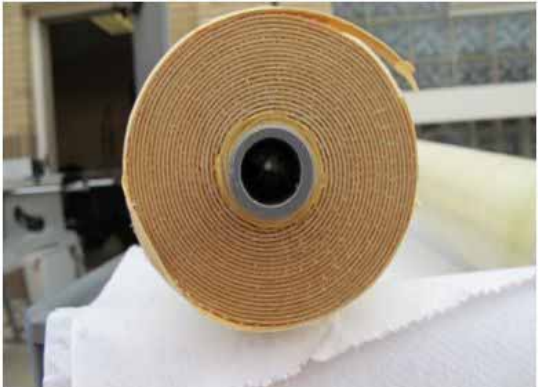




6008014638 UF-UV-H ₂ O ₂ -RO lead element	Brine seal, hard shell (fiberglass outer wrap), ATDs, glue lines of the element were all in good condition. An orange film was prevalent in the plastic wrapping and on the hard shell as well as the feed and brine ends.	
6008014106 UF-UV-H ₂ O ₂ -RO tail element	Brine seal, hard shell (fiberglass outer wrap), ATDs, and glue lines of the element were all in good condition. An orange film was prevalent in the plastic wrapping, and on the hard shell as well as the feed and brine ends.	
6008014687 UF-RO lead element	Brine seal, hard shell (fiberglass outer wrap), ATDs, and glue lines of the element were all in good condition. No visible defects were observed. Both the feed end and brine end of the element were very clean. There were no deposits of scale or organic growth and no unusual features on the hard shell. Clear spacers were observed.	
6008014562 UF-RO tail element	Brine seal, hard shell (fiberglass outer wrap), ATDs, and glue lines of the element were all in good condition. No visible defects were observed. Both the feed end and brine end of the element were very clean. There were no deposits of scale or organic growth and no unusual features on the hard shell. Clear spacers were observed.	

Table D.1. Inspection of Exterior of Membrane Elements Cont'd (Feed and Brine Ends)

Serial No.	ATD Feed End	ATD Brine End
10126184 MBR-RO lead element		
10126171 MBR-RO tail element		
S9790307 MBR-O ₃ -RO lead element		

		
<p>S9790237 MBR-O₃-RO tail element</p>	 	 

6008014638
UF-UV-H₂O₂-RO
lead element



6008014106
UF-UV-H₂O₂-RO
tail element










<p>6008014687 UF-RO lead element</p>	 	 
<p>6008014562 UF-RO tail element</p>		

Table D.2. Inspection of Interior of Membrane Elements

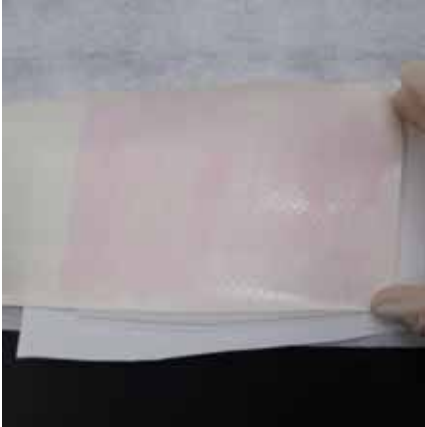





MBR-RO	Lead Element	Tail Element
Serial no.	10126171	10126184
No. of leaves	10	10
Effective surface per leaf	79 cm × 87 cm	87.5 cm × 80 cm
Permeate carrier	Clean	Clean
Feed spacer	Clean	Clean
Membrane support layer	Clean	Clean
Membrane active layer	Thin orange coating along textured surface of active layer on all sheets. Some darker orange spotting observed, some as large as 1–2 cm across.	Some black particulate about 1 mm found on all active layers. Green particulate observed on one of the sheets, size about 1–2 mm.
UF-UV/H₂O₂-RO	Lead Element	Tail Element
Serial no.	6008014638	6008014106
No. of leaves	10	10
Effective surface per leaf	89 cm × 86 cm	86 cm × 87 cm
Permeate carrier	Orange coating	Orange coating
Feed spacer	Orange coating	Orange coating
Membrane support layer	Orange coating	Orange coating
Membrane active layer	Thicker orange coating prevalent on all layers. Small black particulate particles about 1 mm present on all layers as well. Evenly distributed, not noticeably favoring the feed or brine ends.	Thick orange coating prevalent on all layers. Some small black particulate particles about 1 mm present. Evenly distributed, not noticeably favoring the feed or brine ends.
UF-RO	Lead Element	Tail Element
Serial no.	6008014687	6008014562
No. of leaves	10	10
Effective surface per leaf	87.5 cm × 85.5cm	88.5 cm × 85.5 cm
Permeate carrier	Clean	Clean
Feed spacer	Clean	Clean
Membrane support layer	Clean	Clean
Membrane active layer	Few black particulate pieces about 1 mm found on all active layers. Some particulate observed in clusters, forming groups a few millimeters across. Some orange coating present, accumulating on the rough surface of the active layer.	Thin orange coating present on some active layers. Observable black particulate on active layers, all small particles about 1 mm.
MBR-O₃-RO	Lead Element	Tail Element
Serial no.	S9790307	S9790237
No. of leaves	10	10
Effective surface per leaf	63 cm × 83cm	62.5 cm × 84 cm
Permeate carrier	Clean	Clean







Feed spacer	Clean	Clean
Membrane support layer	Clean	Clean
Membrane active layer	Dirty along spacer lines, with some black particulate about 5–10 mm. Orange marks about 5 cm long were present diagonally along spacer lines. Orange stains about 1 cm in diameter throughout.	Thin coating of orange observed on all layers. No particulate observed. A few sheets had thin black scratches visible, forming lines 2–3 cm long.
Serial No. Pretreatment Lead/Tail Element	Active Layer Sample	Active Layer Sample
10126184 MBR-RO lead element		
10126171 MBR-RO tail element		

<p>S9790307 MBR-O₃-RO lead element</p>		
<p>S9790237 MBR-O₃-RO tail element</p>		
<p>6008014638 UF-UV/H₂O₂-RO lead element</p>		

<p>6008014106 UF-UV/H₂O₂-RO lead element</p>		
<p>6008014687 UF-RO lead element</p>		
<p>6008014562 UF-RO tail element</p>		

Table D.3. Dye Test using Rhodamine B Solution

Serial No.	Active Layer	Support Layer
10126184 MBR-RO lead element		
10126171 MBR-RO tail element		
S9790307 MBR-O ₃ -RO lead element		

<p>S9790237 MBR-O₃-RO tail element</p>		
<p>6008014638 UF-UV/H₂O₂-RO lead element</p>		
<p>6008014106 UF-UV/H₂O₂-RO tail element</p>		

<p>6008014687 UF-RO lead element</p>		
<p>6008014562 UF-RO tail element</p>		

Table D.4. MATLAB-Generated Images for F-EEM Analysis

Serial No. Pretreatment Lead/Tail Element	DI Water Extraction	NaOH Extraction
1016184 MBR-RO lead element		
1016171 MBR-RO tail element		
S9790307 MBR-O ₃ -RO lead element		
S9790237 MBR-O ₃ -RO tail element		

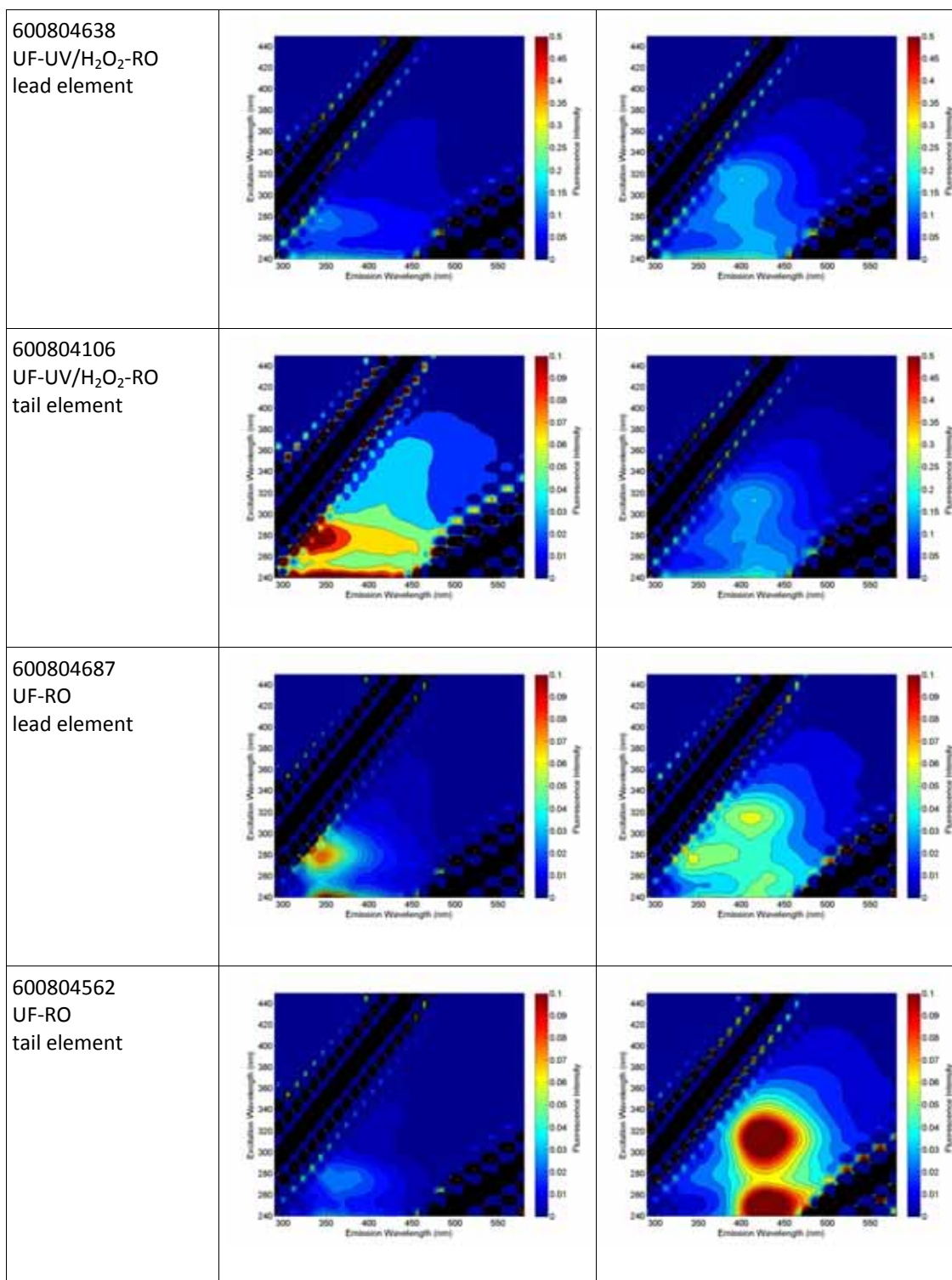


Table D.5. Inductively Coupled Analysis of Membrane Elements in mg of Membrane Surface/cm²

Process	Lead or Tail	Serial No.	Fluoride	Chloride	Bromide	Nitrate-N	Phosphate	Sulfate
DI Extraction								
MBR-RO	Lead	1016184	BDL	0.0044	BDL	0.00006	BDL	BDL
	Tail	1012671	BDL	0.0025	BDL	0.00448	BDL	BDL
MBR-O ₃ -RO	Lead	S9790307	BDL	0.0004	BDL	0.00835	BDL	BDL
	Tail	S9790237	BDL	0.0009	BDL	0.00008	BDL	BDL
UF-UV/H ₂ O ₂ -RO	Lead	6008014638	BDL	0.0051	BDL	0.00021	BDL	BDL
	Tail	6008014106	BDL	0.0032	BDL	0.00004	BDL	BDL
UF-RO	Lead	600814687	BDL	0.0010	BDL	0.00007	BDL	BDL
	Tail	6008014562	BDL	0.0055	BDL	0.00014	BDL	BDL
0.1 M NaOH Extraction								
MBR-RO	Lead	1016184	BDL	0.0042	BDL	0.00020	BDL	BDL
	Tail	10126171	BDL	0.0014	BDL	0.00076	BDL	BDL
MBR-O ₃ -RO	Lead	S9790307	BDL	0.0023	BDL	0.00099	BDL	BDL
	Tail	S9790237	BDL	0.0007	BDL	0.00004	BDL	BDL
UF-UV/H ₂ O ₂ -RO	Lead	6008014638	BDL	0.0044	BDL	0.00016	0.0031	BDL
	Tail	6008014106	BDL	0.0015	BDL	0.00017	BDL	BDL
UF-RO	Lead	6008014687	BDL	0.0008	BDL	0.00000	BDL	BDL
	Tail	6008014562	BDL	0.0037	BDL	0.00105	BDL	BDL

Table D.6. ICP Results in mg of Membrane Surface/cm²

Element	:															
	MBR-RO				MBR-O ₃ -RO				UF-UV/H ₂ O ₂ -RO				UF-RO			
	Lead	Lead	Tail	Tail	Lead	Lead	Tail	Tail	Lead	Lead	Tail	Tail	Lead	Lead	Tail	Tail
	DI	Acid	DI	Acid	DI	Acid	DI	Acid	DI	Acid	DI	Acid	DI	Acid	DI	Acid
Al	BDL	BDL	BDL	0.00034	BDL	0.00036	BDL	0.00055	BDL	0.00013	BDL	0.00047	BDL	0.00035	BDL	0.00051
Ba	BDL	0.00008	0.00002	0.00028	0.00004	0.00012	0.00003	0.00011	0.00003	0.00009	0.00002	0.00011	BDL	0.00012	BDL	0.00018
Ca	0.0006	0.0013	0.00095	0.00202	0.00077	0.00114	0.00063	0.00134	0.00119	0.00209	0.00081	0.00130	0.00047	0.00093	0.00047	0.00106
Fe	0.0002	0.00045	0.00002	0.00047	0.00008	0.00104	0.00009	0.00090	0.01154	0.01429	0.00716	0.00814	0.00027	0.00091	0.00034	0.00105
K	0.0010	0.00072	0.00180	0.00105	0.00135	0.00100	0.00100	0.00015	0.00130	0.00067	0.00085	BDL	0.00133	0.00022	0.00124	0.00045
Na	0.0041	0.00159	0.00148	0.00354	0.00003	0.00008	0.00003	0.00006	0.00005	0.00009	0.00002	0.00004	0.00001	0.00003	0.00002	0.00007
P	BDL	BDL	BDL	BDL	0.00212	0.00057	0.00031	0.00381	0.00700	0.00601	0.00435	0.00109	0.00026	0.00164	0.00125	0.00465
S	BDL	BDL	0.00016	BDL	BDL	BDL	BDL	BDL	0.00250	0.00222	0.00100	0.00125	BDL	BDL	BDL	BDL
Si	0.0003	0.00077	0.00031	0.00175	0.00026	BDL	0.00017	BDL	0.00012	BDL	BDL	BDL	BDL	BDL	BDL	BDL
Sr	0.0000	0.00000	0.00000	0.00001	0.00209	0.00191	0.00037	0.00273	0.00073	0.00221	0.00110	0.00199	0.00099	0.00161	0.00031	0.00313
Mg	BDL	BDL	BDL	0.00006	BDL	0.00001	BDL	BDL	0.00001	0.00002	0.00005	0.00003	BDL	0.00012	BDL	0.00001

Note: BDL= Below Detection Level

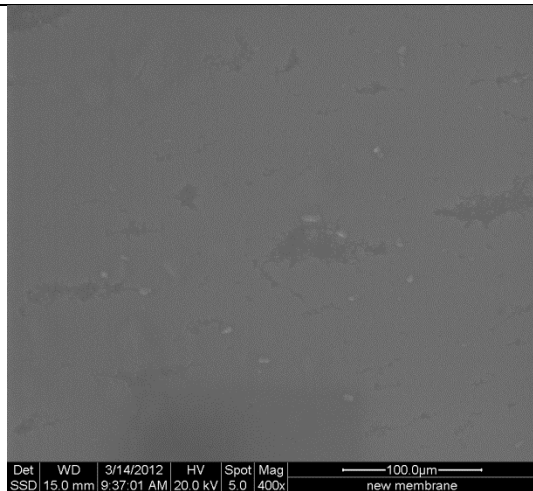


Figure D.1.1. ESEM micrograph of virgin membrane surface at magnification of $\times 400$. The membrane is smooth with a particle-like polymer structure.

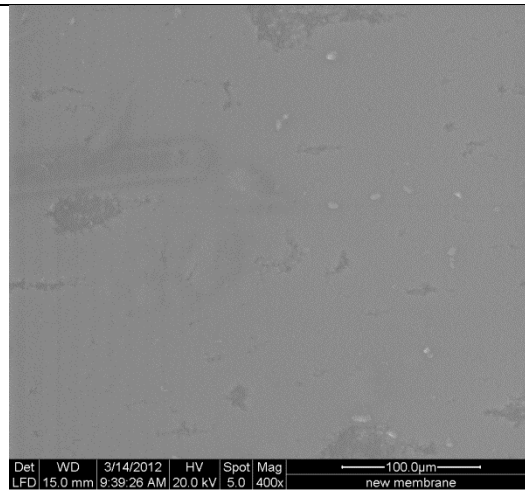


Figure D.1.2. ESEM micrograph of virgin membrane surface at magnification of $\times 400$.

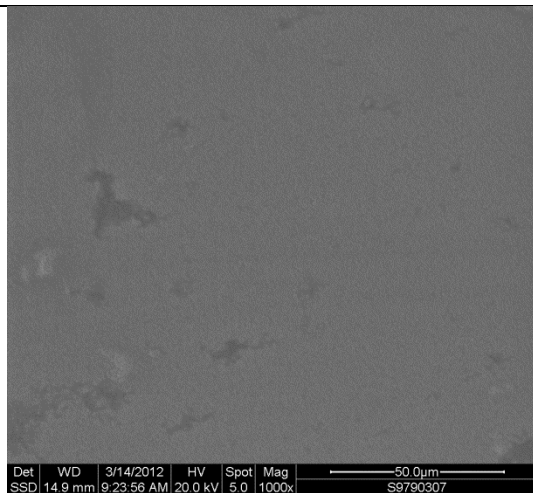


Figure D.1.3. ESEM micrograph of virgin membrane surface at magnification of $\times 1000$.

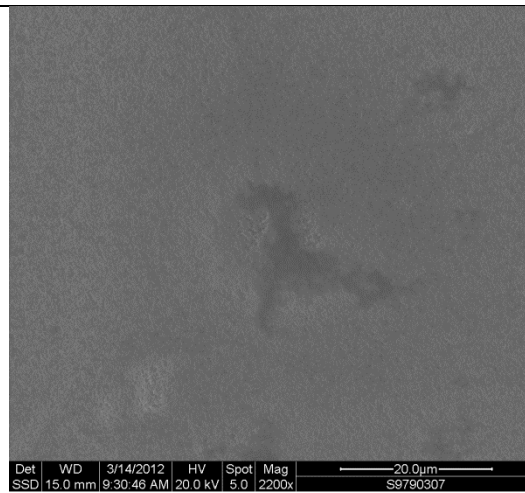


Figure D.1.4. ESEM micrograph of virgin membrane surface at magnification of $\times 2200$.

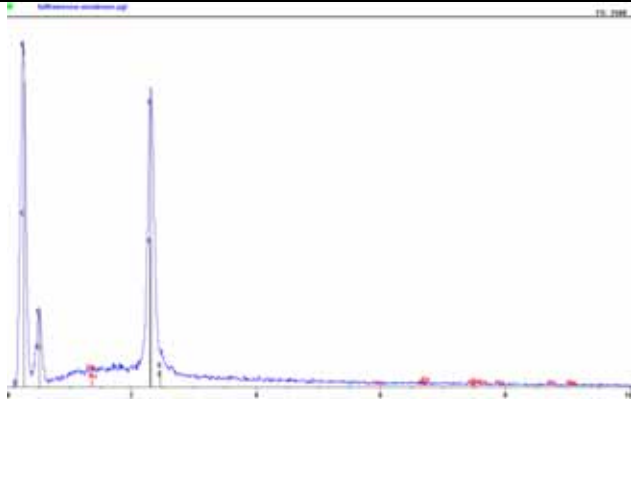


Figure D.1.5. EDS spectrum of the virgin membrane. The major elements are C, O, and S.

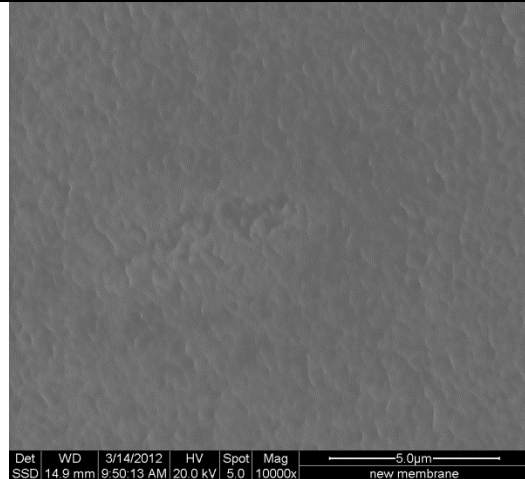


Figure D.1.6. ESEM micrograph of virgin membrane surface at magnification of $\times 10,000$.

Figure D.1. SEM micrographs and EDS spectra of virgin membrane.

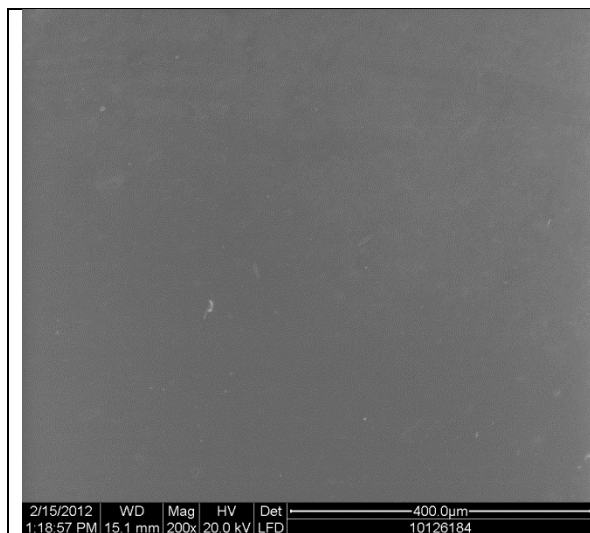


Figure D.2.1. ESEM micrograph of MBR-RO lead element at magnification of ×400.

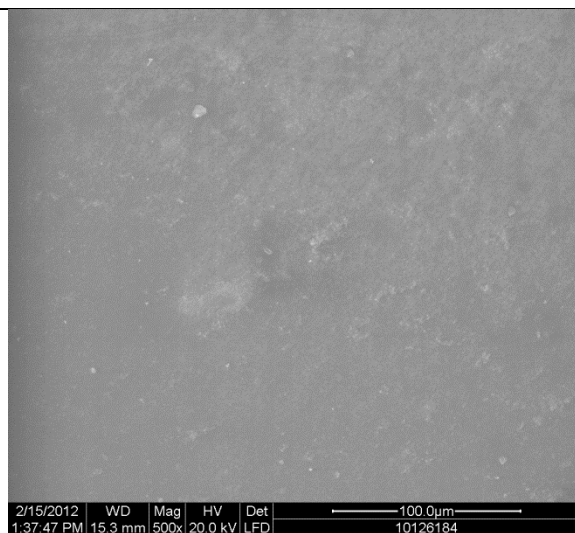


Figure D.2.2. ESEM micrograph of MBR-RO lead element at magnification of ×500. The fouling layer is thin and heterogeneous.

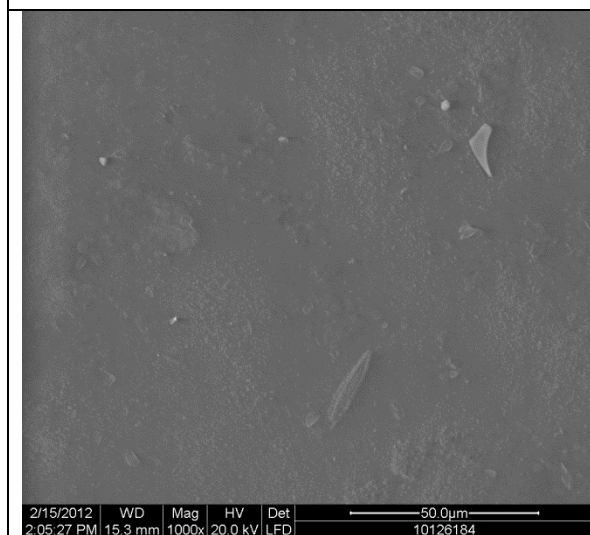


Figure D.2.3. ESEM micrograph of MBR-RO lead element at magnification of ×1000.

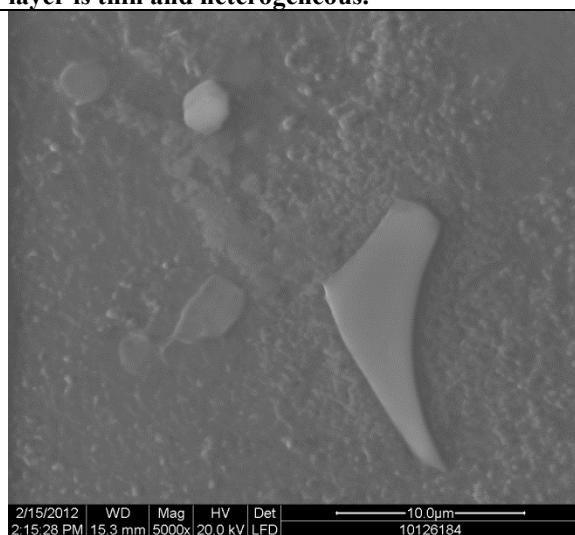
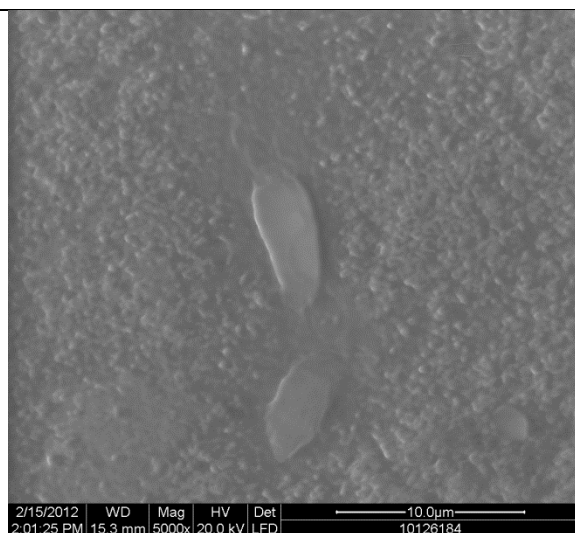
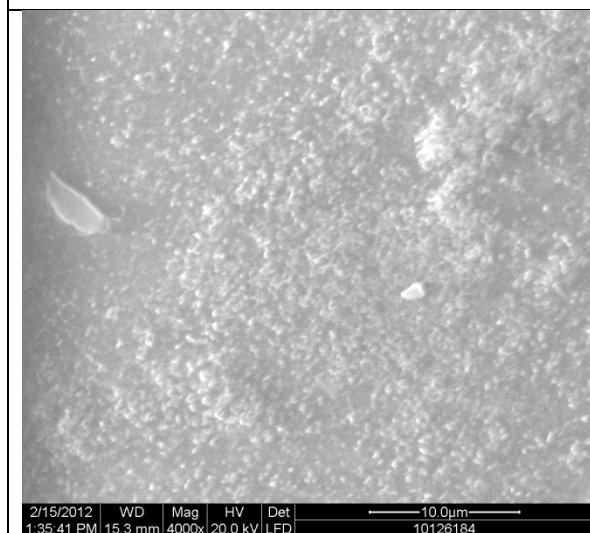
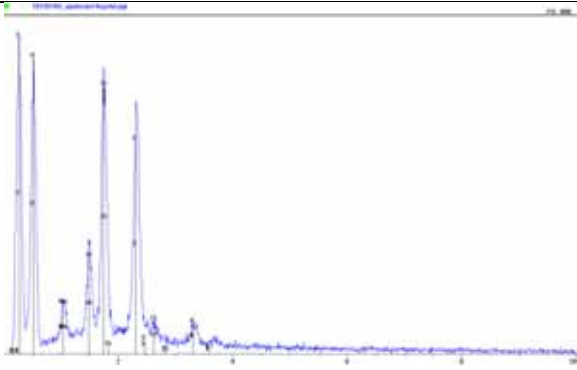


Figure D.2.4. ESEM micrograph of MBR-RO lead element at magnification of ×5000. The EDS indicates the major elements of the flake-like foulants and particles are inorganics Al, Si, and S with trace amounts of Na, Cl, and K, as shown in Figure D.2.7



<p>Figure D.2.5. ESEM micrograph of MBR-RO lead element at magnification of $\times 4000$.</p>	<p>Figure D.2.6. ESEM micrograph of MBR-RO lead element at magnification of $\times 5000$. The EDS indicates the major elements of the flake-like foulants are inorganics Al, Si, and S with trace amounts of Na, Cl, and K.</p>
 <p>The figure shows an EDS spectrum with several sharp peaks. The x-axis represents energy in keV, ranging from 0 to 10. The y-axis represents intensity. The most prominent peaks are labeled with their corresponding elements: Al (Aluminum) at approximately 1.5 keV, Si (Silicon) at approximately 1.7 keV, and S (Sulfur) at approximately 2.3 keV. There are also smaller peaks for Na (Sodium) at approximately 1.0 keV, Cl (Chlorine) at approximately 2.0 keV, and K (Potassium) at approximately 3.9 keV. The spectrum is relatively flat after 4 keV.</p>	
<p>Figure D.2.7. EDS spot scanning of the particles in Figure D.2.4.</p>	

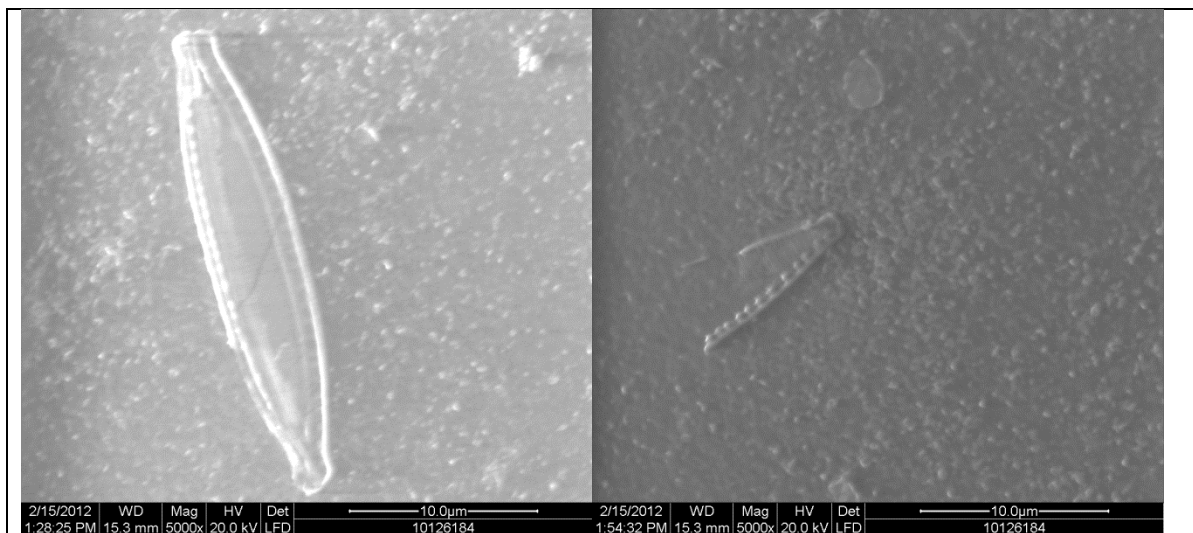
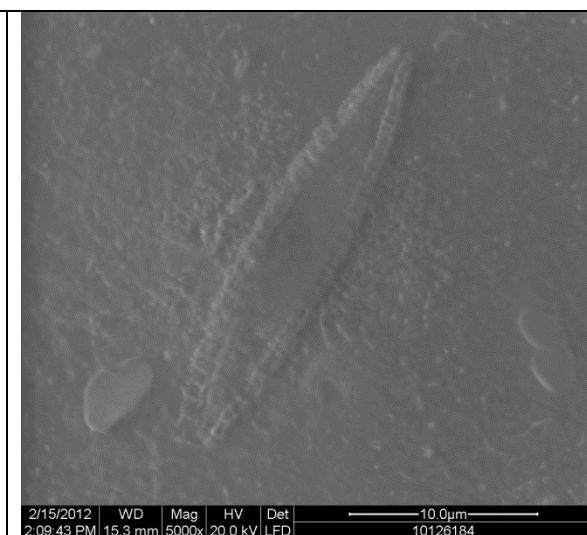


Figure D.2.8. ESEM micrographs of diatoms on membrane surface or embedded in biofilm.



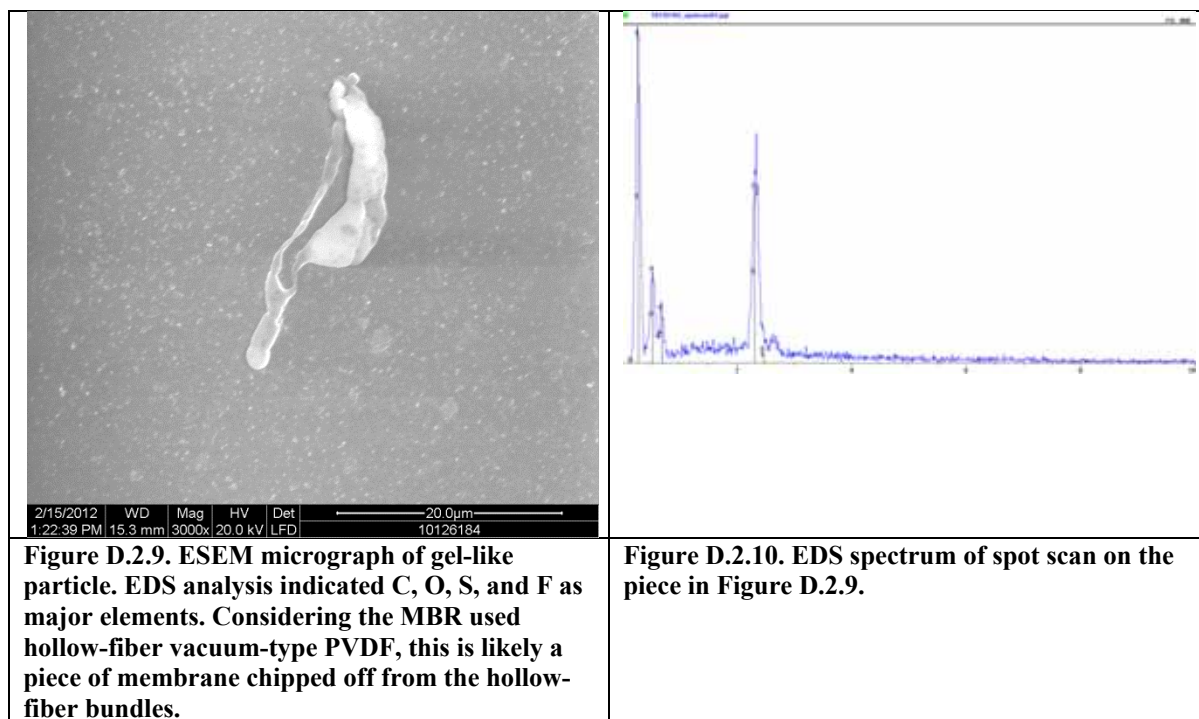


Figure D.2. SEM micrographs and EDS spectra of MBR-RO lead element 10126184.

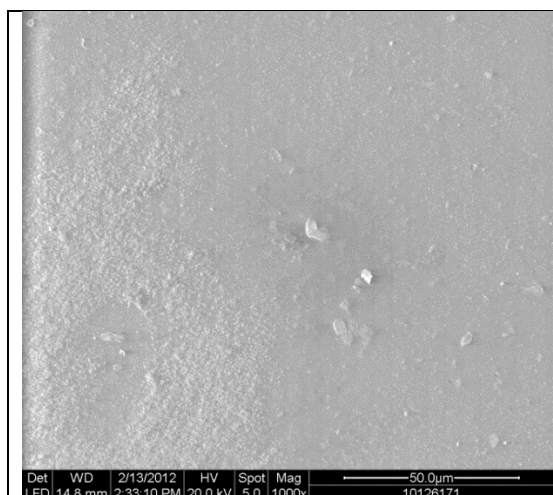


Figure D.3.1. ESEM micrograph of MBR-RO tail element at magnification of ×1000. The fouling layer is more homogeneous and more organic in nature than is the MBR-RO lead element.

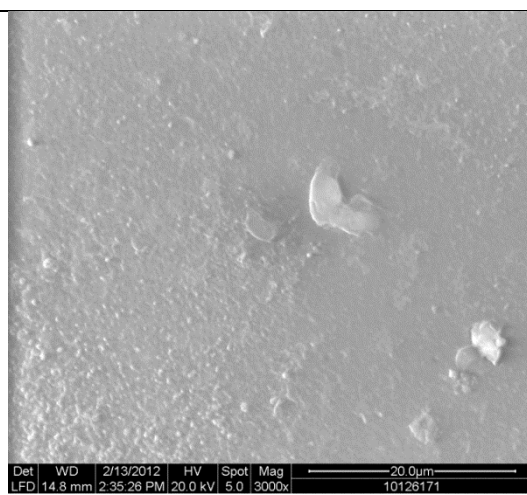


Figure D.3.2. ESEM micrograph of MBR-RO tail element at magnification of ×3000.

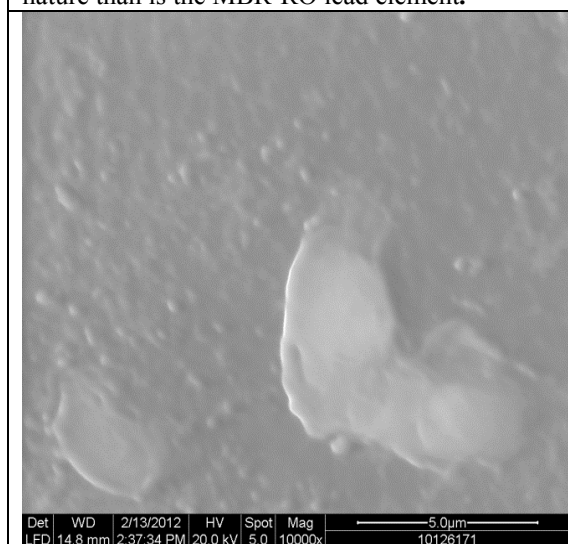


Figure D.3.3. ESEM micrograph of MBR-RO tail element at magnification of ×10,000.

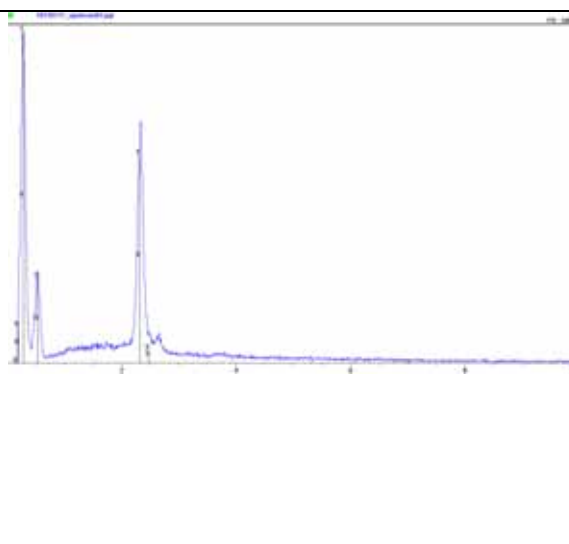


Figure D.3.4. The EDS indicates the major elements of the flake-like foulants in Figure 3.3 are of organic nature.

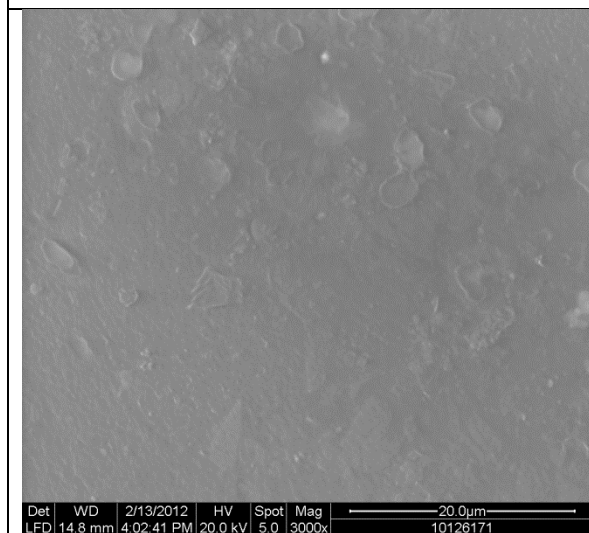


Figure D.3.5. ESEM micrograph of MBR-RO tail element at magnification of ×3000.

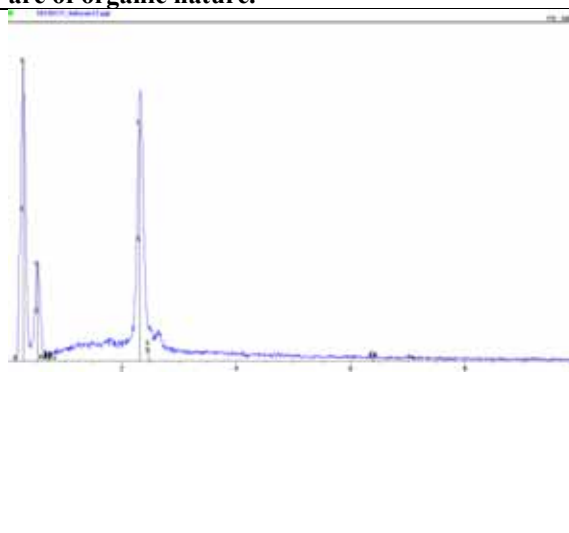


Figure D.3.6. The EDS indicates the major elements of the flake-like foulants in Figure D.3.5 are of organic nature.

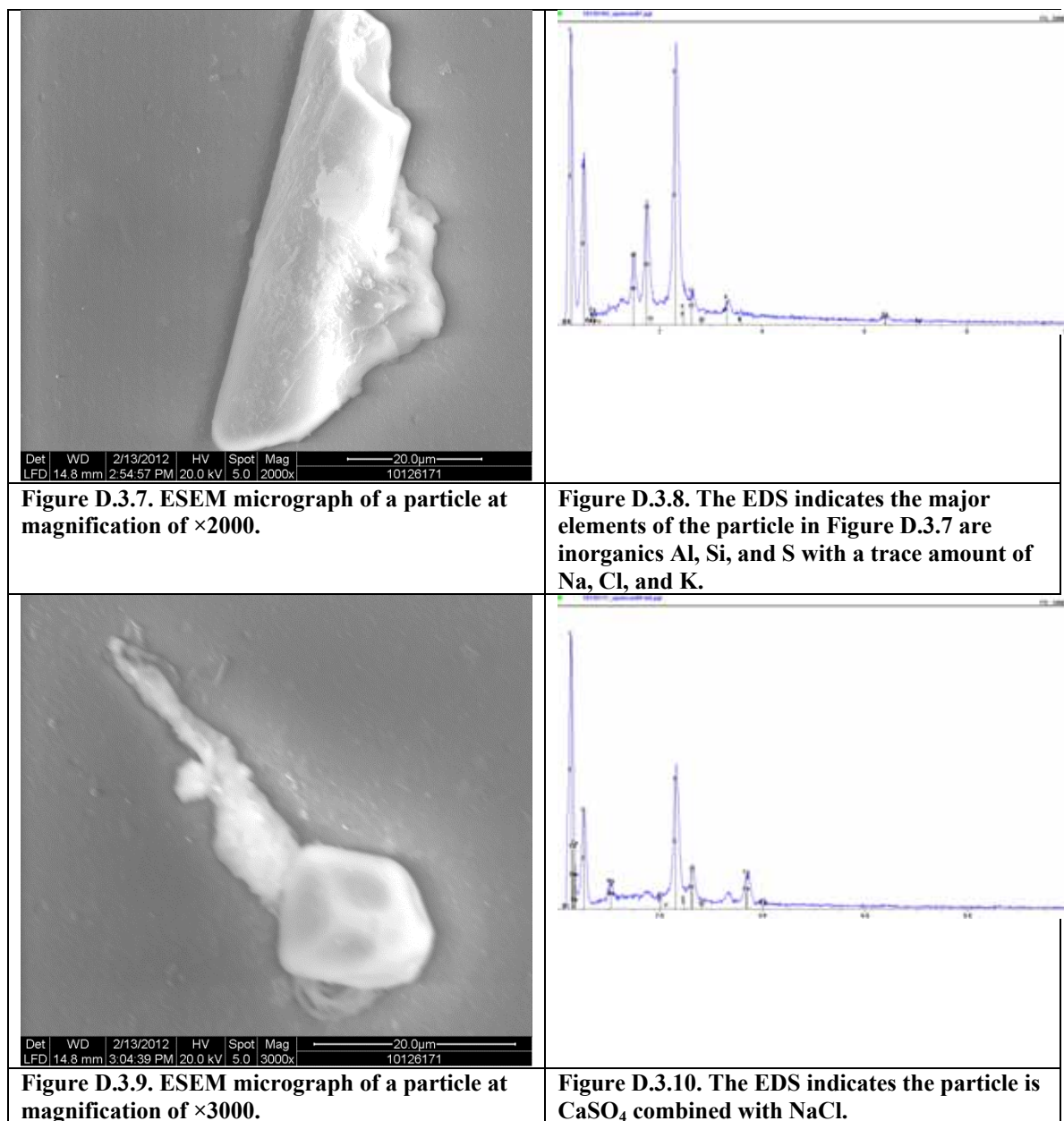


Figure D-3. SEM micrographs and EDS spectra of MBR-RO tail element 10126171.



Figure D.4.1. ESEM micrograph of MBR-O₃-RO lead element at magnification of ×30. Membrane surface was quite clean, similar to virgin membrane.



Figure D.4.2. ESEM micrograph of broken hollow-fiber membrane pieces at magnification of ×200.

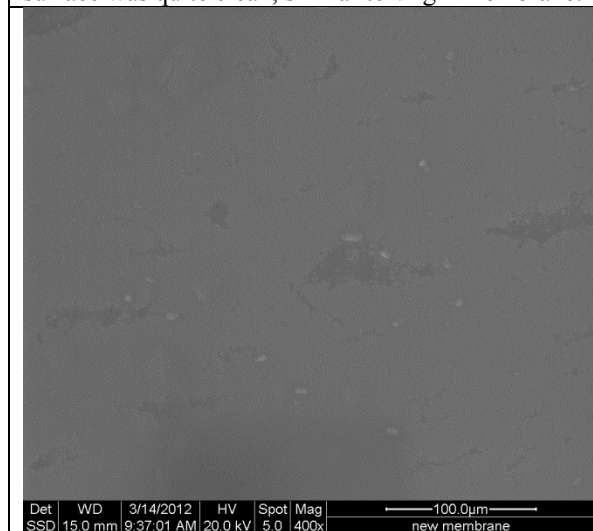


Figure D.4.3. ESEM micrograph of MBR-O₃-RO lead element at magnification of ×400.

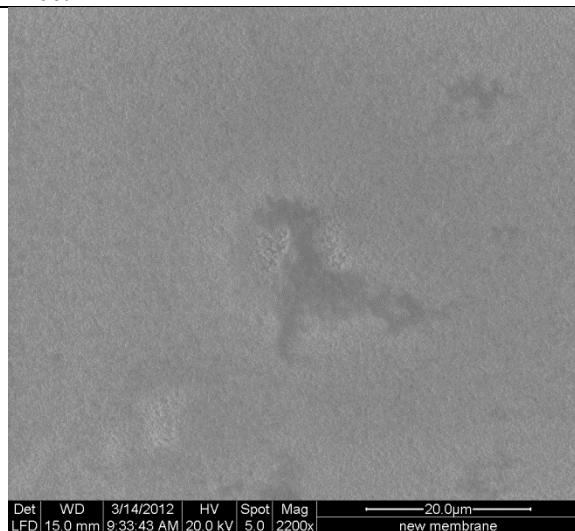


Figure D.4.4. ESEM micrograph of MBR-O₃-RO lead element at magnification of ×2200.

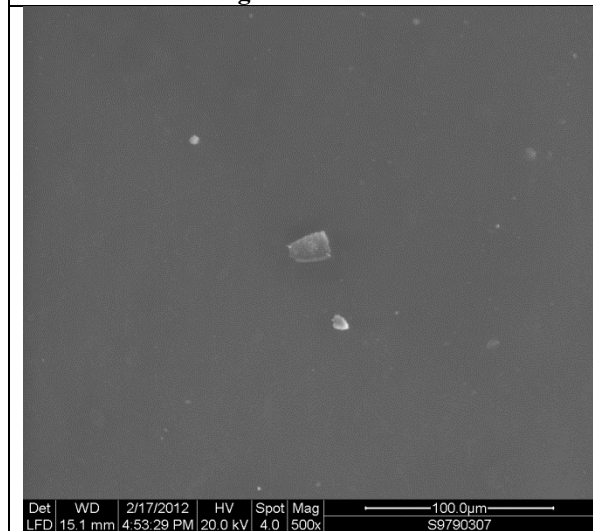


Figure D.4.5. ESEM micrograph of silica particles on membrane surface at magnification of ×500.

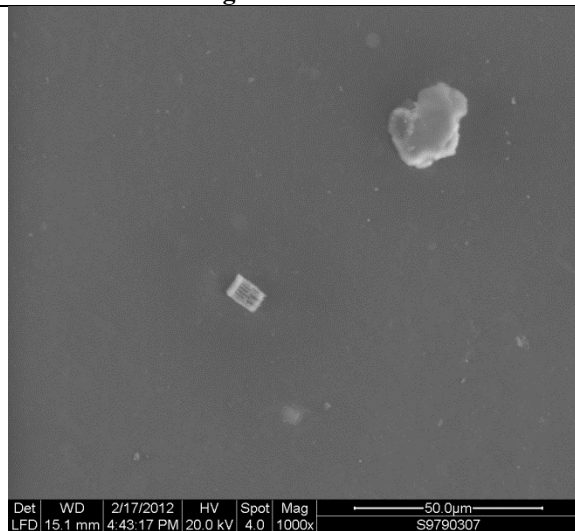


Figure D.4.6. ESEM micrograph at magnification of ×1000. The EDS indicates the particles are silicate and Al-silicate with a small amount of Fe.

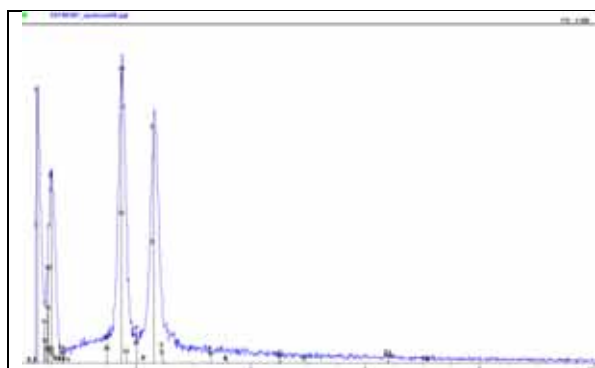


Figure D.4.7. EDS spot scanning of the particles in Figure D.4.5.

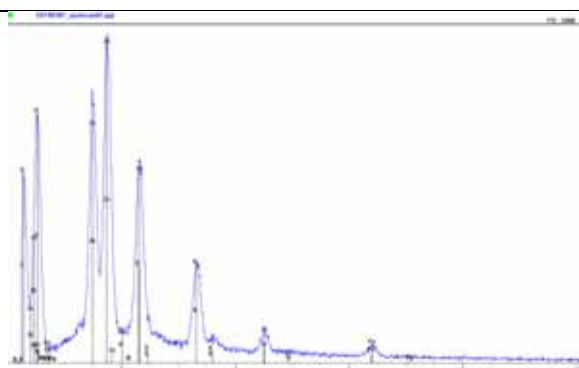


Figure D.4.8. EDS spot scanning of the particles in Figure D.4.6.

Figure D-4. SEM micrographs and EDS spectra of MBR-O₃-RO lead element S9790307.

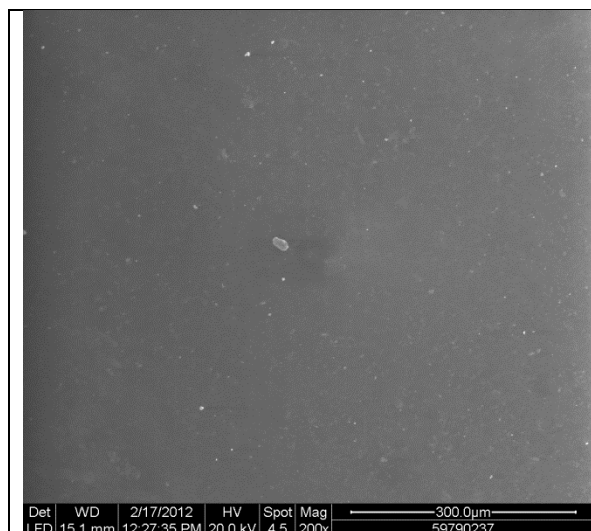


Figure D.5.1. ESEM micrograph at magnification of ×200. There is a thin fouling layer with more particles than the MBR-O₃-RO lead element.

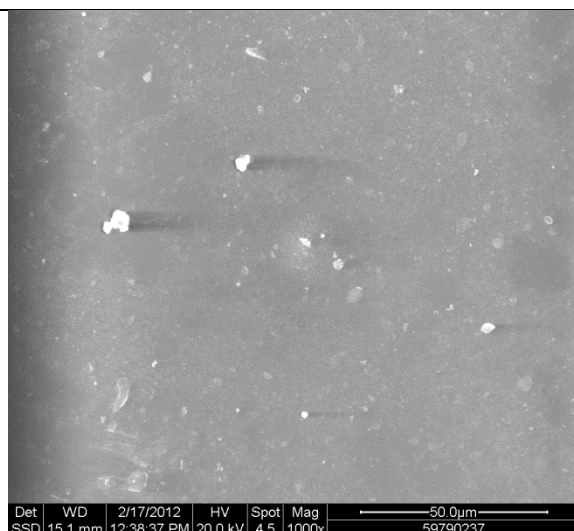


Figure D.5.2. ESEM micrograph at magnification of ×1000.

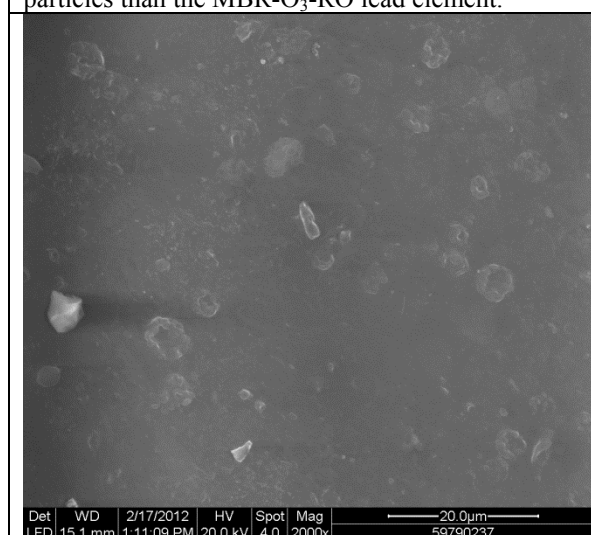


Figure D.5.3. ESEM micrograph of fouling layer at magnification of ×2000.

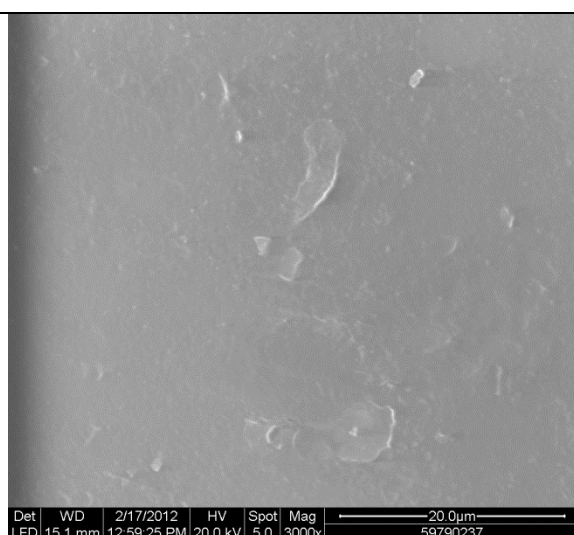


Figure D.5.4. ESEM micrograph of thin fouling layer at magnification of ×3000.

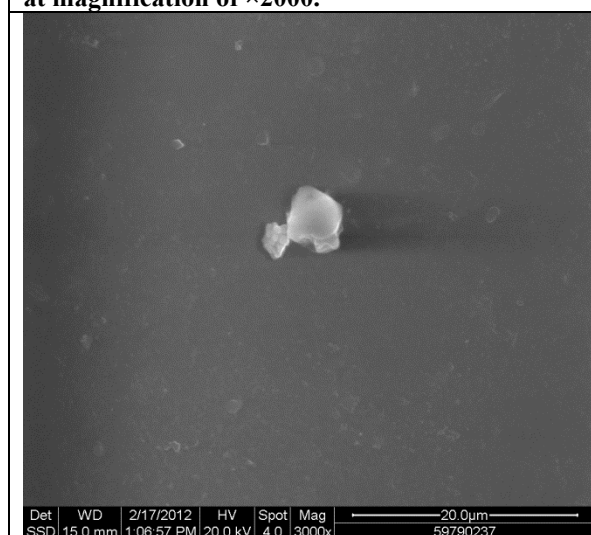


Figure D.5.5. ESEM micrograph of MBR-O₃-RO tail element at magnification of ×3000. The particle is Al-silicate with K.

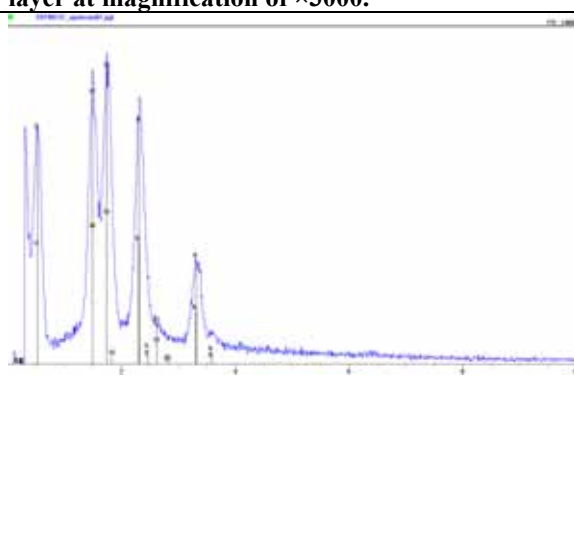


Figure D.5.6. EDS spot scan spectrum of the particle in Figure D.5.5.

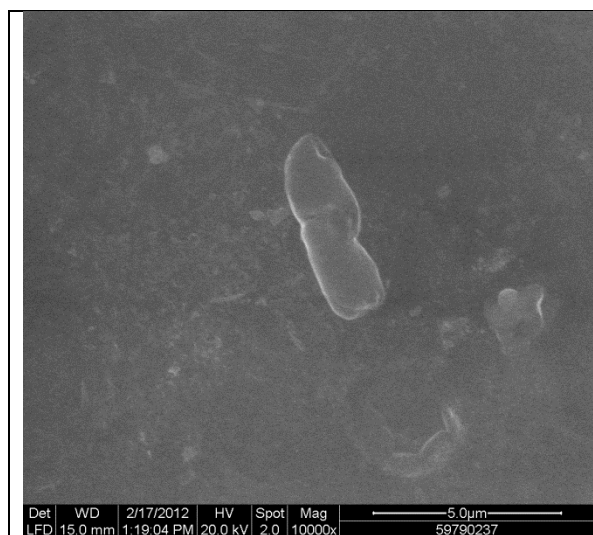


Figure D.5.7. ESEM micrograph of bacteria at magnification of $\times 10,000$.

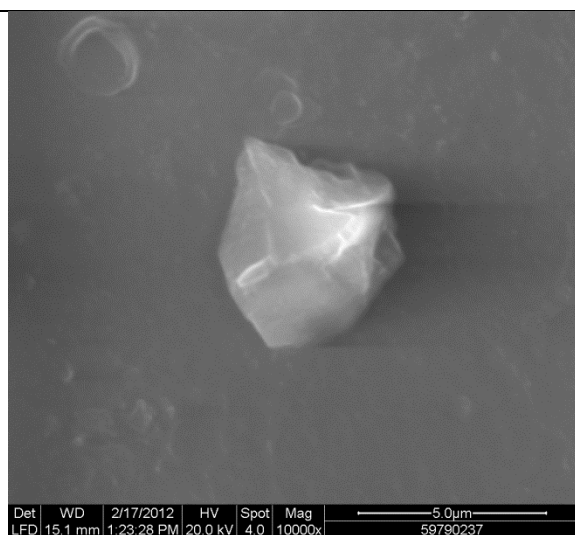


Figure D.5.8. Al-silicate particle with trace amounts of Na, Cl, and K.

Figure D.5. SEM micrographs and EDS spectra of MBR-O₃-RO tail element S9790327.

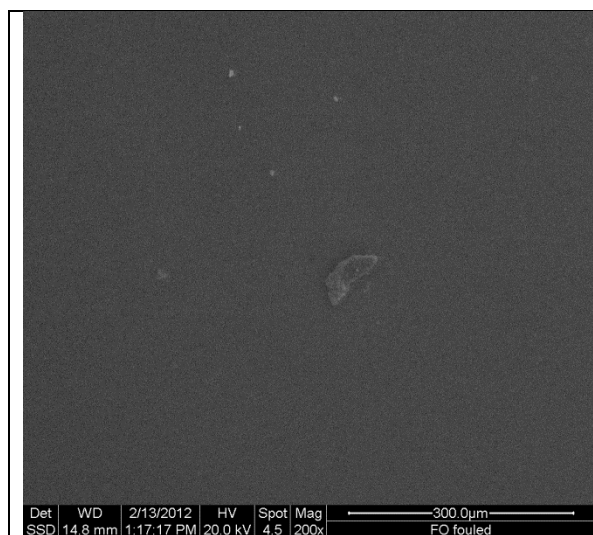


Figure D.6.1. ESEM micrograph of UF-RO lead element at magnification of $\times 200$. Membrane surface was very clean, similar to virgin membrane, but had particles of various sizes. EDS analysis indicates the particles shown in this images are Al-silicate, CaSO₄, and a trace amount of Fe-based chemical.

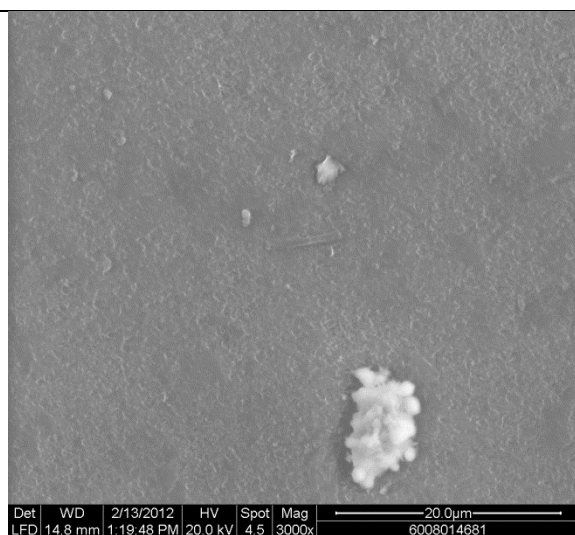


Figure D.6.2. ESEM micrograph of Fe-based particles.

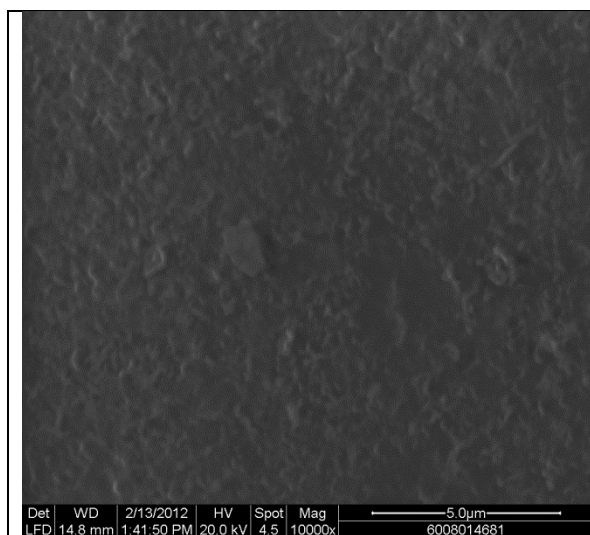


Figure D.6.3. ESEM micrograph of clean area at magnification of $\times 10,000$.

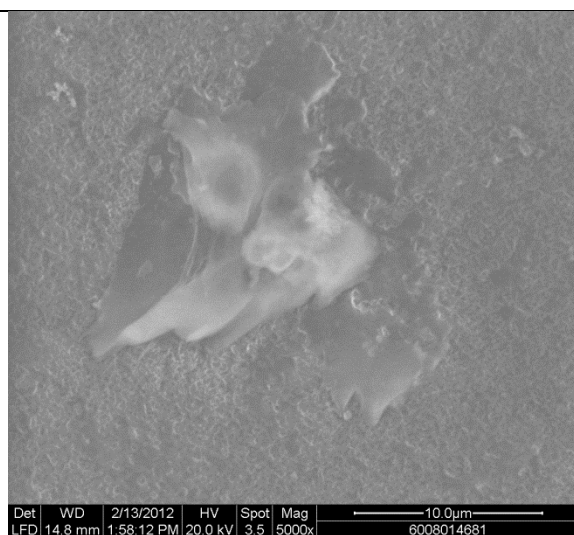


Figure D.6.4. ESEM micrograph of biofouling formation at magnification of $\times 5000$.

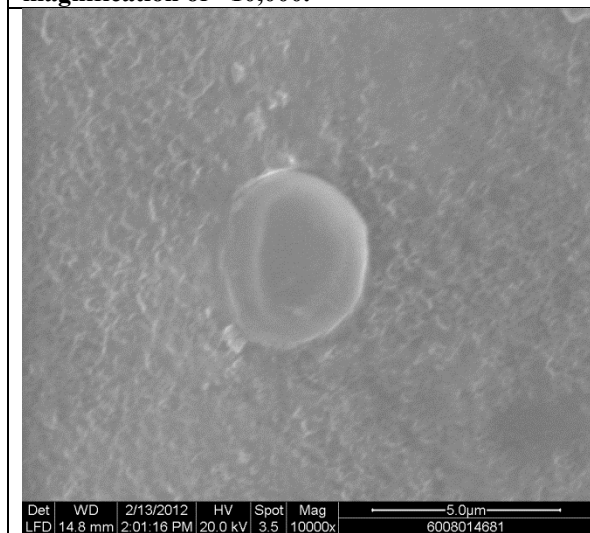


Figure D.6.5. ESEM micrograph of a bacterium on membrane surface at magnification of $\times 10,000$.



Figure D.6.6. ESEM micrograph of biofilm formation at magnification of $\times 13,000$.

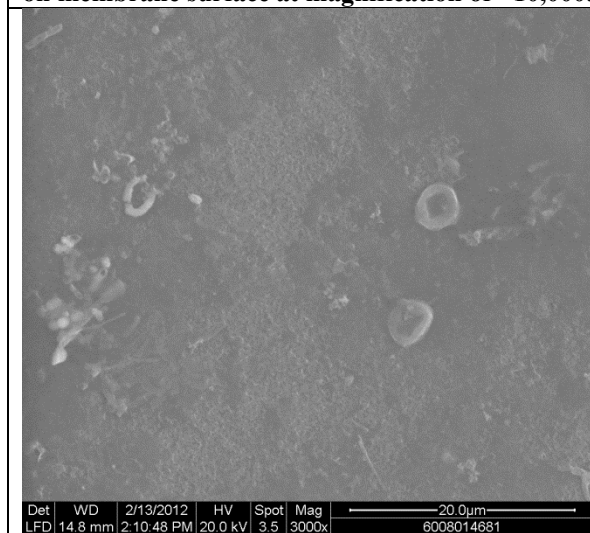


Figure D.6.7. ESEM micrograph of bacterial cells.

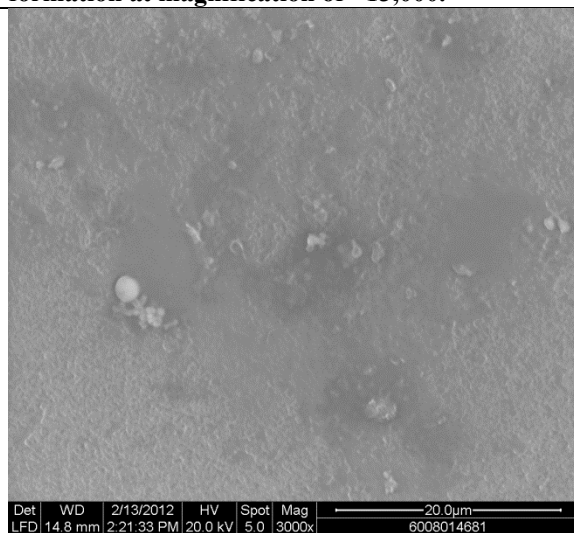


Figure D.6.8. ESEM micrograph of bacterial cells.

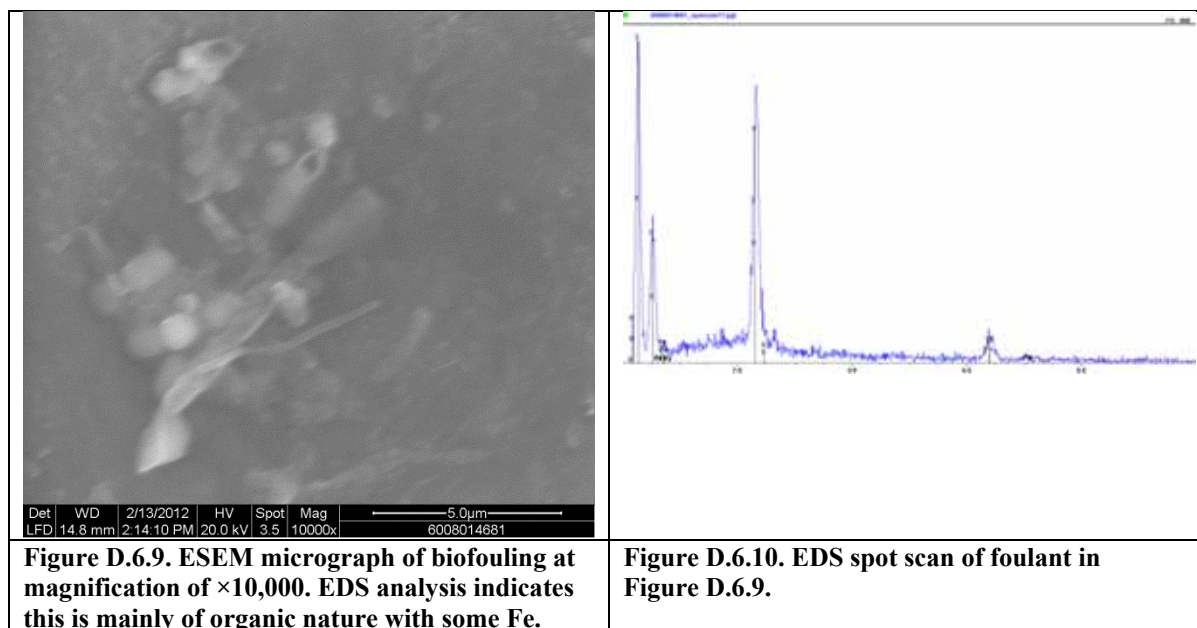
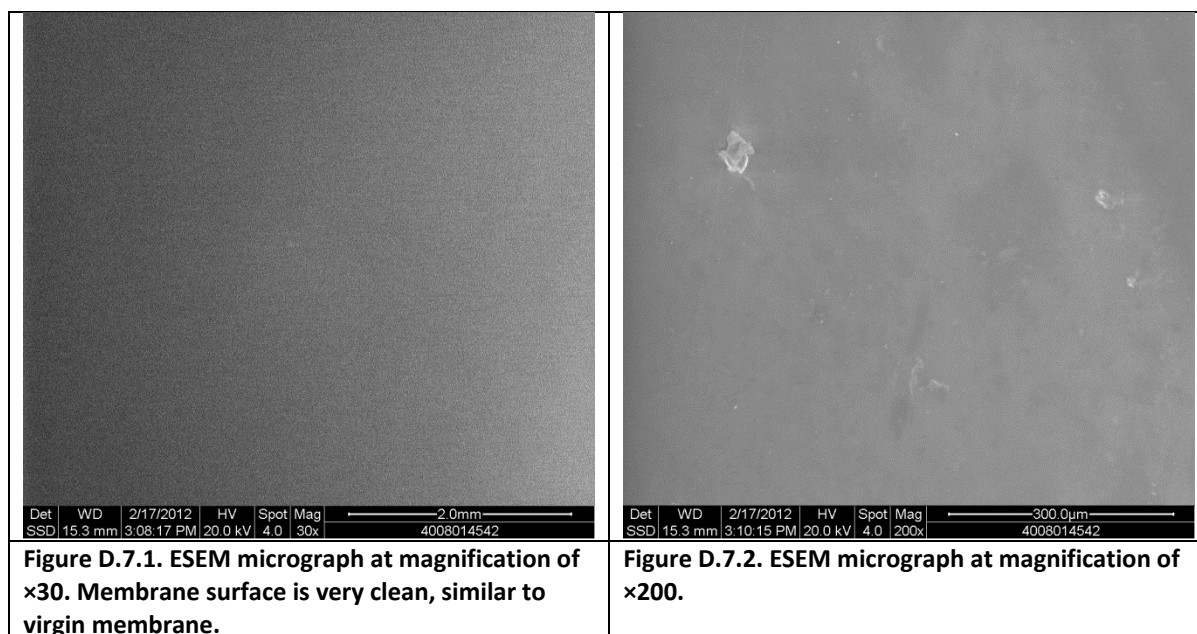


Figure D.6. SEM micrographs and EDS spectra of UF-RO lead element 6008014687.



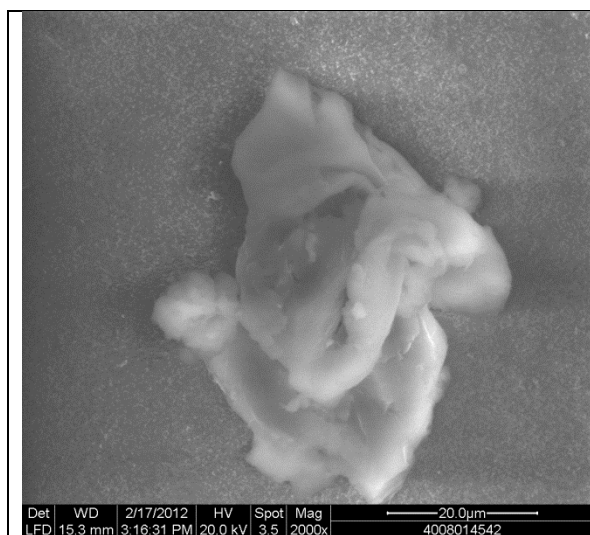


Figure D.7.3. ESEM micrograph of an organic piece at magnification of ×2000.

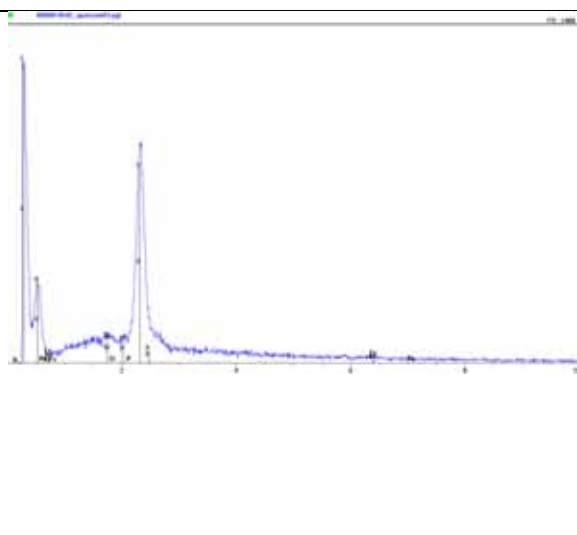


Figure D.7.4. EDS spot scan spectrum of the particle in Figure D.7.3.

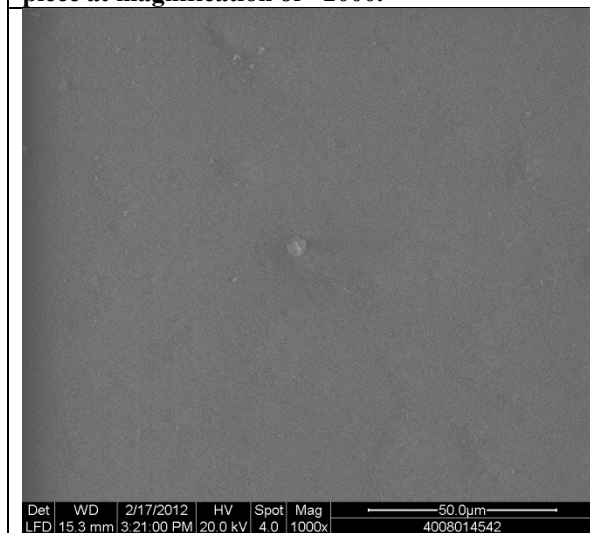


Figure D.7.5. ESEM micrograph at magnification of ×1000.

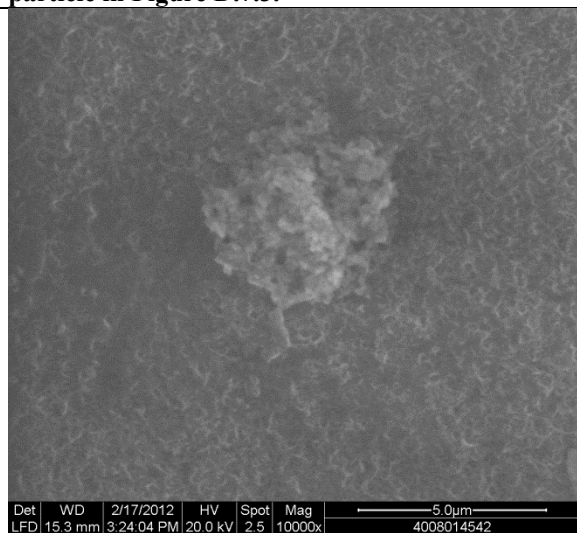


Figure D.7.6. ESEM micrograph at magnification of ×10,000. Membrane surface is clean.

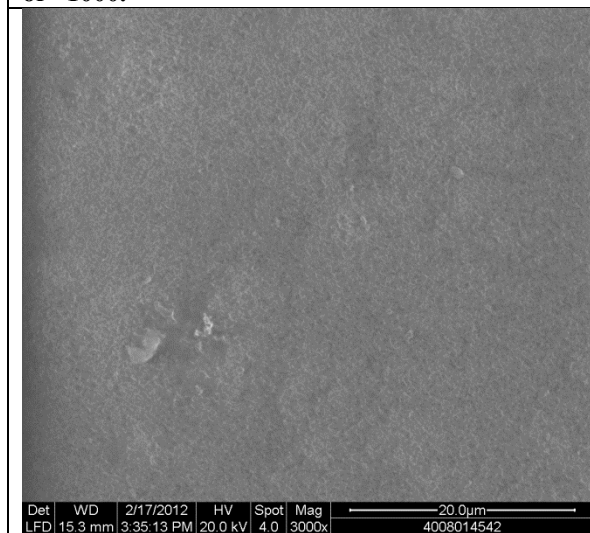


Figure D.7.7. ESEM micrograph at magnification of ×3000.

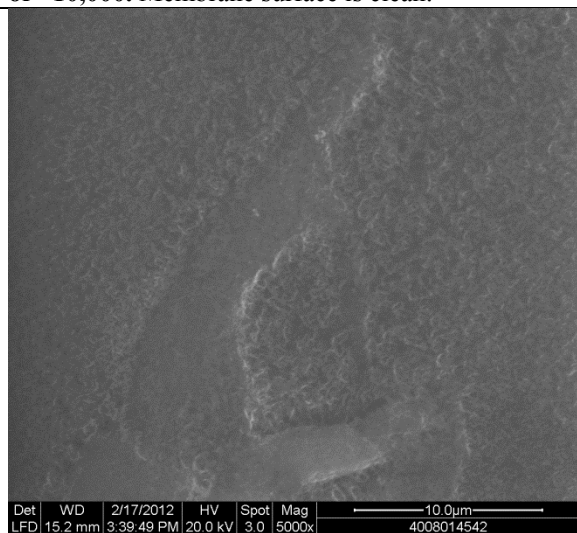


Figure D.7.8. ESEM micrograph at magnification of ×5000. Membrane surface is clean.

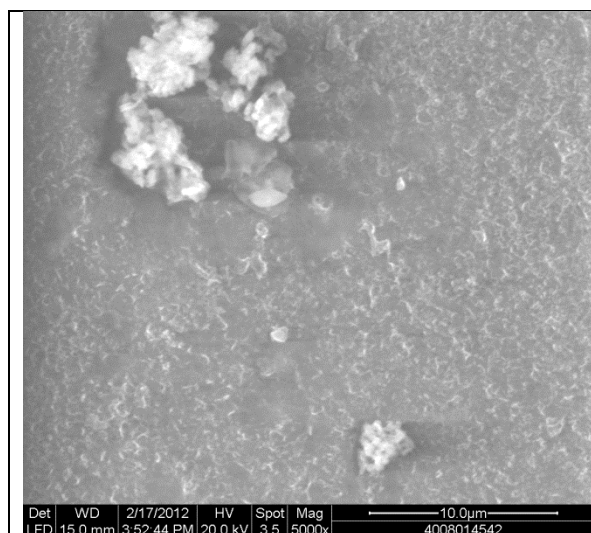


Figure D.7.9. ESEM micrograph of Fe-based precipitates at magnification of ×5000.

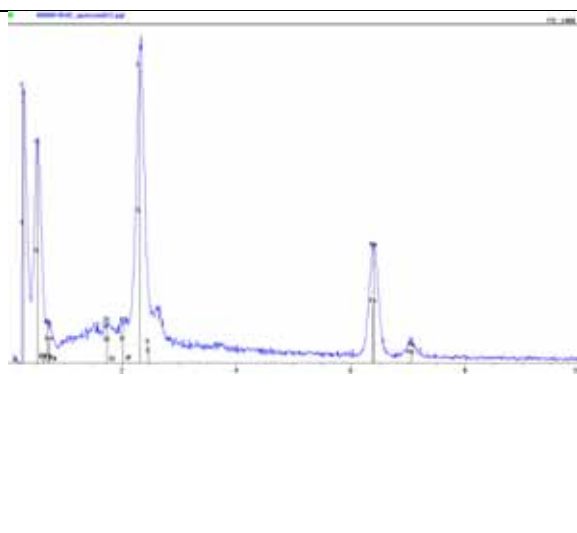


Figure D.7.10. EDS spot scan of Fe-based precipitates in Figure D.7.9.

Figure D.7. SEM micrographs and EDS spectra of UF-RO tail element 600804562.

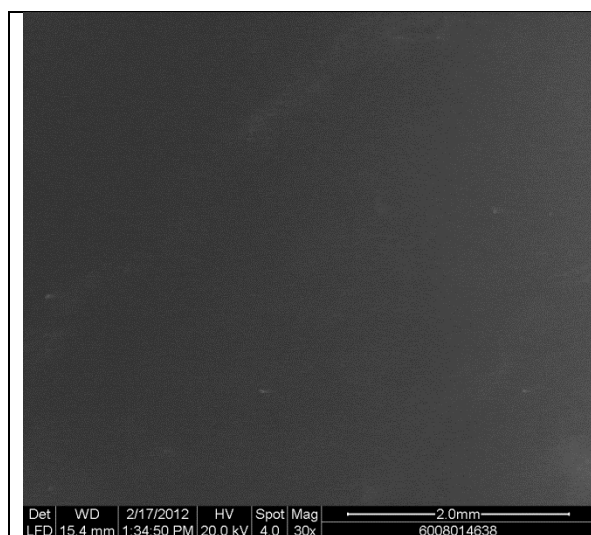


Figure D.8.1. ESEM micrograph of UF-UV/H₂O₂-RO lead element at magnification of ×30. The fouling layer is heterogeneous, some area has a very thick Fe-based fouling layer, whereas some area is as clean as virgin membrane.

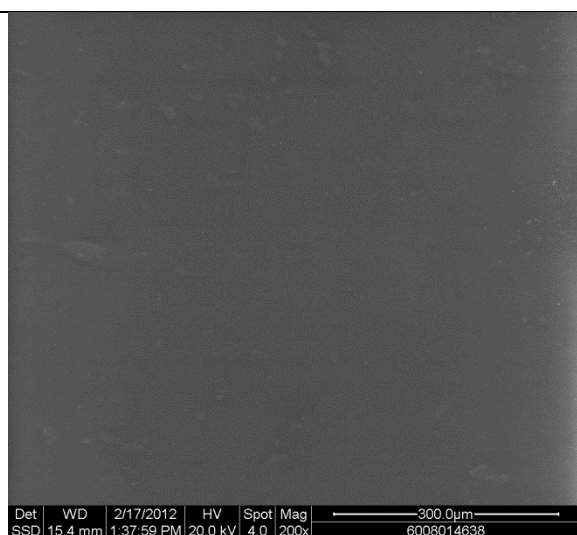


Figure D.8.2. ESEM micrograph of UF-UV/H₂O₂-RO lead element at magnification of ×200.

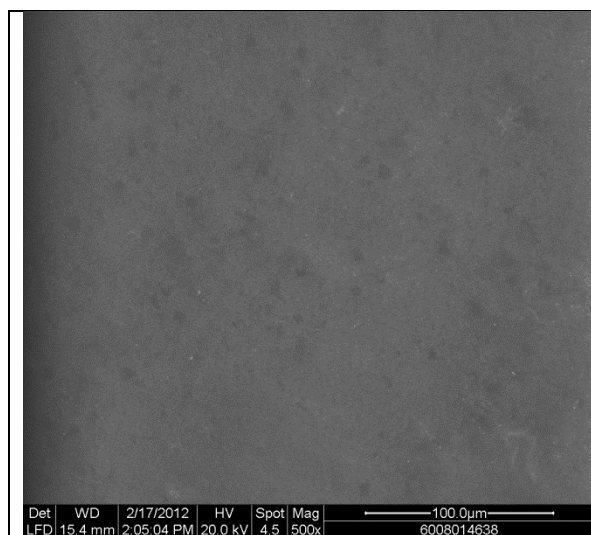


Figure D.8.3. ESEM micrograph of relatively clean area of UF-UV/H₂O₂-RO lead element at magnification of ×500.

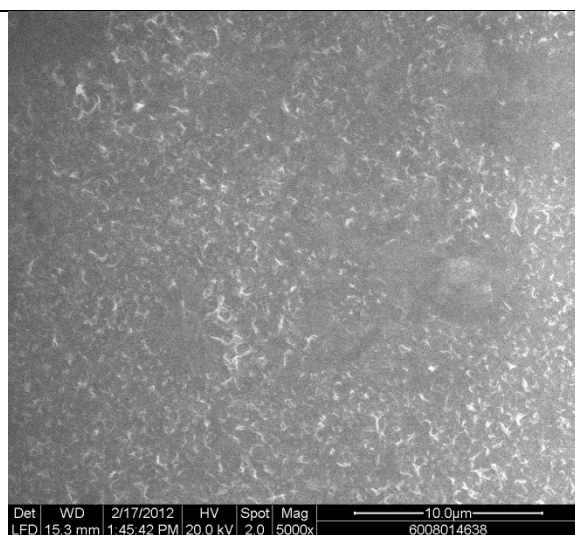


Figure D.8.4. ESEM micrograph of clean area of UF-UV/H₂O₂-RO lead element with biofouling formation at magnification of ×5000.



Figure D.8.5. ESEM micrograph of thin biofilm at magnification of ×5000.

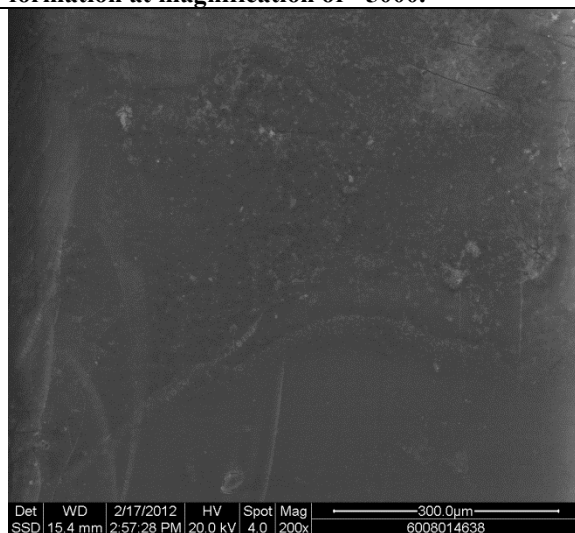


Figure D.8.6. ESEM micrograph of thick fouling layer, which is a combination of biofilm and Fe precipitates, at magnification of ×200.

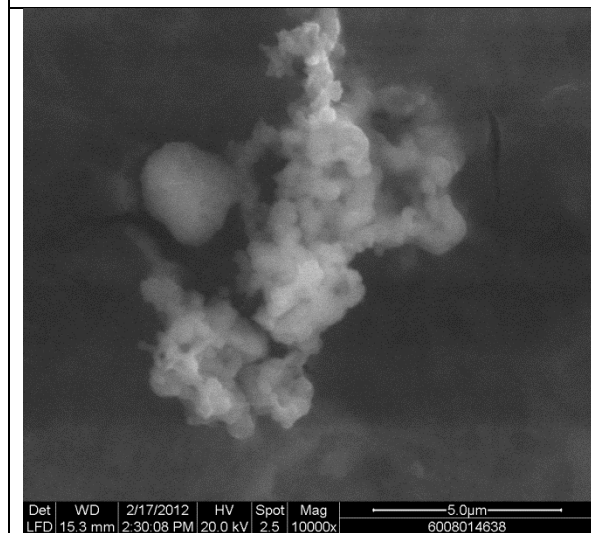


Figure D.8.7. ESEM micrograph of Fe-based particles with small amount of silicate and calcium phosphate.

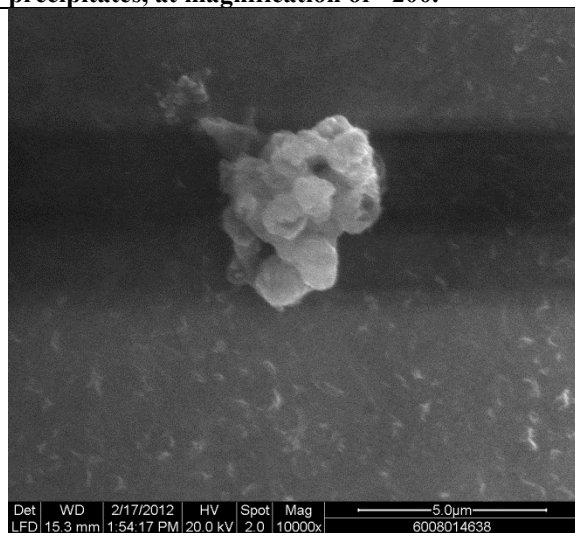


Figure D.8.8. ESEM micrograph of Fe-based particles.

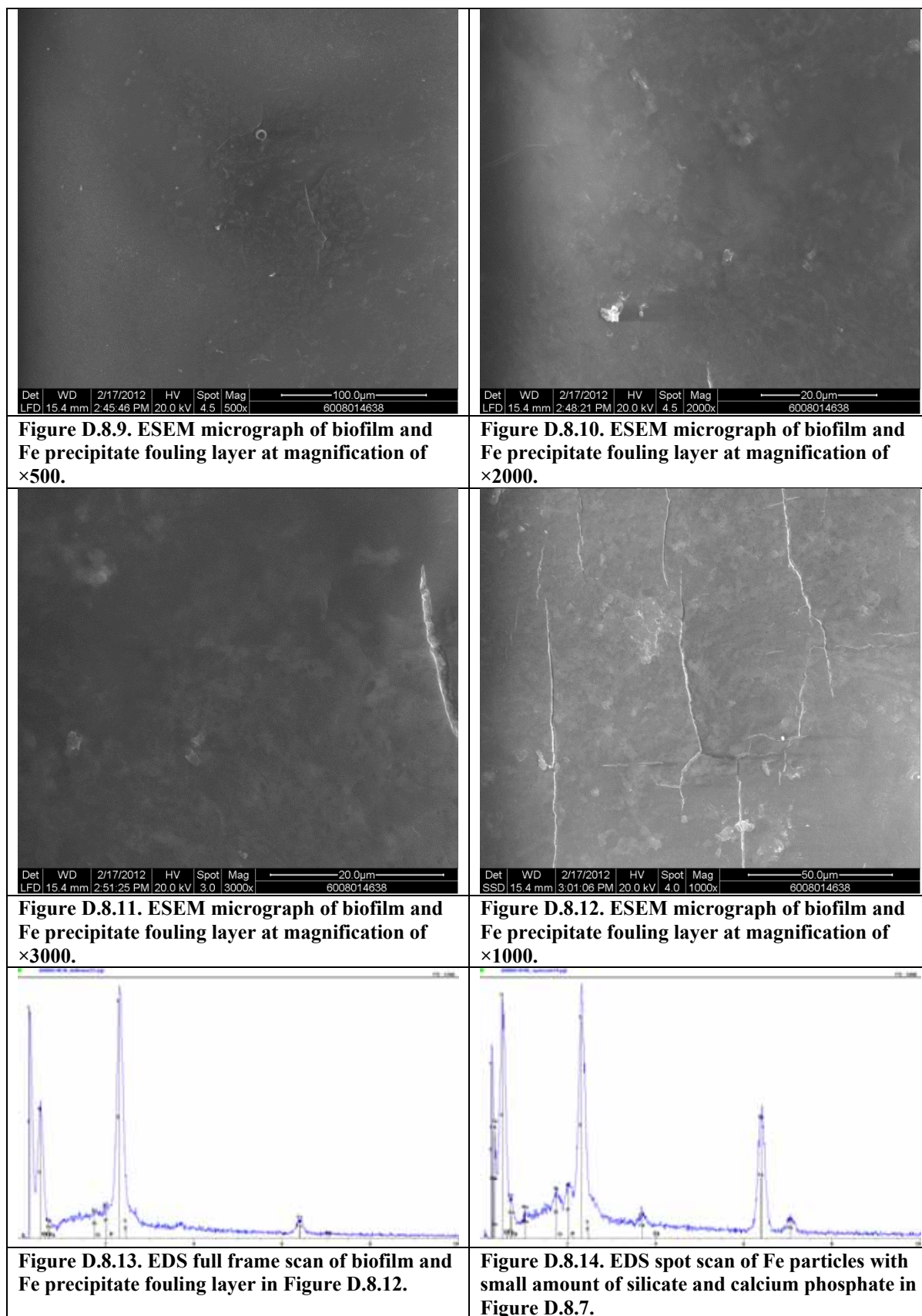


Figure D.8. SEM micrographs and EDS spectra of UF-UV/H₂O₂-RO lead element 600804638.

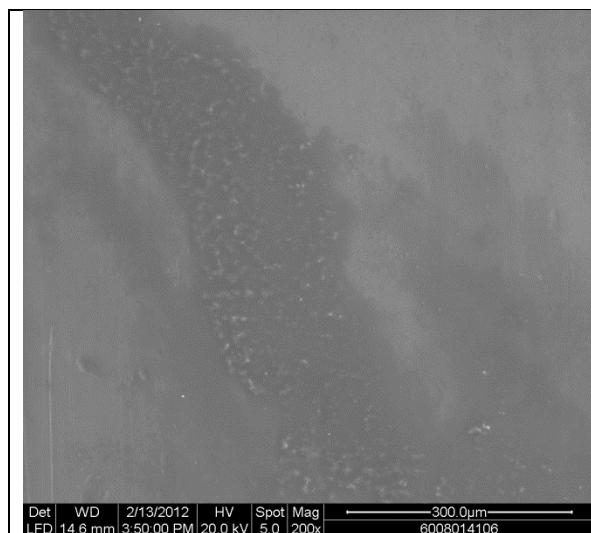


Figure D.9.1. ESEM micrograph of heterogeneous fouling layer at magnification of $\times 200$. Membrane surface is moderately clean; some areas are similar to virgin membrane.

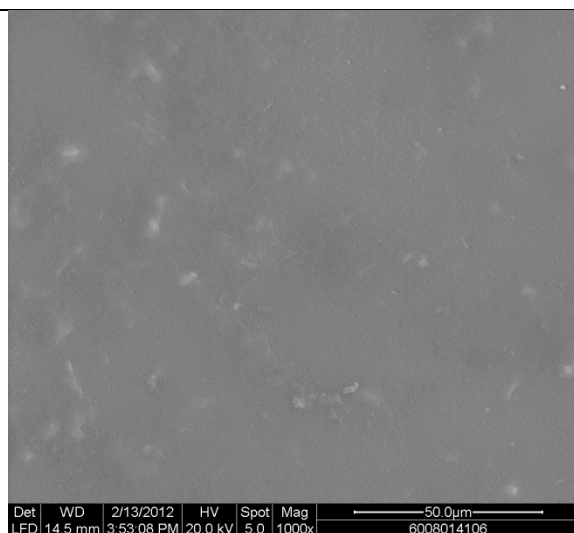


Figure D.9.2. ESEM micrograph of biofilm and Fe precipitate fouling layer at magnification of $\times 1000$.

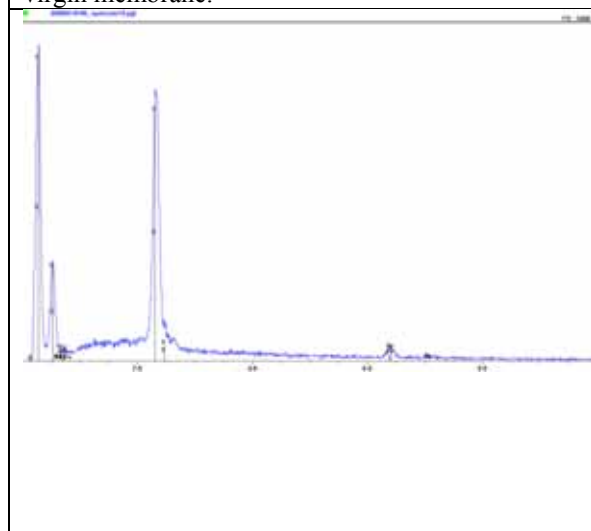


Figure D.9.3. EDS spot scan spectrum of the particle in Figure D.9.2.

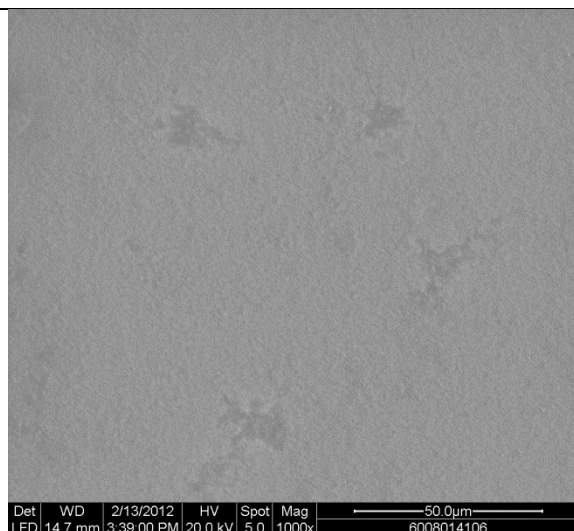


Figure D.9.4. ESEM micrograph of relatively clean area at magnification of $\times 1000$.



Figure D.9.5. ESEM micrograph of biofilm formation at magnification of $\times 10,000$.

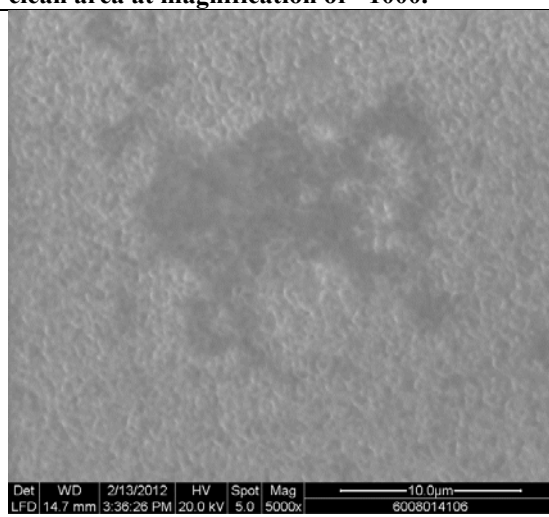


Figure D.9.6. ESEM micrograph at magnification of $\times 5000$. Membrane surface is clean.

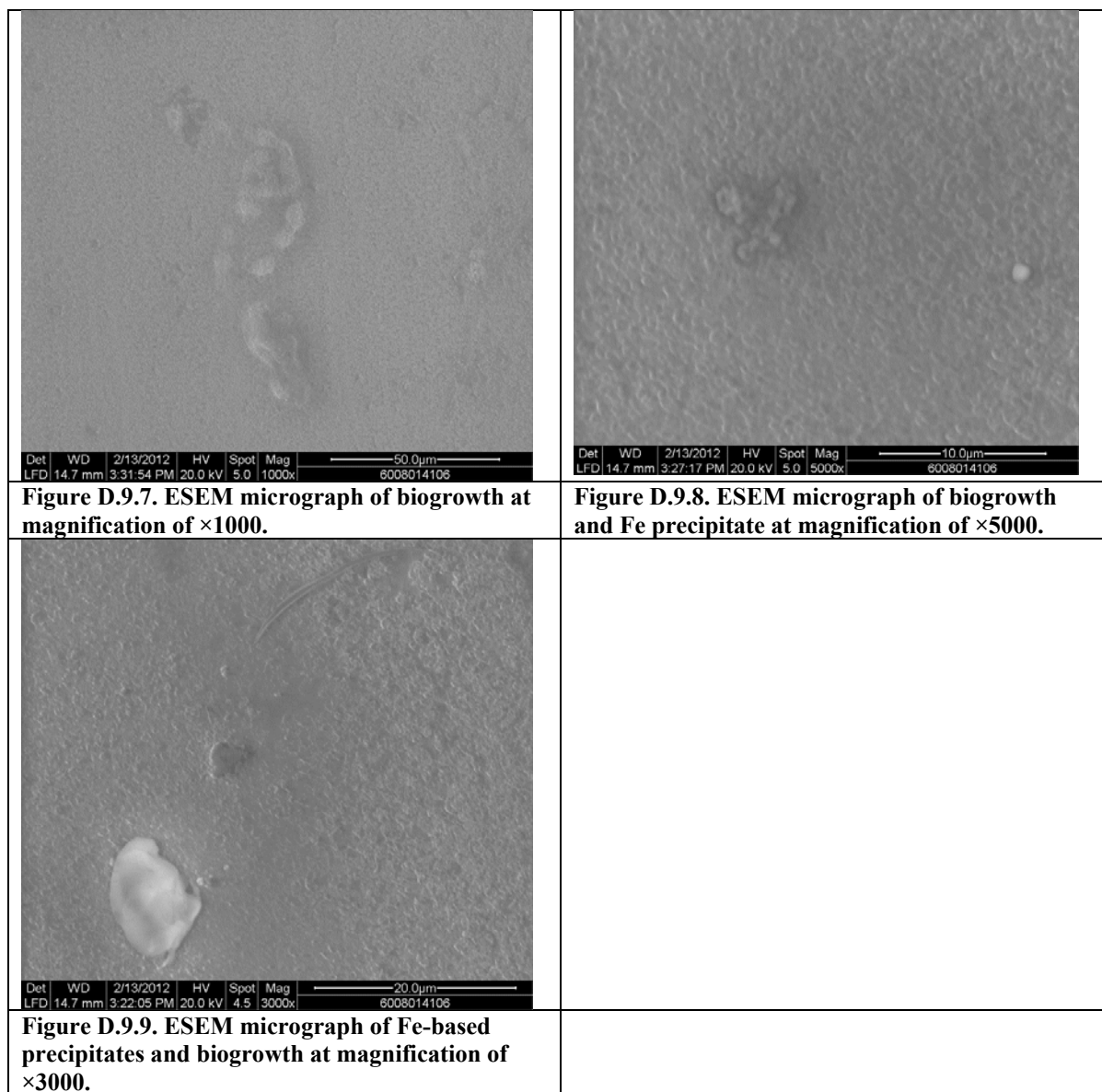


Figure D.9. SEM micrographs and EDS spectra of UF-UV/H₂O₂-RO tail element 600804106.

Advancing the Science of Water Reuse and Desalination



1199 North Fairfax Street, Suite 410
Alexandria, VA 22314 USA
(703) 548-0880
Fax (703) 548-5085
E-mail: Foundation@WateReuse.org
www.WateReuse.org/Foundation